A Novel System Impedance Measurement for Power System Analysis and Improvement in Power Quality

Ben Palethorpe, M.Eng.

Submitted to the University of Nottingham for the degree of Doctor of Philosophy.
April 2002.

Acknowledgements

I would like to thank all those who have helped me throughout the course of this work. I would also like to thank all those that have not helped academically but have helped to make this time so enjoyable.

In particular I would like to express my gratitude to my supervisors Mark Sumner and Dave Thomas, Mark Sumner for his guidance, support and advice in every aspect of this work and to Dave Thomas for his help during the work and in reading of the thesis.

Thanks also to all the members of the Power Group, past and present, who helped me with my experimental work and in whiling away the many hours spent in the lab.

Finally thanks to my family and friends for putting up with me during those periods when I thought I would never finish !

Contents

1 Introduction **1**

1.1 Background to the nature of the National Grid 1

1.2 Power quality 5

1.3 Tackling harmonic distortion 6

1.3.1 Reducing harmonic current at the source 6

1.3.2 Reducing harmonic current at the system level 7

1.4 Power quality regulations 9

1.4.1 BS IEC 61000-3-4 9

1.5 Power system impedance measurement 12

1.6 Objectives of this work 12

1.7 Thesis structure 13

2 Introduction to Impedance Measurement **16**

2.1 Introduction 16

2.2 Why use on-line impedance measurement ? 17

2.3 Terminology 18

2.4 Power system modelling 19

2.4.1 Choosing the correct model 22

2.5 System impedance with non-linear models 22

2.6 Previous work 24

2.6.1 Single measurement, steady state techniques 24

2.6.2 Double measurement, linear disturbing load, steady state techniques 26

2.6.3 Double measurement, non-linear disturbing load, steady state techniques 30

2.6.4 Transient disturbance measurement 31

2.6.5 Steady state, single frequency injection measurement 34

2.6.6 Steady state, wideband injection measurement 36

2.7 Conclusions drawn from reviewed work 38

2.8 Summary 40

3 Description of the Experimental System **41**

3.1 Introduction 41

3.2 The Active Filter System 42

3.2.1 System overview 42

3.2.2 Control 45

3.2.2.1 PWM generator and WATCHDOG 48

3.2.2.2 General purpose board 49

3.2.2.3 Analogue to digital boards 49

3.2.2.4 Transducers 50

3.2.3 Software 50

3.2.4 Protection 53

3.3 The Impedance Measurement System 56

3.4 Summary 59

4 Linear impedance measurement techniques **60**

4.1 Introduction 60

4.2 Requirements for on-line measurement techniques 61

4.3 Short term measurement technique 64

4.4 Medium term injection technique 66

4.5 Signal processing techniques 68

4.5.1 Periodogram approach 69

4.5.2 Correlation approach 72

4.6 Minimization of spectral leakage 74

4.6.1 Steady state cancellation 75

4.6.2 Windowing 75

4.7 Short term injection signal processing 76

4.8 Medium term injection signal processing 80

4.9 Estimating the transfer function from impedance versus frequency values . 81

4.10 Generalized measurement approach 83

4.10.1 Unbalanced system 84

4.10.2 Balanced system 87

4.11 Practical implementation of injection techniques 90

4.11.1 Short term injection 90

4.11.2 Medium term injection 91

4.12 Simulation work 92

4.12.1 Short term injection simulations 95

4.12.2 Medium term injection simulations 102

4.12.3 Summary of simulation results 108

4.12.4 Injection strength in practice 108

4.13 Conclusion 110

5 Impedance measurement results for linear systems 112

5.1 Introduction 112

5.2 Experimental Procedure 113

5.2.1 IM1: Short term injection with supply connection 113

5.2.2 IM2: Medium term injection with supply connection 114

5.2.3 IM3: Discrete frequency calibration injection 115

5.2.4 IM4: Short term injection without supply connection 116

5.3 Test circuits 117

5.3.1 Test circuit 1 (c1) 118

5.3.2 Test circuit 2 (c2) 119

5.3.3 Test circuit 3 (c3) 120

5.3.4 Test circuit 4 (c4) 120

5.3.5 Test circuit (c5) 121

5.3.6 Test circuit 6 (c6) 121

5.3.7 Test circuit 7 (c7) 122

5.3.8 Test circuit 8 (c8) 123

5.4 Experimental results 123

5.4.1 Experimental data before parameter estimation 124

5.4.2 Parameter estimation from experimental results 143

5.4.3 Statistical variation of experimental results 154

5.4.4 Conclusions from experimental results 158

5.5 Summary 159

6 Measurement results in the presence of non-linear loads 160

6.1 Introduction 160

6.2 Experimental circuits 161

6.3 Medium term injection 161

6.3.1 Medium term injection results 161

6.3.2 Discussion of medium term injection results 169

6.4 Short term injection 173

6.4.1 Short term injection results 173

6.4.2 Discussion of circuit A results 181

6.4.3 Discussion of short term injection results 187

6.5 Improved measurement using Prony method 188

6.5.1 Short term injection time 191

6.5.2 Prony extrapolation of time domain signals 193

6.5.3 Experimental verification of the Prony based algorithm 194

6.6 Conclusion 198

7 Using impedance estimates for prediction of load current 200

7.1 Introduction 200

7.2 Load current prediction 200

7.3 Current prediction summary 204

7.4 Voltage detection active power filters 205

7.5 Active shunt filter reference generation 206

7.6 Active filters using supply impedance within reference generation 208

7.6.1 Reference generation using supply impedance transfer function . . 209

7.7 Control of the ASF 215

7.7.1 Control parameter design 221

7.8 Experimental results 222

7.8.1 Voltage distortion compensation with no load 223

7.8.2 Voltage distortion compensation with load connected 227

7.8.3 Voltage distortion compensation with incorrect parameters 231

7.9 Summary 234

8 Conclusions and further work 235

8.1 Objectives 235

8.2 Conclusions 236

8.2.1 Objective 1 236

8.2.2 Objective 2 239

8.2.3 Objective 3 240

8.3 Suggestions for further work 242

A Impedance relationships **257**

B Simulation schematics for impedance measurement **260**

C Active shunt filter implementation **263**

C.1 Control derivation 263

C.2 ASF controller performance 265

D Publications by the author **269**

D.1 Publications by the author 269

List of Figures

1.1 Current distortion due to non-linear load 2

1.2 Rectifier circuits and line current waveforms 4

1.3 Harmonic filter topologies 8

2.1 On-line impedance measurement terminology 18

2.2 Impedance measurement at harmonic frequencies 20

2.3 Current Source non-linear load (CS-NLL) 21

2.4 Voltage Source non-linear load (VS-NLL) 21

2.5 VS-NLL and CS-NLL models with additional filtering 22

2.6 Complete power system with NLLs 23

2.7 Equivalent circuit for impedance measurement using Lemoine's technique, h is harmonic order. h not equal to 1 25

2.8 Equivalent circuits for impedance measurement using Crevier's technique . 27

2.9 Equivalent circuit for impedance measurement using Duggan's technique . 30

2.10 Equivalent circuit for impedance measurement using transient measurement 32

2.11 Equivalent circuit for impedance measurement using harmonic generator . . 37

3.1 Overview of the active filter system 43

3.2 The control scheme 47

3.3 Overview of host and DSP software 52

3.4 Protection features of the experimental rig 54

3.5 Impedance measurement stand alone data acquisition system 57

4.1 Measurement system overview 61

4.2 ASF control scheme 62

4.3 Ideal short term injection 65

4.4 Ideal medium term injection 67

4.5 Single input, single output (SISO) system 69

4.6 Option 1 sampling arrangement 77

4.7 Option 2 sampling arrangement 79

4.8 Spectral leakage from a 50.1Hz sinusoid 80

4.9 Balanced three phase system transient 88

4.10 Single phase equivalent transient 88

4.11 Example three phase system and equivalent single phase system 89

4.12 Active shunt filter for current injection 90

4.13 Simulation supply models 92

4.14 Simulation system for supply model 1 93

4.15 Simulation 1. Ideal simulation conditions: no measurement noise and perfect steady state cancellation 98

4.16 Simulation 2. 51.151kHz experimental sampling frequency and additive measurement noise used 99

4.17 Simulation 3. 51.151kHz experimental sampling frequency and additive measurement noise used. 50.1Hz supply frequency. Results shown with and without pre-processing 100

4.18 Simulation 4. Supply model 2. 51.151kHz experimental sampling frequency and additive measurement noise used. 50.1Hz supply frequency . . 101

4.19 Simulation 5. Ideal simulation conditions: no measurement noise and perfect steady state cancellation 104

4.20 Simulation 6. 51.151kHz experimental sampling frequency and additive measurement noise used 105

4.21 Simulation 7. 51.151kHz experimental sampling frequency. Additive measurement noise. 50.1Hz supply frequency. Results shown using Hanning window 106

4.22 Simulation 7. Hanning window not applied 106

4.23 Simulation 8. Supply model 2. 51.151kHz experimental sampling frequency and additive measurement noise used. 50.1Hz supply frequency . . 107

4.24 Short term injection strength 109

4.25 Medium term injection strength 110

5.1 Practical injection system for IM1 and IM2 114

5.2 Practical injection system for IM3 115

5.3 Practical injection system 117

5.4 Circuit 1: Line-Line circuit 118

5.5 Circuit 2: Line-Line circuit 119

5.6 Circuit 3: Line-Line circuit 120

5.7 Circuit 4: Line-Line circuit 121

5.8 Circuit 5: Line-Line circuit 121

5.9 Circuit 6: Line-Line circuit 122

5.10 Circuit 7: Line-Line circuit 122

5.11 Circuit 8: Line-Line circuit 123

5.12 Short term injection results: c1 126

5.13 Medium term injection results: c1 127

5.14 Short term results: c2 128

5.15 Medium term injection results: c2 129

5.16 Short term injection results: c3 130

5.17 Medium term injection results: c3 131

5.18 Short term injection results: c4 132

5.19 Medium term injection results: c4 133

5.20 Short term injection results: c5 134

5.21 Medium term injection results: c5 135

5.22 Short term injection results: c6 136

5.23 Medium term injection results: c6 137

5.24 Short term results: c7 138

5.25 Medium term injection results: c7 139

5.26 Short term injection results: c8 140

5.27 Medium term injection results: c8 141

5.28 Parameter estimation from experimental results: c1 145

5.29 Parameter estimation from experimental results: c2 146

5.30 Parameter estimation from experimental results: c3 147

5.31 Parameter estimation from experimental results: c4 148

5.32 Parameter estimation from experimental results: c5 149

5.33 Parameter estimation from experimental results: c6 150

5.34 Parameter estimation from experimental results: c7 151

5.35 Parameter estimation from experimental results: c8 152

5.36 Mean and standard deviation of experimental results: c1 155

5.37 Mean and standard deviation of experimental results: c3 156

5.38 Mean and standard deviation of experimental results: c6 157

6.1 Experimental circuits 162

6.2 Medium term injection for circuit A (CS-NLL) and supply c1 163

6.3 Medium term injection for circuit A (CS-NLL) and supply c3 164

6.4 Medium term injection for circuit B (VS-NLL) and supply c1 165

6.5 Medium term injection for circuit B (VS-NLL) and supply c3 166

6.6 Medium term injection for circuit C (combined NLL) and supply c1 167

6.7 Medium term injection for circuit C (combined NLL) and supply c3 168

6.8 Impedance of supplies and of passive load connected to the rectifier output for circuit A 170

6.9 Impedance of supplies and of passive load connected to the rectifier output for circuit B 171

6.10 Impedance of supplies and of passive load connected to the rectifier output for circuit C 172

6.11 CS-NLL measurements. Phase 1 current: Blue. Phase 2 current: Red. Phase 3 current: Green 174

6.12 Measurement 1. Short term injection for circuit A (CS-NLL) and supply c1. 175

6.13 Measurement 2. Short term injection for circuit A (CS-NLL) and supply c1 176

6.14 Measurement 3. Short term injection for circuit A (CS-NLL) and supply c1 177

6.15 Measurement 1. Short term injection for circuit A (CS-NLL) and supply c3 178

6.16 Measurement 2. Short term injection for circuit A (CS-NLL) and supply c3 179

6.17 Measurement 3. Short term injection for circuit A (CS-NLL) and supply c3 180

6.18 VS-NLL measurements. Phase 1 current: Blue. Phase 2 current: Red. Phase 3 current: Green 182

6.19 Measurement 1. Short term injection for circuit B and C, supply c1 183

6.20 Measurement 2. Short term injection for circuit B and C, supply c1 184

6.21 Measurement 1. Short term injection for circuit B and C, supply c3 185

6.22 Measurement 2. Short term injection for circuit B and C, supply c3 186

6.23 Conduction between phases 2 and 3 188

6.24 Simulation circuit used for demonstration of Prony technique 190

6.25 Rectifier input current and voltage 191

6.26 Transient injection signals 192

6.27 Estimated supply impedance 193

6.28 Injection signals and extraploated signals using the Prony algorithm. 195

6.29 Estimated supply impedance after Prony extrapolation 196

6.30 Application of the Prony based algorithm on realistic simulation data 197

7.1 Experimental system 201

7.2 Predicted current distortion results. 202

7.3 Active filter connection 206

7.4 Power system with ASF 209

7.5 ASF equivalent connection 211

7.6 ASF control scheme in dq reference frame 216

7.7 ASF harmonic controller 218

7.8 Voltage feedback for current error generation 220

7.9 Single axis controller 221

7.10 Experimental circuit 222

7.11 Supply impedance for c3 (per phase) 224

7.12 Line voltage distortion before(blue) and after(red) controllers turned on . . 225

7.13 Line voltage harmonics before(blue) and after(red) controllers activated . . 225

7.14 Control action of 5th and 7th frame DQ controllers 226

7.15 Line voltage distortion before(blue) and after(red) control action 228

7.16 Line voltage harmonics before(blue) and after(red) control action 228

7.17 Control action of 5th and 7th frame DQ controllers 229

7.18 Line current waveforms during ASF operation 230

7.19 Supply impedance for c1 and c3, blue: c1, red: c3 232

7.20 Line voltage harmonics before(blue) and after(red) control action 233

7.21 Control action of 11th harmonic dq frame controllers. 234

B.1 Simulated single phase system 261

B.2 Data acquisition system for impedance estimation 261

B.3 Active shunt filter 262

B.4 Transient sources for short term and medium term injection 262

C.1 Single phase equivalent of the ASF connection 263

C.2 Steady state 5th harmonic injection. (a) Line current. (b) controller output, reference is 10. (c) Line current in the frequency domain. 266

C.3 Steady state 7th harmonic injection. (a) Line current. (b) controller output, reference is 10. (c) Line current in the frequency domain. 267

C.4 Steady state 5th and 7th harmonic injection. (a) Line current. (b) controller output, reference is 10. (c) Line current in the frequency domain. 268

List of Tables

1.1 Stage 1 limits for BS IEC 61000-3-4 11

1.2 Stage 2 limits for BS IEC 61000-3-4 11

3.1 ASF parameters 45

4.1 Injection pattern for well-conditioned matrix 86

4.2 Simulation Parameters 94

5.1 Legend for experimental result figures 125

5.2 Legend for Curve fitting results figures 144

5.3 Averaged standard deviation 158

7.1 Current prediction results using laboratory supply 203

7.2 Control parameters 222

7.3 Admittance terms for calculation of current references 224

7.4 Admittance terms for calculation of current references 232

Abstract

This thesis presents an investigation of on-line supply impedance measurement. Network impedance values are invaluable for power system modelling and simulation. Without knowledge of a network structure and the impedances that make up that structure it is impossible to simulate or predict harmonic propagation within a plant. If the impedance structure for a plant is known then it may be possible to alleviate voltage distortion problems by simply redistributing sensitive loads to points of low harmonic distortion. Alternatively distorting loads may be repositioned thus removing the need for additional filters or compensation equipment. The supply impedance, in particular, is of interest. At a simple level it is important for wiring, fuse and circuit breaker calculations. It is also important when designing filters for power factor correction or harmonic attenuation.

Two novel on-line impedance measurement techniques are presented. Both techniques apply a small disturbance to a power network, using measurements of the subsequent transients it is possible to identify the system impedance at the point of measurement. These techniques are implemented both in simulation and experimentally. Excellent identification was possible for linear impedance networks. The performance of the techniques was also investigated in the presence of various non-linear loads. Limitations to both approaches are identified.

An active shunt filter was designed and constructed for this work. Experimental impedance measurement was undertaken using this hardware. It was therefore possible to demonstrate the possibility of impedance measurement using an existing active shunt filter and during its normal operation. Finally experimental measurement data was used to demonstrate the operation of the active shunt filter using reference currents determined from supply voltage and supply impedance.

Chapter 1

Introduction

1.1 Background to the nature of the National Grid

The British National Grid system has been developed over time to produce a power network employing a small number of high capacity generators, with a total capacity of approximately 70GW [1]. These are connected to customers via the transmission and distribution networks mainly comprising of transformers and cabling [2]. Traditionally, large quantities of power were consumed by power factor lagging loads such as heating and direct on-line induction motors driving pumps and fans. In fact about 43% of electrical power is still consumed by induction motors [3]. Power factor correction (PFC) capacitors were introduced from an early date in order to improve the power factor to reduce transmission losses and allow maximum power flow through the existing network. Modern power electronic technology and the desire for greater efficiency, to reduce both the cost and environmental impact, have led to a shift away from this situation.

The installation of power factor correction capacitors has increased [4] in an attempt to increase power supply efficiency. The disadvantage of these extra components is that they will create resonant circuits [5]. Such resonances do not occur at frequencies near the fundamental frequency and therefore do not immediately pose a problem. But when this is

combined with the rise in use of power electronic equipment there is potential for harmonic problems to arise.

Harmonic distortion is not a new phenomenon in power networks. Early synchronous generators were not able to generate a purely sinusoidal output. Instead a distorted waveform was produced rich in harmonic voltage components [6]. In modern times it is the increasing use of non-linear loads that is causing the rise in harmonic distortion on the power system. A non-linear load (NLL) is defined by Dugan et al. [5] as: *an electrical load which draws current discontinuously or whose impedance varies throughout the cycle of the input a.c. voltage waveform.* Figure 1.1 shows an example of this definition.

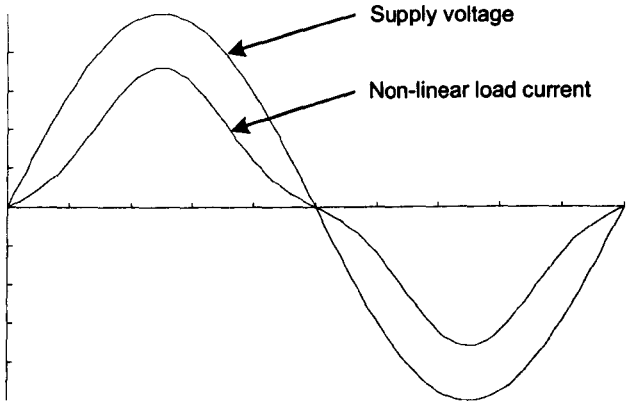

Figure 1.1: Current distortion due to non-linear load

Until recent years the only significant NLLs were the controlled rectifiers used to power d.c. motor drives [7]. The development of power electronics has changed this situation and has led to a fundamental change in electrical power consumption. Power electronic circuits have affected both industrial and domestic power consumption. The adjustable speed drive (ASD) has led to an increase in the efficiency of motor drives for the manufacturing industry. The switch mode power supply has provided cheap and compact d.c. power supplies for personal computers and other domestic electronic apparatus. Mohan et al. [8] have estimated that 50% of electrical power consumed in the USA is through such power electronic converters. These examples of power electronic equipment use a rectifier input to convert a.c. voltage to d.c.. This non-linear circuitry draws non-sinusoidal current from the power

supply. The most common power electronic circuits directly connected to the power network are uncontrolled rectifier circuits. Figure 1.2 shows both inductively smoothed and capacitively smoothed rectifier circuits and the current harmonics drawn by each circuit when fed from a sinusoidal supply.

Voltage distortion is created in the network as the result of this harmonic current flowing through the system impedance. This increase in distortion has led to the installation of passive filters designed to attenuate voltage distortion at certain frequencies. Passive filters alter the system impedance at certain frequencies by blocking the path of harmonic current (series filter) or to provide a low impedance sink for the harmonic current (shunt filter). Power electronic equipment also gives rise to other power quality problems, as described in the next section.

Deregulation of the electricity supply combined with the increased development of, so called, renewable energy sources has led to a significant change in the structure of generation and distribution. The shift has been away from very few centralised generators to a more distributed system of generation whereby small generators may be connected to the power system throughout the network [9]. Such generation is known as Distributed, or Embedded, generation. Examples of embedded generation include industrial combined heat and power (CHP) plants, municipal waste burning power plants, wind turbine generators and photo-voltaic power generation. Small capacity generation using alternative energy sources is environmentally beneficial as is the overall efficiency gain achieved from CHP plant generation. Such generation increases the complexity of the grid network and can lead to problems with control of frequency and voltage.

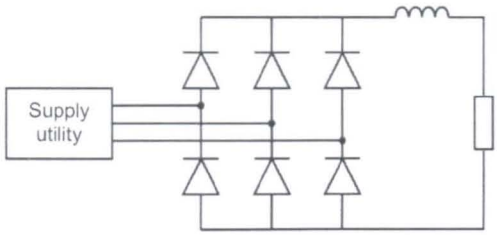

(a) Inductively smoothed uncontrolled rectifier

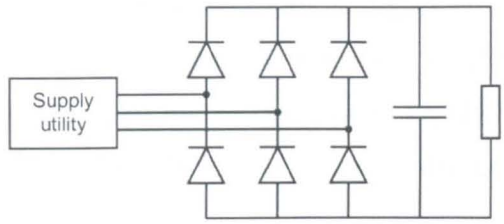

(b) Capacitively smoothed uncontrolled rectifier

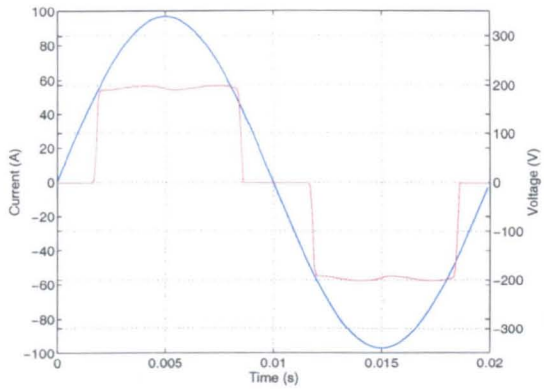

(c) Phase voltage and line current waveform

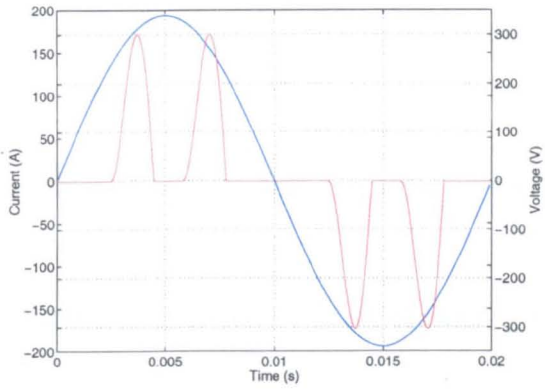

(d) Phase voltage and line current waveform

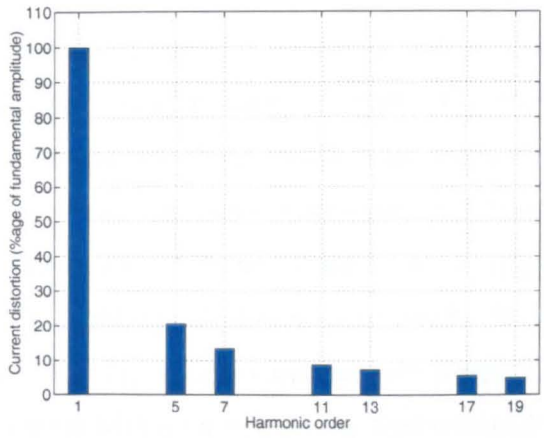

(e) Line current harmonics

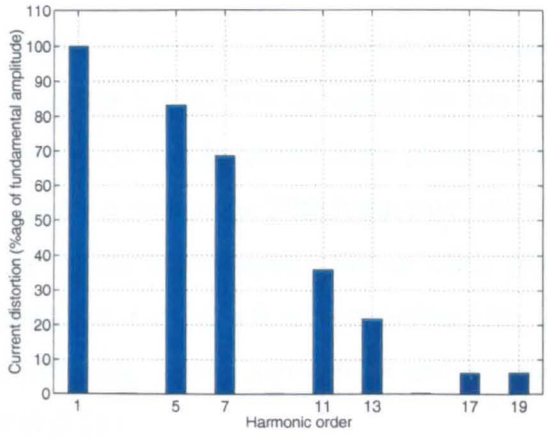

(f) Line current harmonics

Figure 1.2: Rectifier circuits and line current waveforms

1.2 Power quality

As a result of developments in power electronics and embedded generation the instances of power quality problems have increased dramatically. Power quality is the term used to refer to the quality of the power supply. It is therefore a measure of the voltage that is supplied to consumers. The quality of the voltage waveform is defined in terms of many different quantities [5]:

- Short duration voltage variations. This includes sags, swells and short supply interruptions.
- Voltage imbalance in multiphase systems.
- Waveform distortion. This includes harmonic distortion, interharmonic distortion, notching and noise.
- Voltage fluctuation. This describes systematic or continuous voltage changes giving rise to flicker.
- Frequency variations.

This work concentrates on steady state power waveform distortion. In particular, harmonic distortion was of primary concern. The experimental facility was designed for the compensation of low order steady state harmonic distortion in a balanced three phase system. In this work 'low order' harmonics is defined as those below the 20th harmonic. Alternative hardware solutions would be more appropriate for the compensation of other power quality problems. Problems concerned with imbalance require a four wire active filter system [10] [11], voltage variations are better tackled using a series active filter and frequency variations with a unified power flow controller [12] [13].

Voltage distortion is undesirable for many reasons. Transmission losses are increased when transmitting harmonic currents. These losses can result in overheating of transmission apparatus such as transformers. Voltage distortion may result in this equipment being derated in order to ensure reliability and safety. Induction motor losses are also increased

if fed from a non-sinusoidal supply. A further detrimental effect in motors is that torque pulsations may also occur. Over voltage conditions may arise in power electronic rectifier circuits in the presence of high voltage distortion. This can affect performance and can result in unwanted tripping of equipment. To counter this, electronic power supplies must be designed in order to withstand greater variations in supplied voltage. This inevitably leads to increased equipment cost. Power converters, d.c. drives for instance, often rely on zero crossing points in the voltage cycle to synchronise switching instants. This can obviously be affected by a heavily distorted supply. High frequency harmonic distortion can cause interference with telecommunication circuits [5]. it is clear that harmonic voltage distortion can severely affect the normal operation of the power network.

1.3 Tackling harmonic distortion

There are two general approaches that may be used in order to tackle the problem of harmonic distortion. The first approach is to reduce the level of harmonic current produced by the the operation of connected loads. The second method is to connect additional circuits in order to mitigate the effects of harmonic current.

1.3.1 Reducing harmonic current at the source

The most common form of power interface is the uncontrolled rectifier as shown in figure 1.2. As can be seen the level of harmonic distortion in the line current is high. This type of circuit is used extensively for reasons of cost and reliability. Alternative rectifier circuits are available for both 3 phase and single phase operation. Two diode bridge rectifiers may be used to feed the same d.c. link. This requires shifting the phase of the input to one of the rectifiers. This may be achieved using two feed transformers, one connected in a star-star configuration and the other in a star-delta configuration. This method is often used at present for high power installations and can reduce the harmonic current drawn by the load [14]. Active rectifier circuits are also available that utilize one or more switching

devices in the rectifier circuit in order to reduce the harmonic content. In terms of additional complexity the single switch rectifier [15] is the simplest of these circuits as only one additional switching element is required. At the other end of the complexity scale is the Sinusoidal Front End [16]. This circuit employs a switching element in parallel to every diode in the uncontrolled rectifier. The level of harmonic current may be almost eliminated using a suitably high switching frequency. Whilst these alternative circuits are capable of drastically reducing the level of current harmonic drawn they increase the complexity of the design and hence the cost and reliability of the equipment requiring a d.c. source.

1.3.2 Reducing harmonic current at the system level

Harmonic filters may be used in order reduce the level of harmonic current in a power system. Harmonic filters can either be constructed from passive components (passive filters) or use a power electronic converter in order provide compensation (active filter). Both passive and active filters may be implemented as series or shunt filters. Figure 1.3 shows the general form of a series and a shunt filter. The series filter acts to block harmonic currents so that harmonic current does not pass through the supply impedance. Hence voltage distortion will be reduced on the supply side of the filter. The shunt filter offers a path of low impedance for harmonic currents of certain frequencies. The filter thus acts like a local sink for these harmonic currents. The supply voltage distortion is again reduced.

Passive filters can be implemented in various forms [5] and are reliable and simple to construct. The simplest form of passive series filter is a set of line inductors connected in series with the load. Such a filter is often connected to a capacitively smoothed rectifier circuit input. Tuned filters can introduce extra resonances due to interaction with the supply impedance, therefore, it is very important to design them carefully and to carry out extensive studies before installation.

Active filters are based upon controlled power converter technology. They potentially offer many advantages over passive filters such as size, flexibility and the fact that extra resonances need not be introduced into the supply. The cost of active filters will continue to fall

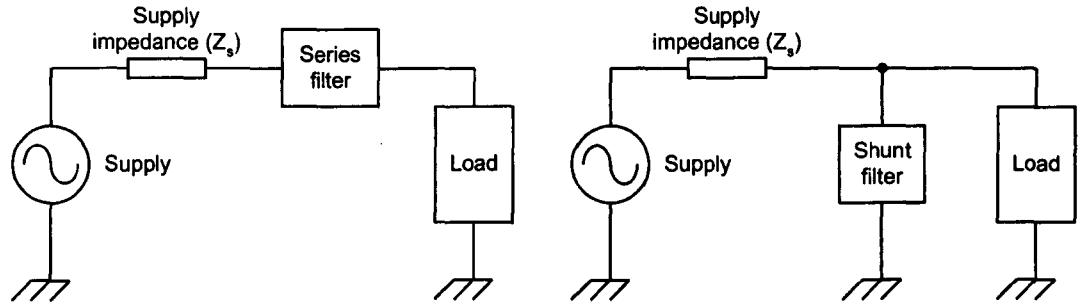

(a) Series filter (b) Shunt filter

Figure 1.3: Harmonic filter topologies

as semiconductor technology progresses and their use becomes more widespread. Much research has been carried out on active filter topologies. Shunt and series active filters have been developed as well as more elaborate circuits that offer additional power quality functionality such as the dynamic voltage restorer (DVR) for compensation of voltage flicker and the unified power flow controller (UPFC) for controlling power flow, harmonics and flicker [12]. Many control strategies have been researched for use to control active filters. Controllers have been designed using instantaneous reactive power theory [17], synchronously rotating reference frames [18] [19] [20] [10], deadbeat controllers [21], hysteresis controllers [22], fuzzy logic [23] and sliding mode controllers [24]. In each system a knowledge of power supply impedance is required for stable control operation. In this work an active shunt filter (ASF) was employed using current controllers based upon synchronously rotating frames of reference, see chapter 7.

1.4 Power quality regulations

Standards and regulations have been introduced in order to provide harmonic guidelines for both suppliers and consumers of electrical power in an attempt to limit harmonic distortion and its undesirable effects. In the USA, IEEE519 [25] sets standards for both suppliers and consumers. The supplier standards are defined in terms of the quality of the voltage that the supplier provides to its customers. The customer standards set out the acceptable levels of harmonic current that a customer may draw from the electrical utility. In the UK, engineering recommendation G5/4 [26] sets out similar limits for acceptable voltage distortion and harmonic current limits. The British Standard BS IEC 61000-3-4 [27] sets standards for the level of harmonic current that may be drawn from by a consumer connected to the public low voltage distribution system. All the standards are applied at the point of common coupling (PCC) between the supplier and the consumer, also the point of metering in most instances. Actual limits shall be shown for BS IEC 61000-3-4 to put the standards in context and to illustrate the format. Similar classifications and acceptable harmonic current levels are given in both IEEE519 and G5/4 for low voltage loads. All the harmonic standards have been developed in order to try and define an acceptable level of distortion. This level must be a balance between:

- the additional equipment cost associated with countering or preventing harmonic voltage distortion and
- the costs due to increased network losses, derating of equipment and supply interruptions.

1.4.1 BS IEC 61000-3-4

A measure is made as to the relative size of the customer load when compared to the capacity of the distribution network. This measure, the short circuit ratio, is made because the ultimate aim of imposing such a standard is to limit the voltage distortion on the network. Therefore when a load drawing low levels of harmonic current is connected to a

very strong supply (small supply impedance) the limits are relaxed. Conversely, if a highly distorting power load is connected to a weak supply (high supply impedance) then the harmonic current limits must be much more stringent, for a similar level of voltage distortion to be present on the system in both cases. The short circuit ratio, R_{sce} is defined as the ratio of supply short circuit current and the maximum fundamental load current of the consumer.

$$R_{sce} = \frac{i_{sc}}{i_l}$$

where i_{sc} is the supply short circuit current and i_l is the maximum fundamental load current of the consumer.

The limits are applied in three stages, dependent on the value of R_{sce}:

Stage 1:: If $R_{sce} \geq 33$ then the limits are as shown in table 1.1

Stage 2: For equipment not meeting the limits in table 1.1, higher emissions are allowed providing $R_{sce} > 33$ and they meet the limits in table 1.2 (for balanced 3-phase equipment). There is an additional set of limits for single phase, interphase and unbalanced three-phase equipment.

Stage 3: If the limits detailed in table 1.2 are exceeded, it still may be possible to connect the equipment based on the power of the installation. In this case the local supply authorities requirements will apply (as set out in standard G5/4 stage 2 [26]). For equipment having an input current > 75A per phase, stage 3 requirements should be applied in addition to stage 1 or stage 2.

The limits in table 1.1 and table 1.2 show the currently acceptable levels of harmonic distortion. As levels of voltage distortion change and trends in new equipment alter these levels may well be changed as appropriate.

Harmonic Number	Admissible harmonic current i_n/i_1 (%)	Harmonic Number	Admissible harmonic current i_n/i_1 (%)
3	21.6	21	$\leq$0.6
5	10.7	23	0.9
7	7.2	25	0.8
9	3.8	27	$\leq$0.6
11	3.1	29	0.7
13	2.0	31	0.7
15	0.7	$\geq$33	$\leq$0.6
17	1.2		
19	1.1	Even	$\leq 0{\cdot}8/n$ or $\leq 0{\cdot}6$
i_1 = rated fundamental current; i_n = harmonic current component			

Table 1.1: Stage 1 limits for BS IEC 61000-3-4

Minimal R_{sce}	Admissible harmonic current distortion factors (%)		Admissible individual harmonic current i_n/i_1 (%)			
	THD	PWHD	i_5	i_7	i_{11}	i_{13}
66	16	25	14	11	10	8
120	18	29	16	12	11	8
175	25	33	20	14	12	8
250	35	39	30	18	13	8
350	48	46	40	25	15	10
450	58	51	50	35	20	15
$\geq$600	70	57	60	40	25	18
Note 1: The relative value of even harmonics shall not exceed $16/n$%						
Note 2: Linear interpolation between successive R_{sce} values is permitted						

Table 1.2: Stage 2 limits for BS IEC 61000-3-4

1.5 Power system impedance measurement

Detailed modelling is required in order to predict the effect of installation of new loads or harmonic filters. Such modelling obviously requires accurate information concerning the nature of the network, such as interconnection details, load characteristics and network impedance values [28] [29] [30]. Without this information the most economic solutions will not necessarily be chosen. Without knowledge of a network structure and the impedances that make up that structure it is impossible to simulate or predict harmonic propagation. If the impedances are known then it may be possible to alleviate voltage distortion problems by simply redistributing sensitive loads to points of low harmonic distortion. Alternatively non-linear loads may be repositioned thus removing the need for additional filters or compensation equipment. System impedance is also important for wiring, protection relays, fuse and circuit breaker calculations. It is of vital importance when designing passive filters for harmonic attenuation. This is especially true when designing a passive filter for an application where a large amount of voltage distortion is present [31].

Although system impedance is a fundamental quantity for the analysis of power networks direct measurement is not normally undertaken for technical reasons. Measurement of impedance must be conducted during normal network operation as it is not feasible to interrupt the supply for measurement purposes. Such measurements are not undertaken routinely although some research has been conducted on this topic, as described in chapter 2. Instead impedance values at harmonic frequencies are normally extrapolated from fundamental name plate data using simplified assumptions.

1.6 Objectives of this work

The aim of this work was to investigate how to improve power quality using an on-line supply impedance measurement. The original motivation came from the desire to combine work undertaken at the University of Nottingham in the areas of active filtering and power network protection. The specific objectives of the project may be summarised as:

- To develop impedance measurement techniques specifically designed to be embedded in an existing piece of power electronic equipment such as an active filter.
- To determine whether it is possible to make power system impedance measurements in a real power network in the presence of many locally connected pieces of power electronic equipment.
- To experimentally demonstrate power quality improvement using knowledge of the system impedance.

These objectives have been addressed both by simulation and experimental work. Simulation work was undertaken using the SABER power electronic simulation package and with the MATLAB/SIMULINK data processing package. The methods developed from this simulation work were experimentally verified using a 45kVA experimental facility. This facility was purposefully built as part of the project work.

1.7 Thesis structure

Chapter 2 presents a review of previous on-line impedance measurement work. Features common to all experimental impedance measurement techniques are discussed such as experimental limitations and assumptions relating to power networks. The various measurement techniques are split into different categories according to their mode of operation. The advantages and disadvantages of each category are considered. This chapter also introduces steady state models used in the analysis of non-linear loads. This was necessary in order to comprehensively assess previous techniques for on-line power system impedance measurement.

Chapter 3 outlines the experimental rig purpose built for this work. The fully functional active shunt filter is described, including details of the circuit topology, the control system and the protection circuitry employed. Furthermore, the additional data acquisition circuitry required for the impedance measurement work is also described. This hardware is

used throughout the experimental work in the rest of this thesis.

Chapter 4 introduces two proposed techniques for on-line impedance measurement, the 'Short Term Measurement' and the 'Medium Term Measurement'. Both techniques involve the application of a disturbance onto the power network. Measurement of the transient response of the network to the disturbance is taken and used to provide data for the estimation of the system impedance. Signal processing techniques for this purpose are considered. Practical data processing schemes are developed for each injection method. These are designed to minimize the effects of experimental error and system non-linearities. The focus of this work is on balanced three phase systems but a generalized measurement approach is outlined so that the techniques described can be applied to unbalanced systems. Simulations are included in order to assess the viability of the methods developed.

Chapter 5 shows experimental results for both the short term and medium term injection techniques. A variety of linear supply configurations were constructed in order to test the measurement techniques. Experimental results are shown for these different supply circuits as well as alternative measurements made for comparison. The curve fitting routines introduced in chapter 4 are implemented and a statistical analysis is provided to demonstrate the repeatibility of both measurement methods.

Chapter 6 investigates the performance of both proposed techniques in the presence of power converter loads. From this investigation the limitations of the methods are highlighted and guidelines are provided for the practical application of these methods. Whereas previous measurement work has assumed linearity, it is the aim of this chapter to refine this assumption and suggest instances where a non-linearity is present but these methods may remain applicable.

Chapter 7 utilizes the impedance estimates made experimentally in order to demonstrate the operation of an active shunt filter, using a measurement of the supply voltage and the supply impedance estimate. A suitable method of reference generation is derived in terms of measured voltage distortion and harmonic supply impedance. An active filter controller is then described that incorporates this method of reference current generation. Such an

active filter would compensate for voltage distortion at the point of connection. This would be particularly suitable for providing pure supplies for sensitive equipment, use by utilities for bus conditioning or for use in an isolated power network such as an oil platform for example [32]. Practical results are shown to demonstrate the stable operation of the system using this method. Finally, the performance is demonstrated using an inaccurate impedance estimate. The importance of the impedance estimate is thus highlighted for this application.

Chapter 8 concludes this work. A summary of the work undertaken is provided and the various conclusions drawn are brought together. Further work in this field is also suggested.

Chapter 2

Introduction to Impedance Measurement

2.1 Introduction

This work is concerned with on-line, as opposed to off-line, measurement of the local supply impedance. Off-line measurement involves disconnecting the supply. A measurement is then made of the de-energized network or load in question. This is a relatively simple task compared to the on-line approach whereby the supply remains connected and measurements must be made during normal network operation. It is particularly important that an on-line approach should not affect the power network, that is being characterized, in such a way as to interrupt normal operation. This places a significant restriction on all approaches to on-line measurement. This work has concentrated on identifying impedance values in the range of frequencies between d.c. and 1kHz, that is, up to the twentieth harmonic of the fundamental 50Hz supply. The majority of harmonic distortion lies within this range of the low order harmonics.

2.2 Why use on-line impedance measurement ?

The reasons why a supply impedance estimate may be required have been outlined in chapter 1. Traditionally, the fault level associated with a point of connection has been used to calculate the fundamental frequency impedance of the supply at that point [2]. This may be sufficiently accurate for most purposes at the fundamental frequency, although in many cases even this is not true [33]. This is primarily because load characteristics are not considered in the fault level calculation. These should not be ignored. It is certainly not acceptable to predict the impedance at higher frequencies from fault level information as modern power networks are likely to contain many components that will affect the impedance at all frequencies.

Power factor correction (PFC) capacitors at the transmission level, or installed by a customer, will affect the system impedance and possibly introduce system resonances. Similarly, tuned filters designed to reduce levels of harmonic currents will introduce further resonant points. Non-linear loads connected to the grid will also affect the impedance of the supply at harmonic frequencies. Even if these components are not utilized, the resistance and reactance of cabling and transformers is found to vary significantly at low order harmonic frequencies [34] [35] [5].

An alternative to using fault levels at non-fundamental frequencies for impedance calculations might be to use circuit diagrams and wiring diagrams in order to calculate impedance values. In practice, sufficient information concerning the power system and connected loads will not be available for this approach to be viable. Even if such information is available it is important to note the supply impedance will vary with time, depending on the loads connected at remote points in the power grid. Knowledge of remote load connection is almost certainly unavailable so this method of identification is not feasible for accurate measurement. On-line measurement is the only alternative solution. Experimental measurement requires no *a priori* knowledge of the network structure and no information concerning connected loads. By repeated measurement over time significant changes in impedance may also be tracked, as in [36] where the supply impedance variations was monitored over a 24 hour period.

2.3 Terminology

Previous work has considered the measurement of load impedance, supply impedance and the system impedance. In order to clarify the terminology and distinguish between these cases consider figure 2.1. This figure shows a very simplified power network. The voltage source,E, is a sinusoidal source of frequency f_s. Z_s is a Thevenin equivalent of the the network to the point of measurement (POM). Z_L is a load, or Thevenin equivalent of several loads, connected at the POM. I_M is some arbitrary current source injecting currents at non-fundamental frequencies into the network and hence introducing voltage distortion. This current may be introduced by some non-linearity in the circuit, by an existing non-linear load or by some measurement apparatus. Referred to the POM, the supply impedance is Z_s and the load impedance is Z_L. Some work has been specifically directed at measuring the impedance of specific loads, Z_L. This work is primarily concerned with the system impedance, that is, the impedance measured at the POM. The system impedance in this case is Z_s in parallel with Z_L. The techniques for the identification of the different components are the same. The only difference lies in which quantities are measured. It is clear that to identify Z_L data records for I_L and V_M must be obtained. Similarly, to identify Z_s some measurement of I_s and the voltage across Z_s must be made.

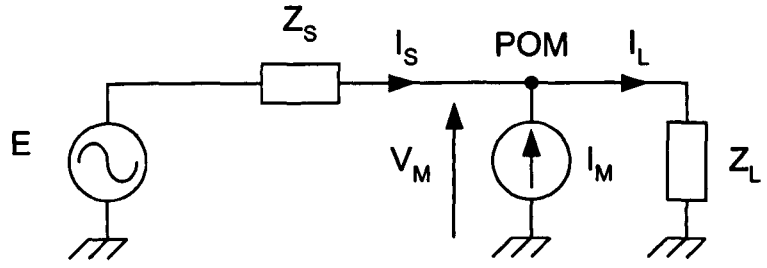

Figure 2.1: On-line impedance measurement terminology

2.4 Power system modelling

An equivalent circuit modelling the power supply at the point of connection is required. This work is more relevant at the distribution level, for example for small to medium industrial loads, as opposed to the higher voltage transmission level as it will be concerned with the 415V supply level. With this perspective in mind, equivalent components are required to model the voltage supply, the supply impedance and load impedances due to both linear and non-linear loads. For the purposes of a short duration measurement the supply may be considered to be a constant frequency and sinusoidal voltage supply. A lumped Thevenin equivalent may be calculated for the linear supply impedance. Finally, non-linear elements within the network must be considered.

The most common form of NLL connected to a power system is a rectifier circuit for supplying a d.c. current from the a.c. supply [37]. In the steady state these loads may be most simply modelled as a current source at each harmonic frequency at which the load draws current [37]. This model does not account for power flow at these harmonic frequencies. Therefore a better model includes an impedance in parallel with the current source in order to account for this power flow [35]. This impedance will be different for each harmonic frequency and will only be of a fixed value in the steady state.

Historically the most the important NLLs have been d.c. drives [7]. A large smoothing reactance is used for such a drive on the d.c. side of the converter that has generally been considered as an infinite impedance [38]. Using this assumption it is clear that the first equivalent circuit described is satisfactory, especially when considering a network with little harmonic distortion. Assuming an infinite d.c. side impedance implies that all the power flow is at the fundamental frequency which is again a satisfactory, and useful, assumption for most applications.

Figure 2.2 shows a simple steady state power system equivalent circuit. A Thevenin equivalent has been derived for the supply and linear loads whilst a Norton equivalent has been derived for all non-linear loads using the model described. E is a voltage source operating at a fundamental frequency, f_s. Z_s represents all linear network impedances. The harmonic

current flow due to the non-linear loads is represented by I_h, where h denotes the harmonic order. Z_h represents the impedance at each harmonic frequency associated with the non-linear loads. Z_h is different for each harmonic, is only applicable in the steady state and depends upon the operating point of the system.

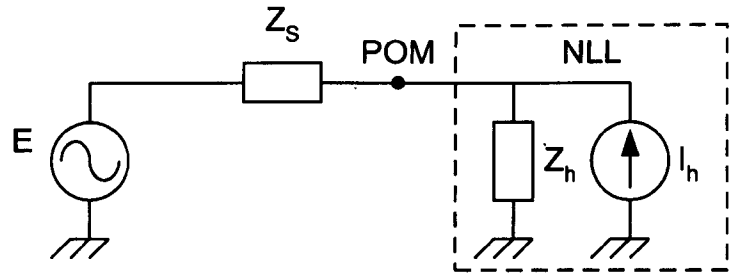

Figure 2.2: Impedance measurement at harmonic frequencies

In both [37] and [35] the power network was considered primarily from a transmission perspective. In this case the equivalent circuit shown in figure 2.2 is generally accepted. In [38] the authors stated that a harmonic equivalent circuit for a power converter may be a Norton equivalent, as shown in figure 2.2, or alternatively as a Thevenin equivalent. This approach was developed further by Peng, [39] [40], at the distribution level. Power converters were split into two categories depending upon the converter characteristics.

The first category of NLL uses a Norton equivalent circuit and the second uses a Thevenin equivalent. A power converter utilizing a d.c. line reactance is classed as a current source type harmonic source. The notation used by Peng, [39] [40], has been adopted, hence this class of NLL shall be referred to as a Current Source NLL (CS-NLL). Figure 2.3 shows a typical single phase converter of this type and an equivalent circuit.

This type of load is insensitive to small changes in harmonic voltage distortion at the PCC. Hence its behaviour is like that of a constant amplitude current source. The equivalent circuit parameters, I_h and Z_h, will vary for each harmonic and are dependent on the operating point of the system. This equivalent is equally valid for a thyristor controlled bridge assuming that switching instants are not highly dependent upon the harmonic content of the voltage at the converter supply.

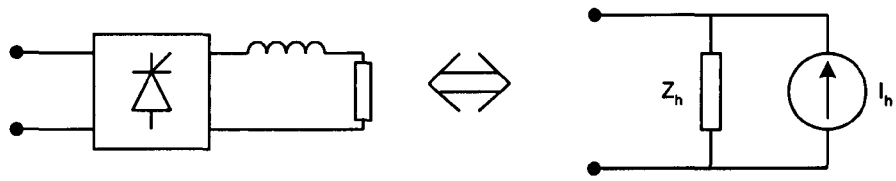

Figure 2.3: Current Source non-linear load (CS-NLL)

The second category of NLL uses a Thevenin equivalent circuit in order to model a power converter with a capacitively smoothed d.c. link. Figure 2.4 shows a typical single phase converter of this type and an equivalent circuit. In this case the current drawn by converter is highly dependent upon the supply voltage. Again parameters are required for V_h and Z_h for each harmonic.

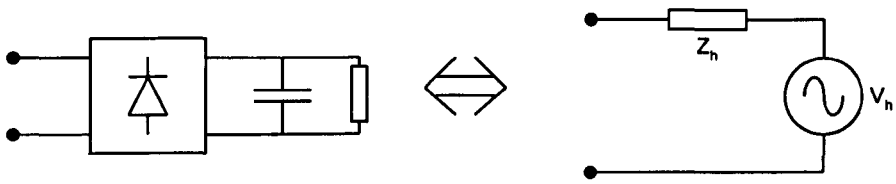

Figure 2.4: Voltage Source non-linear load (VS-NLL)

Both models are applicable for modelling steady state operation. The parameters for each harmonic are also only applicable about a single operating point due to the non-linearity of the converter circuits. It is possible to obtain a useful insight as to the behaviour of each category of load in a transient or measurement situation although in doing so it should be noted that the limitations of both models are being reached. Before attempting such an analysis it is worth considering NLLs that lie somewhere between the definition of the CS-NLL and the VS-NLL.

2.4.1 Choosing the correct model

In many cases line chokes are connected to a VS-NLL in order to reduce the harmonic current drawn by such a load. If the voltage drop across the diodes is assumed to be zero and the diode commutations are assumed to be instantaneous then the current drawn by the loads shown in figures 2.5(a) and 2.5(b) will be the same in the steady state [41].

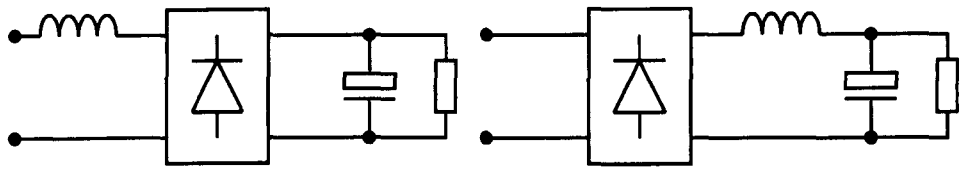

(a) VS-NLL with additional line inductance

(b) CS-NLL with d.c. link smoothing capacitance

Figure 2.5: VS-NLL and CS-NLL models with additional filtering

The circuit shown in figure 2.5(b) is now a hybrid version of the CS-NLL and the VS-NLL. If the network is considered from a transmission perspective, every VS-NLL will have considerable line inductance provided by its' feed transformer. Therefore such a circuit may in fact be considered to be more like a CS-NLL, depending upon the ratio of L and C in figures 2.5(a) and (b). It can thus be seen that the distinction made by Peng [39] [40], that power converters may be split into two distinct categories, does not contradict the earlier models but merely provides further detail if the network is considered from the distribution level.

2.5 System impedance with non-linear models

Figure 2.6 shows one phase of a complete power system including NLL models of the types described. In figure 2.6 all linear loads have been incorporated into Z_t and Z_{dl} as part of the Thevenin equivalent. NLLs are represented by a single CS-NLL and VS-NLL. If a supply network has a significant number of NLLs with a large power rating then the impedance

at harmonic frequencies may be markedly different from the linear impedance ($Z_t + Z_{d1}$), with respect to PCC. This gives rise to two different means of measuring the impedance of a power network.

- If the impedance values are measured at the actual harmonic frequencies using the equivalent network shown in figure 2.6 then they will only be valid at this operating point. Furthermore, a system impedance measured at one harmonic frequency only applies to that frequency and cannot be used to infer the impedance at other harmonic, or interharmonic, frequencies.
- If the impedance is measured over a range of interharmonic frequencies then it is possible to derive a linear transfer function, ($Z_t + Z_{d1}$), and hence estimate the impedance at other interharmonic frequencies. At harmonic frequencies this transfer function will only predict the linear part of the impedance.

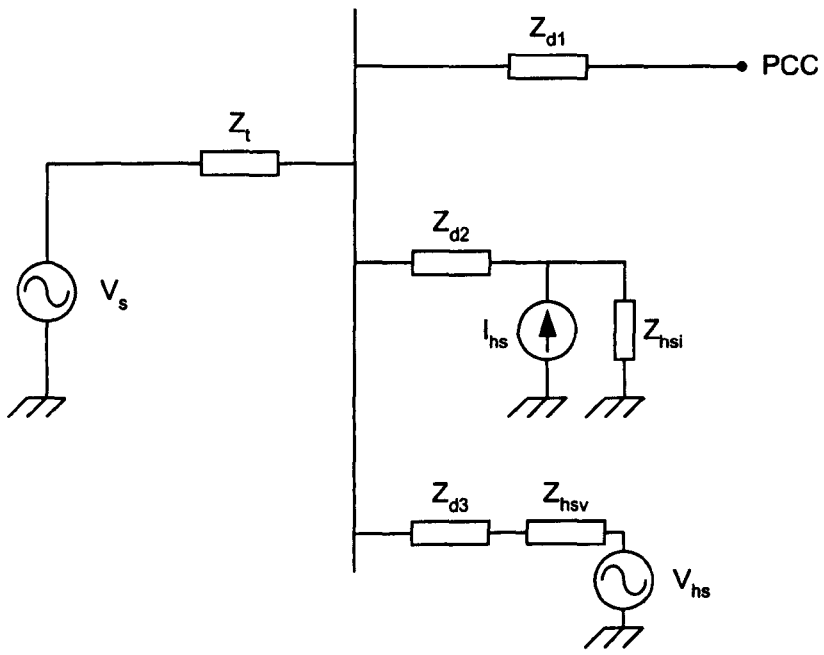

Figure 2.6: Complete power system with NLLs

Both approaches have been used in previous work on this subject. Non-linear characteristics of supposedly linear apparatus, such as saturation in transformers, is generally not

considered. Non-linear loads that create interharmonics, such as arc furnaces [35], are not considered either due to their unpredictable time varying nature. The model described only predicts non-linear interaction at harmonic frequencies. It may also be possible that interaction will occur at non-harmonic frequencies between a disturbance, due to a measurement procedure for example, and the non-linear loads. In this case the non-linear load output is correlated with the measurement signal. It is assumed that this interaction does not occur in all of the reviewed papers. Such interaction is considered further in chapter 6.

2.6 Previous work

Various approaches have been considered for on-line measurement, both in simulation and experimentally. These approaches shall be reviewed in terms of the complexity, in the authors opinion, of the underlying concept.

Assumptions concerning system linearity were made in the vast majority of all the reviewed literature. These shall be outlined for all the reviewed work. A stationary system must be assumed for all the techniques described. This means that the connected network must remain the same throughout the measurement process. The fundamental supply frequency is also assumed to remain constant during the measurement process. Measurement techniques that require the shortest measurement period will be the least prone to errors caused due to these assumptions not being completely satisfied.

2.6.1 Single measurement, steady state techniques

In 1977 Lemoine [42] introduced the simplest method of estimating the supply impedance using the harmonic distortion from the France-England d.c. link. This technique was also described by Oliveira et al [43]. Figure 2.7 shows the assumed equivalent single phase circuit for this method, for all frequencies other than the supply frequency.

At the fundamental frequency, ($h = 1$), the supply voltage will be required in order to cal-

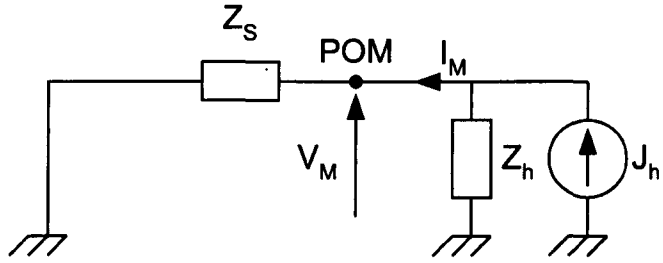

Figure 2.7: Equivalent circuit for impedance measurement using Lemoine's technique, h is harmonic order. h not equal to 1

culate the impedance. At all other frequencies the supply voltage source can be considered as a short circuit. The harmonic current source will act as an open circuit at all frequencies. Steady state voltage and current records were taken at the POM. At each harmonic, h, of the supply frequency the system impedance was then calculated using Ohm's law:

$$Z_s = \frac{V_{Mh}}{I_{Mh}}$$

This calculation could be performed in the frequency domain using a discrete Fourier transform (DFT). In this case it was actually performed on a harmonic by harmonic basis. A fundamental notch filter was initially applied to the signals followed by a very narrow band pass filter centred at the harmonic frequency being measured. The voltage, V_h, and current, I_h, signals were then extracted by arithmetic means and the impedance at the filtered frequency was calculated in real and imaginary terms. Presumably the DFT was not used due to the computational limits at the time. Three phase measurements were taken for both voltage and current. The harmonic impedance was then calculated in terms of symmetrical components with the positive and negative sequences assumed to be equal.

This technique assumes that there is no other distortion on the network other than that due to the single harmonic source considered. In other words, if the France-England d.c. link was removed then the voltage measured at the POM would be a pure sinusoidal signal at the fundamental frequency. This is clearly a major simplification although it may have

been more justified at the time of the work due to there being fewer NLLs connected and due to the sheer scale of the harmonic source chosen. Impedance measurements were only possible at frequencies where there were measurable current components. In this case impedance values were calculated at the 5th, 7th, 11th, 13th, 17th and 19th harmonics. As the only source of current harmonics considered was the source used for measurement the impedance values should be continuous through the harmonic frequencies. Experimental results were presented although it was not possible to validate the accuracy of these results by any other means. Unfortunately this is a common problem with all experimental work of this nature.

2.6.2 Double measurement, linear disturbing load, steady state techniques

Several authors have extended the previous technique in an attempt to compensate for the background distortion from non-linear loads remote from the point of measurement. In 1978 Crevier and Mercier [44] proposed the first such scheme. Steady state measurements were recorded at the POM before and after the switching of capacitor banks. Oliveira et al. [43] generalized this approach, noting that the steady state measurements may be made before and after the addition of any known impedance, not necessarily a capacitor bank. Various aspects of this method were developed further in [45] [46] [47] and [48]. A formulisation of this technique similar to that in [45] is shown to explain the technique for a single phase system. Figures 2.8(a) and 2.8(b) show a power system at some harmonic of the supply frequency, h, before and after the addition of a known admittance Y_d.

In figure 2.8 E_h and Z_{sh} are the Thevenin equivalent that models the network supplies, all linear impedance and all remotely positioned non-linear loads at each harmonic frequency. Therefore E_h is not only a fundamental source but has voltage components at harmonic frequencies due to the background distortion. These components model the distribution system. The distribution system is assumed to be unaffected by the measurement process. The POM is situated at the connection between this distribution system and a customer load. The customer load is modelled as a CS-NLL. At each harmonic it is shown as a

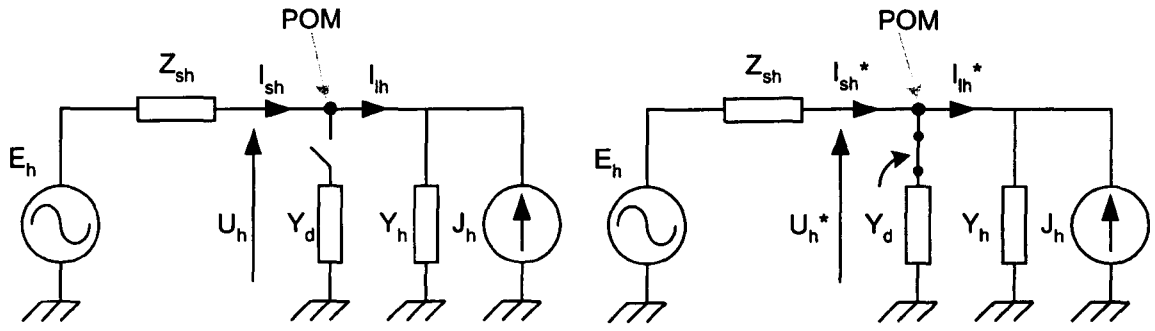

(a) Pre disturbing load

(b) Post disturbing load

Figure 2.8: Equivalent circuits for impedance measurement using Crevier's technique

current source, J_h, and an admittance, Y_h.

Steady state measurements are made before and after the addition of the admittance Y_d. Two equations describe the system during the first set of measurements, these are equations 2.1 and 2.2.

$$U_h = \frac{1}{1 + Y_h Z_{sh}} E_h - \frac{Z_{sh}}{1 + Y_h Z_{sh}} J_h \tag{2.1}$$

$$I_h = \frac{Y_h}{1 + Y_h Z_{sh}} E_h - \frac{1}{1 + Y_h Z_{sh}} J_h \tag{2.2}$$

On addition of the disturbing admittance, Y_d, two more equations may be derived under certain assumptions. These equations are 2.3 and 2.4, * notation is used to denote values measured after the system has been changed. The first assumption is that the system is a stationary system. Hence E_h, Z_{sh}, J_h and Y_h are all assumed to remain constant. All of these quantities contain non-linear components so this assumption will not necessarily be true. In [45] this assumption is justified by assuming that the system behaves in a linear manner about the operating point. As a result the impedance calculated from this method should be considered as the impedance value about the operating point at which

measurements were taken. The author goes on to state that the disturbing load should not change the load voltage rms value by more than 5%. This restriction is applied in order to stay close to the system operating point and to restrict further, potentially disruptive, harmonic distortion. Furthermore, any independent load changes on the whole network that occur during the measurement periods will affect the accuracy of the method, as described in section 2.5.

$$U_h^* = \frac{1}{1 + (Y_h + Y_d)\, Z_{sh}} E_h - \frac{Z_{sh}}{1 + (Y_h + Y_d)\, Z_{sh}} J_h \tag{2.3}$$

$$I_{sh}^* = \frac{Y_h + Y_d}{1 + (Y_h + Y_d)\, Z_{sh}} E_h - \frac{1}{1 + (Y_h + Y_d)\, Z_{sh}} J_h \tag{2.4}$$

Four equations have now been constructed with four unknown values. It is possible to solve for E_h, Z_{sh}, J_h and Y_h. In this work only Z_{sh} and Y_h are of interest. Equations 2.5 and 2.6 show the respective calculations required for these values.

$$Z_{sh} = \frac{U_h - U_{sh}^*}{I_{sh}^* - I_{sh}} \tag{2.5}$$

$$Y_h = \frac{I_{lh} - I_{lh}^*}{U_h - U_{sh}^*} \tag{2.6}$$

Equation 2.6 has been displayed in terms of the load current I_{lh} to clarify later discussion. U_h and Z_d are both known so it is possible to determine I_{lh} from Kirchoff's second law. Impedance estimates with this method are only possible at frequencies where harmonic distortion exists as current and voltage signals will not be sufficiently large to enable accurate measurement at other values. Therefore measurements will only be possible at several harmonic frequencies.

Equations 2.5 and 2.6 are composed of difference terms, that is, the difference between the voltage distortion is required, measured before and after the load change. Similarly

for the current measurements. From these equations it can therefore be seen that a further restriction is applied. It is not sufficient that the harmonic distortion can be measured, it is also necessary that the differences, before and after the load change, can be measured with reasonable accuracy. This is in conflict with the earlier statement demanding that the load change should not shift the operating point unduly. From a practical point of view this method is difficult to implement accurately as the voltage and current waveforms are required with great precision so that the differences may be calculated with sufficient accuracy to yield a consistent and valid impedance measurement. Practical aspects of this method are discussed in [47] and experimental results show limited success in implementing this technique.

Although it was stated in [43] that any known admittance may be used as the disturbing load, in practice capacitor switching has been used in all studied examples of this method. The main reason for this is that capacitor banks are present on distribution networks. Therefore only measurement equipment is required and knowledge of the capacitor switching instant. A further benefit of using a capacitor is due to the fact that the impedance of a distribution system is generally inductive and so the effect of adding a capacitor is to potentially create a resonance. As a result there is more distortion that will aid the accuracy of the method. On the other hand this increased distortion may prove too much for the system and the supply may be affected detrimentally. It was even been suggested in [46] that measurements could be made with a variety of capacitor values in order to provide resonances over the whole frequency range in an attempt to improve the signal to noise ratio of measured signals. This method was outlined for a single phase system although it would be possible to extend it for a three phase network. In [44] three phase measurements were made using unbalanced capacitor switching, the work in [48] also considered three phase circuits.

The impedance values from this technique will only be valid at the current operating point of the network and care should be taken if these values are to be used to infer the impedance at other frequencies, as discussed in section 2.5

2.6.3 Double measurement, non-linear disturbing load, steady state techniques

The next method can be viewed as an extension to the previous one. Instead of using a known linear impedance to act as a disturbing load an additional non-linear load is connected at the POM. This technique is the final method described in [43] and was also the subject of [49]. The same assumptions that were applied to the previous method are applied here. In this case the parameters of the disturbing load are not known so a complete solution for all the equivalent circuit parameters, as presented for the previous method, is not possible. It is still possible to identify the supply impedance at the POM which is the aim of this work. Figure 2.9 shows an equivalent circuit to illustrate the identification.

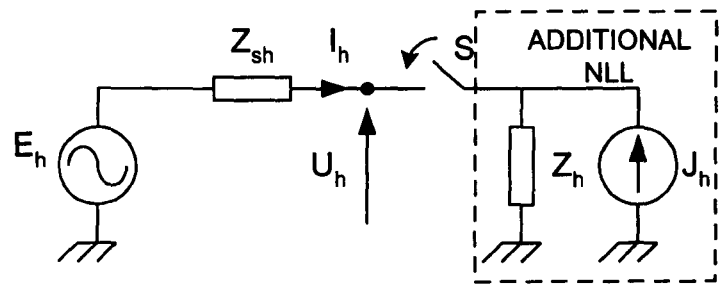

Figure 2.9: Equivalent circuit for impedance measurement using Duggan's technique

E_h and Z_{sh} are the Thevenin equivalent of the network to the POM including background voltage distortion. Again this is assumed to remain constant throughout the measurement procedure. Initially the voltage, U_h, is measured at the POM with the additional NLL disconnected, switch S open,to characterize the background distortion. The disturbing load is then connected, switch S is closed, and steady state measurements are made of the voltage U_h^* and current I_h^*. In [49] the two states required were provided by taking measurements at different times. This assumes that there will be a natural variation in the total non-linear load. In [43] an uncontrolled six pulse rectifier load was used.

The supply impedance Z_{sh} may be calculated at each disturbed harmonic frequency using

equation 2.7

$$Z_{sh} = \frac{U_h - U_h^*}{I_h^*} \tag{2.7}$$

An interesting application of the steady state load change was presented in [50]. The authors presented a piece of equipment that continuously monitored the current and voltage at the point of connection. Sudden variations in the voltage or current were automatically detected. These sudden variations were attributed to a load change somewhere on the network. Steady state measurements were recorded after the trigger and stored values retrieved from immediately before the trigger. These two sets of data were used in order to calculate the impedance as described previously.

The last two methods described were heavily reliant on very accurate measurement. The background distortion must be subtracted very carefully as the required signals are very small compared to the fundamental component. Even slight supply frequency variations between measured data could result in poor cancellation that will wreck any chance of a successful measurement.

2.6.4 Transient disturbance measurement

The final three categories of impedance measurement methods are not restricted to the measurement of impedance solely at harmonic frequencies. Interharmonic impedance values are not generally affected by non-linear distortion. Consequently these values may be used at any network operating point, as absolute values. If a range of these interharmonic values are known then it is possible to derive a transfer function for the linear impedance and hence to predict the impedance at other frequencies where non-linear distortion is not present. As the section title suggests, this category of methods use transient disturbances on a power network for identification purposes. If a power network undergoes a sudden transient such as a switching operation then a whole a range of frequencies will be injected into the system. Measurements may be taken during this period and the impedance calculated at the excited frequencies.

The required transient may be provided by a variety of different methods. The most common method used in the literature has been the switching transient due to capacitor banks being switched into a distribution system. This is the approach that was used in [51] [52] [53] [54] [55] and [56]. The first five references used existing capacitor banks on a network. In normal network operation these capacitor banks are switched on and off at various times. By using data from these switching events no additional disturbance is applied to the network. In [56] experimental apparatus that includes a capacitor bank was attached to the system allowing complete control of the transient switching. Other means of introducing a transient disturbance have also been used. In [53] transformer tap changing disturbances were also used and in [57] transformer inrush current was used. Finally, in [58] low frequency oscillations were investigated in North America using a load pulse from 'Chief Joseph', a 1400MW dynamic brake unit. Figure 2.10 shows a single phase equivalent network diagram to illustrate this technique.

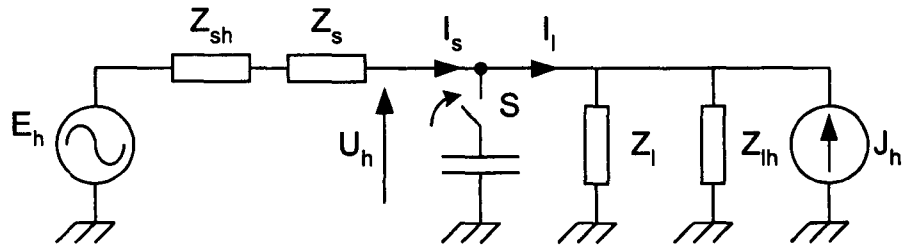

Figure 2.10: Equivalent circuit for impedance measurement using transient measurement

A capacitor bank has been used to provide the transient disturbance although this would equally apply to other disturbing sources. In order to clarify the injection measurement at interharmonic frequencies both the supply and load impedances have been split into linear and non-linear components. E_h and Z_{sh} are again a Thevenin equivalent to model the background distortion present at the POM. Additionally Z_s has been included to represent the linear part of the transmission network. Similarly the load is comprised of J_h and Z_{lh} that describe non-linear loads at each harmonic and Z_l to represent the linear part of the load. At harmonic frequencies all the loads shown will be identified and at interharmonic frequencies only the linear impedances, Z_s and Z_l, will be identified. A stationary system is assumed for all of the referenced methods.

In both [51] and [52] the impedance characteristic of a distribution feeder was being investigated, hence the current I_l and the voltage U were measured during the capacitor switching transient. The entire transient must be recorded for accurate identification. In both papers two methods were suggested for calculating the impedance from the transient data. The first method involves calculating the DFT of the current and frequency and applying Ohms law at each excited frequency. The alternative estimates the impedance using a transfer function estimation method based upon the power spectral densities of the two signals [59]. The direct calculation method is shown as equation 2.8 and the power spectra method is shown as equation 2.9, $\Im$ is used to denote the discrete Fourier transform. $P_{vv}(f)$ and $I_{iv}(f)$ are the auto power spectrum of the voltage and the cross power spectrum of the current and voltage respectively. These power spectra are calculated from the Fourier transform of the relevant auto- and cross- correlation functions.

$$Z(f) = \frac{\Im(U(t))}{\Im(I(t))} \tag{2.8}$$

$$Z(f) = \frac{P_{vv}(f)}{P_{vi}(f)} \tag{2.9}$$

Both methods require the same data to be measured. Both techniques are considered further in chapter 4.

In [51] the recorded signals were passed through a fundamental frequency notch filter and in [52] the time records were notch filtered at both the fundamental and 5th harmonic frequencies. The power spectra method was used with the aim of reducing non-linear effects at harmonic frequencies. In [53], [56], [54] and [57] the direct calculation method was used. The first two of these references used background distortion cancellation. Voltage and current measurements were made prior to the transient injection and were subtracted from the transient measurement to remove steady state distortion. This is similar to the differential technique described in section 2.6.2 and similarly requires very accurate transducers in order to cancel the harmonic components precisely. An alternative is to merely discard impedance values at distorting harmonic frequencies and use some form of interpolation.

This would ensure only the linear part, Z_s, of the supply impedance would be measured and similarly for the load impedance. The transformer inrush transient used in [57] is such that the power network is excited at all harmonic frequencies. As harmonic producing loads generally distort the odd harmonics this method only uses impedance values for the even harmonics. In this manner the linear part of the impedance is measured and no steady state data measurements are required.

Using unbalanced transient switching or by staggering the transient on each phase will enable the measurement of the mutual impedance terms between the phases, as described in [54] and [53].

The range of frequencies at which excitation is sufficient to allow an impedance to be estimated is determined by both the network and the capacitor bank, or other source of transient disturbance. The level of injection may be affected at resonances or anti-resonances such that impedance estimation is not possible in certain frequency ranges. The accuracy of this method is heavily dependent on the assumption made that the system is stationary during the measurement period. NLLs may affect this assumption at interharmonics as well as harmonic frequencies. If a harmonic source output is correlated with the transient injection then the results may be affected at other non-harmonic frequencies. In [55] simulation was used to measure the impedance of a network containing a CS-NLL with some success. In [60] it was found that a VS-NLL degraded experimental results measured using a similar method that is discussed in section 2.6.6. This topic shall also form the basis of chapter 6

2.6.5 Steady state, single frequency injection measurement

One restriction of the previous techniques is that the impedance measurement must take place at a point where some network disturbance can be created or where an additional load can be connected. An alternative approach is to construct a piece of measurement apparatus that may be connected to the network at the desired point of measurement. Such a piece of equipment was built in [56] using the transient disturbance approach. An alternative approach was developed in [36] [61] [62] [63] [64] [65]. In each case a piece

of equipment was constructed that was capable of injecting small sinusoidal current waveforms at the point of connection. By injecting a current signal at an individual frequency and measuring the subsequent voltage distortion it was possible to calculate the impedance at that frequency from Ohms law. This approach again assumes that the system is linear and stationary during the measurement period. Measurements at harmonic frequencies will be invalid assuming that there is some harmonic voltage distortion at the point of measurement at that frequency.

In [36] a power electronic injection unit was purpose built so that the system impedance could be measured at remote points in the UK national grid. This equipment was also used in [61] for field testing. Measurements were conducted at frequencies between 75Hz and 975Hz at 50Hz intervals. The measurement frequencies were chosen as interharmonic values. By using these interharmonic values no background distortion cancellation was necessary as it can be safely assumed that there will be no background voltage distortion at these frequencies. A further assumption was made that the impedance at a harmonic frequency could be linearly interpolated from the impedance values for the two closest measurements. The same assumption was also specified in [65]. It will only be true if there are few, or no, harmonic distorting loads connected. If this is not true then the impedance values calculated at harmonic frequencies should represent the linear part of the system impedance.

In [62], [63] and [64] similar measurement apparatus was developed. In this case the frequency spacing was programmable and results were shown at 10Hz intervals. A fundamental frequency notch filter was connected between the equipment and the power network to protect the measurement apparatus. A measurement at the fundamental frequency was therefore not possible and interpolation was used for this point. Measurements were made at some harmonic frequencies on a real network and these were found to be meaningless due to the background distortion. These methods implicitly assume that the harmonic producing loads distorting output will not be correlated with the injected signals at the interharmonic frequencies.

There are many advantages to this technique to counter the main objections of having to

construct a dedicated measurement system. Measurements made at interharmonic frequencies should not disturb the normal network operation. Signals may be injected over several fundamental voltage cycles in order to reduce the affects of random noise. A potential downside is the measurement time for this method. Full steady state cycles of injected current must be applied at each measurement frequency, if there are many frequencies then the measurement may be prohibitively time consuming.

2.6.6 Steady state, wideband injection measurement

The final method to be reviewed may be considered to be an extension of either the steady state, single frequency, injection measurement, section 2.6.5, or alternatively the transient disturbance measurement, section 2.6.4.

A purpose built measurement system has been developed to inject steady state current signals for measurement purposes on power networks as in the previous section. In this case the injected current signal is not at a single frequency but is a wideband signal. This method was first introduced by Banta et al. [66]. In this work a 3Ω load resistor was connected across distribution lines for random periods using switching transistors. A current waveform of approximately 50A and 50% duty cycle was injected into the network as a random noise source. The transistor switching times were controlled by an electronic noise generator. A passive notch filter was again used at the output of the apparatus in order to reject fundamental frequency voltage and hence to protect the measuring equipment. Both the voltage and current were measured and impedance was calculated using the direct calculation method,equation 2.8. The injected current was a band limited source of white noise. The injected current was meant to excite the system over all frequencies, limited only by the maximum switching frequency of the transistors. The authors stated that the impedance component at fundamental frequency, 60Hz in this case, should be found from linear interpolation of neighbouring points. It is clear from this statement that the measurement is focused upon the linear part of the network impedance and values calculated at frequencies at which harmonic distorting loads are present should be discarded. This is confirmed by the discontinuities in the impedance magnitude results at all the odd harmonics up to the

11th harmonic.

A similar procedure has been developed in the series of references [45], [47], [46], [67] and [60]. A single phase device was developed to inject transients on a periodic basis, hence this method may be considered as an extension of section 2.6.4. An equivalent circuit is shown in figure 2.11 to illustrate the, so called, harmonic generating device (HGD).

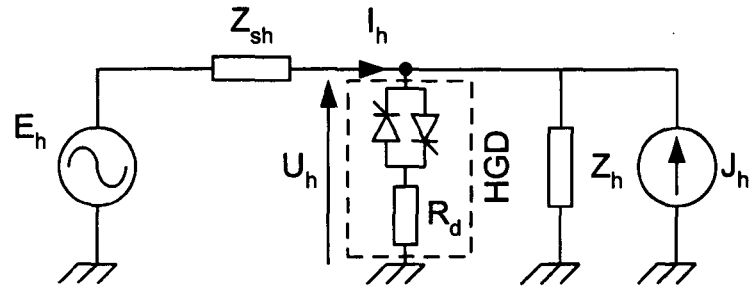

Figure 2.11: Equivalent circuit for impedance measurement using harmonic generator

One of the two thyristors was fired every half fundamental voltage cycle, at a point 250μs before the zero crossing. Therefore the injected disturbance was two narrow current spikes, each of 250μs duration situated at the voltage zero crossings. The resistor, R_d, was used to limit the injected distortion, a value of 0.5Ω was used for the networks investigated. The harmonics produced excited the network at the odd harmonics. It was also noted that by only using one thyristor the even harmonics could be excited. This was due to a d.c. component being injected in this case. The experimental procedure used was identical to the method used in the same reference in section 2.6.3 apart from the fact that the HGD was used as a substitute for the disturbing capacitor load. Results were far superior for this impedance measurement as the injection levels could be controlled by varying the resistor R_d and the injection bandwidth could be controlled by varying the thyristor pulse widths.

The same experimental hardware was used in [67], figure 2.11, although a different experimental procedure was followed. One thyristor of the HGD was used to generate a transient every third fundamental voltage cycle. Current and voltage data was recorded for 48 fundamental voltage cycles while the injection was taking place. This data was split into 48 sections, two containing steady state data and one centred about the HGD disturbance. The

data section preceding each transient section was then subtracted from the transient section in question in order to remove the background distortion. This approach was taken, as opposed to storing the steady state data in a continuous record, to reduce the effects of a non-stationary system. The direct method, equation 2.8, of impedance calculation was then applied. The impedance was calculated at intervals of $(\frac{50}{3})$Hz. The author decided to discard those values at harmonic frequencies. This changes the impedance measurement method significantly. If the harmonic estimates are ignored the resultant measurement will only consider the linear part of the network impedance. Hence the previous assumption that the values are only valid at the network operating point is not required. It is still necessary that the harmonic producing load output cannot be significantly correlated with the disturbance signal at interharmonic values, an assumption required for all the described methods. This alternative method can also be interpreted as a transient disturbance measurement repeated 16 times. As a consequence the random errors introduced by this method are reduced compared to a single transient disturbance. It is particularly important that the HGD is appropriately controlled so that the transient disturbance decays to zero sufficiently quickly so that the whole transient is captured and does not interfere with the next steady state data period.

2.7 Conclusions drawn from reviewed work

Five different on-line impedance measurements from the literature have been described. Although each of these methods are different, many conclusions may be reached that apply to all. Similarly, many of the assumptions were common to all techniques. It is clear that, which ever method is used, the accuracy of the measurement at a particular frequency depends on the amount of disturbance provided at that frequency. This is not only dependent on the source of the disturbance, but also, on the impedance of the network at that frequency. An acceptable balance must be reached between using a high injection strength, resulting in accurate measurement results, and disturbing the normal operation of the loads connected to the network. Again, the acceptable level of disturbance will be dependent on the nearby loads to the point of measurement. It is possible to minimize the potential

disruption, this can be done by disturbing the system at frequencies at which there is little steady state distortion such as the methods that only measured impedance at interharmonic frequencies. Alternatively natural system disturbances can be used. The standard deviation of the results using any of the methods described may be reduced by repeated measurement and averaging the results. If the measurement errors are assumed to be random then the standard deviation is proportional to $\left(\frac{1}{\sqrt{n}}\right)$, n being the number of repetitions. If small disturbances are used then the experimental measurements must be completed with a high degree of accuracy. Most of the described methods involve cancelling background distortion from transient signals. For these methods very small signals must be extracted from quite large signals which may result in large measurement errors.

It is assumed that the measurement disturbance will not interact with the steady state operation of the non-linear loads. Impedance estimates made at harmonic frequencies will contain non-linear impedance terms that only apply at the operating point of the system at the time of measurement. It is possible to use interpolation about the harmonic frequencies in order to estimate the linear part of the impedance at that frequency. A further advantage of interpolating at the harmonic frequencies is that the background distortion cancellation used in many of the techniques is less critical. Obviously only the methods that calculate impedance at interharmonic frequencies may use interpolation. The correlation between the system disturbance and non-linear load at non-harmonic frequencies was briefly addressed in [60] and [53] although neither was able to characterize the behaviour or compensate.

The effect of non-linear interaction will vary depending on the connected loads and the point of measurement. Finally, it should be noted that the accuracy of any experimental results are very difficult to verify. Clearly, disconnection of the supply is not possible and so measurements are restricted to the on-line approaches described.

2.8 Summary

This chapter has provided a review of previous impedance measurement and an analysis of possible power system equivalent circuits. In the reviewed work the supply impedance was measured in two different ways. This distinction was described in section 2.5. The first method measures the supply impedance at harmonic frequencies but is only valid at the network operating point at the time of the measurement. The second method measures interharmonic impedance and derives harmonic impedance from interpolation. Both approaches are valid and may be suited to different applications. Various assumptions have been made concerning the loads connected to power systems.

In all the reviewed work existing harmonic distortion was assumed to be present due to the connection of CS-NLLs. This assumption may have been based upon convenience, practical experience, or the historical nature of NLLs. In order to justify this approach it is necessary to assume that VS-NLLs are connected such that at remote points in the network these behave as CS-NLLs, as in section 2.4.1. These assumptions shall be considered further during the design and implementation of the impedance measurement techniques in the following chapters.

Chapter 3

Description of the Experimental System

3.1 Introduction

The aim of this chapter is to describe the experimental systems that were constructed in order to verify the methods developed and to evaluate their performance in a real system. This chapter is split into two parts, the former describing the active filter and the latter describing the impedance measurement system. The active filter hardware was based upon a commercially available IGBT voltage source inverter [68]. This inverter has been incorporated into an active shunt filter with additional circuitry, a replacement control system and additional protection measures. These modifications are the focus of the hardware description for the active filter. The control system software and user interface are also described in this chapter. The impedance measurement system utilised both the active filter and an additional data acquisition system. The data acquisition system is described as well as the interface between it and the active filter system. Changes were also made to the active filter control software to enable this system to be used as the basis for the impedance measurement work.

3.2 The Active Filter System

3.2.1 System overview

An overview of the active shunt filter experimental rig is shown in figure 3.1. The inverter shown is an ID9001-II series Heenan Drives 45kW IGBT voltage source inverter [68]. This was used to provide the power electronic basis of the active filter. The inverter was connected with the various other components shown to form the active shunt filter (ASF). Additional protection features were also required as the inverter was connected in a manner unforeseen in its design. These are described in section 3.2.4. A new control system was designed and constructed. This replaced the existing controller and was interfaced with the inverter gate driver circuits and internal protection circuitry of the inverter. The control is described in section 3.2.2. The basic parameters that determined the potential performance of the ASF must first be established. These parameters are:

- V_{DC}, the d.c. link voltage
- f_s, the inverter switching frequency
- L, the line inductor value
- V_s, the supply voltage at the PCC of the ASF

The 45kW inverter uses six 1200V 300A IGBT switching devices. A 1.5mF d.c. link capacitance is used. The rated voltage of the six individual electrolytic capacitors that comprise the d.c. link is 400V. These are connected in such a way that the d.c. link rated voltage is 800V. As a consequence of these voltage ratings the ASF d.c. link operating voltage,V_{DC}, was chosen as 680V. The d.c. link voltage was measured as part of the ASF control as shown in figure 3.1, see section 3.2.2 for further details of this measurement.

The ID9001-II Heenan Drives inverter was designed to operate at a switching frequency of 4kHz. As the gate driver circuits and some protection features of the drive were maintained

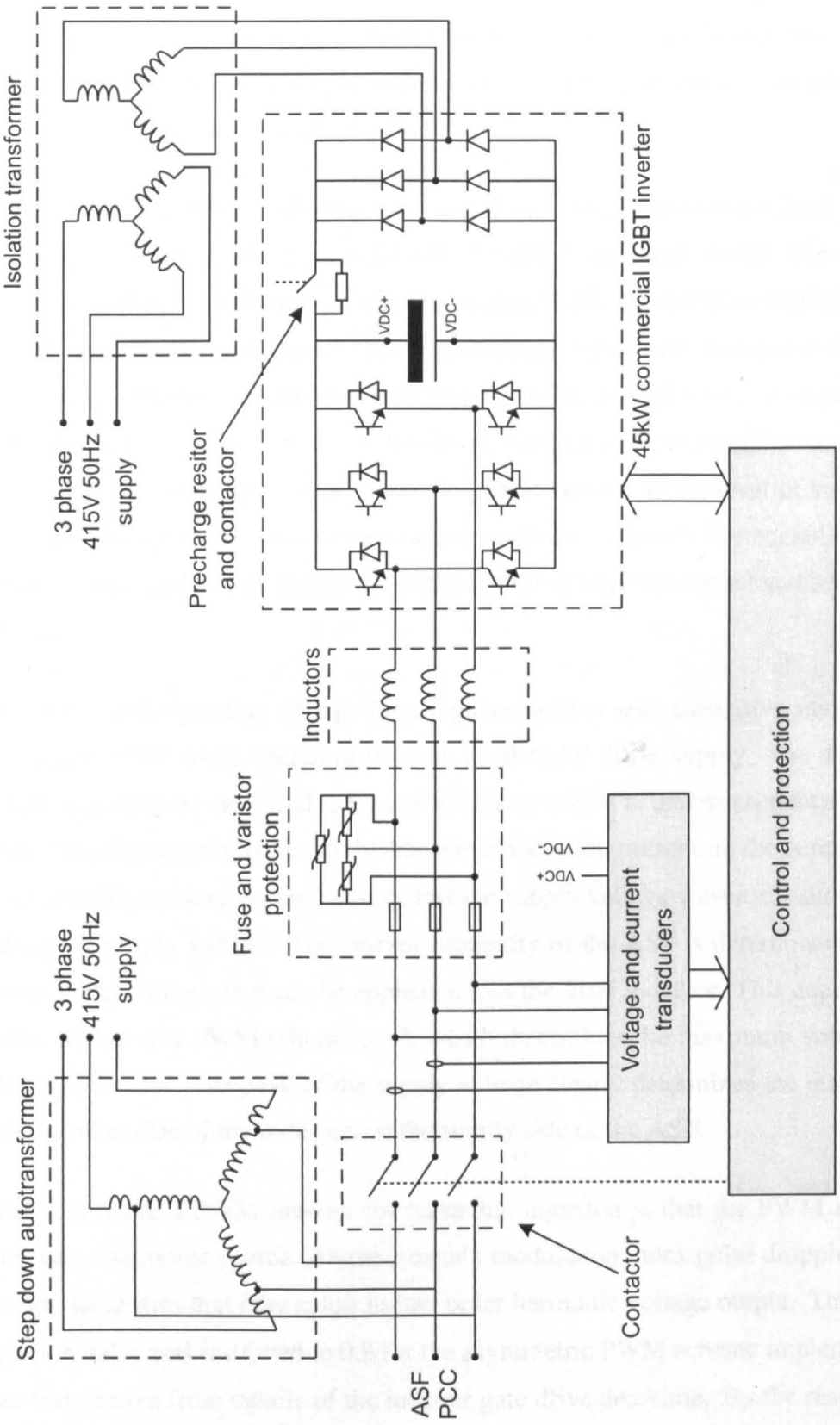

Figure 3.1: Overview of the active filter system

this switching frequency was adopted for the ASF as well. This switching frequency is typical for a drive system operating at power levels between about 10kVA and several hundred kVA. By using this switching frequency control techniques can be experimentally evaluated for ASFs over this range of ratings.

A set of three phase multi-tapped inductors wound on a single core were used as line inductors. The available tappings were 2.5mH, 5.0mH, 7.5mH and 10mH. The control bandwidth is limited by the inductor size chosen. A small inductor size allows a high bandwidth current controller to be designed. The experimental rig current rating also depends on the inductance. Higher current levels are possible with a small value of inductance. The disadvantage of using small inductors lies in the fact that switching ripple current will be increased. The 2.5mH tapping was chosen for the inductors. If the level of switching frequency ripple current is deemed to be excessive switching frequency filters could be implemented to reduce the level of disturbance although these were not considered necessary for this work.

The standard d.c. link operating voltage for a 6 pulse rectifier with capacitive smoothing, under no load, is 587V when operating from an ideal 415V 50Hz supply. The d.c. link voltage for this circuit was measured to be approximately 620 V at the experimental supply connection. This discrepancy is due to the harmonic distortion present on the supply. The fifth and seventh harmonics, in particular, distort the supply voltage waveform and consequently the peak supply voltage. The current capability of the ASF is determined by the maximum available voltage that can be applied across the filter inductor. This depends on the d.c. link voltage and PWM scheme used, which determines the maximum voltage on one side of the inductor. The peak of the supply voltage clearly determines the maximum voltage on the other side of the inductor, on the supply side of the ASF.

A problem with using a PWM inverter for harmonic injection is that the PWM scheme itself can act as a harmonic source. Above a certain modulation index pulse dropping may introduce non-linearities that may result in low order harmonic voltage output. Therefore the modulation index was restricted to 0.9 for the asymmetric PWM scheme implemented. This value was chosen from details of the inverter gate drive deadtime. By the restricting

Inverter rating	45kW
d.c. link capacitance	1.5mF
d.c. link voltage	680V
Line inductors	2.5mH
Switching frequency	4kHz
Supply voltage	300V
Supply frequency	50Hz

Table 3.1: ASF parameters

the modulation index the current capability of the ASF was restricted. In order to preserve this capability the ASF input voltage was stepped down using a transformer. A three phase auto-transformer was used, see figure 3.1, to step the supply voltage from 415V to 300V line to line. If an ASF was purpose built for the 415V supply a higher d.c. link voltage would be possible if higher rated devices and capacitance were used. With the reduced supply voltage it is possible to operate the PWM in its linear region and to operate at a higher current level while using the available electronic equipment.

The isolation transformer shown was required in order to pre-charge the d.c. link, to satisfy part of the inverter built in protection and to power the cooling fans. This is discussed further in section 3.2.4 along with a description of the fuse and varistor protection and the contactor shown in figure 3.1. To summarize this section table 3.2.1 shows the relevant ASF parameters.

3.2.2 Control

The control system is shown in figure 3.2. The inverter control board has been replaced with an inverter interface board that allows the ASF controller to interface with the existing inverter gate drivers and internal protection features. A detailed description of the interface board is given in [69]. The gate driver board requires four signals, these are U, V, W and RUN. U V and W are signals determining the switching positions of the three

inverter output legs. RUN combines all the trip values into a single signal that determines whether the inverter is active or switches it into a tripped mode. This is described further in section 3.2.4. The rest of the control system is comprised of the actual controller and the control peripherals.

A Texas Instruments 320TMSC44 microprocessor [70], referred to as the C44, is used to implement the control strategy. This is mounted on a Blue Wave Systems QPC/C40S ISA motherboard that is mounted in a host PC [71]. The C44 processor is a 32bit floating point processor with a clock frequency of 50MHz. This processor was chosen in order to implement complex control strategies without the need to reduce the sampling frequency or spend an excessive amount of time optimizing the code. Development time was reduced using a floating point processor as calculations were possible without the scaling factors required when using a fixed point processor. The ASF code was written in the Texas C programming language. A supervisory control and data acquisition (SCADA) interface was written for the host PC. This program allows the operator to vary control parameters on-line and to request data from the C44. This host software communicates with the C44 via an 8K area of Dual port RAM (DPRAM). This software was written in C++ for the Microsoft Windows95 operating system. The software is considered in section 3.2.3.

The QPC/C40S motherboard has a 24 line I/O port that the C44 can control. The port was connected via high speed buffers to a hardware backplane configured as a communication bus. 16 lines were configured as bidirectional data lines and 8 lines were configured as unidirectional address lines controlled by the C44. This communication bus allows the processor to communicate with hardware peripherals. Communication is controlled by the C44 processor. Each hardware board has a unique 4 bit address. To communicate with a particular peripheral the correct address must be written on the address bus. Control options may be set using the further 4 address lines or data may be sent to the peripheral using the data bus. This results in a system that may have up to 16 peripheral boards that can each communicate with the processor. Four such boards were designed and built for the ASF experimental rig. Each board, and other associated components, shall be described in turn.

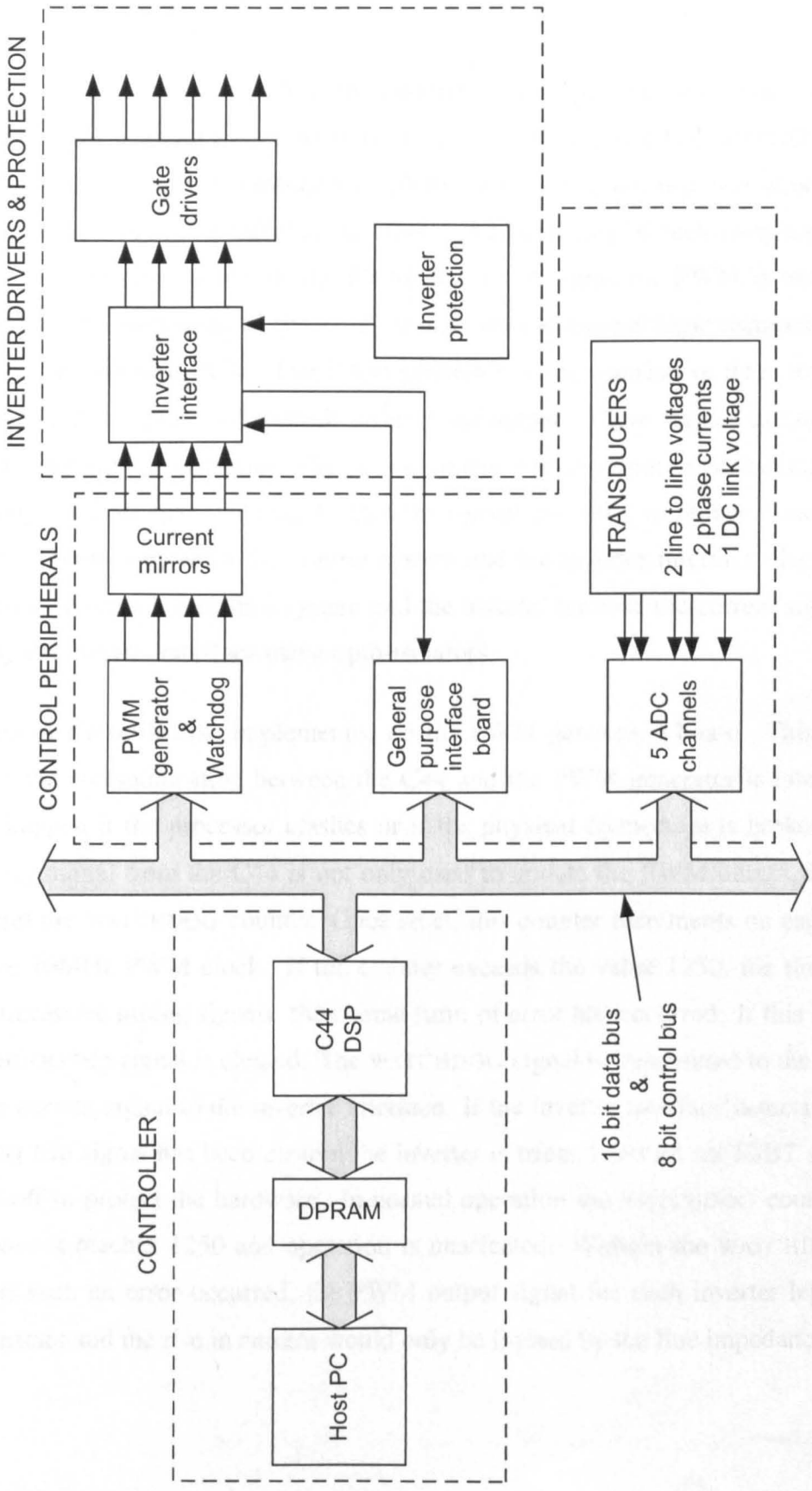

Figure 3.2: The control scheme

3.2.2.1 PWM generator and WATCHDOG

Three 16 bit values are transferred from the C44 to the PWM generation unit each sampling period. Each value is an integer between 0 and 1250 and corresponds to a switching time between 0 and 125μs with a resolution of 100ns. Each value corresponds to one leg of the inverter output. A timing signal is also sent at the beginning of each sampling period, this forces the generator to update the PWM output. Asymmetric PWM is used, as in [72]. An Intel 8254 three channel timer chip is used with additional logic required in order to implement asymmetric PWM. The PWM generator output consists of three logic level voltage signals that correspond to each inverter leg output. These signals are sent to an intermediate current mirror circuit. The current mirror circuit outputs a current signal that is sent to the inverter interface board. Current signals are used to reduce noise effects on the coaxial cables between the control system and the inverter interface. Isolation is also achieved between the control system and the inverter because the current signals are received by the inverter interface using opto-isolators.

A WATCHDOG circuit is also implemented on the PWM generation board. This is used to detect if the communication between the C44 and the PWM generator is interrupted. This may happen if the processor crashes or if the physical connection is broken. Each PWM timing signal from the C44 is not only used to update the PWM output, it is also used to reset the WATCHDOG counter. Once reset, this counter increments on each rising edge of the 10MHz PWM clock. If the counter exceeds the value 1250, the time taken between successive timing signals, then some form of error has occurred. If this happens the WATCHDOG trip signal is cleared. The WATCHDOG signal is transmitted to the inverter by another current signal to the inverter interface. If the inverter interface detects that the WATCHDOG trip signal has been cleared the inverter is tripped and all six IGBT switches are turned off to protect the hardware. In normal operation the WATCHDOG counter will be reset once it reaches 1250 and operation is unaffected. Without the WATCHDOG trip function, if such an error occurred, the PWM output signal for each inverter leg would remain constant and the rise in current would only be limited by the line impedance.

3.2.2.2 General purpose board

This board is primarily used for the input and output of logic level signals. It consists of 8 logic level outputs, 8 logic level inputs, 8 LED indicators and a 4 channel digital to analogue converter (DAC). Three of the outputs are used in normal operation, the others are used for debugging software and for future expansion. The 3 outputs are TRIGGER, ENABLE and ACTIVE CONTROL. TRIGGER is used by the impedance measurement system and is described later in this chapter. ENABLE is a trip signal that is passed to the inverter interface. It is isolated by being sent as a current signal and received using an opto-isolator. This signal is cleared, hence tripping the inverter, if the C44 software detects that a measured quantity lies outside the range of normal operation. Both measured line voltages, both line currents and the d.c. link voltage are checked each sample period to determine the state of ENABLE. ACTIVE CONTROL is a further signal sent to the contactor box shown in figure 3.1, this is described in section 3.2.4. Only one input logic signal is used at present, the others are reserved for future expansion. TRIP STATUS is a signal returned from the inverter to the controller, if the inverter interface has detected any trip this signal notifies the controller. Again, this is an isolated signal. The LED indicators are used for debugging and showing the user various information. The DACs are used for outputting variables to an oscilloscope and software debugging.

3.2.2.3 Analogue to digital boards

Two peripheral boards were constructed, each containing four 16 bit ADC channels with an input range between -10V and +10V. This circuit was based upon a design previously used in Nottingham [73] [74]. Each ADC channel may be triggered individually, alternatively any number may be triggered simultaneously. The maximum sampling rate for these successive approximation converters is 100kHz although for this application 8kHz is used. Once the ADC output is ready a pin is set to indicate that conversion is complete, after approximately 7μs. This signal is not used by the control system. Instead 10μs is left between triggering the ADCs and reading the values from the ADC buffers. Synchronous sampling is used in conjunction with the asymmetric PWM routine. Therefore samples are

taken, on average, at the centre of the PWM pulses. By using this technique the voltage and current noise components due to the IGBT switching edges are minimized.

3.2.2.4 Transducers

The final part of the control system shown in figure 3.2 is the transducer section. Three voltages are measured using PSM voltage transposers. The voltage transposers have a bandwidth of 50kHz, provide 1kV isolation and have a linearity of 0.1% across the full output range. The transposer gain is set using a resistor. Gain and offset adjustments have been provided for each channel although final calibration has been achieved in software. Each measured quantity is passed to the ADC boards using shielded cables. The output level in each case is designed to match the input level of the ADC converters, between -10V and +10V. The two line voltage transducers measure in a range between -800V and +800V. The d.c. link transducer makes use of the offset adjustment in order to measure a range between 0 and +800V. Two line currents are also measured, using LEM current transducers. Gain and offset adjustments are available although, once more, final calibration is achieved in software. The LEM tranducers have a similar accuracy to the voltage measurements and the bandwidth is 100kHz. The measurement range was restricted to between -80A and +80A for each channel.

3.2.3 Software

Two software programs were written for the control of the ASF. The main control code was written, in C, for the C44. This is interrupt driven code operating in real time. A timer interrupt is triggered from an internal clock every 125μs, this corresponds to a sampling frequency of 8kHz. The interrupt routine contains all of the necessary code to control the ASF. Care must be taken to ensure that the interrupt routine takes less than 125μs to complete or else the subsequent sampling instant will be missed and the WATCHDOG protection will trip the inverter. A background routine, or part of the background routine, is executed during the time after an interrupt routine has finished and before the next interrupt

is called. This background routine controls non time critical communications with the host PC via the 32K block of DPRAM. The user interface is a C++ program written for the host PC. This SCADA software controls the communication between the C44 and the host PC. Figure 3.3 shows an overview of the main tasks of the host PC software and the C44 control software.

The user interface is a menu driven system that operates in the Microsoft Windows95 environment. The user may change control variables, update parameters or request data from the C44. Another useful feature is the periodic updating of a selection of the most important variables on the screen for the users information. All communication with the C44 is made through the DPRAM. Once the user has entered one or more options a semaphore system is used to communicate relevant information and requests to the C44. The C44 background routine reads this information from the DPRAM and takes the appropriate action, although this may not happen instantly if the interrupt routine is called during this period.

There are two mechanisms for data acquisition. The first mechanism involves periodically, at approximately 1 second intervals, updating a selection of relevant variables to the host program for display on the screen. This information is provided to give the user a visual indication of the present state of the ASF. The second mechanism is used to capture short periods of data from the C44. Any number of variables may be stored at a sampling rate that is either the control sampling rate or a multiple of that rate. This data is stored directly to the DPRAM. The only restriction is that no more than 6K data values can be captured at once due to DPRAM capacity. Once all data has been stored the host reads it and stores it to a file. This data may then be analyzed by the user.

Certain tasks in the C44 software are time critical. At the start of each interrupt period a timing signal is output to the PWM generator, see section 3.2.2.1, to update the PWM output to that calculated at the end of the previous interrupt cycle. In order to achieve synchronous sampling the ADCs must also be triggered at this time. The rest of the interrupt routines various tasks are then completed. The total duration of the interrupt routine varies depending on selected options such as whether or not data is required by the host and the length of control method chosen. In general the entire interrupt routine takes approxi-

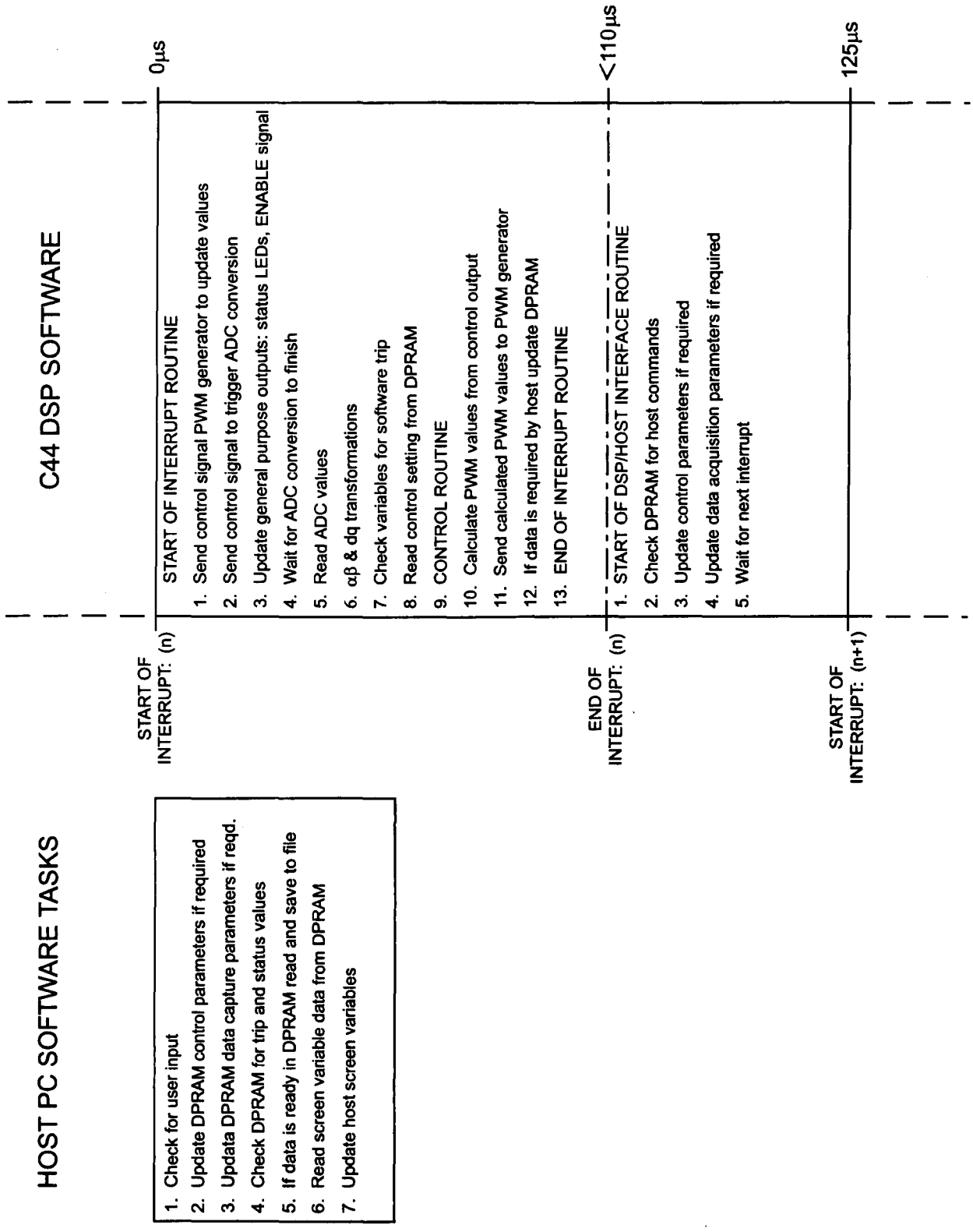

Figure 3.3: Overview of host and DSP software

mately 110μs. The control section of the interrupt routine calculates reference voltages for the PWM software function. This then converts these voltages into 16 bit timing values for the PWM generator. This information is transferred to the PWM generator buffers. It is not until the next interrupt cycle commences that this PWM information is updated. Hence the total processing delay of the control system delay is 1 complete sampling period of 125μs.

3.2.4 Protection

Various protection measures have been implemented in the experimental rig. Some of these were built in to the inverter hardware and others have been added due to the unconventional way that the inverter has been connected to the supply. The protection measures are explained during a description of the starting procedure for the ASF. Figure 3.4 shows the protection mechanisms implemented.

Both contactors, 1 and 2, are initially open. Contactor 1 is operated by the user. On closure the inverter d.c. link is pre-charged. Above a threshold voltage, approximately 500V, the pre-charge contactor automatically closes short circuiting the pre-charge resistor. An isolation transformer is used so that the d.c. link is able to float with respect to the supply. Potential short circuit paths that could exist once contactor 2 closes are thus eliminated. The inverter SUPPLY FAIL trip circuit is also satisfied as the normal supply voltage is applied to the rectifier input. Cooling fans are also operated from this supply.

The next stage required is to commence inverter switching. The gate driver circuits for the upper IGBT in each inverter leg are powered by a charge pump power supply. In order to initiate switching of the upper switches the lower IGBT in each inverter leg must be switched on for 10ms. After this period normal switching patterns may be used. A specific software routine controls this process. Prior to this the inverter trips and WATCHDOG trips must be reset manually by user operated switches. Assuming that no faults are present the charge pumping procedure begins. After the charge pump priming is completed the output of the inverter is controlled to match the output of the supply auto-transformer.

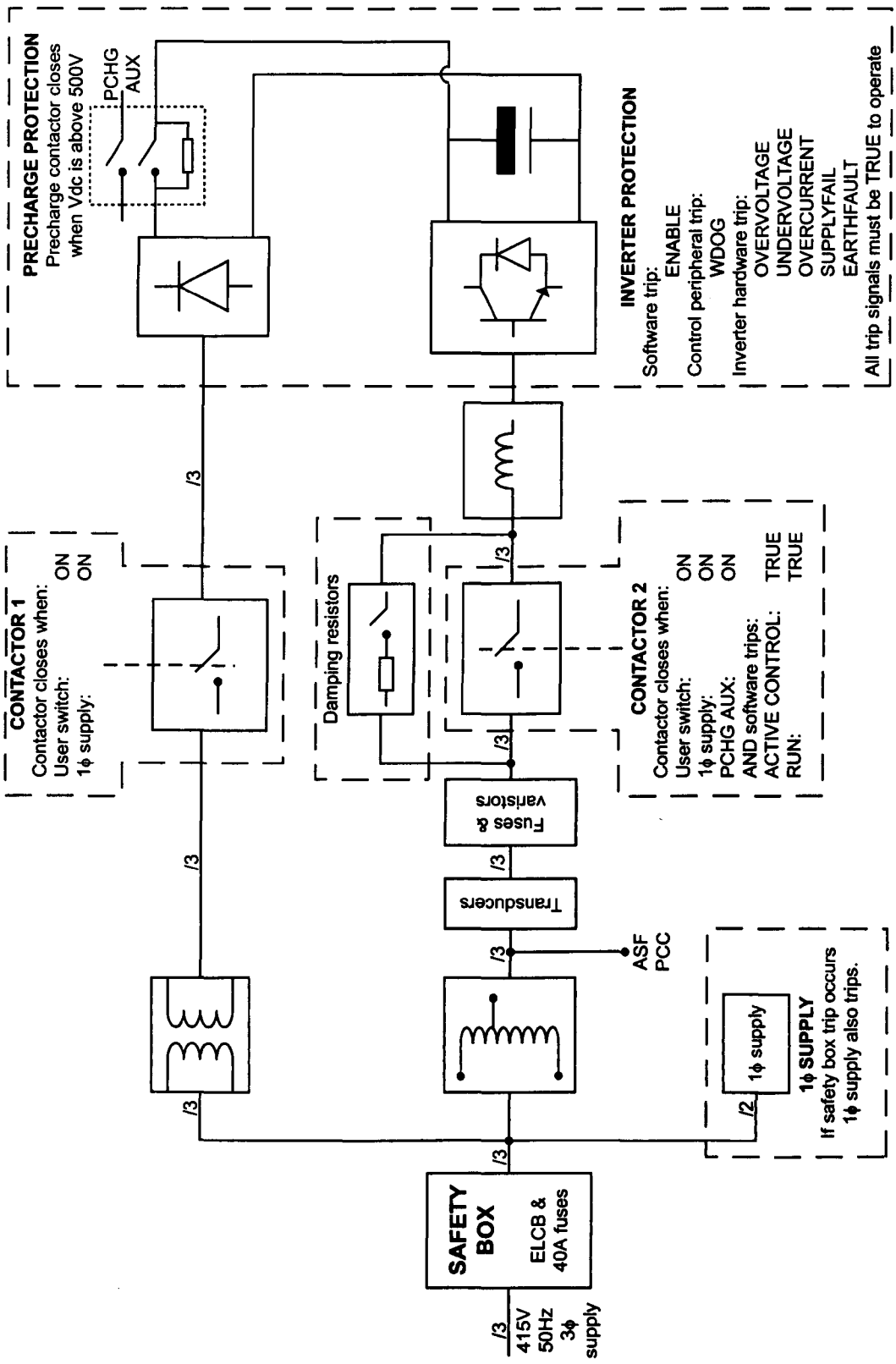

Figure 3.4: Protection features of the experimental rig

The voltage matching procedure is conducted so that contactor 2 may be closed without creating any large current surges that might trip, or potentially damage, the inverter. Even if the voltages are matched very accurately this contactor closure can still cause current spikes and electromagnetic interference that may affect the inverter detrimentally. As a result damping resistors have been added to the experimental rig, figure 3.4. These damping resistors are operated manually. They are only used for the short period once voltage control is established before contactor 2 is closed. After the contactor closes they are short circuited and no longer serve any purpose.

It is vital that the voltage matching control is operational before contactor 2 closes. If it is allowed to close in any other situation the full supply voltage may be applied to the inverter, in this case the current will only be limited by the line inductors and the inverter could easily be damaged. Accordingly, the contactor 2 control has been designed to be foolproof. In order for the contactor to close various conditions must be met, these are shown in figure 3.4. In order to initiate voltage matching control, it is a pre-requisite that the pre-charge contactor is closed and the single phase supply is switched on. The RUN trip signal must be set, indicating that the inverter is operational. The ACTIVE CONTROL signal is sent by the control system indicating that voltage matching control is in use. Finally, the user must operate a switch to close the contactor. If a fault occurs during subsequent ASF operation there are several mechanisms by which contactor 2 will be opened in order to protect the inverter. If a software trip is detected the ACTIVE CONTROL signal is cleared, causing operation to the circuit to be broken. Similarly if an inverter trip is detected the RUN signal is cleared and the circuit is again broken. Major faults such as a pre-charge fault or single phase supply fault will also break the ASF circuit.

When contactor 2 is finally closed the voltages are such that no current should flow between the ASF supply and the inverter output. Some high frequency current will flow due to the PWM nature of the control although this will be minimal as the inductor impedance is very large at the switching frequency. As this is an open loop control the d.c. link voltage slowly ramps towards the OVERVOLTAGE level. When the d.c. link voltage reaches a certain threshold, before the OVERVOLTAGE level is reached, the controller automatically initiates the ASF control scheme. Current control and d.c. link voltage control is activated. The d.c.

link voltage is controlled to 680V. When the d.c. link voltage rises above the rectified level, approximately 620V, no current will flow from the isolated transformer supply. This will effectively be disconnected leaving the ASF control to maintain the d.c. link voltage level.

During normal operation the rig may be tripped by the software trip routine. This will trip the rig if line currents exceed a predetermined level or if the d.c. link voltage is outside its safe limits. The inverter protection can also halt operation if any of the faults shown in figure 3.4 are triggered. If a trip does occur data is automatically stored by the C44 for diagnostic purposes. All hardware trip signals are also latched for diagnosis by the user. These must manually be reset before operation is allowed to continue.

Fuse and varistor protection is also provided as a last resort safety measure. 70A semiconductor fuses are positioned to limit the device current in the inverter. The varistors provide an alternative current path if one of the fuses blows preventing dangerous voltage spikes that may damage the IGBT devices. The varistors also protect the IGBT switches from voltage spikes from the supply and due to the switching operations of contactor 2.

3.3 The Impedance Measurement System

The impedance measurement system uses the entire experimental rig previously described. An additional data acquisition system (DAS) was constructed for the required measurements and some additional interfacing has been implemented between the ASF control system and the DAS. The overall system is shown in figure 3.5.

For the experimental impedance measurement work, the supply impedance was varied although the voltage must still be stepped down in order to ensure correct ASF operation. As a consequence the step down auto-transformer has formed part of the supply in all the experimental measurement work. To vary the supply impedance additional elements were connected at the output of the auto-transformer or at the PCC of the ASF.

The DAS is controlled by a Siemens 167 microcontroller. This is in turn controlled by a

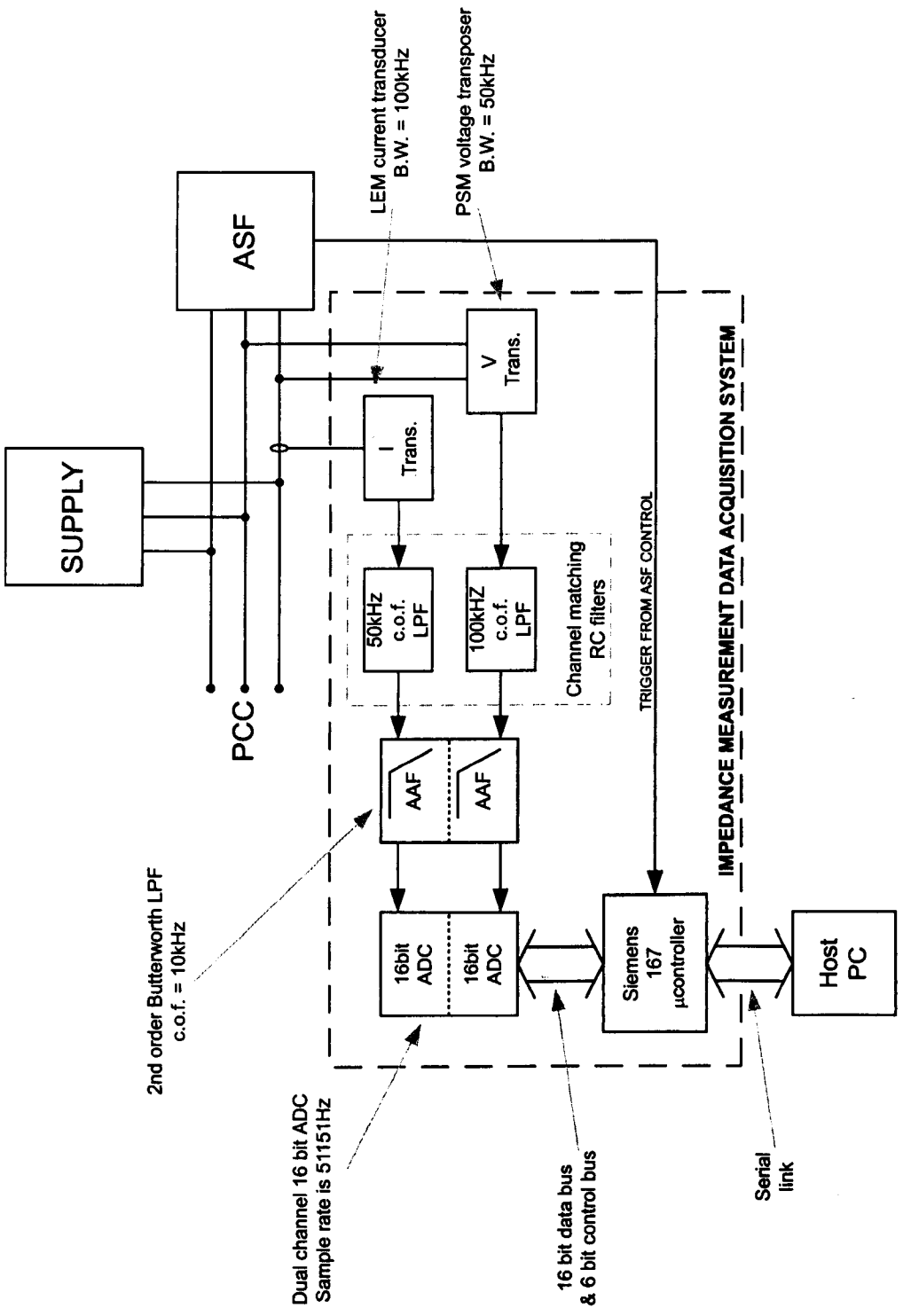

Figure 3.5: Impedance measurement stand alone data acquisition system

simple user interface on the host PC. Communication between the host PC and the microcontroller is via a serial link. A simple control program was written for the microcontroller in C, this controls the ADC sampling and sends stored data to the host PC for off-line processing.

One current transducer and one voltage transducer are used for the impedance measurement data capture, as shown in figure 3.5. An LEM current transducer was used for current measurements and a PSM voltage transposer was used for the voltage channel. The data sheets for these transducers claim that the bandwidths are 100kHz and 50kHz respectively. It is also stated that the roll off characteristics are first order. A single order passive filter is used on each channel in order to balance the frequency response characteristics of the two channels. This was achieved by applying a filter to each channel that had the same characteristics as the other channel transducer. This matching is important for accurate impedance measurement 4.5.

Second order Butterworth anti-aliasing filters were used with a cut off frequency of 10kHz. These circuits were constructed with precision resistors and trimming capacitors, for fine tuning the response of each channel. During construction the two channels were calibrated, in terms of phase response, using test signals. The trimming capacitors were used in order to vary the phase response in order to match the response of each channel. This was achieved with some degree of success, in the frequency range between 0 and 2kHz. The phase difference between the two channels for sinusoidal test signals was less than 1 degree. The ratio of voltage magnitude to current magnitude at the output of the anti-aliasing filters was also tested. This ratio did not vary by more than 1% in the frequency range. Therefore it was decided that no additional calibration was required apart from a d.c. calibration implemented in software. 16 bit ADCs were used with an input range of between -10V and +10V. The sampling rate was fixed at 51151Hz. This frequency was chosen to be as close to 51.2kHz as possible. This target sampling rate was chosen in order to store 8192 samples in 8 fundamental voltage supply cycles for ease of DFT processing.

One trigger signal is sent from the ASF controller to initiate sampling. On receiving this signal 16384 samples are recorded for both channels and stored in the microcontroller

RAM. This data can be passed to the host PC and saved to file using the user interface. Impedance measurement calculations were conducted off-line using MATLAB on the host PC. The ASF trigger signal is set to initiate sampling one sampling period prior to the transient injection. The transient injection is controlled by the ASF software. After the control algorithm has been processed the three reference voltages for the ASF output are available. The transient voltage signal is added to these references to provide an open loop transient signal. The updated references are subsequently passed to the PWM software routine before being output to the control hardware.

3.4 Summary

This chapter has explained the important features of the experimental rig. The control system and software has been ~~been~~ described as well as the protection features implemented for safety and to protect the experimental hardware from damage. The impedance measurement has been described as an extension of the ASF experimental rig. Experimental results using the systems described in this chapter follow in the next two chapters.

Chapter 4

Linear impedance measurement techniques

4.1 Introduction

This chapter aims to introduce two new proposed techniques for on-line impedance measurement. The two methods shall be described as:

1. Short term injection
2. Medium term injection

Many features of both techniques, including the hardware platform and signal processing techniques, are common to both and shall be dealt with as such. This chapter shall be approached as follows:

The basic requirements of the measurement system shall be outlined and common assumptions for both schemes will be described. Both injection strategies shall then be introduced. For clarity both methods are described for the impedance measurement of a single phase

circuit, the three phase approach is described for both schemes later in this chapter. Signal processing techniques are discussed and suitable procedures are defined for both methods. A generalized three phase approach to impedance measurement is outlined and applied to the proposed methods. Finally the practical implementation of the methods is described using the ASF.

4.2 Requirements for on-line measurement techniques

The first requirement of both proposed schemes is that each shall be embedded into the normal operation of an ASF. Figure 4.1 shows a simple overview of the system. The methods will actively inject current waveforms into the supply from the ASF in order to disturb the network. Measurements of the current injection and subsequent voltage disturbance will be used in order to estimate the system impedance at the point of connection of the ASF. The hardware platform for each method is the same, the two methods differ in their injection strategies.

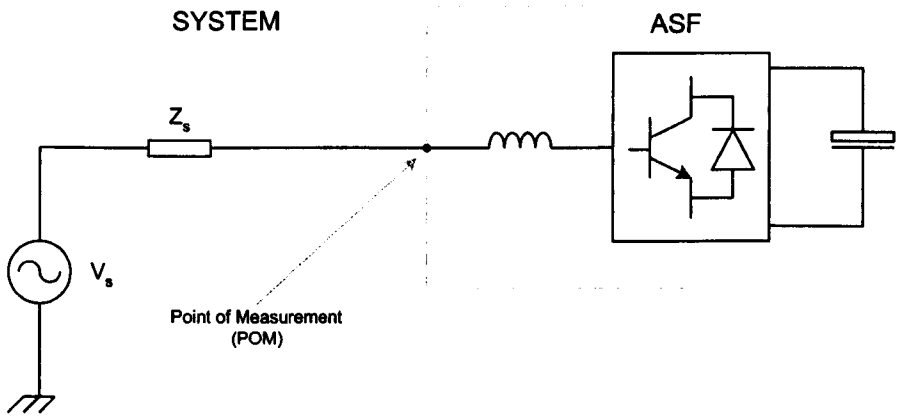

Figure 4.1: Measurement system overview

The ASF hardware consists of a voltage source inverter and a set of line inductors. The ASF controls the current in the output line inductors in order to operate as a controllable current source. A *per phase* representation of the ASF is shown in figure 4.2.

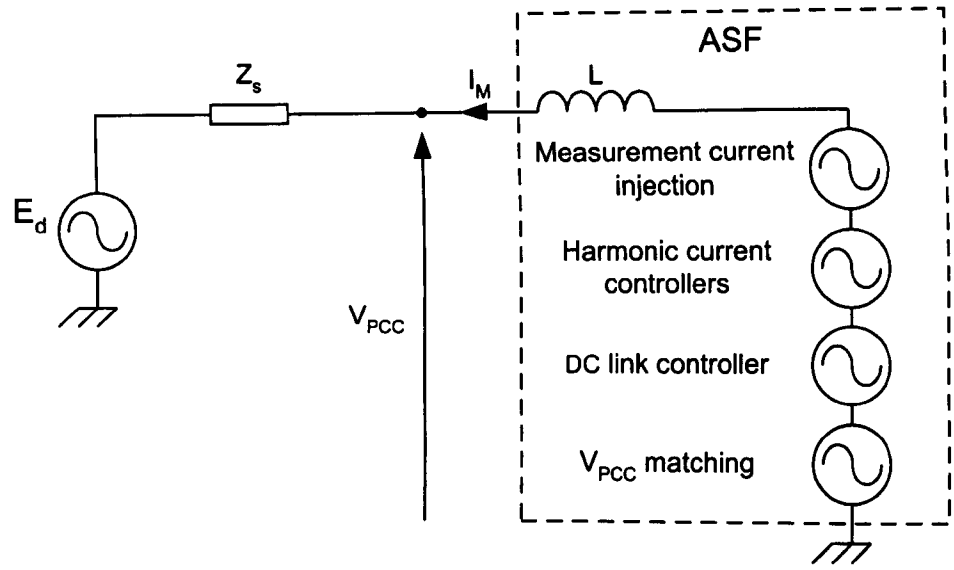

Figure 4.2: ASF control scheme

The power system supply is represented by E_d and Z_s. E_d incorporates harmonic distortion present on the supply that is due to remotely connected NLLs and Z_s is the supply impedance. The ASF line inductance is L. The voltage source inverter acts as a controllable voltage source. The voltage source may be considered as the sum of four separate voltage components, each component is generated by a software routine within the ASF controller. These components are:

1. Supply matching component. Without any active control present the first objective of the ASF control is to ensure that no current should flow in the line inductors. This is achieved with a voltage output that is equal to the voltage measured at the PCC, V_{PCC}. The PWM output of the inverter means that high frequency voltages will be present across the inductors although only a small current will flow.

2. d.c. link controller. The d.c. link controller applies a voltage such that real fundamental power is drawn from the supply to maintain the d.c. link voltage at a predetermined value.

3. Harmonic current controllers. The harmonic current controllers apply a further voltage in order to inject 5th and 7th harmonic current to achieve the compensating ob-

jective of the ASF.

4. Injection source. Finally, an uncontrolled voltage output for measurement current injection may be applied.

The proposed techniques shall aim to accurately measure system impedance at the point of measurement in the range of frequencies between d.c. and 1kHz. All simulation and experimental work shall be conducted in the range between d.c. and 2kHz in order to investigate the limits of the methods. The system requirements were such that the measurement process should measure impedance during normal circuit operation without unduly affecting normal network operation. Furthermore the time of injection must be controlled by the system so that measurements may be triggered on demand.

Both methods will measure the system impedance at frequency values that do not correspond with the frequencies at which harmonic producing loads inject current into the system. To estimate the impedance at these harmonic frequencies some form of interpolation will be applied using the neighbouring values. The interpolation method chosen is discussed further in section 4.9. This constraint is equivalent to stating that only the linear part of the system impedance shall be measured. Harmonic producing non-linear loads have a non-linear relationship between current and voltage at the harmonic producing frequencies. Therefore the impedance for such loads at these harmonics will depend on the operating point of the load. Consequently the act of measurement will affect the voltage-current relationship. By using interpolation only the linear part of the impedance will be measured at these frequencies. This is a common assumption made in the literature, see chapter 2. It has the further advantage of eliminating measured impedance points at harmonic frequencies. these points are particularly prone to large measurement errors, due to steady state current and voltage components interfering with transient measurements.

Certain common assumptions shall be made regarding the nature of the measured system. These assumptions are:

- The supply frequency, f_s, remains constant during a measurement period.

- The measured impedance, Z_s, remains constant during a measurement period.
- Non-linear loads that produce time varying interharmonic currents, such as arc-furnaces [5], are ignored.
- The measurement injection is assumed to be uncorrelated with the system at all non-harmonic frequencies. This assumption is investigated further in chapter 6.

The measurement period should be as short as possible in case the first two assumptions are not completely satisfied. A long term injection method, as described in [63], was ruled out due to the time varying nature of power systems. Such a measurement process must inject a current disturbance at each frequency of interest for at least one supply voltage cycle. A complete sweep of all frequencies between d.c. and 2kHz at 10Hz intervals would therefore require a minimum of 200 supply cycles to complete. This yields a measurement time in excess of 4 seconds. This was deemed as too time consuming for an on-line measurement technique, especially if used for the determination of reference currents for an active filter. Work has thus focused on methods that allow an impedance estimate to be reached in a much smaller time period.

4.3 Short term measurement technique

The short term measurement technique uses a single injection of a wideband current disturbance in order to perturb the system. Measurements of the current and voltage transients are made in the steady state immediately before the injection is applied. A second set of measurements is made to capture the transient disturbance. The ASF is used to inject the disturbance whilst in steady state operation. Complete control of the injection is possible. It is possible to commence the measurement process at any point in the supply cycle and to repeat measurements automatically at a set interval. Previous techniques, with one exception, that have used a wideband injection have relied upon switching phenomenon beyond the control of the measurement system such as capacitor bank switching, transformer tap changing or transformer inrush. In [60] a power electronic device, named as a harmonic

generating device (HGD), was developed that allowed some control of a wideband injection. In this case a thyristor and resistor combination was used, described in more detail in chapter 2. No phase control of the point of injection was possible in this case. The HGD was a specific piece of measurement equipment, in this work an existing ASF is used for this purpose.

An introduction to this method is given in [75] using an ideal current disturbance and a stationary linear single phase system. In this preliminary work an ideal current source was used to inject a triangular current pulse, of width t_{pulse} and magnitude I_{max}. A triangular waveform was chosen as a realizable approximation to an impulse function. Such a current injection is not possible using the available experimental systems although this will provide a useful starting point in order to understand the nature of the disturbing signal. In the single phase system a current pulse of the form shown in figure 4.3(a) is injected into the system from the ideal current source.

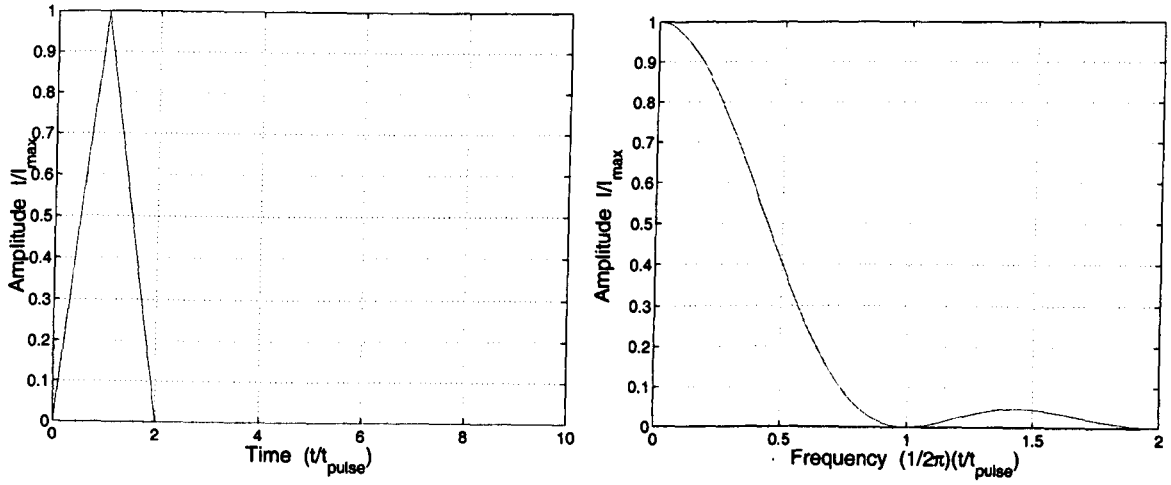

(a) Time domain

(b) Frequency spectrum

Figure 4.3: Ideal short term injection

In a balanced three phase system, section 4.10.2, the injected current in phase 1 would be that shown in figure 4.3(a). The transient current injection in phases 2 and 3 are determined such that the total current injection in all three phases sums to zero. The injection in phases 2 and 3 will be of the same form as for phase 1 although the amplitude of the triangular

injection will be $\frac{-I_M}{2}$. The spectral content of this signal, I_{M1}, is shown in figure 4.3(b).

The peak injection disturbance occurs at d.c., this is determined by the peak amplitude of the current injection. The duration of the current injection determines the rate of decay of amplitude with increasing frequency. A wideband measurement must inject a sufficient disturbance across the whole range of frequencies that are of interest. With reference to figure 4.3(b) the upper frequency limit for measurement should be positioned at a frequency considerably below the first duration at $f = \frac{1}{2\pi t_{pulse}}$. Otherwise the injection level at frequencies that reside in the upper region of interest will be significantly lower than the lower frequency injection level, resulting in a poor signal to noise ratio. The actual values for t_{pulse} and I_{max} are constrained by the experimental system. These are determined in section 4.11. The ASF is operated as a controlled current source but the control bandwidth and d.c. link voltage limitation is such that it is not possible to exactly replicate the injection signal described. Due to these limitations the system impedance will have some affect on the injection. The experimental parameters were chosen in order to disturb the system sufficiently for impedance measurement up to 1kHz.

4.4 Medium term injection technique

The second injection technique is referred to as the medium term injection technique. This refers to the nature of the injected transient and not to the overall measurement duration. This method will again use two sets of measurements. One set is taken in the steady state immediately prior to the transient injection to account for the background distortion levels. The second set of measurements are taken during the medium term injection. The steady state data is subtracted from the transient data in the same way as for the short term injection. The total duration of the measurement is 16 fundamental supply cycles comprised equally of steady state and active data records. This technique also applies a wideband injection signal to the network. In this case a longer duration input disturbance that is not intended to approximate an impulse disturbance. A current input is applied for the entire 8 active fundamental voltage cycles. The current disturbance is designed to disturb the sys-

tem for a longer duration than the short transient applied by the short term technique. By applying a longer disturbance it is possible to reduce the current magnitude, for a similar signal to noise ratio. The applied current injection is shown below in figure 4.4(a). This waveform contains a non zero d.c. component in order to excite even harmonics of the fundamental injection frequency as well as the odd harmonics. The same injection is shown in the frequency domain in figure 4.4(b). The current disturbance waveform was designed with certain features in mind, these were:

- The supply frequency impedance is very important. The injection was designed so that the low frequency injection is high, in fact the injection strength decays exponentially with frequency.
- The injection strength at harmonic frequencies is unimportant as the measured impedance at such frequencies is ignored. Instead, the harmonic impedance values are calculated by interpolation of interharmonic values. Therefore the injection strength at harmonic frequencies should ideally be zero. This effect could be generated with a single positive and single negative step although this would create injection minima every 12.5Hz. The two positive and two negative step was adopted as injection minima were only present every 25Hz.

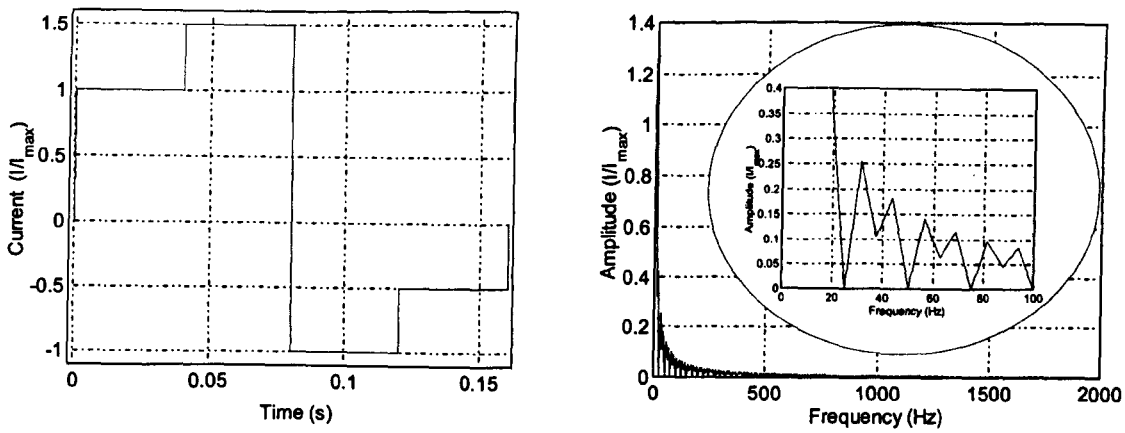

(a) Time domain

(b) Frequency domain

Figure 4.4: Ideal medium term injection

The current injection was again applied in an open loop manner. An additional d.c. voltage was added to the inverter output voltage, figure 4.2. This voltage was stepped to approximate the desired injection current. The success of this process is dependent upon the output voltage capability of the inverter.

4.5 Signal processing techniques

Methods based upon the Fourier transform have been adopted for the signal processing stage of the measurement process. Fast Fourier transforms (FFT) are very computationally efficient hence making them ideal for an on-line measurement procedure. Parametric techniques are available that may serve the same purpose and yield superior results such as auto-regressive techniques, Pisarenko harmonic decomposition or Prony analysis [76]. These alternatives rely on additional information in the form of parameters for an assumed model of the system under consideration. While such methods have the ability to provide more useful spectral information, in practice this may not be the case. High signal to noise ratio [76] or poor parameter selection [77] may result in inferior performance than that provided by the FFT based approaches. Furthermore, such schemes use computationally intensive algorithms [78] that are not suited to an on-line measurement procedure. Although more efficient algorithms may be available the investigation of such methods was beyond the scope of this work.

A theoretically defined discrete Fourier transform (DFT) uses a time domain signal that is periodic and present for all time. An FFT, by definition, must use a finite data window. The FFT therefore estimates the frequency components of the input signal with some variance. The sampled data sequences also contain errors, both random noise due to natural variation of the power system or experimental error and other non-random errors associated with the system or measurement procedure. If the non-random errors are eliminated then the sampled data series' form part of a stationary stochastic process. That is, the statistical variation in the sampled data will be governed by fixed statistical properties. It is the aim of this section to determine a signal processing scheme so that an impedance estimate may

be calculated with minimum computational power and yet with a minimum error from the actual impedance measured and with a minimum fluctuation, or variance, about the true impedance.

At non-harmonic frequencies the supply impedance shall be considered as a linear transfer function, as shown in figure 4.5 with the input being the current disturbance and the output being the subsequent voltage transient.

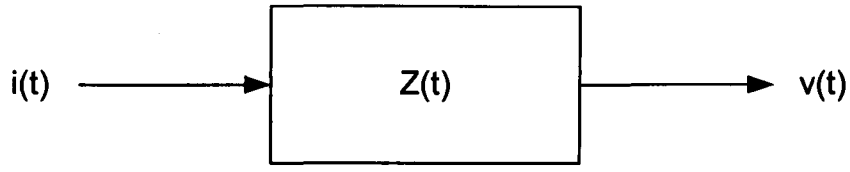

Figure 4.5: Single input, single output (SISO) system

It is shown by Jenkin and Watts [59] that the transfer frequency response function, Z_f, may be calculated in the frequency domain by equation 4.1. In this equation $P_{vi}(f)$ is the cross power spectrum (or cross spectral density (CSD)) of v and i and P_{ii} is the auto power spectrum (or power spectral density (PSD))of the current input i. In practice these quantities are merely estimates of the true CSD and PSD because the true cross- and auto-power spectra may only be calculated given input signals of an infinite length.

$$Z(f) = \frac{P_{vi}(f)}{P_{ii}(f)} \tag{4.1}$$

It is necessary to consider various means by which $P_{vi}(f)$ and $P_{ii}(f)$ may be estimated so that the method best suited to this application may be chosen.

4.5.1 Periodogram approach

Kay [76] states that the simplest and crudest form of power spectrum estimator is the periodogram. The periodogram is a spectral estimate calculated from the square of the mag-

nitude of the FFT of the given signals. The basic definition for the CSD is shown in equation 4.2, the PSD of x is simply P_{xx}. $\Im$ is used to define the fast Fourier transform (FFT) for a finite length input signal

$$P_{xy}(f) = |\Im(x(t))\Im(y(t))|^2 \tag{4.2}$$

Using this definition it is possible to redefine equation 4.1 as equation 4.3. It should be noted that this is not a generalized mathematical derivation and is only possible as all sampled values of current and voltage are real and by definition do not contain a complex part.

$$Z(f) = \frac{\Im(v(t))}{\Im(i(t)} \cdot \frac{\Im(i(t))}{\Im(i(t)} \tag{4.3}$$

From simple cancellation of terms it can be seen that the forms shown in equation 4.3 and equation 4.4 are equivalent. Equation 4.4 is the intuitively obvious solution found by dividing the Fourier transform of the voltage by the Fourier transform of the current. Thus the simplest means of calculating the impedance of the supply in the frequency domain is to apply equation 4.4 at each frequency of interest, f. Unfortunately the accuracy of this method is highly dependent on the noise present in the system [76] due to the simple means used to derive the spectral densities.

$$Z(f) = \frac{\Im(v(t))}{\Im(i(t))} \tag{4.4}$$

Although the periodogram is a commonly used estimator for spectral densities its' variance is large [76] and does not decrease with record length [79] [59]. Furthermore poor results can be expected if noise in the input signals is not random noise. In the practical case investigated signal noise is partially due to A/D quantization errors, transducer error and

system noise which may all be considered as random noise sources. Other sources of error are due to imperfect cancellation of supply voltage harmonics, imperfect cancellation of steady state current injected into the system by the ASF and are also due to the non-linear nature of some connected loads. This second class of error are not random and will therefore severely affect the accuracy of the impedance estimate. It is hence clear that equation 4.4 may not provide a good estimate of impedance with frequency in terms of its statistical variance. In fact this method of calculation has provided satisfactory results for many studies and has the advantage of simplicity and computational efficiency over more complicated algorithms. Whilst this method may provide adequate results, for systems with high noise levels, a high degree of non-linearity and a low level of injection disturbance a superior spectral density estimator should be sought.

Welch's averaged periodogram technique is a commonly used improvement to the method described. In this technique the time domain recorded samples are split into several equal length records, for example 8192 recorded points may be split into 8 sections each of length 1024 points. Each section of data is treated individually for initial processing. The PSD of each section is calculated using the periodogram method described. The overall PSD of the entire sample is found by averaging the individual sections. This technique provides a smoothed estimator of the PSD as the frequency resolution is decreased. The frequency resolution will be 8 times lower if the recorded data is split into 8 sections. The advantage of this method lies in the fact that the variance will also be reduced by a factor of approximately 8. This process overcomes the fact that the variance of a periodogram does not decrease with increased data length. For the particular application in this work the majority of non-random noise is expected to lie at the harmonic frequencies and be due to non-ideal cancellation of steady state quantities or non-linear effects. With this in mind it was intended that impedance values at the harmonic frequencies should be discarded and values for these frequencies should be calculated by interpolation. It is this prior knowledge of the system that dictates that a smoothed estimator of the PSD is not appropriate in this situation. A smoothed estimator will spread the inaccuracy at the harmonic frequencies to neighbouring frequency points thereby reducing the accuracy of these points also. For these reasons Welch's averaged technique has not been adopted.

4.5.2 Correlation approach

Alternative estimator functions for PSD and CSD are available that do not involve the use of equation 4.2 although these are invariably computationally more demanding. The cross power spectrum may also be defined as the Fourier transform of the cross-correlation function of the inputs. The auto power spectrum is therefore defined as the Fourier transform of the auto-correlation function of its input. The cross-correlation and auto-correlation functions may be estimated in the time domain. It is not possible to calculate exact values for these functions, again because only limited time domain information is available. The ideal cross-correlation function is defined in equation 4.5 as γ_{xy} for an infinite time series, E denoting the expected value. This definition applies only when all elements of both x and y are real.

$$\gamma_{xy}(m) = E\{x_n y_{(n+m)}\} \tag{4.5}$$

Several estimator functions, R_{xy}, are defined for the calculation of the cross correlation sequence in the time domain with a finite length time series. A cross-correlation sequence is used to quantify the amount of correlation between the signals, the overall aim of the method is to reject components of the signals that are not highly correlated such as random noise, or steady state background distortion in this case. A cross-correlation sequence is calculated with a value of correlation corresponding to each point in the input signals. Equation 4.6 shows an unbiased estimator. This definition gives the cross-correlation at a single position, m in the input signals.

$$\hat{R}_{xy}(m) = \frac{1}{N-m} \sum_{n=0}^{N-m-1} x(n+m)y(n) \tag{4.6}$$

Equation 4.7 shows a an alternative definition, a biased estimator of the cross-correlation.

$$\hat{R}_{xy}(m) = \frac{1}{N} \sum_{n=0}^{N-m-1} x(n+m)y(n) \tag{4.7}$$

The unbiased estimator has the same expected value as the ideal definition given in equation 4.5 but the variance of the estimator increases with the length of the time record. In contrast the biased estimator does not have the same expected value as shown in equation 4.5 but its variance decreases with record length. A full discussion of this topic is given in [59] and [76] but it is sufficient to note here that the biased estimator is more commonly applied as the mean-squared error is generally lower for this method.

This section has described two methods of estimating the supply impedance based upon power spectral density functions. The first method defined the spectral density estimate using periodogram functions calculated from the squared magnitude of the Fourier transform, equation 4.3. It was shown that this method is equivalent to calculating the impedance by simply dividing the Fourier transform of the voltage by the Fourier transform of the current, the most intuitive solution. Due to the nature of applying Fourier transforms to finite data records this method has a high variance. The second method employs correlation functions applied in the time domain followed by the application of Fourier transforms. This technique has a far greater computational demand although the variance of the solution is reduced.

The overriding factors determining the accuracy of the technique lie in the overall injection strength of the disturbance and the correct interpretation of the impedance estimate close to harmonic frequencies. The first factor is system dependent and will be a compromise between nuisance interference and impedance estimate accuracy. The second factor will be directly combated by only considering interharmonic values. Therefore it was not found necessary to use the second impedance estimate derivation based upon correlation series. The simpler and more intuitive method directly applying the Fourier transform to the data series was thus adopted.

Both Girgis & McManis [52] and Morched & Kundur [51] suggested the use of the more complicated algorithm using the power spectra. In both cases little background distor-

tion was present. In fact steady state cancellation of background distortion was not even required due to such low distortion levels, notch filters were used to suppress the fundamental in [51] and both the fundamental and fifth harmonic in [52]. It is clear that these studies had different signal processing requirements from this work.

4.6 Minimization of spectral leakage

Attention is now turned to the application of the chosen signal processing technique. The impedance estimates at the harmonic frequencies shall be disregarded for reasons of non-linearity and cancellation of background distortion. It is therefore important that the impedance estimates close to the harmonic frequencies are very accurate. Otherwise an interpolation algorithm will be passed inaccurate data and the impedance estimates at harmonic frequencies will be flawed. This is particularly important for the estimation of impedance below the fundamental frequency. A mechanism is required to calculate the $\Im(v(t))$ and $\Im(i(t))$ with maximum accuracy at interharmonic frequencies, particularly those frequencies that lie close to the harmonic frequencies.

When applying a DFT an infinitely long periodic signal is assumed to be present in the time domain. The period of this signal is equal to the length of the sampled data record. The act of sampling the finite length data record is equivalent to multiplying the infinitely long signal by a window function. The simplest such function being a rectangular window whereby all data within the sampled period is given equal weighting and all data outside of the sampling window is weighted to zero. When considered in the frequency domain this multiplication is equivalent to a convolution of the ideal spectrum with the window function spectrum. This convolution smears the ideal frequency spectrum resulting in what is termed as spectral leakage. In [76] spectral leakage in the frequency domain is described as being due to the energy in the main lobe of a spectral response *leaking* into the side lobes. This effect distorts the surrounding spectral response. Time domain records with large steady state components at the fundamental supply frequency and its harmonics will be the greatest source of spectral leakage in this application.

4.6.1 Steady state cancellation

The simplest means of reducing spectral leakage close to the harmonic frequencies is to exactly cancel the steady state components by subtracting a steady state measurement from the transient data record. If the supply components are removed then spectral leakage about these points will be eliminated. If total cancellation is not possible due to problems of resolution then at least the leakage affects will be reduced, especially about the fundamental frequency component. This cancellation is implemented for all impedance measurements. Two sets of data are recorded, steady state data and transient data. In the time domain the transient signals are $v_t(t)$ and $i_t(t)$ and the steady state signals are $v_s(t-T)$ and $i_s(t-T)$. T is the time between the steady state measurement and the transient measurement and must be an integer number of fundamental supply cycles. The background distortion is removed from the transient signal by a simple subtraction as shown in equations 4.8 and 4.9.

$$v(t) = v_t(t) - v_s(t-T) \tag{4.8}$$

$$i(t) = i_t(t) - i_s(t-T) \tag{4.9}$$

The success of the cancellation is dependent on the data acquisition system used. The data acquisition must be triggered exactly so that the steady state harmonics exactly match the steady state harmonics present in the transient record. The mechanism implemented to successfully achieve this task is considered in more detail later in this chapter. Complete cancellation of the steady state components cannot be guaranteed in practice due to experimental limitations. Complete cancellation is not assumed and must be considered during the remainder of the signal processing.

4.6.2 Windowing

In a periodic stationary system, that is a periodic system whose statistical properties remain constant with time, a rectangular window that exactly encompasses an integer number of periods will, in theory, result in no spectral leakage [35]. In practice this will not be the

case, mainly due to practical problems involved in sampling over an exact number of periods or because the system is not perfectly stationary. A phase locked loop PLL may be used to track the fundamental frequency and hence it may be possible to divide the time of one period into a suitable number of divisions for an FFT to minimize the spectral leakage. Dedicated hardware is normally required for a PLL which will further complicate the experimental hardware. If this approach is not possible the FFT performance may be improved with the use of alternative windowing functions.

Spectral leakage may be reduced by the use of non-rectangular windowing functions such as the Hamming or Hanning window. These may reduce the side lobe leakage but have the effect of reducing the frequency resolution by widening the main lobe. All non rectangular windowing functions taper the edges of the data set to zero. For current injection data this will have the effect of attenuating the injection strength of the disturbance, especially at the window boundaries. Therefore a window should be positioned such that the greatest time domain disturbance occurs at the centre of the chosen window. In the case of the rectangular window this is not important.

4.7 Short term injection signal processing

The impedance measurement data acquisition hardware is fully detailed in chapter 3. Two data acquisition channels are used, one measures voltage and the other measures current. The phase response characteristics over the frequency range considered of both channels have been accurately matched. The data acquisition is capable of sampling at a rate of 51.151kHz with 16 bit accuracy. The desired sampling frequency was 51.2kHz, chosen in order to sample 8192 samples in eight 50Hz supply voltage cycles. Unfortunately the micro-controller used for the data acquisition was not able to time A/D conversions at the required interval, 51.151kHz was the closest possible with the 40ns timer resolution available. The entire measurement process consists of 8192 samples of steady state data from each channel and 8192 samples of transient data from each channel. Each record length is marginally longer than 8 fundamental 50Hz supply voltage cycles, this would

correspond to 8184 samples. This slight discrepancy may introduce a slight degree of spectral leakage as a non-integer number of supply cycles are recorded. In fact this error is negligible when compared to variations in supply frequency.

There are several possible different signal processing options using this approach. The simplest sampling solution is to assume that the supply frequency is constantly 50Hz and to sample with a rectangular sampling window. This case is shown in figure 4.6. The steady state data is recorded in the eight cycles following the transient record in this case. The steady state data was recorded after the transient data for practical triggering reasons only.

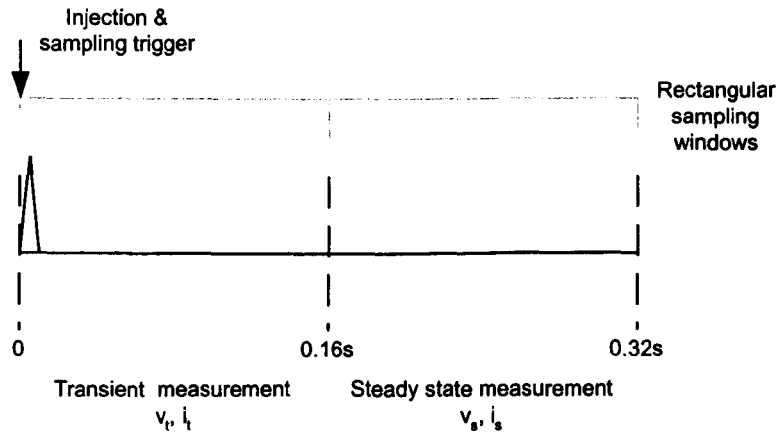

Figure 4.6: Option 1 sampling arrangement

In theory this realization of the measurement technique results in no spectral leakage, in reality the fundamental supply frequency may not be exactly 50Hz. Measurements at the University of Nottingham showed measured variations of up to 0.1Hz at any particular time. In the UK, the Electricity Supply Regulations state that the supply frequency should not exceed 1% variation from 50Hz ($49.5 \leq f_s \leq 50.5$). The system is normally controlled such that the frequency is between 49.8Hz and 50.2Hz [80]. Even a slight variation in supply frequency will affect the voltage cancellation of equation 4.8 massively. As an example consider the supply frequency to be 50.1Hz. For a fundamental voltage with a peak value of 460V the imperfect cancellation would result in a residual fundamental component with a peak value of 25V. This will severely affect the calculated impedance

data points surrounding the fundamental frequency voltage due to spectral leakage.

It is important that the whole transient event is captured and also that it has decayed completely before the steady state measurement. For this reason eight supply cycles of data were chosen. This provided a frequency resolution of 6.25Hz. The current disturbance for this technique is of a very short duration with the consequent voltage disturbance also likely to be short lived unless the response of the system is particularly oscillatory.

After the transient decay is completed the rest of the data record may be considered as *zero padding* unless, of course, the steady state cancellation wasn't successful. Zero padding is the section of the transient data recorded after the system response has decayed to zero, or is so small that the signal noise dominates the data. No further information is contained in this *padding* although by recording it the resolution of the FFT will be affected. In this situation steady state harmonics will remain with the same effect apart from at harmonic frequencies where errors will be present. Zero padding will not actually improve the resolution of the calculated spectrum, although it may give this impression. Zero padding will smooth the spectrum by interpolation [59] [76]. It may be useful to reduce ambiguities due to a lack of spectral resolution and it will allow for more accurate identification of peaks and troughs in a spectrum.

In order to further reduce the effects of spectral leakage a PLL could be considered, as suggested in section 4.6.2. This solution was ruled out due to the additional experimental complication. Alternatively a spectral window could be applied. The disadvantage of this approach lies in the fact that the measurement data is attenuated to zero at the edges of the sampled window. This firstly reduces the effective signal injection. Consequently the transient injection position must be moved to the centre of the sampled window or else it will be severely attenuated. A possible window implementation is shown in figure 4.7.

To achieve the same frequency resolution it can be seen that the total measurement time is 1.5 times greater than for the first option considered. As a result this method was rejected.

A digitally implemented approximation to the PLL was implemented. Data was captured using the initial scheme described and shown in figure 4.6. Once the data was captured

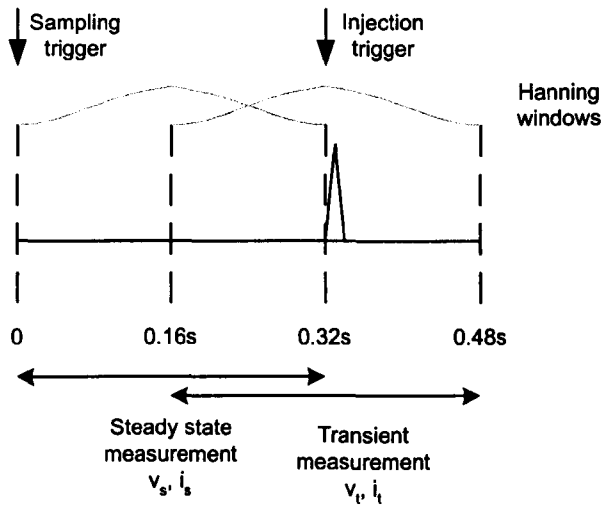

Figure 4.7: Option 2 sampling arrangement

a pre-processing algorithm was applied to ensure that steady state cancellation was effectively carried out.

Initially assuming a 50Hz fundamental supply, the phase of the fundamental supply for the 8th and 16th cycles were calculated using a simple FFT routine on each section, θ_8 and θ_{16} respectively. The phase difference was then used in order to calculate the actual fundamental frequency, equation 4.10

$$2\pi(\delta f)\left(\frac{8 \times 1023.02}{51.151 \times 10^3}\right) = \theta_{16} - \theta_8 \tag{4.10}$$

For this method to succeed the transient response must have decayed completely by the start of the 8'th cycle of data used. It was then possible to relocate the start position of the steady state data section, for both the voltage and current signals, in order to achieve maximum steady state cancellation. The rest of the analysis was completed as for the basic rectangular window method assuming a fundamental frequency of 50Hz. This did not result in significant inaccuracy as the frequency error is very small compared to the frequency resolution. This technique enabled very good cancellation using very little extra processing time.

4.8 Medium term injection signal processing

The same data acquisition system was used to validate the medium term injection technique. The sampling rate and number of samples used were the same as for the short term injection. The medium term injection provides an active disturbance throughout the entire eight recorded cycles of transient data. Therefore it was possible to use a Hanning window in order to reduce the level of spectral leakage. The window was applied to the current signal i and the voltage signal v after steady state cancellation. This windowing procedure lessens the effect of spectral leakage at the expense of frequency resolution which must be accounted for during the interpolation or curve fitting routines. In the short term case all points were discarded that lie at harmonic frequencies whereas in the medium term case the adjacent points should also be discarded.

Figure 4.8 demonstrates the leakage for a sinusoidal 50.1Hz signal. Although the percentage leakage is small in both cases it is sufficient to cause a large impedance error. With the Hanning window applied the lobe at 50Hz is widened but the amount of leakage is drastically reduced.

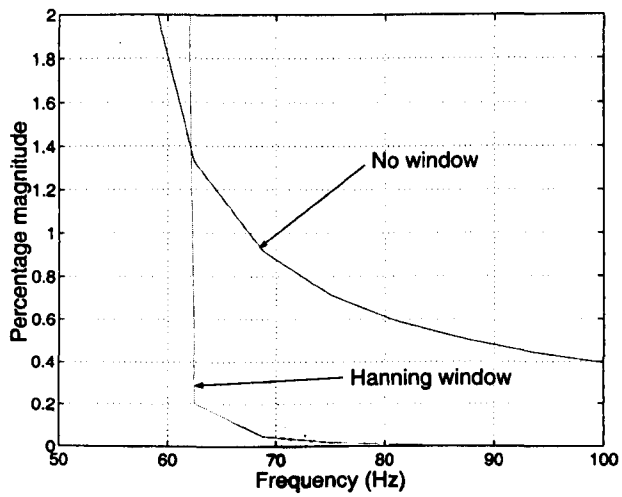

Figure 4.8: Spectral leakage from a 50.1Hz sinusoid

4.9 Estimating the transfer function from impedance versus frequency values

This is the final processing stage required for the calculation of a single phase impedance transfer function. If a graphical representation of impedance is required without a transfer function then this stage may be omitted.

On completion of a transient injection, using either of the techniques, a series of impedance values will be calculated at frequency points between d.c. and the maximum frequency of interest, 1kHz for this application. The impedance values will be spaced at intervals of 6.25Hz, 160 impedance points in all. An s-domain transfer function may be estimated from this data using a suitable algorithm. The algorithm chosen for this complex curve fit is a damped Gauss-Newton least squares formulation, detailed extensively in [81] and [82], and explained at the end of this section.

The curve fitting algorithm requires a series of complex impedance values and corresponding measurement frequencies. In addition the order of both the numerator and denominator of the s-domain transfer function must be specified. These are specified as n and d respectively. The output form of the curve fitting algorithm is in a Pade form shown in equation 4.11. The values of $(B_0 \dots B_n)$ and $(A_0 \dots A_{d-1})$ are automatically constrained to be real and the transfer function (impedance) will be stable.

$$Z(s) = \frac{B(s)}{A(s)} = \frac{B_n s^n + B_{n-1} s^{n-1} + \cdots + B_1 s + B_0}{s^d + A_{d-1} s^{d-1} + \cdots + A_1 s + A_0} \tag{4.11}$$

Only some of the impedance values initially calculated should be passed to the curve fitting algorithm. Initially all data calculated at harmonic frequencies should be discarded for reasons previously discussed. 140 points still remain in the range up to 1kHz. For a low order system $(n, d < 8)$ 140 points is superfluous and will result in unnecessary calculation delay.

In the short term injection case a good curve fit may be achieved using only the interharmonic points spaced evenly between the harmonic frequencies, that is, points that lie at frequencies of $(25(2n+1) \quad , 0 \leq n \leq 19)$. These points are less susceptible to spectral leakage than any others and so will provide the best basis for the transfer function estimate. There are 20 such impedance values available. Using only 20 values will have the advantage of dramatically reducing the computation time taken during this process.

In the medium term injection case it is unwise to use the same points as the midpoints between each harmonic frequency are points at which the ideal injection strength is zero, see figure 4.4. The windowing method used for the medium term injection will smooth the response at these frequencies but errors at these points are still greater than for neighbouring points. Therefore the neighbouring points above each midpoint frequency value were chosen: $(25(2n+1)+6.25 \quad , 0 \leq n \leq 19)$.

The chosen impedance values, $(h(1) \ldots h(n)$, and the corresponding frequencies, $(\omega(1) \ldots \omega(n))$, are passed to the algorithm along with values for the transfer function order, n and d. The algorithm is an iterative procedure that aims to minimize the squared error between the input impedance values and the values generated from equation 4.11. This is shown in equation 4.12.

$$\underset{B_k, A_k}{min} \sum_{k=1}^{n} \left| h(k) - \frac{B(\omega(k))}{A(\omega(k))} \right|^2 \tag{4.12}$$

If the iterative procedure cannot converge then the values for n, d or both n and d should be changed. The algorithm has successfully converged with all data used in this project although if this is not always the case then it is a simple matter to automatically vary the system order for convergence. For practical purposes the values of n and d may be set so that the fitted impedance function has an order greater than or equal to the highest order expected. This will not adversely affect the iterative process as has been found with other curve fitting schemes such as the Prony method [78]. Finally, it is also possible to weight the different impedance values so that some provide more influence than others. This has

not been done although it may be possible to weight the impedance values depending on the injection strength at that frequency so as to give more weight to those values with a higher signal to noise ratio.

4.10 Generalized measurement approach

A general approach for impedance measurement in three phase circuits is described in this section that is applicable to both techniques.

An arbitrary measurement injection will be assumed at each frequency f. I_{Mf1} denotes the current injection at this frequency, f, into phase 1, I_{Mf2} for phase 2 and I_{Mf3} for phase 3. It is assumed that no steady state current or voltage components are present at any values of f chosen. The measurement of three phase three wire systems is the prime aim of this work although the described methods are easily transferred to unbalanced systems and to single phase systems. The unbalanced case is initially considered and then simplified when further assumptions become possible due to the nature of the system.

Equation 4.13 shows a generalized equation relating the phase voltage and current in an unbalanced three phase network in terms of a (3×3) impedance matrix.

$$\begin{pmatrix} v_1 \\ v_2 \\ v_3 \end{pmatrix} = \begin{pmatrix} Z_{11} & Z_{12} & Z_{13} \\ Z_{21} & Z_{22} & Z_{23} \\ Z_{31} & Z_{32} & Z_{33} \end{pmatrix} \begin{pmatrix} i_1 \\ i_2 \\ i_3 \end{pmatrix} \tag{4.13}$$

This equation is given for a particular value of frequency. Such an equation exists at all frequencies with the coefficients of the impedance matrix varying with frequency. An alternative impedance relationship may be defined relating line voltages and currents, equation 4.14. This form will be predominantly used in this work due to the absence of a neutral conductor. Tilde $\tilde{Z}$ notation is used for this relationship in order to differentiate the

impedance matrices in equations 4.13 and 4.14.

$$\begin{pmatrix} v_{12} \\ v_{23} \\ v_{31} \end{pmatrix} = \begin{pmatrix} \tilde{Z}_{11} & \tilde{Z}_{12} & \tilde{Z}_{13} \\ \tilde{Z}_{21} & \tilde{Z}_{22} & \tilde{Z}_{23} \\ \tilde{Z}_{31} & \tilde{Z}_{32} & \tilde{Z}_{33} \end{pmatrix} \begin{pmatrix} i_1 \\ i_2 \\ i_3 \end{pmatrix} \tag{4.14}$$

Only six independent impedance variables are in fact present in equation 4.13 as the mutual coupling between phases is the same irrespective of the direction of measurement,$Z_{12} = Z_{21}$, $Z_{13} = Z_{31}$ and $Z_{23} = Z_{32}$. The same is not true of equation 4.14. Appendix A contains transformation matrices that may be used to convert impedance terms between these systems.

The aim of an impedance measurement technique is to identify all the coefficients of the impedance matrices. This is accomplished using measurements of phase, or line, voltage and current measurements. Most impedance measurement work to date has either considered single phase systems or else certain assumptions have been made concerning the supply network impedance values.

If it is possible to measure all three phase voltages and currents then it is possible to measure all the elements of the impedance matrix using multiple transient events. Nagpal et al. [54] considered the measurement of the entire impedance matrix using capacitor bank switching events. Three independent transient events are required for it to be possible to calculate all nine impedance coefficients. A generalized approach for this measurement shall be described. Simplifications to the method will then be described under the assumption of a balanced supply impedance.

4.10.1 Unbalanced system

The work in this thesis is primarily concerned with three phase three wire systems. The impedance relationship shown in equation 4.14 is adopted as line to line voltage measurements are readily available.

Each row of equation 4.14 may be considered in turn. The first row is shown in equation 4.15 for one frequency.

$$v_{12} = \tilde{Z}_{11} i_1 + \tilde{Z}_{12} i_2 + \tilde{Z}_{13} i_3 \tag{4.15}$$

A determined set of 3 linearly independent equations of this form are required in order to solve the set of simultaneous equations for $\tilde{Z}_{11}$, $\tilde{Z}_{12}$ and $\tilde{Z}_{13}$ [83]. Measurements must be made for v_{12}, i_1, i_2 and i_3 over three transient switching operations. The set of equations formed can be expressed in matrix form, as in equation 4.16 at each particular frequency of interest. Superscript notation labels each set of transient data.

$$\begin{pmatrix} v'_{12} \\ v''_{12} \\ v'''_{12} \end{pmatrix} = \begin{pmatrix} i'_1 & i'_2 & i'_3 \\ i''_1 & i''_2 & i''_3 \\ i'''_1 & i'''_2 & i'''_3 \end{pmatrix} \begin{pmatrix} \tilde{Z}_{11} \\ \tilde{Z}_{12} \\ \tilde{Z}_{13} \end{pmatrix} \tag{4.16}$$

To calculate values for the three impedance terms the matrix of current measurements must be inverted. This matrix should be well-conditioned[83] for computational accuracy.

The chosen injection procedure is applied three times in total so as to allow a set of determined equations to be constructed. In order to achieve such a set of equations it is necessary to apply sufficiently different current injection into each phase for accurate measurement of the differences in voltage and current in each phase to be identified. A procedure shall be described that will achieve these aims while not affecting the ASF operation unduly. There are many possible variations but all are similarly constrained.

To identify an unbalanced impedance it is necessary to apply an unbalanced current injection measurement. Therefore $I_{Mf1} + I_{Mf2} + I_{Mf3} \neq 0$. This will affect the d.c. link voltage level and will disturb the d.c. link controller. This effect should be minimized if possible. The harmonic current controllers will also be disturbed by current injection at the compensation frequencies, this disturbance can only be reduced by reducing the injection strength at these frequencies. Table 4.10.1 shows three injection transients that may be used to construct equation 4.16 as multiples of a base quantity current, I_{Mf}. As the actual injection current is applied in an open loop manner it is impossible to absolutely ensure the current strength relationships shown in table 4.10.1. This is not a problem as the injected

Phase current	$\frac{i1}{I_M}$	$\frac{i2}{I_M}$	$\frac{i3}{I_M}$
Transient 1	2	-1	0
Transient 2	0	2	-1
Transient 3	-1	0	2

Table 4.1: Injection pattern for well-conditioned matrix

waveforms are measured. As long as the relative injection strengths approximate the form shown a well-conditioned set of equations shall be formed.

The transient injections should be applied in quick succession, assuming that the applied transients are given sufficient time to decay completely, so that the measured impedance remains constant. As each injection is unbalanced the d.c. link voltage will be affected. The d.c. link controller has a low bandwidth and so will be unable to control the d.c. link voltage in this time frame. Once all three transients have been applied the net current will be zero and so the d.c. link voltage should be unaffected by the measurement procedure.

The three impedances may now be calculated by inverting the 3×3 matrix,as in equation 4.17. The current waveforms are individually measured so the form will not be exactly that shown in equation 4.17. Assuming the ASF control delivers this injection approximately then there should be no calculation problems due to an ill-conditioned matrix.

$$\begin{pmatrix} \tilde{Z}_{11} \\ \tilde{Z}_{12} \\ \tilde{Z}_{13} \end{pmatrix} = \frac{1}{2I_M} \begin{pmatrix} 2 & -1 & 1 \\ 2 & -2 & 2 \\ 4 & -4 & 2 \end{pmatrix} \begin{pmatrix} V_{12}^1 \\ V_{12}^2 \\ V_{12}^3 \end{pmatrix} \tag{4.17}$$

This process may be repeated for the other 6 impedance terms required to completely characterize the impedance of the network at that frequency. If all six currents and voltages are recorded for the three transients described in this section then the same data may be used in order to calculate the other impedance terms. Therefore three transient data records are required in order to calculate all nine impedance terms. If additional data for transients is

available then a least squares solution may be used in order to improve accuracy. If the impedance matrix is required in terms of phase voltages instead of line voltages then the transformation given in appendix A may be applied.

4.10.2 Balanced system

In this section the impedance of the network is assumed to be balanced. The impedance matrix **Z** may be rewritten as in equation 4.18. Z_s and Z_M are used to define the self and mutual impedances respectively. This equation is defined in terms of phase voltages.

$$\begin{pmatrix} v_1 \\ v_2 \\ v_3 \end{pmatrix} = \begin{pmatrix} Z_s & Z_M & Z_M \\ Z_M & Z_s & Z_M \\ Z_M & Z_M & Z_s \end{pmatrix} \begin{pmatrix} i_1 \\ i_2 \\ i_3 \end{pmatrix} \tag{4.18}$$

If equation 4.18 is considered in terms of symmetrical components [84] the positive and negative sequence impedance are equivalent and equal to $(Z_s - Z_M)$. As the system has no neutral wire the zero sequence circuit becomes an open circuit. For all practical purposes the system can be reconsidered as having three identical self impedance terms and no mutual impedance terms, the impedance is thus redefined in equation 4.19 substituting Z for $(Z_s - Z_M)$

$$\begin{pmatrix} v_1 \\ v_2 \\ v_3 \end{pmatrix} = \begin{pmatrix} Z & 0 & 0 \\ 0 & Z & 0 \\ 0 & 0 & Z \end{pmatrix} \begin{pmatrix} i_1 \\ i_2 \\ i_3 \end{pmatrix} \tag{4.19}$$

If the network being measured is balanced, or is a close approximation, then several simplifications to the experimental system may be made. The main advantage being that it

is possible to calculate the required impedance using only one current transducer and one voltage transducer with a single transient event.

Consider the Thevenin equivalent of the supply impedance to be measured in figure 4.9. Steady state measurements have been subtracted from the transient measurement in order to remove the supply voltage and harmonics and the process is considered for one frequency point. The transient injection current is I_M in phase 1 and $\frac{-I_M}{2}$ in both phases 2 and 3. A balanced injection was hence provided that should not disturb the d.c. link voltage level.

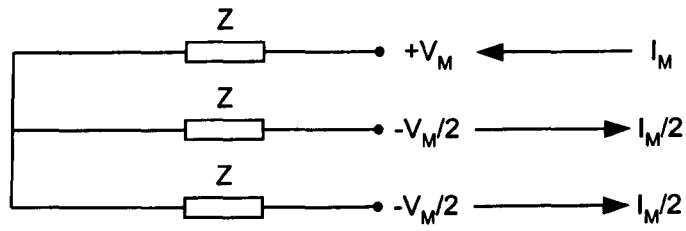

Figure 4.9: Balanced three phase system transient

The circuit shown in figure 4.9 may be redrawn as a single phase equivalent circuit as in figure 4.10. The measurement data from a transient injection is thus stored as a single voltage and current transient, as in the single phase equivalent, figure 4.10. In order to transform the measured impedance into a per phase value it is necessary to scale the measured impedance by a factor of $\frac{2}{3}$.

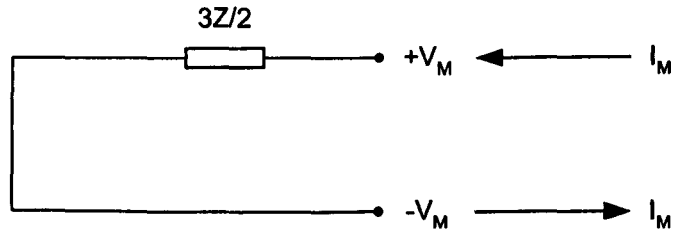

Figure 4.10: Single phase equivalent transient

Care must be taken if calculating component values from the single phase equivalent data. As an example consider the circuit shown in figure 4.11(a). This is transformed into the

single phase equivalent shown in 4.11(b). In this case the capacitors are connected in delta and are of value C in the three phase figure. These are transformed to a capacitor of value 2C in the single phase equivalent. In order to use the conversion factor of $\frac{2}{3}$ it is necessary to transform the impedance into a star connected Thevenin equivalent first.

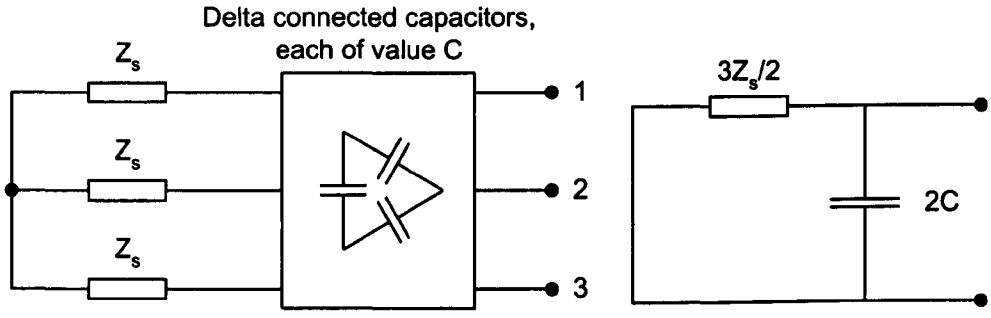

(a) Three phase system (b) Single phase equivalent

Figure 4.11: Example three phase system and equivalent single phase system

This section has described a generalized approach to impedance measurement for an unbalanced three phase three wire system. It was shown that the requirements for the measurement in the case of a balanced system were greatly reduced. The requirements for impedance measurement in a balanced three wire system are the same as the requirements for the measurement of system impedance in a single phase system hence the method is directly applicable to the single phase situation. If the network in question is a three phase four wire balanced system the zero sequence impedance is $(Z_s + 2Z_M)$ in relation to equation 4.18. If the zero sequence impedance is required it is necessary to adopt the approach of section 4.10.1. In this case it is necessary to separately identify the self and mutual impedance terms in order to calculate the zero sequence impedance. Finally, in the case of an unbalanced three phase four wire system the unbalanced approach, section 4.10.1, must again be used.

All experimental work has been focused on the measurement of the supply impedance in the three phase three wire scenario. If this measurement is possible then the unbalanced case should prove to be possible from the outlined method described in this section.

4.11 Practical implementation of injection techniques

The experimental platform for impedance measurement is fully described in chapter 3. Figure 4.12 shows the basic ASF circuitry parameters.

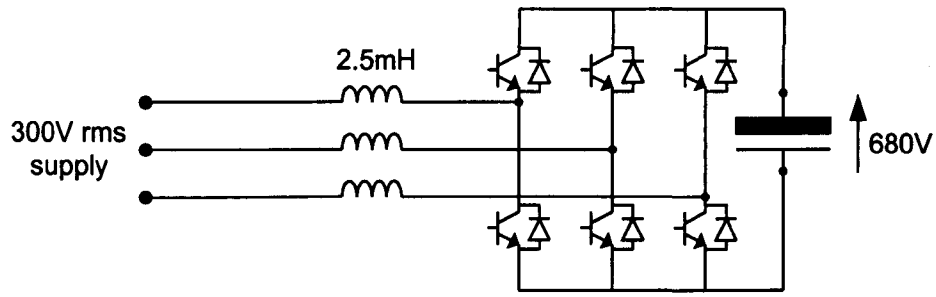

Figure 4.12: Active shunt filter for current injection

4.11.1 Short term injection

The width of the injected pulse is constrained by the sampling frequency of the ASF controller. The ASF sampling frequency is 8kHz which corresponds to a sampling interval that is fixed at 125μs. The total pulse width was chosen to be six sampling intervals, that is, a pulse rise time of 375μs and a decay time of 375μs. In the practical measurement circuit the line inductors limit the rate of rise and fall of injected current. Therefore by reducing the pulse width, in an attempt to increase measurement bandwidth, the peak injected current will fall. This will reduce the effective bandwidth of the system. A compromise was reached with the values shown. The parameters may be varied if the injection level is too high and is hindering the normal network operation. Alternatively the injection pulse width may be increased to increase the injection level if a higher SNR is required.

The injection is an open loop addition to the voltage output as the controller bandwidth is insufficient to provide control. During the injection process the ASF control scheme continues to operate, the control bandwidth is such that very little attenuation of the injected signal will occur. Both the voltage and current disturbances are measured so even if there is

a significant interaction this will not affect the accuracy of the results although the injected signal may be reduced about the 5th and 7th harmonic leading to a lower injection strength and decreased SNR at these points. It should also be noted that the PWM output of the inverter will also affect the shape of the injection pulse and will make it further removed from the ideal case described.

The d.c. link voltage is controlled about a reference value of 680V and the line-line voltage of the supply fundamental is approximately 300V rms (approx. 460V peak). The maximum injection voltage is limited by the difference between the voltages either side of the line inductors. For a balanced three phase system it is important that the applied injection voltage on phases 2 and 3 is as close as possible. Otherwise the assumptions made in section 4.10.2 will not be true, resulting in an incorrect impedance estimate. The ASF output voltage reference should not exceed the maximum PWM output voltage possible. If a reference greater than this is used then PWM saturation will occur, that is, the PWM voltage will be limited by the maximum pulse width allowed and the output voltage will not faithfully output the reference voltage at the PWM input. It is particularly important that this is observed on phases 2 and 3.

The optimum short term injection time was chosen when ($V_{23} = 0$) although measurements are possible commencing at any other point in the cycle as long the PWM is not saturated. At this point the inverter output to both these phases will clearly be equal and any non-linearity in the PWM calculation or inverter switching will be minimized.

4.11.2 Medium term injection

The same applied voltage constraints are applied to the medium term voltage injection. As the injection duration spans several fundamental cycles the start time of the injection is not important.

4.12 Simulation work

All simulation work carried out using a single phase system, although, it is directly applicable to the balanced three phase case. Two test circuits have been used for demonstration purposes, these are termed test model 1 and 2 and are shown in figures 4.13(a) and (b). Test model 1 is a simple LR supply. This was chosen as it will approximate the impedance of many supplies, where Z_s is dominated by the connection transformer. Due to the lack of oscillatory response on current disturbance, the estimated impedance for this model will be the 'worst case scenario' for both injection methods. The second model has power factor correction (PFC) capacitors connected to the original model. Identification is expected to be superior, especially for the short term injection, as the transient response is of a longer duration and will contain more information for the identification algorithms.

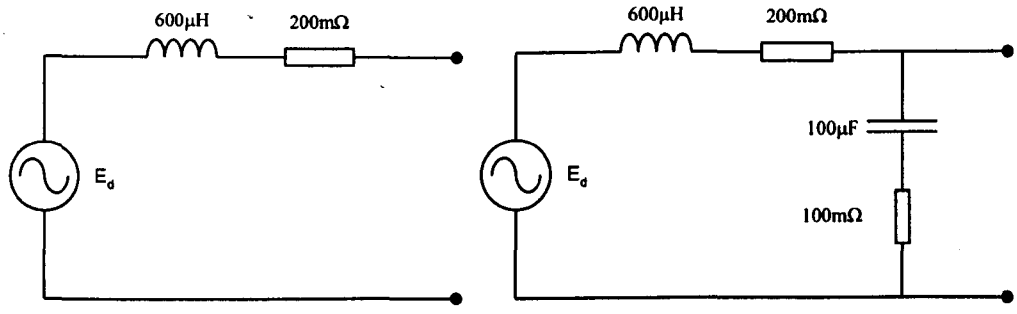

(a) Test model 1 (b) Test model 2

Figure 4.13: Simulation supply models

The *Power System Blockset* in SIMULINK was used to execute the simulations. The overall schematic is shown in figure 4.14. This was used for both the short and medium term injections with appropriate changes made to the injection and data processing units. The full schematics for this simulation are shown in appendix B.

A single phase inverter was simulated with a single current controller with zero reference. In the steady state voltage matching is achieved and zero mean current flows between the ASF and the supply. Simulation parameters are given in table 4.2.

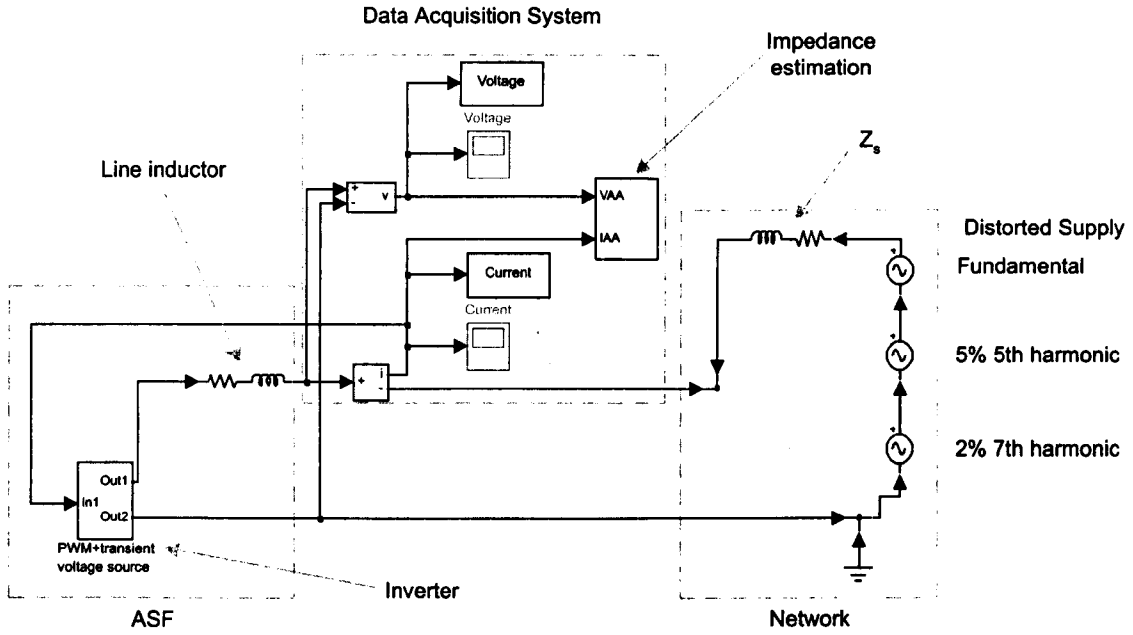

Figure 4.14: Simulation system for supply model 1

Fifth and Seventh harmonic voltage distortion was included in the simulation. This level of distortion was used as this level was found to be present on the laboratory supply.

Four simulation results are shown for each injection method to illustrate various features. Four figures are shown for each example simulation, these are:

- (a). Current transient after cancellation of steady state current. The ASF current controller was supplied with a zero reference. The mean steady state measured current is therefore zero although switching frequency current will be present due to the PWM output.
- (b). Voltage transient after cancellation of steady state voltage. The transient information before cancellation is dominated by the supply voltage, the success of this cancellation step is apparent in this figure for each situation.
- (c). The real part of the estimated impedance.
- (d). The imaginary part of the estimated impedance.

Parameter	Value
Fundamental supply voltage	170V (rms)
5'th harmonic supply voltage	8.5V (rms)
7'th harmonic supply voltage	3.4V (rms)
d.c. link voltage	680V
Switching frequency	4kHz
Line inductance	2.5mH

Table 4.2: Simulation Parameters

Normally distributed additive noise was applied to the measured current and voltage signals in some of the simulations. These are clearly labelled as such. The noise applied to each channel had zero mean and the variance was calculated so that the magnitude of the noise was equivalent to the 12 bit A/D level on each channel ($\approx$95% confidence level).

4.12.1 Short term injection simulations

Simulation 1

The first simulation conducted used ideal simulation conditions. Supply model 1 was used. A sampling frequency of exactly 51.2kHz was used with a 50Hz supply frequency to ensure no spectral leakage at all. No noise was applied to the measurement transducers. Perfect cancellation is achieved in the time domain without any switching frequency components present. The imaginary impedance estimate is virtually identical to the ideal supply imaginary part. Some error is present on the graph showing the real part of the impedance. As a fraction of the impedance magnitude the error is very small although as a fraction of the real part the error is significant. This error is due to quantization introduced by the A/D convertors and truncation error introduced in the estimation calculation. This illustrates how sensitive the calculation can be when using a low injection strength and a very short duration disturbance.

Simulation 2

The first simulation was repeated with alterations made to the sampling frequency and noise content of the measured signals, again using supply model 1. The sampling frequency was changed to the actual experimental value used, 51.151kHz. Additive noise, as described above, was also applied to the measured signals at the transducer inputs. The preprocessing cancellation algorithm for the short term injection method was applied before estimating the impedance. Finally the curve fitting algorithm was applied to the estimated impedance data.

In this case excellent imaginary impedance estimation is achieved again although some random noise is apparent throughout the frequency range. A large error may also be seen due to non-ideal cancellation at 50Hz. Good estimation of the real impedance was achieved with errors again due to random noise and non-ideal cancellation, visible for the fundamental and fifth and seventh harmonics. This simulation clearly illustrates the importance of steady state cancellation. In the time domain figures the steady state components are barely

visible and yet they significantly affect the impedance estimate at these frequencies.

The red crosses in the impedance figures show the values used by the curve fitting algorithm. These have successfully been chosen so as not to be affected by the errors present at the supply harmonic frequencies. The curve fitting algorithm was used to derive a transfer function and from this the red line has been plotted showing that the algorithm has identified the supply impedance very accurately.

Simulation 3

The second simulation was repeated with a supply frequency of 50.1Hz. Supply model 1 was used. Supply frequency deviations have been recorded with a 0.1Hz deviation although such a deviation is probably the largest that will be encountered in the practical experimentation.

The pre-processing algorithm to reduce spectral leakage was required to shift the position of the transient data by 16 samples, relative to the steady state data, in order to achieve optimum cancellation. As a consequence some switching frequency components are present although these should not affect the estimate as they are centred about 4kHz.

To illustrate the importance of optimum cancellation another line has been plotted. Steady state cancellation was still applied in this case although the pre-processing data shifting was not applied. This is shown as a magenta coloured trace. The effects of spectral leakage are clearly present and are shown to detrimentally affect the impedance estimate not only at supply harmonic frequencies but at the surrounding frequencies also. It is not possible to estimate the impedance accurately between the fifth and seventh harmonics at all, hence whole sections of the frequency range become invalid.

The curve fitting algorithm was again successfully applied to the impedance estimate calculated with correct steady state cancellation.

Simulation 4

The final simulation was repeated with the same parameters as simulation 3 although in

this case supply model 2 was used.

The transient response for this circuit could be measured for a much longer duration when compared to the first supply model. Therefore the resulting impedance estimate is greatly improved. Slight errors still remain at the supply frequencies from remaining steady state supply components. The impedance estimate also exhibits slight errors about the resonant frequency although the actual resonant frequency is identified very well.

The curve fitting algorithm was applied again with excellent results.

Short term injection simulation results

The figures for the short term simulations are shown over the next four pages.

Blue	Measured data for the time domain plots, after steady state cancellation.
Blue	Impedance estimates prior to curve fitting in frequency domain plots.
Green	Ideal impedance lines calculated from the supply transfer function
Red crosses	Raw data used for curve fitting
Red	Impedance estimate generated from the curve fitting algorithm.
Magenta	Impedance estimate calculated without spectral leakage reduction.

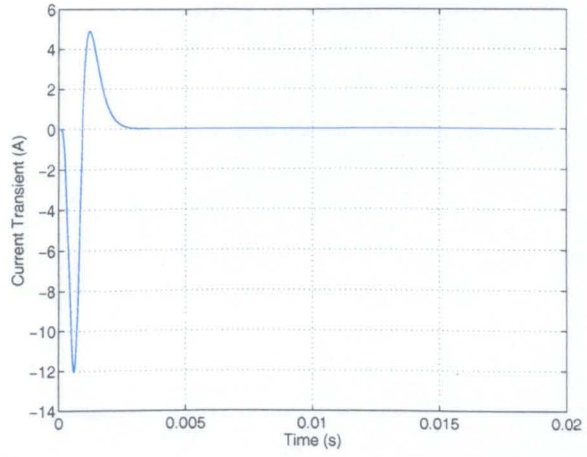

(b) Current signal after cancellation

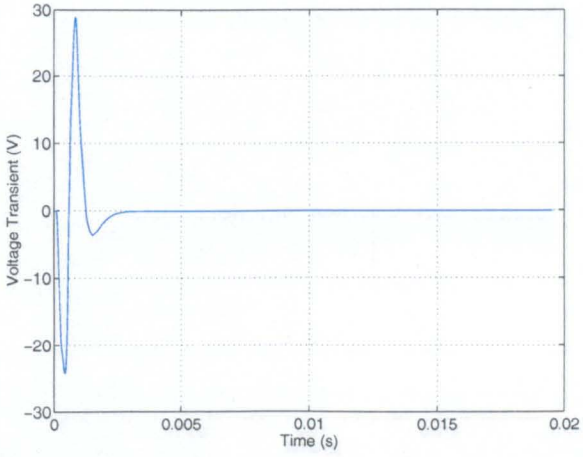

(c) Voltage signal after cancellation

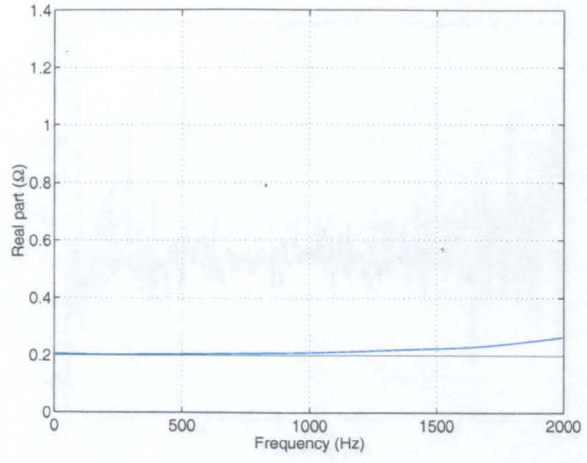

(d) Estimated impedance (real)

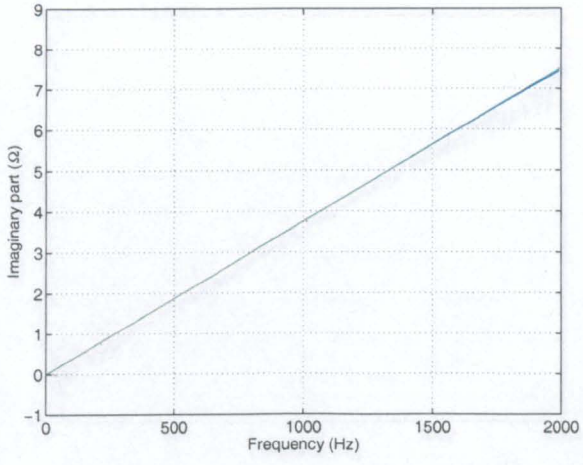

(e) Estimated impedance (imaginary)

Figure 4.15: Simulation 1. Ideal simulation conditions: no measurement noise and perfect steady state cancellation

Blue	Measured data for the time domain plots, after steady state cancellation.
Blue	Impedance estimates prior to curve fitting in frequency domain plots.
Green	Ideal impedance lines calculated from the supply transfer function
Red crosses	Raw data used for curve fitting
Red	Impedance estimate generated from the curve fitting algorithm.
Magenta	Impedance estimate calculated without spectral leakage reduction.

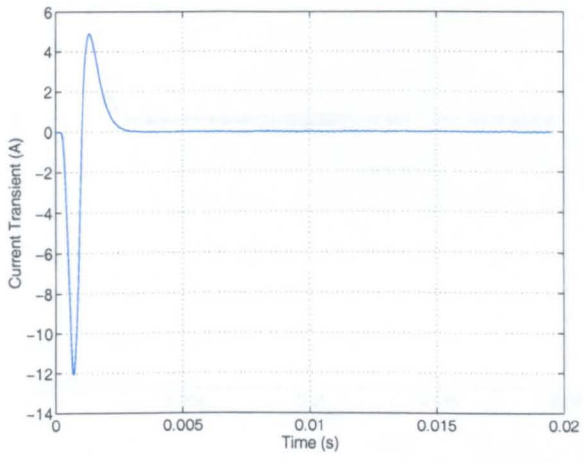

(b) Current signal after cancellation

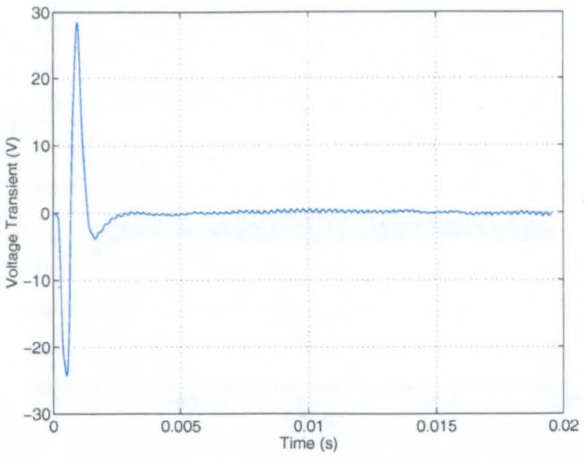

(c) Voltage signal after cancellation

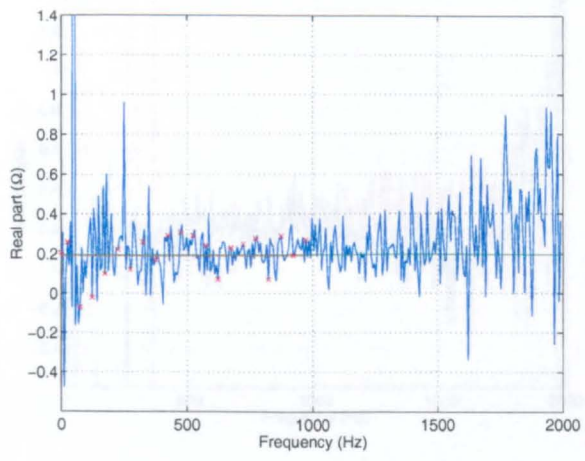

(d) Estimated impedance (real)

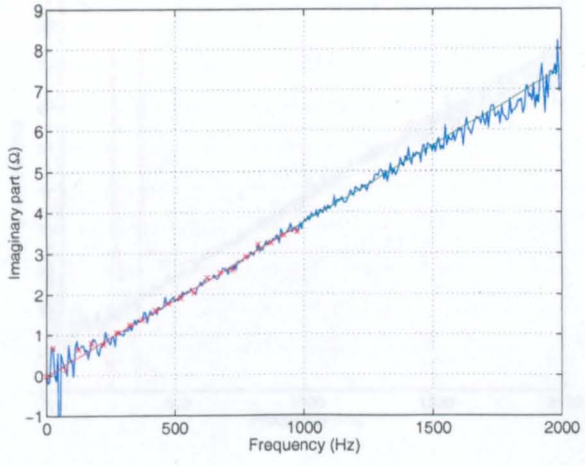

(e) Estimated impedance (imaginary)

Figure 4.16: Simulation 2. 51.151kHz experimental sampling frequency and additive measurement noise used

Blue	Measured data for the time domain plots, after steady state cancellation.
Blue	Impedance estimates prior to curve fitting in frequency domain plots.
Green	Ideal impedance lines calculated from the supply transfer function
Red crosses	Raw data used for curve fitting
Red	Impedance estimate generated from the curve fitting algorithm.
Magenta	Impedance estimate calculated without spectral leakage reduction.

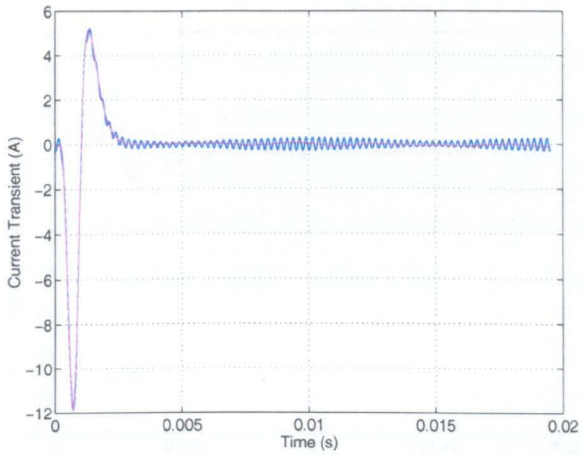

(b) Current signal after cancellation

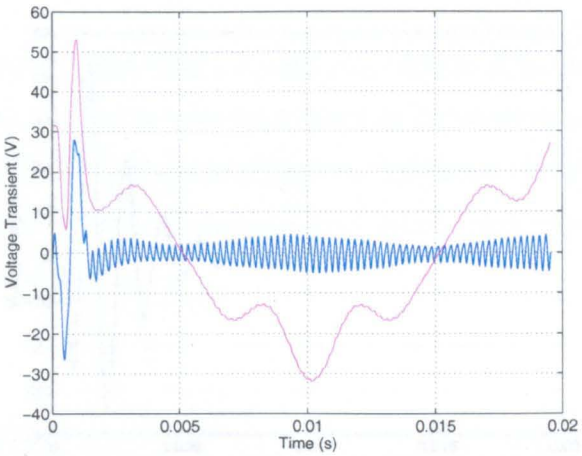

(c) Voltage signal after cancellation

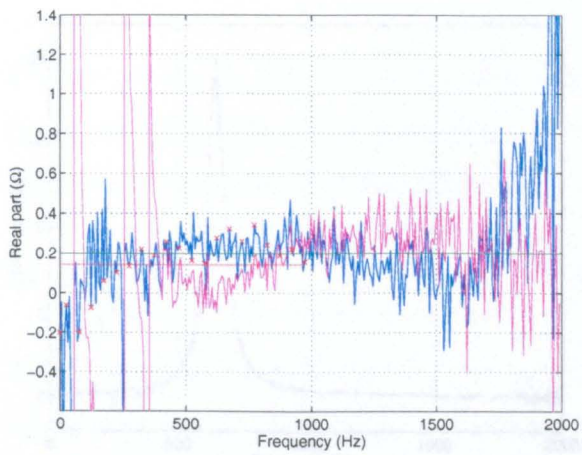

(d) Estimated impedance (real)

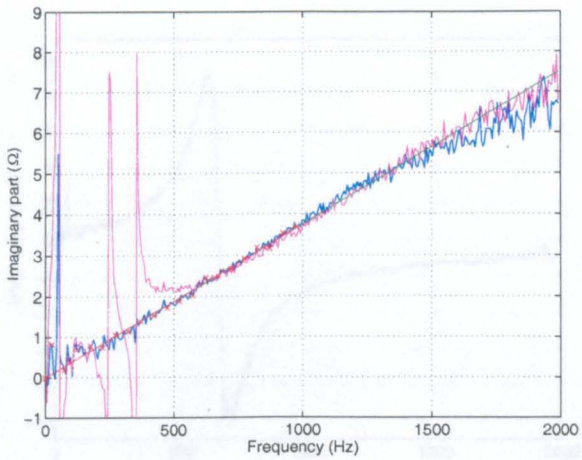

(e) Estimated impedance (imaginary)

Figure 4.17: Simulation 3. 51.151kHz experimental sampling frequency and additive measurement noise used. 50.1Hz supply frequency. Results shown with and without preprocessing

Blue	Measured data for the time domain plots, after steady state cancellation.
Blue	Impedance estimates prior to curve fitting in frequency domain plots.
Green	Ideal impedance lines calculated from the supply transfer function
Red crosses	Raw data used for curve fitting
Red	Impedance estimate generated from the curve fitting algorithm.
Magenta	Impedance estimate calculated without spectral leakage reduction.

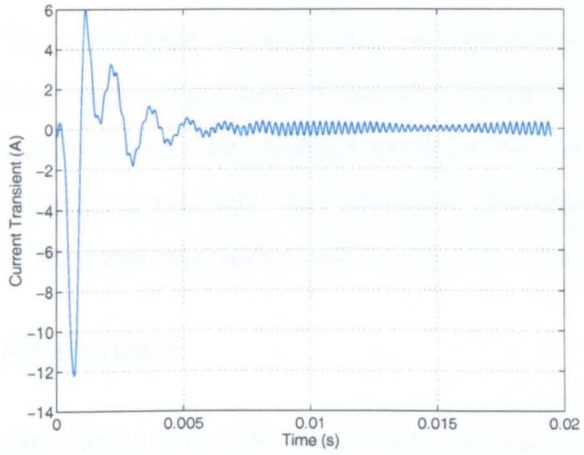

(b) Current signal after cancellation

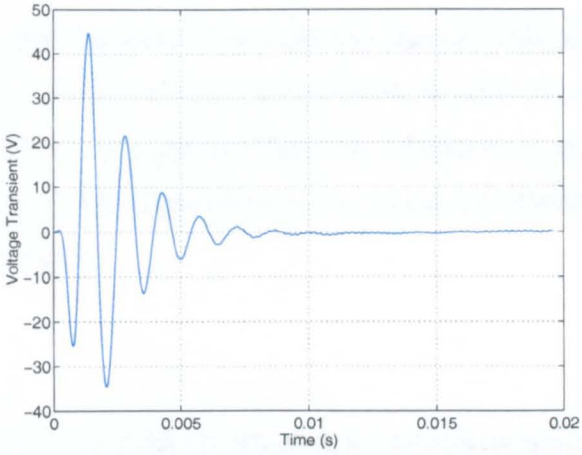

(c) Voltage signal after cancellation

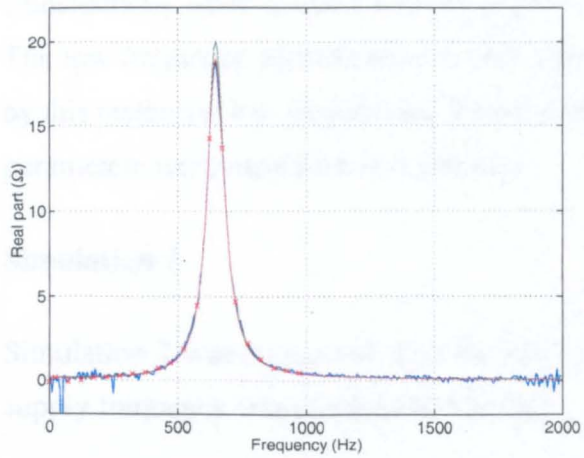

(d) Estimated impedance (real)

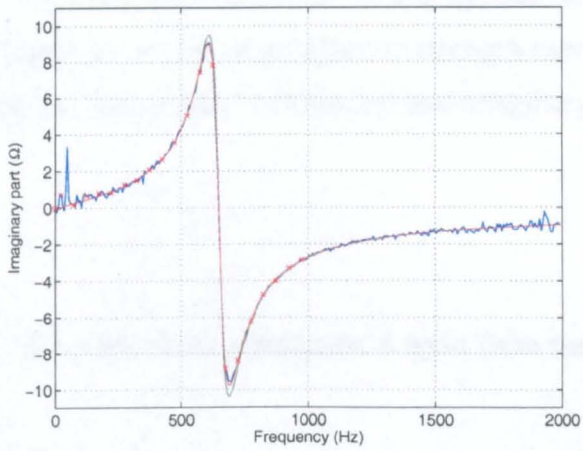

(e) Estimated impedance (imaginary)

Figure 4.18: Simulation 4. Supply model 2. 51.151kHz experimental sampling frequency and additive measurement noise used. 50.1Hz supply frequency

4.12.2 Medium term injection simulations

Simulation 5

The first simulation conducted using the medium term injection method was for the ideal case. Supply model 1 was used. A sampling rate of 51.2kHz was used with a 50Hz supply and without a noise source on either the current or voltage channel.

The impedance results in this case show some deviation from the ideal impedance. This error is due to the action of the current controller. This error was not evident in the short term simulations as the injection duration was so short. It is random ~~random~~ influence on the impedance estimate. The estimated impedance in this case shows a very good correlation to the ideal impedance, especially at low frequencies.

Simulation 6

Simulation 6 uses the actual sampling rate used, 51.151kHz, in addition to transducer noise components. Supply model 1 was used.

Considerably more random noise is present in the impedance estimates for this simulation. The low frequency identification is still very good due to the large injection strength used by this method at low frequencies. Curve fitting was successful, both the real and imaginary parameters were identified very closely.

Simulation 7

Simulation 7 was conducted with the same parameters as for simulation 6 apart from the supply frequency was changed to 50.1Hz.

The medium term injection reduces the effects of spectral leakage by applying a Hanning window to the measured data after steady state cancellation. For comparison the impedance has also been estimated without the windowing procedure, these results are shown in figures4.22(a) and (b). These clearly show that it is essential to apply the window

with this technique.

The transient voltage signal contains steady state supply components that are present because the supply frequency is not 50Hz. As a result the impedance values at these frequencies are corrupted. The figures show that these are discarded by the curve fitting routine.

Simulation 8, supply model 1

The final medium term injection simulation uses the second supply model. All other parameters are the same as for simulation 7.

The match between estimated impedance and the ideal values is again excellent. Significant errors are still present at the supply frequencies but influence of these errors is very restricted.

Medium term injection simulation results

The figures for the medium term simulations are shown over the next four pages.

Blue	Measured data for the time domain plots, after steady state cancellation.
Blue	Impedance estimates prior to curve fitting in frequency domain plots.
Green	Ideal impedance lines calculated from the supply transfer function
Red crosses	Raw data used for curve fitting
Red	Impedance estimate generated from the curve fitting algorithm.
Magenta	Impedance estimate calculated without spectral leakage reduction.

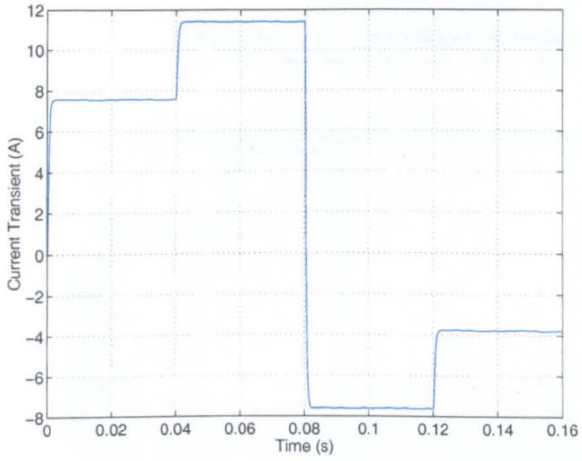

(b) Current signal after cancellation

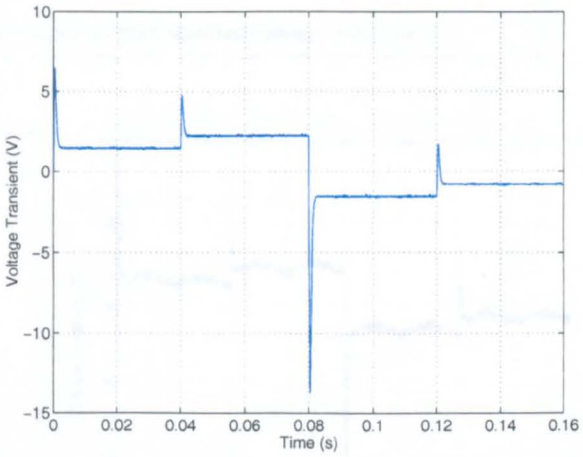

(c) Voltage signal after cancellation

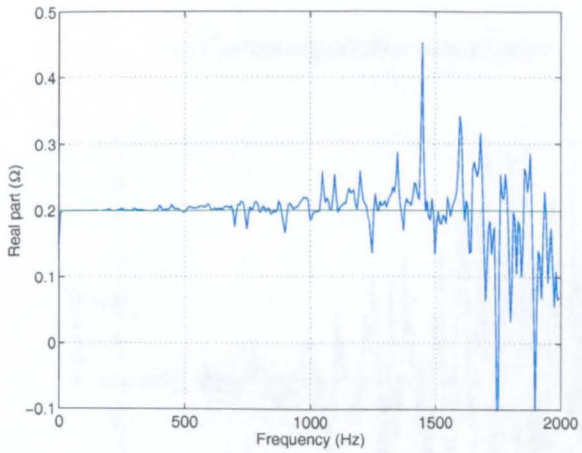

(d) Estimated impedance (real)

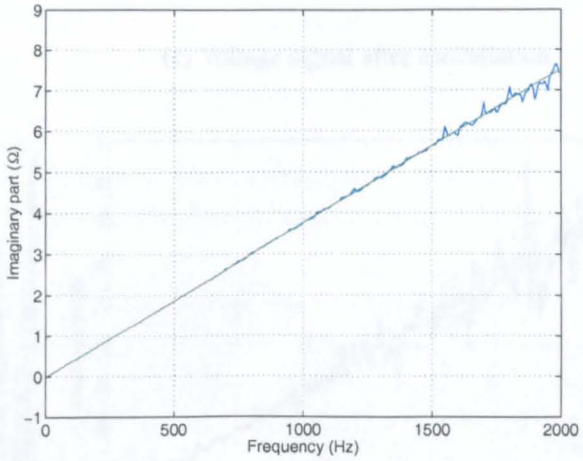

(e) Estimated impedance (imaginary)

Figure 4.19: Simulation 5. Ideal simulation conditions: no measurement noise and perfect steady state cancellation

Blue	Measured data for the time domain plots, after steady state cancellation.
Blue	Impedance estimates prior to curve fitting in frequency domain plots.
Green	Ideal impedance lines calculated from the supply transfer function
Red crosses	Raw data used for curve fitting
Red	Impedance estimate generated from the curve fitting algorithm.
Magenta	Impedance estimate calculated without spectral leakage reduction.

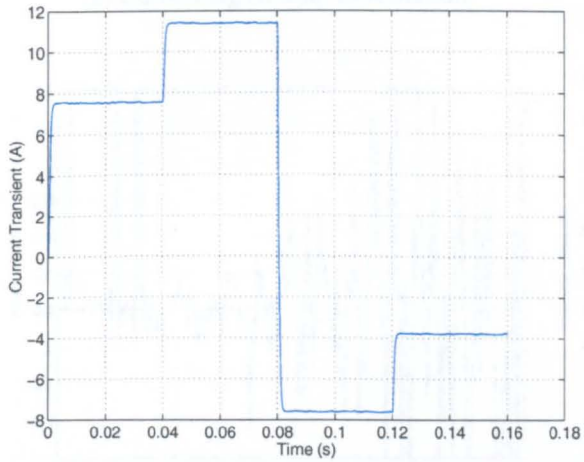

(b) Current signal after cancellation

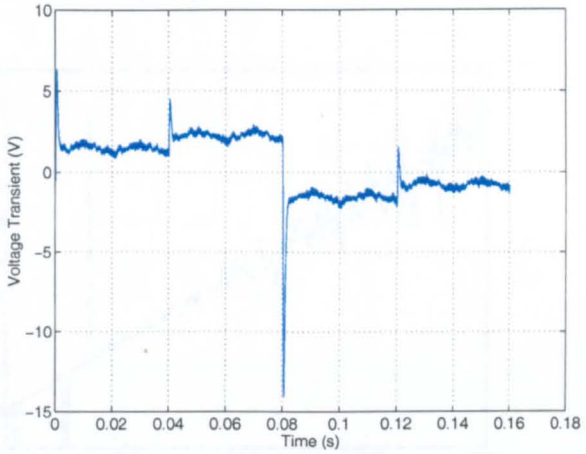

(c) Voltage signal after cancellation

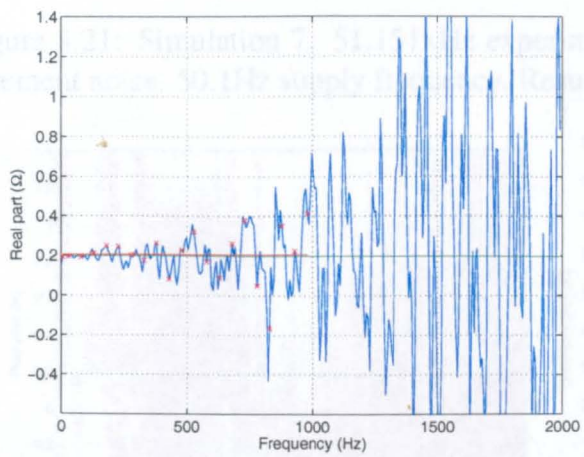

(d) Estimated impedance (real)

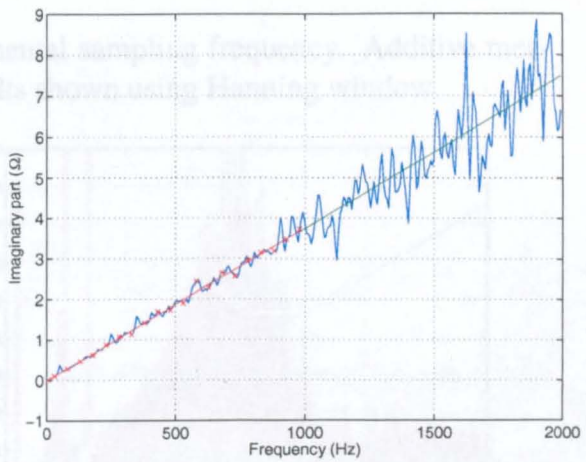

(e) Estimated impedance (imaginary)

Figure 4.20: Simulation 6. 51.151kHz experimental sampling frequency and additive measurement noise used

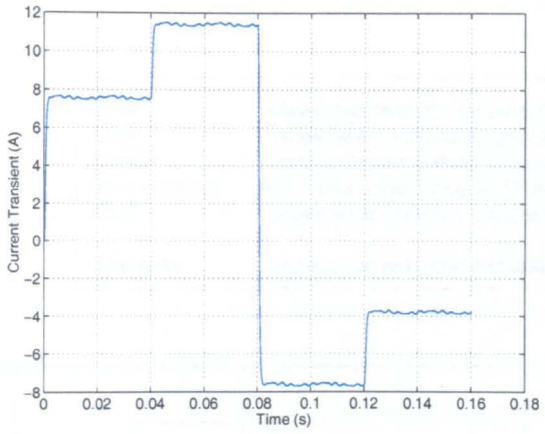

(a) Current signal after cancellation

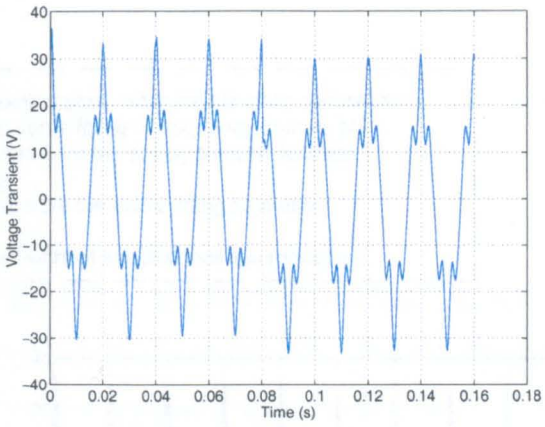

(b) Voltage signal after cancellation

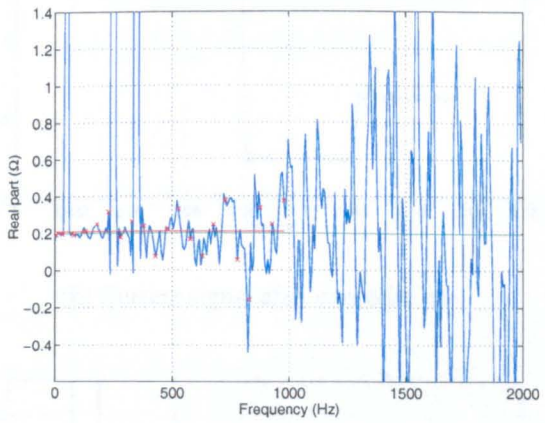

(c) Estimated impedance (real)

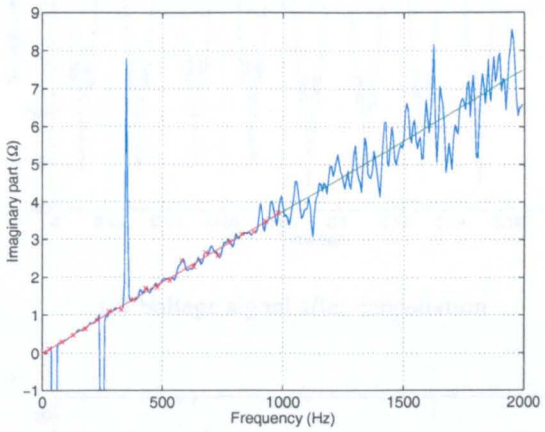

(d) Estimated impedance (imaginary)

Figure 4.21: Simulation 7. 51.151kHz experimental sampling frequency. Additive measurement noise. 50.1Hz supply frequency. Results shown using Hanning window

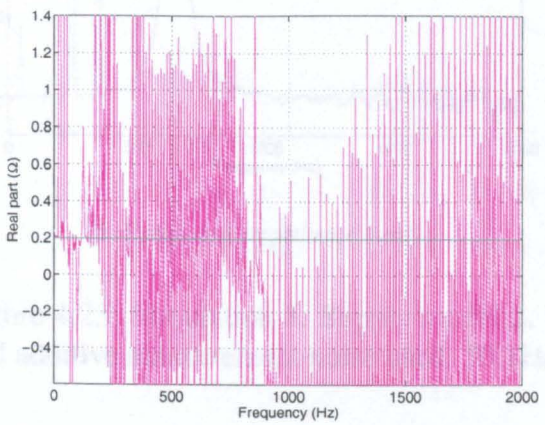

(a) Estimated impedance (real)

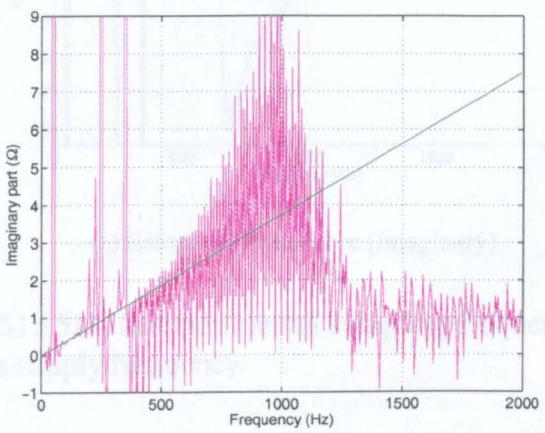

(b) Estimated impedance (imaginary)

Figure 4.22: Simulation 7. Hanning window not applied

Blue	Measured data for the time domain plots, after steady state cancellation.
Blue	Impedance estimates prior to curve fitting in frequency domain plots.
Green	Ideal impedance lines calculated from the supply transfer function
Red crosses	Raw data used for curve fitting
Red	Impedance estimate generated from the curve fitting algorithm.
Magenta	Impedance estimate calculated without spectral leakage reduction.

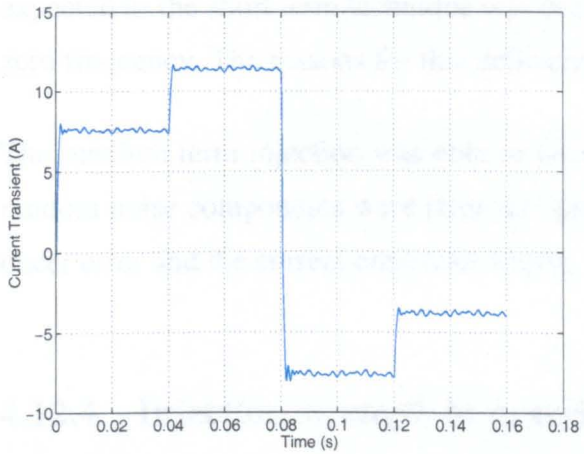

(b) Current signal after cancellation

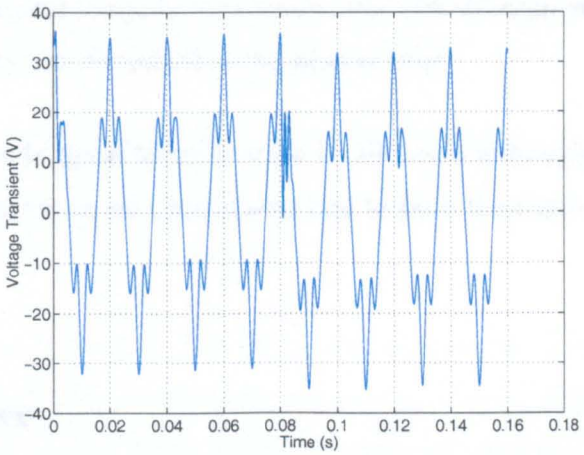

(c) Voltage signal after cancellation

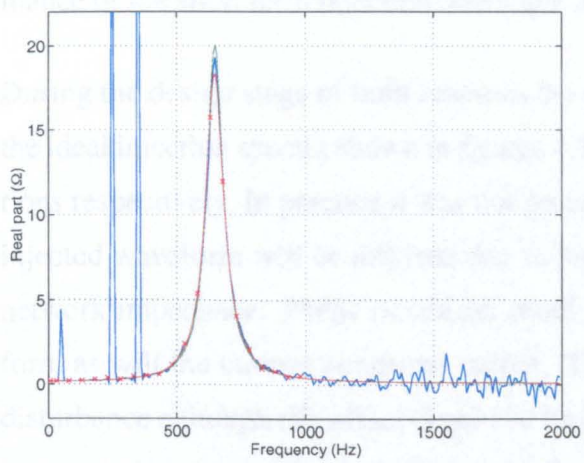

(d) Estimated impedance (real)

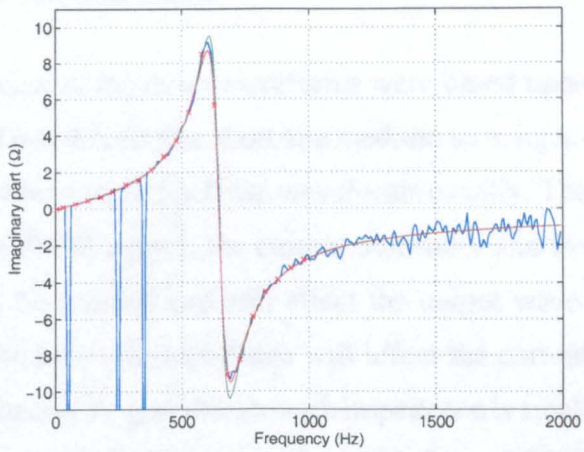

(e) Estimated impedance (imaginary)

Figure 4.23: Simulation 8. Supply model 2. 51.151kHz experimental sampling frequency and additive measurement noise used. 50.1Hz supply frequency

4.12.3 Summary of simulation results

The simulation results have shown that both techniques are capable of good supply impedance identification. Various expected sources of error were included and acceptable performance was still possible.

The short term injection technique showed a large error at lower frequencies, this was not expected as the short term technique was designed to apply maximum injection strength at zero frequency. The reasons for this deficiency are discussed in the next section.

The medium term injection was able to provide good identification in all cases although random noise components were large and present in all simulations due to both the transducer error and the current controller action.

4.12.4 Injection strength in practice

Finally, a brief section has been included with the intention of explaining the poor performance of the short term injection technique at low frequencies.

During the design stage of both schemes the current injection waveforms were based upon the ideal injection spectra shown in figures 4.3 and 4.4, for the short and medium term injections respectively. In practice it was not possible to replicate these waveforms exactly. The injected waveform will be affected due to the PWM output, the current controller and the network impedance. PWM saturation should be avoided and will affect the output waveform as will the current controller output. The network impedance will affect the current disturbance although this effect should be limited as long as the network impedance is small in comparison to the line inductance. In the case of the short term injection figure4.24(a) and (b) shows both the ideal injection waveforms and injection waveforms taken from simulation data.

Ideal conditions were used for the simulation, that is, a 50Hz supply, a sampling frequency

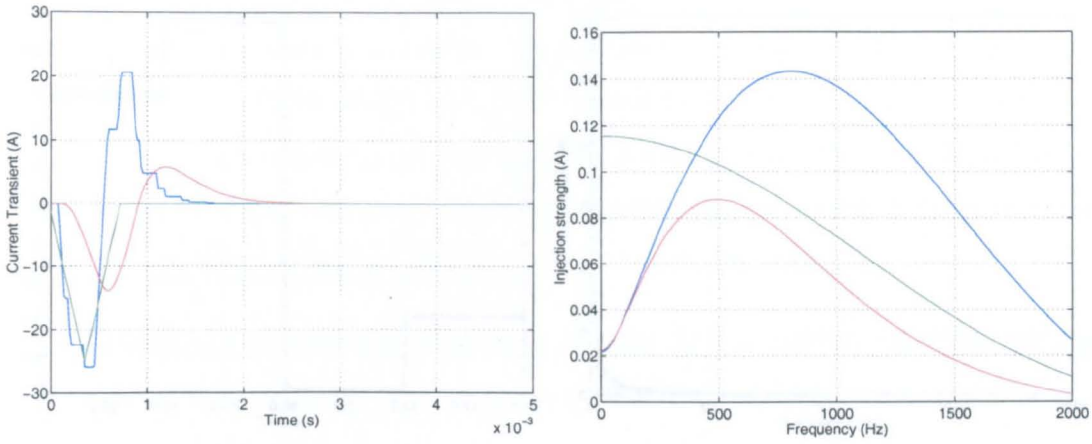

(a) Transient current waveform (time domain)

(b) Transient current waveform (frequency domain)

Figure 4.24: Short term injection strength

of 51.2kHz, no noise signals and zero supply impedance. The green traces show the ideal injection waveforms from section 4.3 using parameters from the simulation circuit. The blue traces show the equivalent simulated waveforms and the red traces show the measured waveforms, after application of the anti aliasing filters. Figure 4.24(b) confirms that the short term injection strength at low frequencies is below the intended level. Consequently the low frequency performance of the short term injection method is lower than initially expected.

The medium term injection was not significantly affected using the simulation parameters above. Figures 4.25(a) and (b) show the injection waveforms for the medium term injection. In this case the current disturbance is executed with excellent agreement to the initial designed waveforms. The medium term injection is less demanding upon the ASF with the only slight deviation from the ideal waveforms being due to the finite bandwidth of the current controller. In the experimental work several current controllers are applied that may distort the injected disturbance to a greater extent than shown here.

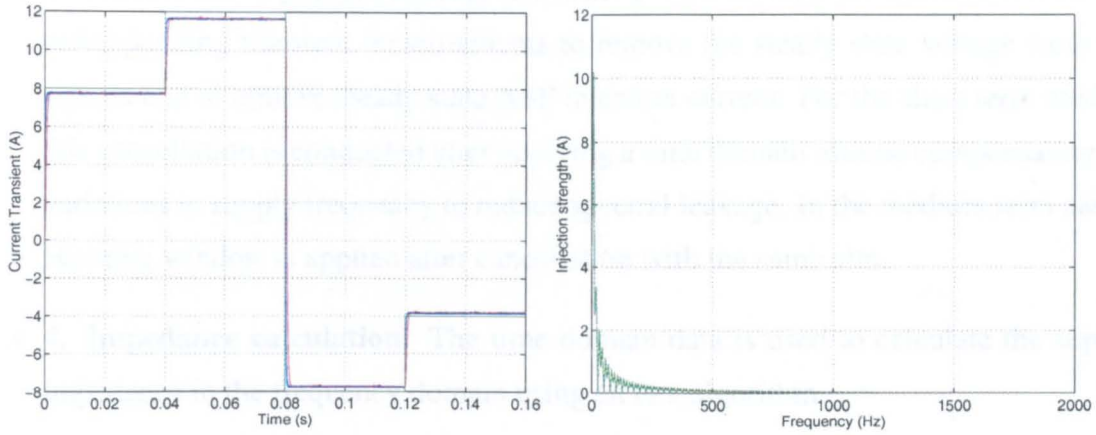

(a) Current signal after cancellation (b) Current injection strength

Figure 4.25: Medium term injection strength

4.13 Conclusion

Two methods have been proposed for on-line impedance measurement. The major sources of error in the time domain are expected to be due to imperfect cancellation. Using the chosen approach these errors may be confined to known positions in the frequency domain and as a result these errors will subsequently be almost eliminated by interpolating about the harmonic frequencies. The signal processing methods were chosen for computational efficiency and are suited to an on-line measurement approach using an existing ASF.

To summarize, the final procedure for impedance estimation is thus defined as:

- **1. Define injection parameters.** The short term or medium term injection strategy is chosen. The appropriate transducer measurements are chosen depending on the system model. For this work a balanced three wire three phase system is considered, requiring only one voltage and one current measurement.
- **2. Experimental measurement.** Steady state and transient measurements are recorded. For research purposes the total duration of each method is 0.32s although further optimization may be possible.

- **3. Time domain pre-processing.** The steady state records are subtracted from the corresponding transient measurements to remove the steady state voltage from the signals and to remove steady state ASF injection current. For the short term method this cancellation is conducted after applying a time domain routine compensating for variations in supply frequency to reduce spectral leakage. In the medium term case a Hanning window is applied after cancellation with the same aim.
- **4. Impedance calculation.** The time domain data is used to calculate the supply impedance in the frequency domain using an FFT algorithm.
- **5. Model parameter calculation.** Interharmonic impedance estimates are used in order to calculate the parameters of a linear impedance model.

These techniques have been described for single measurements. The experimental verification shall also deal with single measurements. To improve the SNR it is possible to repeat measurements over time. If the method errors are assumed to be random then it is possible, by application of the central limit theorem, to show that the standard deviation of the error is proportional to $\frac{1}{\sqrt{n}}$ [85].

Certain practical features of the system have not been considered such as permitted injection strength. The maximum injection strength without disturbing normal circuit operation should be applied. This clearly depends on the particular system measured.

Both techniques are practically implemented in the next chapter.

Chapter 5

Impedance measurement results for linear systems

5.1 Introduction

The previous chapter contained a description of the short and medium term injection techniques to be evaluated. The results from the experimental work in order to achieve this are described in this chapter.

Both of the techniques that have been introduced were applied to a variety of test circuits within the laboratory. The test circuits were chosen to cover a whole range of supply configurations in order to rigorously test the methods. The impedance estimates obtained were compared with independently measured impedance estimates using another experimental means for comparison. Statistical analysis was performed on a selection of the test circuits in order to quantify the measurement noise level. Finally, impedance transfer functions equivalent were derived using the complex curve fitting algorithm described in the previous chapter.

5.2 Experimental Procedure

Four different types of experimental measurement were made for each test circuit. The first two are the techniques described in the previous chapter. The second two are supplementary measurements taken in order to verify the proposed techniques and to assess their accuracy. Not all of the experimental results measured exactly the same circuit configurations due to practical constraints. The four techniques applied were:

1. Short term injection with supply connection.
2. Medium term injection with supply connection.
3. Discrete frequency calibration injection.
4. Short term injection without supply connection.

These methods shall be referred to as injection method 1 (IM1) to injection method 4 (IM4). Each shall be discussed in turn in order to provide an overview and to establish precisely which quantities were measured in each instance.

5.2.1 IM1: Short term injection with supply connection

In this case the complete short term injection technique was applied, as described in chapter 4. Figure 5.1 is a schematic representation of the supply and injection hardware. All values are referred to the secondary of the experimental rig transformer, that is, the point of measurement. The point of measurement is shown as PCC in figure 5.1. Z_{s1} is a Thevenin equivalent, per phase, of the total supply impedance measured to the 100A laboratory supply bus, including the impedance due other loads connected to the laboratory supply. Z_{s2} is a Thevenin equivalent, per phase, of the impedance of the experimental rig transformer. The total supply impedance, $(Z_{s1} + Z_{s2})$, was measured using IM1.

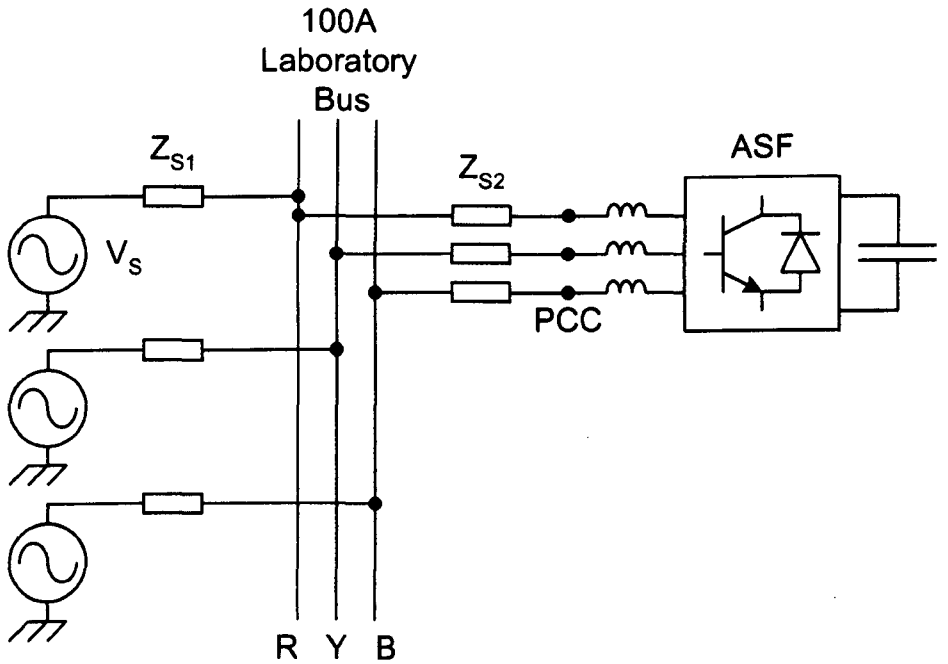

Figure 5.1: Practical injection system for IM1 and IM2

The ASF harmonic current references were set at zero so as to draw zero fifth harmonic and seventh harmonic currents in the steady state. The fundamental controller was left to maintain the d.c. link voltage at the reference level of 680 V. Data was captured on the dedicated data acquisition system. Further details of the signal processing for this technique are shown in section 4.7.

5.2.2 IM2: Medium term injection with supply connection

The medium term injection technique was implemented, as described in chapter 4. Figure 5.1 shows the experimental system. The ASF references were maintained in the same way as for the short term injection method. Signal processing aspects of this technique may be found in sections 4.4 and 4.8.

5.2.3 IM3: Discrete frequency calibration injection

IM3 was a long term injection using alternative measurement hardware conducted in order to verify the novel methods being tested. This was completed off-line, that is, on a de-energised system. This was necessary for practical reasons that shall be discussed. Thus the primary connection of the experimental rig feed transformer was disconnected from the supply and short circuited. In this case only the impedance Z_{s2}) shall be measured. This system is shown in figure 5.2.

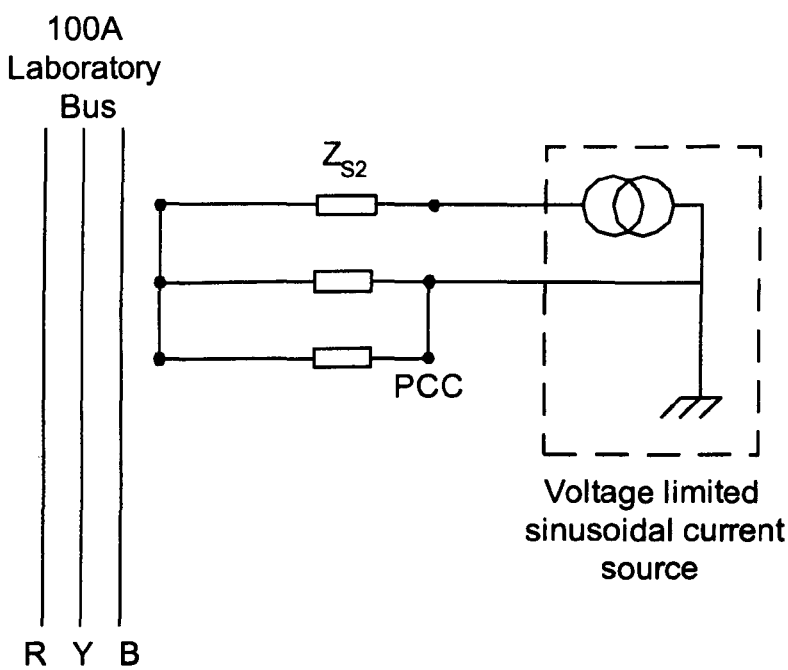

Figure 5.2: Practical injection system for IM3

A Datron Wavetek Calibrator was used in conjunction with a Ballantine transconductance amplifier so as to act as a controlled current source to inject a sinusoidal current waveform at the PCC. This process was repeated through a range of predetermined discrete frequencies. At each frequency ten complete cycles of steady state current and voltage data was recorded using an IMM differential voltage probe and a Tektronix current probe. The data was stored on an eight bit LeCroy digital storage scope and was subsequently transferred and processed on a PC. An impedance estimate was made at each frequency using the

following procedure.

One complete cycle was calculated for both the measured voltage and current by averaging the ten recorded cycles, thus yielding voltage and current signals $V_i(t)$ and $I_i(t)$. A DFT was applied to these signals. The impedance of the network at the particular frequency, f_i was then calculated from equation 5.1.

$$Z_i = \frac{\Im(V_i(t))}{\Im(I_i(t))} \tag{5.1}$$

The current source output voltage was limited to 15 V. Hence it was not possible to connect the current source to the test circuit with the supply connected. Therefore the measurement was made off-line. Consequently the impedance measured using this method will not include the supply impedance beyond the experimental rig transformer, Z_{s1}. Fortunately this impedance was small compared to the total impedance measured as the supply impedance was dominated by the experimental rig transformer. The output voltage limit also limited the magnitude of the current injection at certain frequencies. The largest magnitude possible was an rms current of 2A but this had to be reduced, depending on the impedance at each particular frequency, to as little as 100mA rms.

5.2.4 IM4: Short term injection without supply connection

The short term injection method (IM1) was also applied to each test circuit without a supply connection. This method was used in order to provide a direct comparison to IM3. This scheme is shown in figure 5.3.

The d.c. link voltage of the ASF was maintained by the separate supply used by the ASF for pre-charge protection, see chapter 3 for further details. It was not possible to maintain the ASF control whilst applying this method. The output of the ASF was instead controlled to provide zero output using a fixed 50 % duty cycle on each phase. The required steady state data was captured in this state.

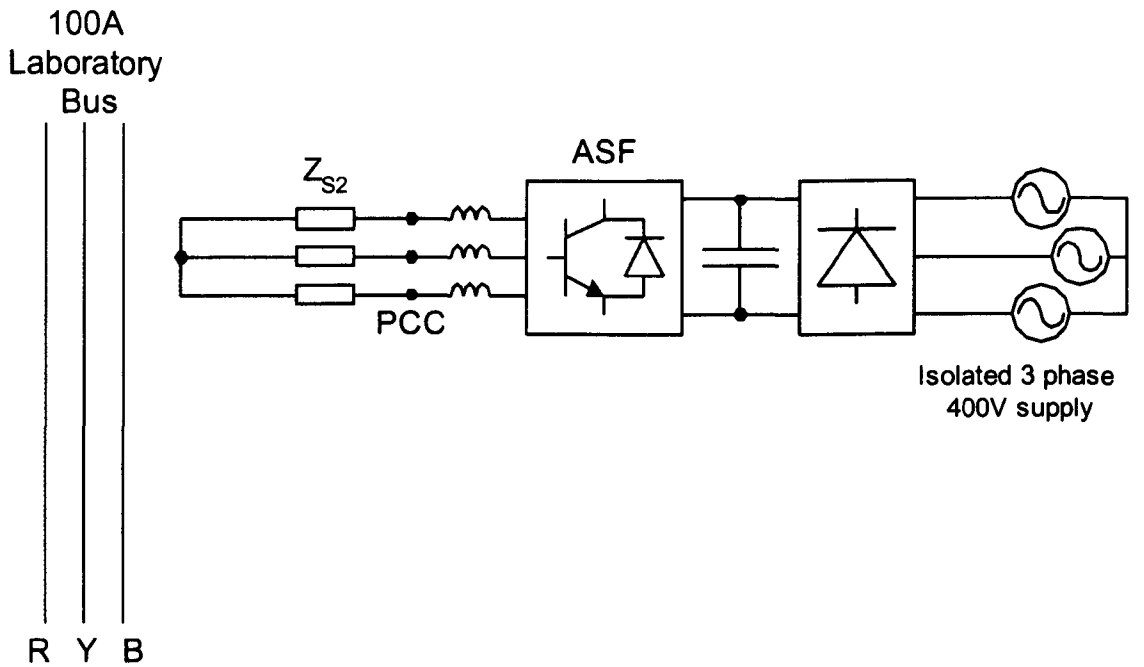

Figure 5.3: Practical injection system

5.3 Test circuits

Eight different test circuits have been constructed in order to test the measurement techniques over a wide range of supply possibilities. The basic supply connection is through the 100kVA experimental rig star-star step down auto-transformer. This is the simplest connection possible and is the first test circuit. Different combinations and sizes of passive components have been connected between the secondary of the main transformer and the ASF connection to create further test circuits. These components have been chosen so as to provide resonant points that might be present on a real supply due to power factor correction capacitors or tuned filters for harmonic reduction. Each of the test circuits, c1 to c8, shall be described in turn.

5.3.1 Test circuit 1 (c1)

Circuit 1 is the experimental system supply alone. A 1MVA 11kV - 415V transformer feeds the main laboratory. A 415V 100A supply ring feeds the individual experimental rigs within the laboratory. The 100kVA star-star auto-transformer is connected to this ring. The secondary voltage is stepped down to 300V rms, this is the supply connection for circuit 1. Figure 5.4 shows the line-line circuit for one phase of the supply. The entire supply network impedance is shown as a Thevenin equivalent, Z_s. Z_s is referred to the secondary side of the transformer, that is, to the point of measurement.

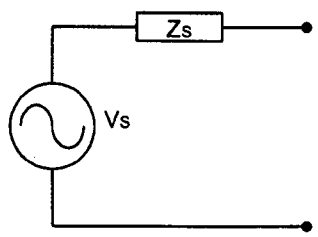

Figure 5.4: Circuit 1: Line-Line circuit

Injection methods 1 and 2 will measure Z_s whereas injection methods 3 and 4 will measure only the impedance of the experimental supply transformer. With reference to figure 5.1, injection methods 1 and 2 will measure Z_s, the sum of Z_{s1} and Z_{s2}, whereas injection methods 3 and 4 will only measure Z_{s2}. This is due to the fact that the primary side of the experimental transformer is short circuited during these tests and no supply is present.

A simple way of modelling the supply impedance would be to assume that the total impedance is due only to the experimental rig transformer and the main laboratory transformer, as these will dominate the supply impedance. Weedy [2] suggests that a transformer may in turn be represented by a single inductance and suggests an approximate value of impedance as 10% per unit. Using these assumptions the approximate impedances of the experimental rig transformer and the laboratory transformer will be 600μH and 30μH respectively. From these figures it may be noted that injection methods 3 and 4 should measure 95% of the total supply impedance for this supply.

A further measurement complication is introduced due to the fact that the impedance Z_{s1} will vary depending on the loads connected at remote points from the PCC. Hence this impedance will vary with time in an unpredictable manner. This variation should have only a small influence on the measurement results as Z_{s1} is small compared with the fixed impedance Z_{s2}.

The most comprehensively studied circuit was circuit 1. This was firstly because a transformer connection is a very common form of supply connection and was the actual means of connecting the ASF for other work. Secondly, it was the hardest supply to measure as the transient response was very short, due to there being little oscillation in either the current or voltage waveform.

5.3.2 Test circuit 2 (c2)

An additional inductor was connected in series to each phase of circuit 1 in order to create the second test circuit, circuit 2. The name plate value for this additional inductance was 250μH per phase. This circuit was used to verify that the proposed methods were capable of measuring a range of supplies with predominantly inductive impedances. Figure 5.5 shows a line-line equivalent circuit.

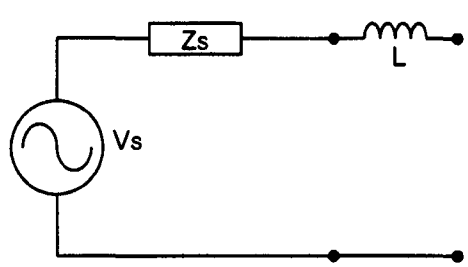

Figure 5.5: Circuit 2: Line-Line circuit

5.3.3 Test circuit 3 (c3)

Circuit 3 was constructed in order to model a supply with power factor correction (PFC) capacitors. This supply circuit was developed using circuit 1 and additionally connecting 50μF capacitors in delta formation at the secondary side of the transformer. The line-line circuit is shown in figure 5.6.

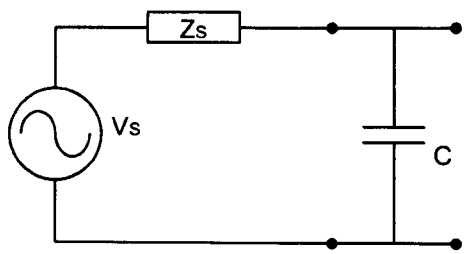

Figure 5.6: Circuit 3: Line-Line circuit

As an example, consider a linear three phase load connected to the circuit 1 supply drawing 50A rms per phase with a fundamental displacement factor of 0.80. On addition of the PFC capacitors the displacement factor would be corrected to a value of 0.90. This circuit had a resonant point within the frequency range of interest.

5.3.4 Test circuit 4 (c4)

Circuit 4 is the same as circuit 3 but extra inductance was added between the PFC capacitors and the the point of connection. The name plate value for this inductor was 250μH. This situation would realistically occur if the point of measurement was separated from the PFC capacitors by a significant length of cabling or another transformer. Figure 5.7 shows the line-line equivalent for circuit 4.

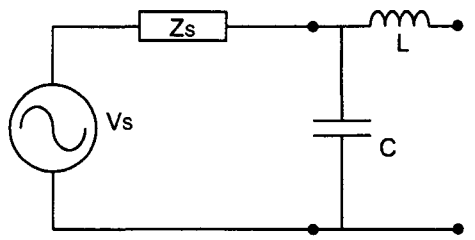

Figure 5.7: Circuit 4: Line-Line circuit

5.3.5 Test circuit (c5)

Circuit 5 was constructed to provide a supply circuit with two resonant points. It was based on circuit 4 with additional capacitance at the point of connection. 25μF capacitors were connected in delta to provide a small secondary resonant point at a higher frequency. It was then possible to establish how the methods were able to perform at higher frequencies. Figure 5.8 shows the line-line configuration for circuit 5.

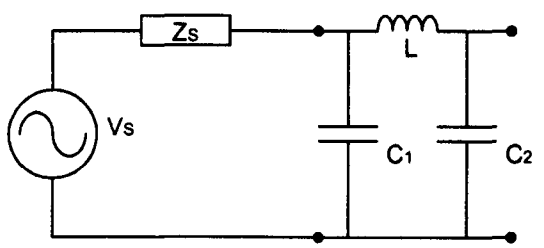

Figure 5.8: Circuit 5: Line-Line circuit

5.3.6 Test circuit 6 (c6)

This circuit was built to test the measurement methods with a tuned filter connected to the supply. An LC filter was connected in delta as shown in the line-line circuit, figure 5.9. The LC filter was comprised on each phase of a 50μF capacitor in series with a 250μH inductor.

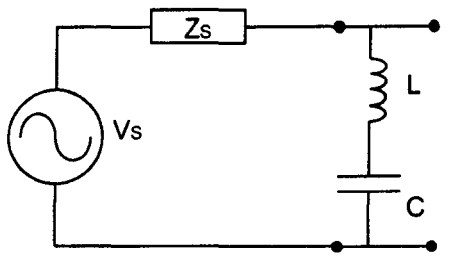

Figure 5.9: Circuit 6: Line-Line circuit

5.3.7 Test circuit 7 (c7)

Circuit 7 was an extension of circuit 1 in order to establish the performance of the techniques when a linear load was connected to the point of measurement. In this case there was a steady state current flowing into the load which may affect the accuracy of the measurements. The load impedance was high in comparison to the supply impedance resulting in a very similar impedance to circuit 1. The load was constructed using a resistor and inductor in series between each phase. Figure 5.10 shows the line-line configuration for circuit 7.

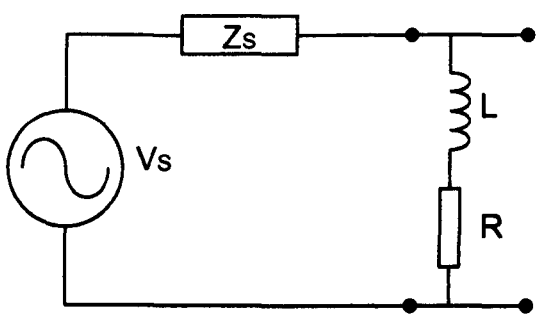

Figure 5.10: Circuit 7: Line-Line circuit

5.3.8 Test circuit 8 (c8)

The final test circuit was an extension to circuit 3. As for circuit 7, a linear load was connected to the supply to examine the measurement performance in the presence of a steady state current at the point of measurement.

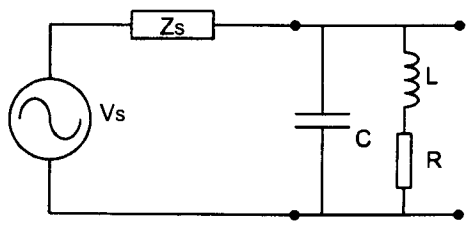

Figure 5.11: Circuit 8: Line-Line circuit

The eight test supply circuits have now been described. Experimental results are shown in the next section using these topologies in order to investigate the performance of the proposed impedance measurement techniques.

5.4 Experimental results

The experimental results were split into three sections. The first section shows typical injection results in the time domain and frequency domain. In this section the supply impedance is calculated at all frequencies and parameters are not estimated for each supply. It is the aim of this section to show typical 'raw' data before any post processing is conducted. the second section takes the results from the first section and estimates circuit parameters for the frequency range of interest. Finally, the third section was designed to show the statistical variation of the techniques for a selection of the test circuits.

5.4.1 Experimental data before parameter estimation

For each of the measurements carried out several results have been displayed. These were:

- The current and voltage measurements have been shown, after cancellation of steady state components. These signals were the result of subtracting the steady state measurements from the transient data. A phase current, i_1, was plotted. The line voltage, V_{12} was plotted. Only a portion of the transient period has been displayed for ease of viewing, in most cases this was the first fundamental supply cycle.
- Spectral data showing the injected signal strengths for both the current and voltage signals in the frequency range from 0 to 2kHz. The current and voltage spectra are shown for each of the methods.
- Impedance estimates were displayed in terms of real and imaginary parts. Estimates are shown at all frequencies including the harmonic frequencies.

Typical results for IM1 and IM2 are displayed for each test circuit. In each case these were plotted with the IM3 results. IM4 results were also plotted alongside the IM1 results. They are shown in the order of the test circuits. These figures were intended to give the reader a brief overview of the results before detailed analysis. A general discussion of these results is given following the figures. The figures have been ordered by test circuit. IM1 results precede the IM2 results for each circuit. The figure colour scheme is shown overleaf.

Injection method	Injection technique	Trace colour
IM1	Short term injection method with supply connected. Total supply impedance is measured.	Blue
IM2	Medium term injection with supply connected. Total supply impedance is measured.	Blue
IM3	Discrete frequency injection with no supply connection. Impedance measured to primary of rig feed transformer	Green
IM4	Short term injection method with no supply connection Impedance measured to primary of rig feed transformer	Red

Table 5.1: Legend for experimental result figures

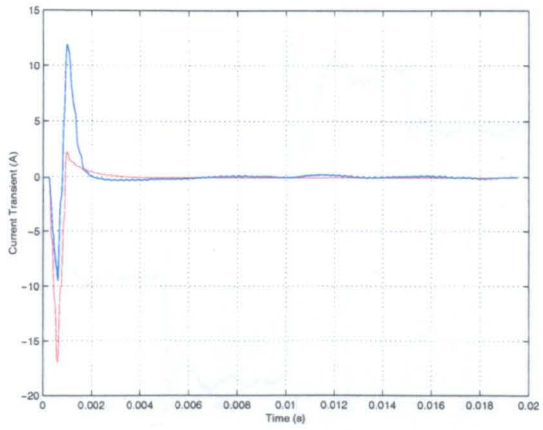

(a) Current transient.

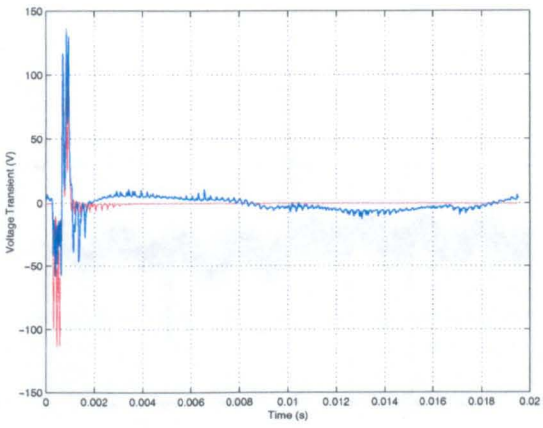

(b) Voltage transient.

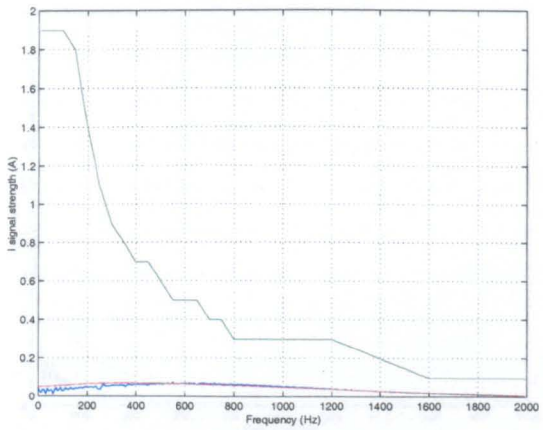

(c) Current spectrum.

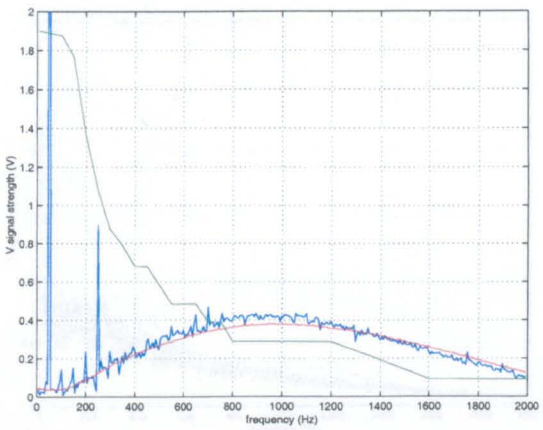

(d) Voltage spectrum.

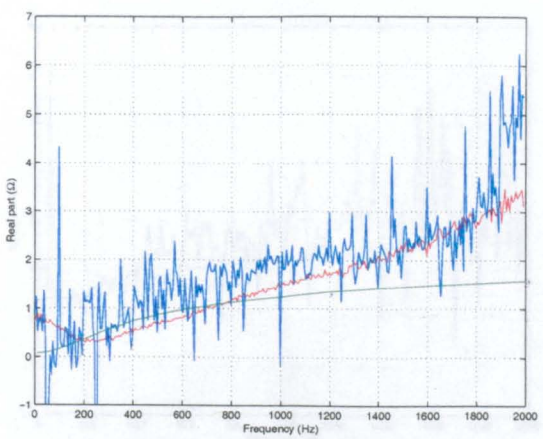

(e) Real impedance.

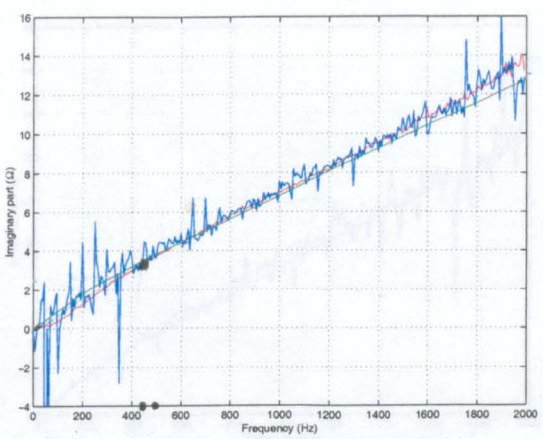

(f) Imaginary impedance.

Figure 5.12: Short term injection results: c1

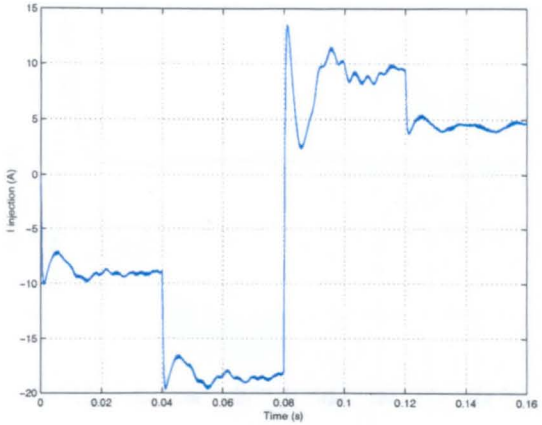

(a) Current transient.

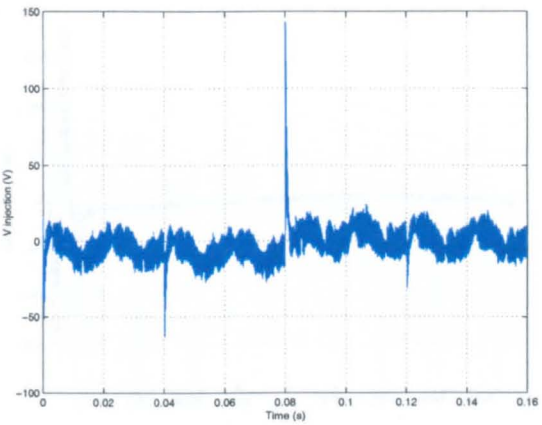

(b) Voltage transient.

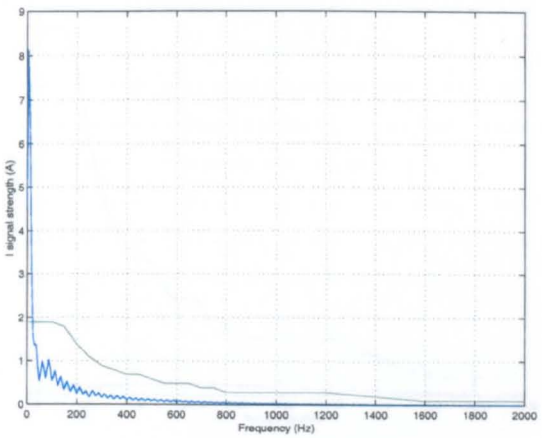

(c) Current spectrum.

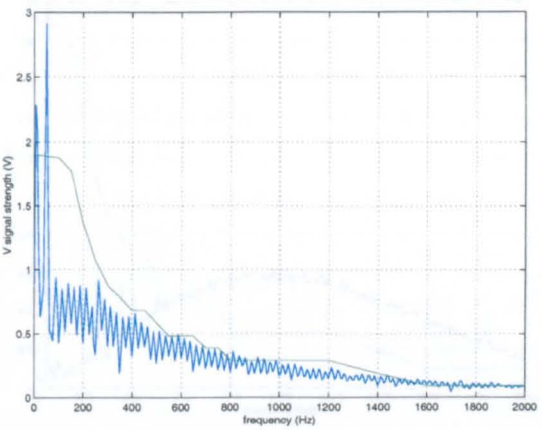

(d) Voltage spectrum.

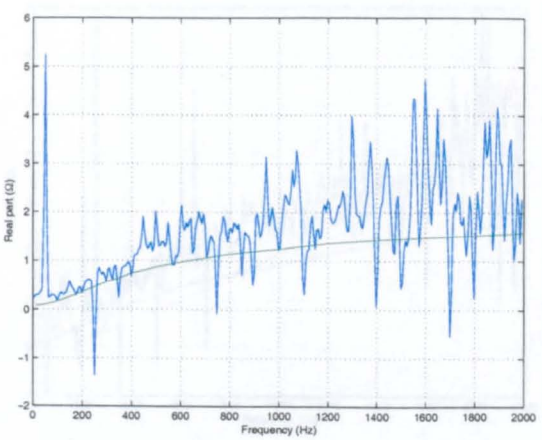

(e) Real impedance.

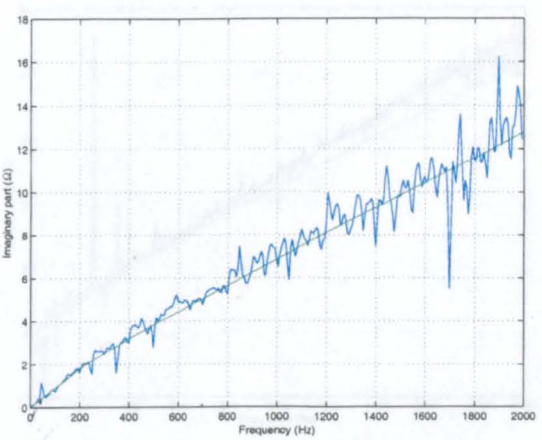

(f) Imaginary impedance.

Figure 5.13: Medium term injection results: c1

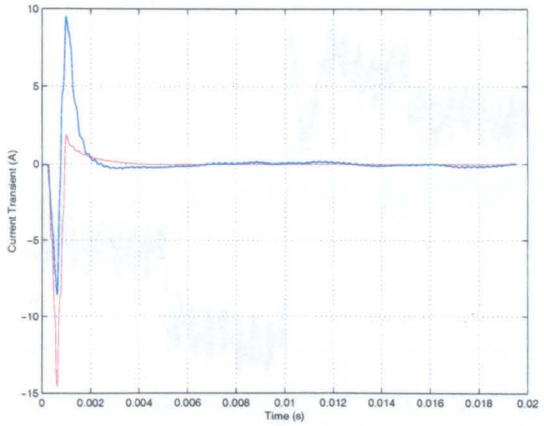

(a) Current transient.

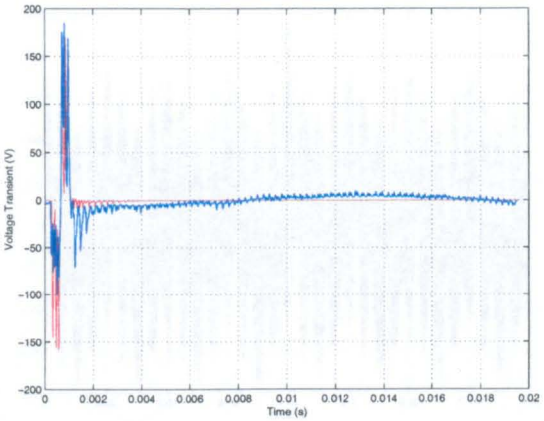

(b) Voltage transient.

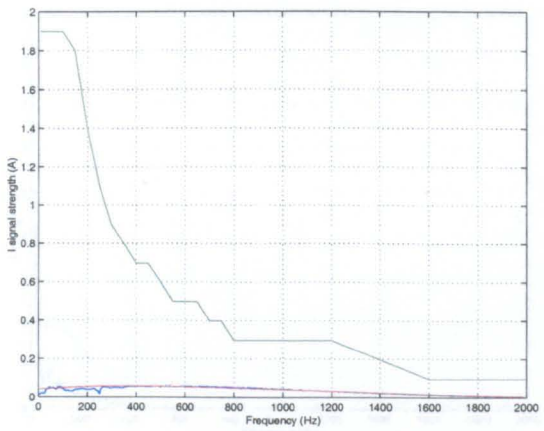

(c) Current spectrum.

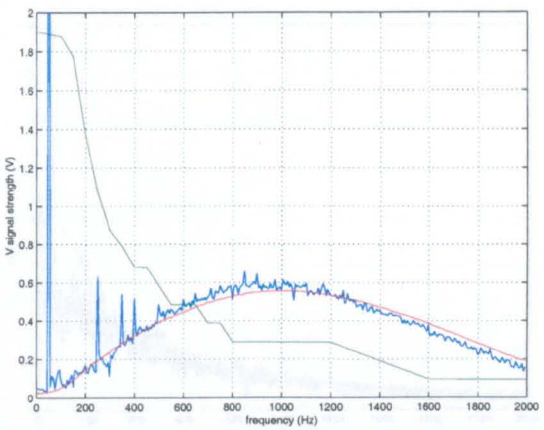

(d) Voltage spectrum.

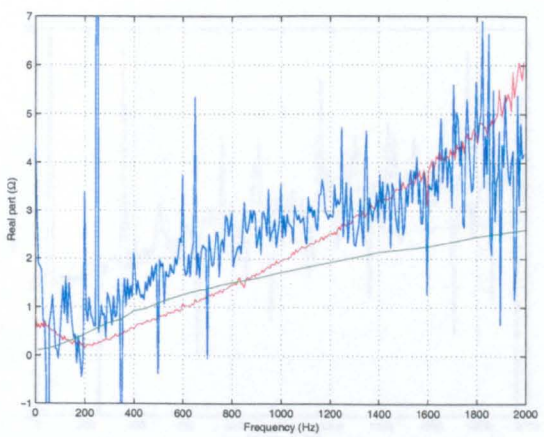

(e) Real impedance.

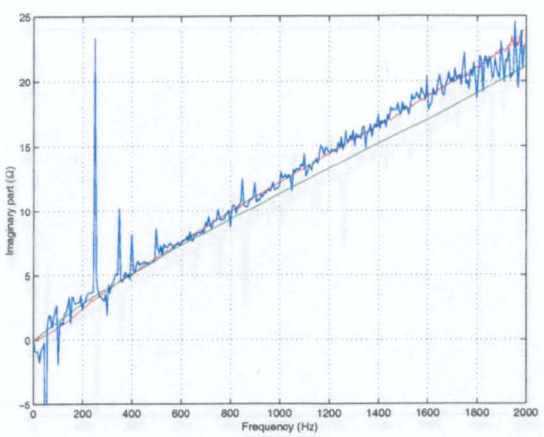

(f) Imaginary impedance.

Figure 5.14: Short term results: c2

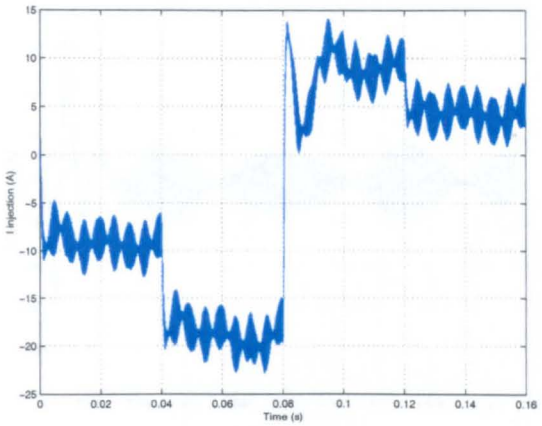

(a) Current transient.

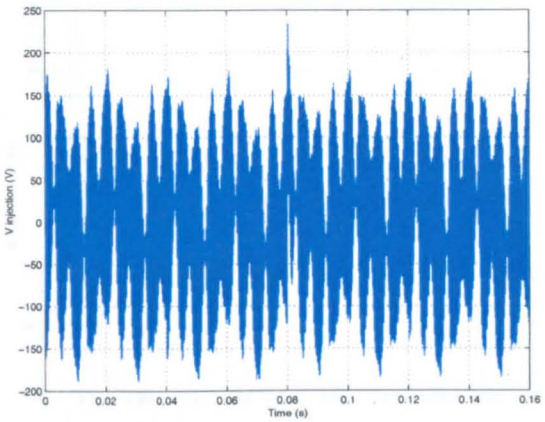

(b) Voltage transient.

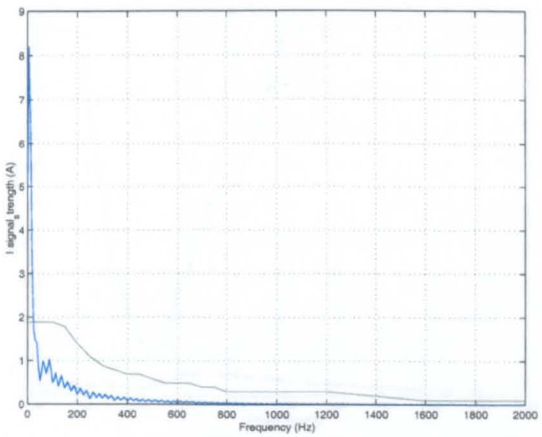

(c) Current spectrum.

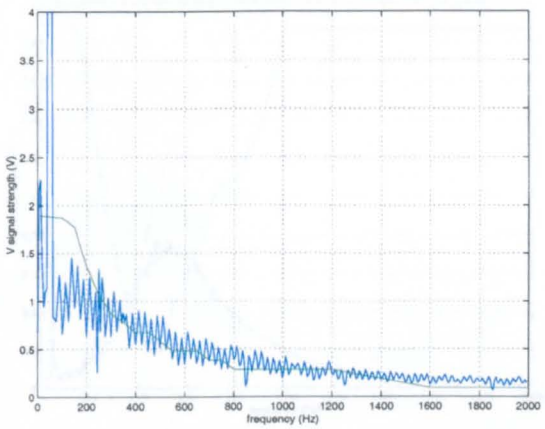

(d) Voltage spectrum.

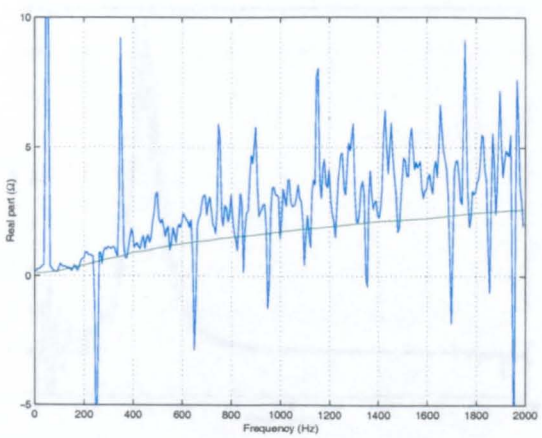

(e) Real impedance.

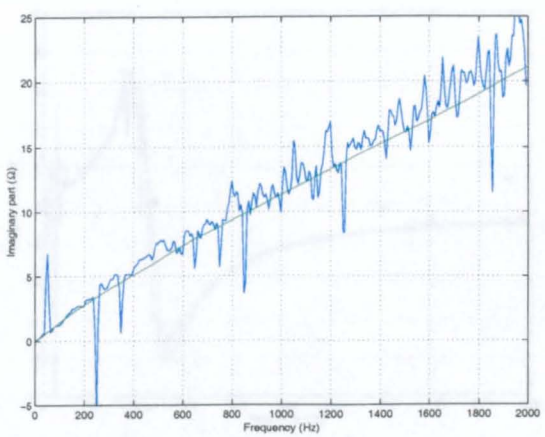

(f) Imaginary impedance.

Figure 5.15: Medium term injection results: c2

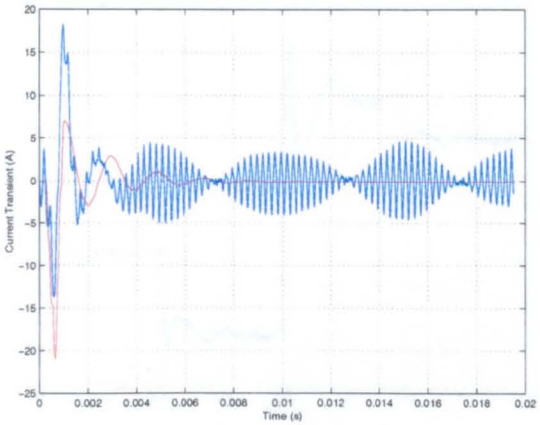

(a) Current transient.

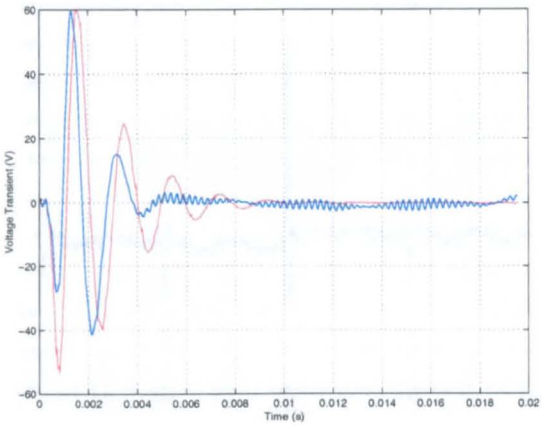

(b) Voltage transient.

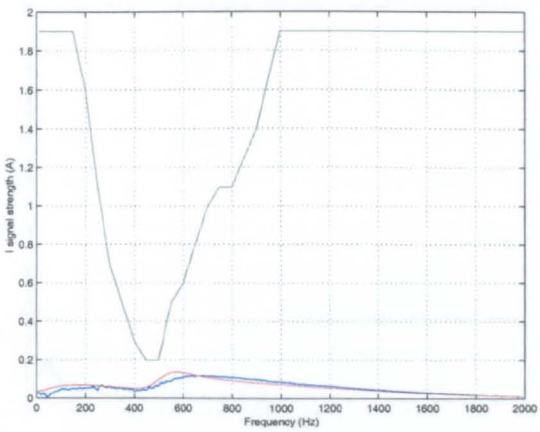

(c) Current spectrum.

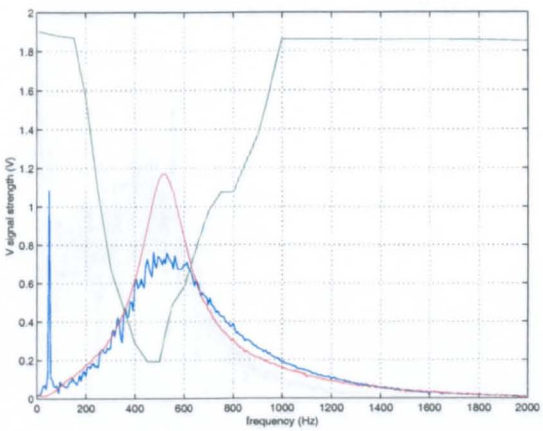

(d) Voltage spectrum.

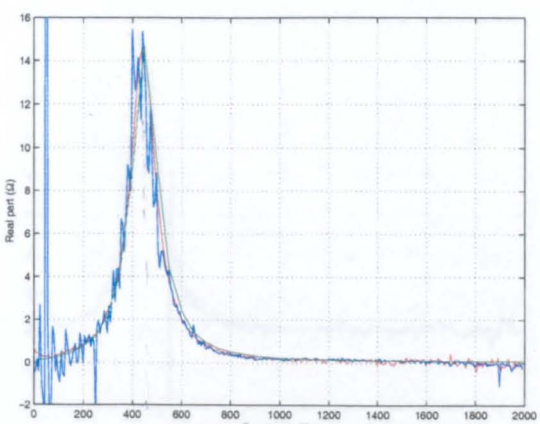

(e) Real impedance.

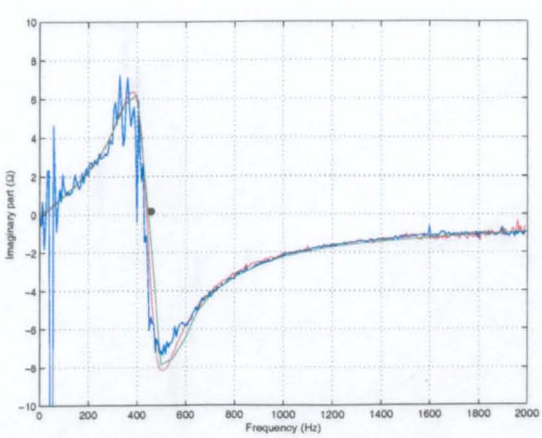

(f) Imaginary impedance.

Figure 5.16: Short term injection results: c3

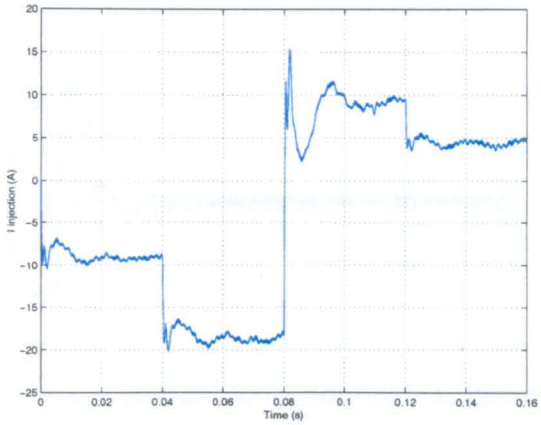

(a) Current transient.

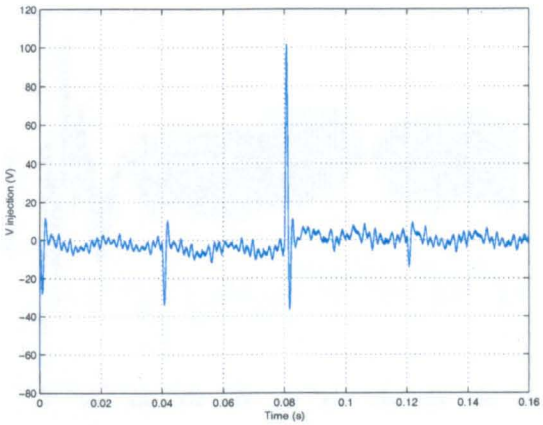

(b) Voltage transient.

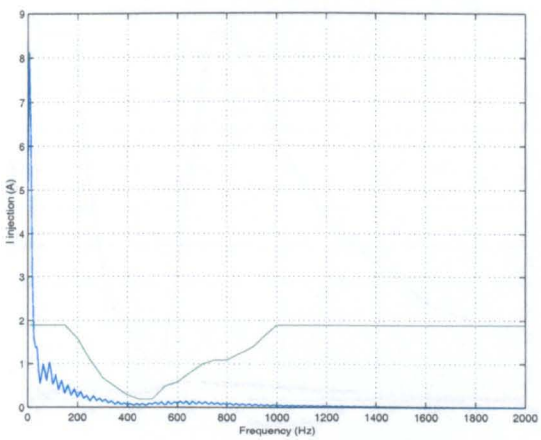

(c) Current spectrum.

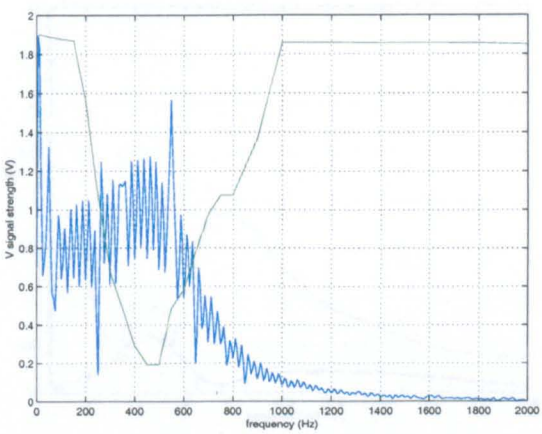

(d) Voltage spectrum.

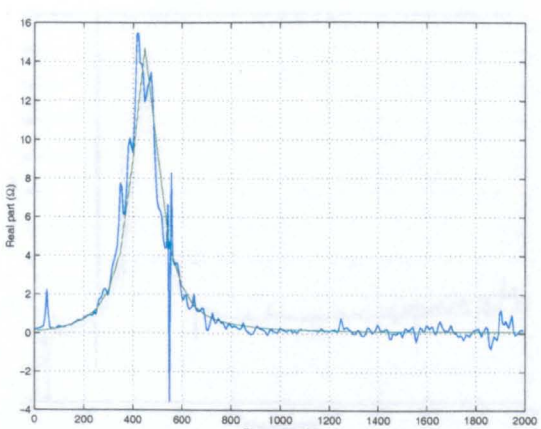

(e) Real impedance.

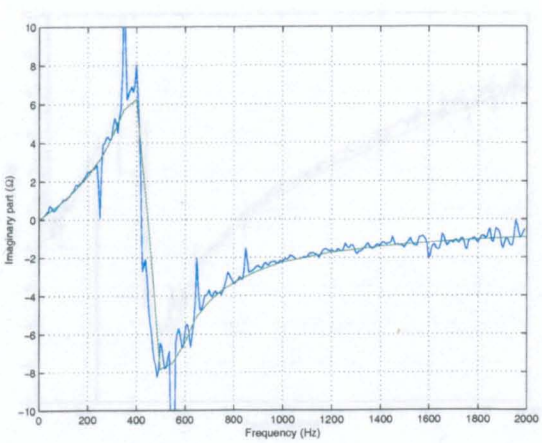

(f) Imaginary impedance.

Figure 5.17: Medium term injection results: c3

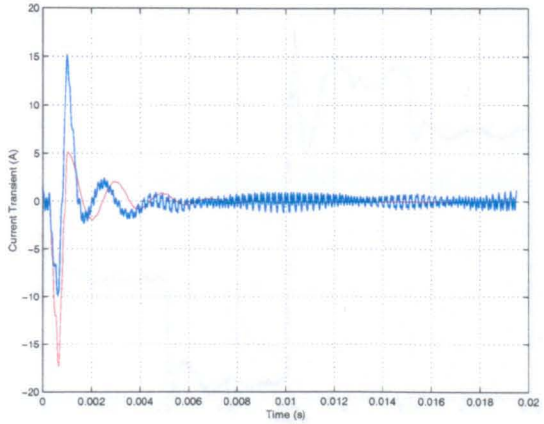

(a) Current transient.

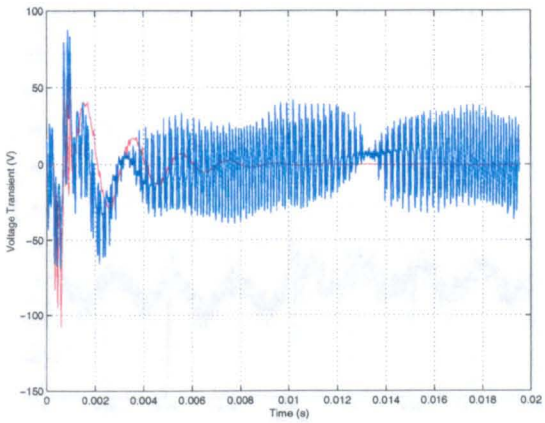

(b) Voltage transient.

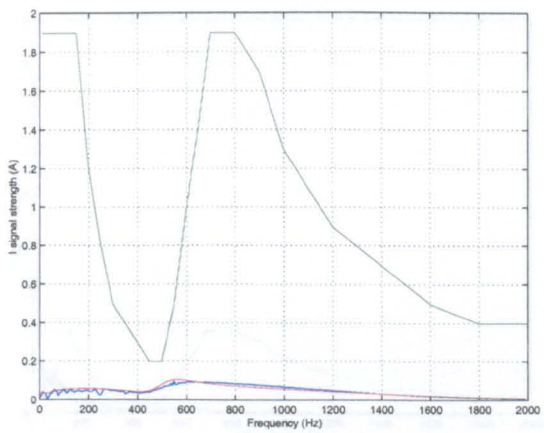

(c) Current spectrum.

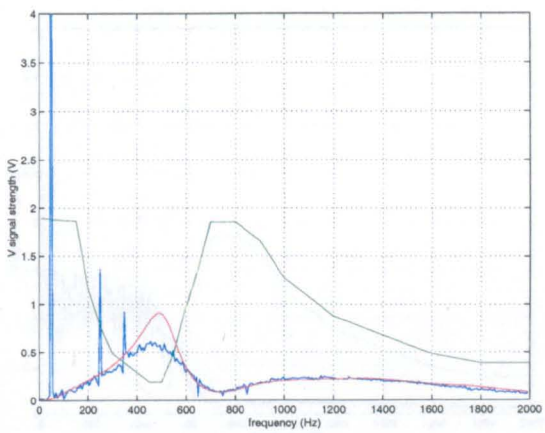

(d) Voltage spectrum.

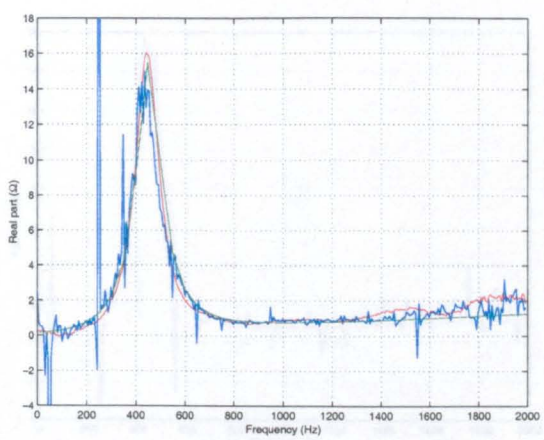

(e) Real impedance.

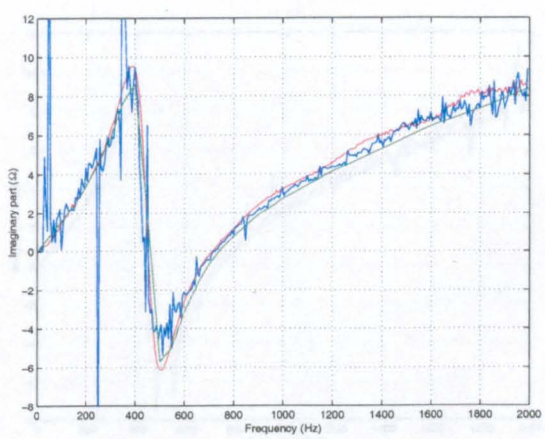

(f) Imaginary impedance.

Figure 5.18: Short term injection results: c4

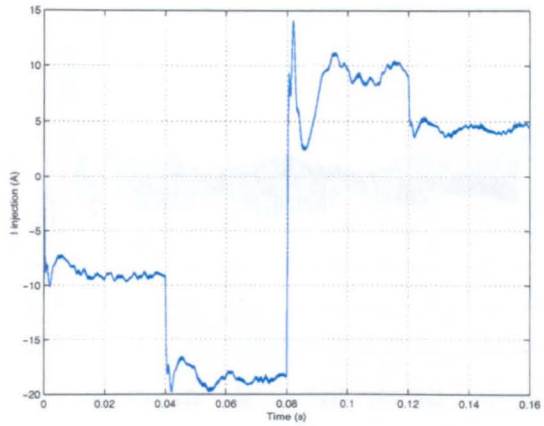

(a) Current transient.

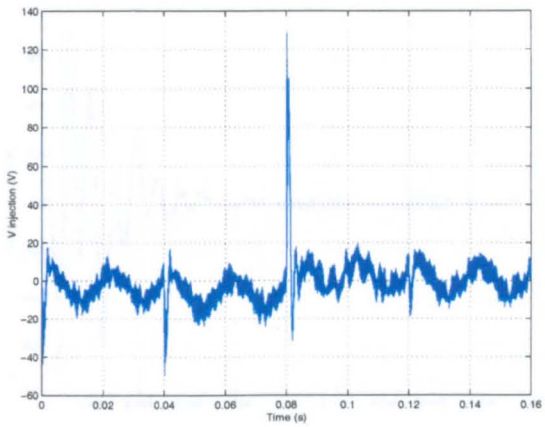

(b) Voltage transient.

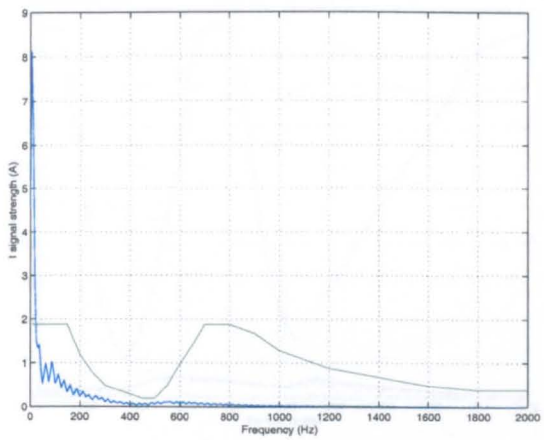

(c) Current spectrum.

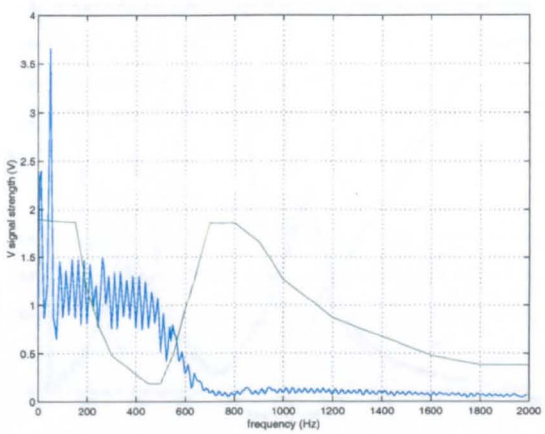

(d) Voltage spectrum.

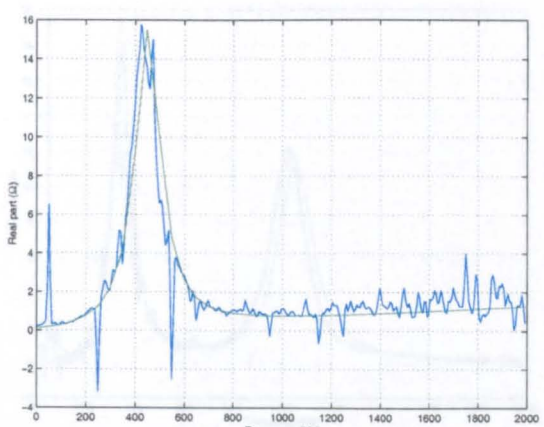

(e) Real impedance.

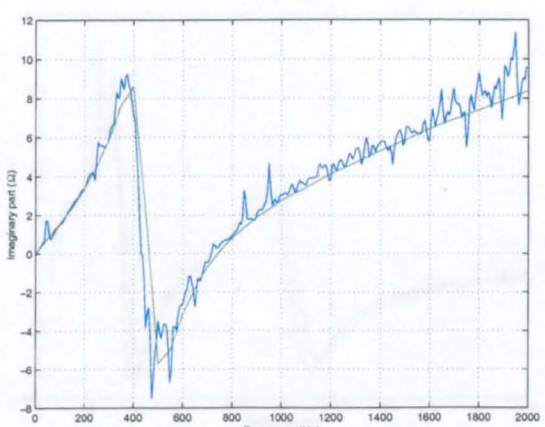

(f) Imaginary impedance.

Figure 5.19: Medium term injection results: c4

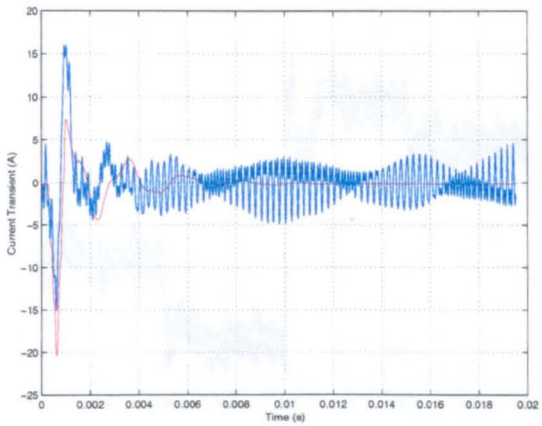

(a) Current transient.

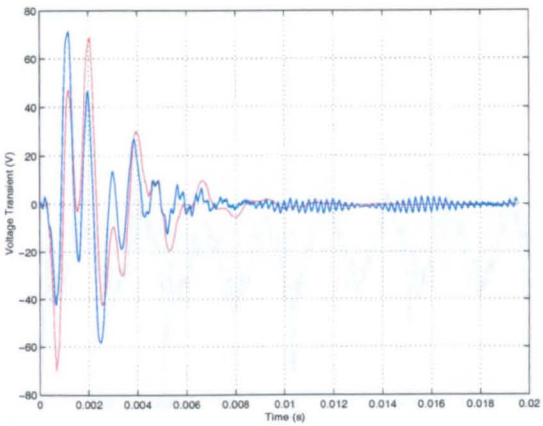

(b) Voltage transient.

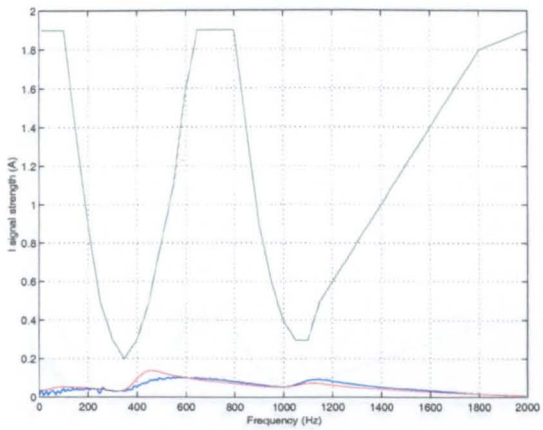

(c) Current spectrum.

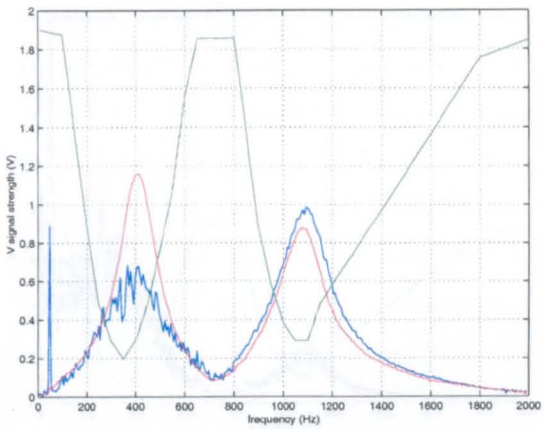

(d) Voltage spectrum.

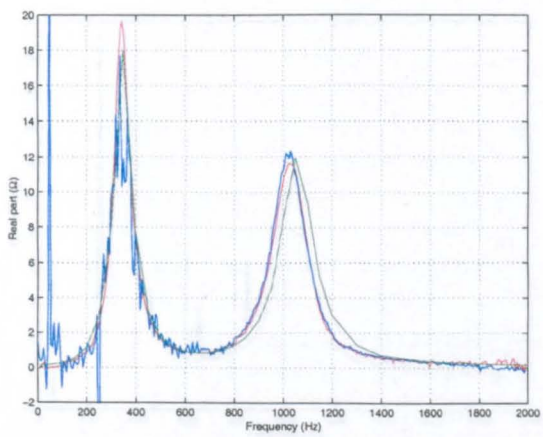

(e) Real impedance.

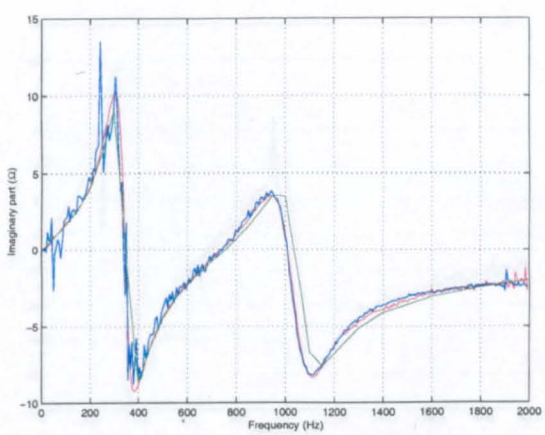

(f) Imaginary impedance.

Figure 5.20: Short term injection results: c5

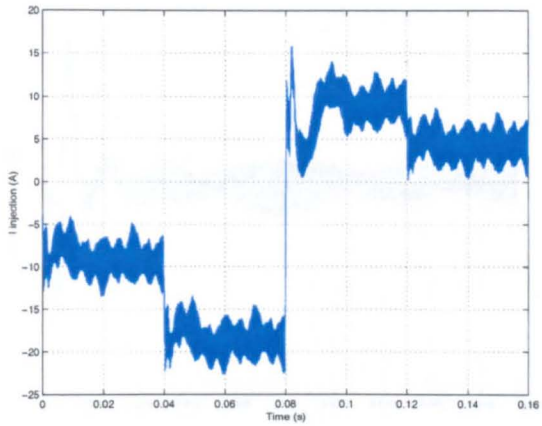

(a) Current transient.

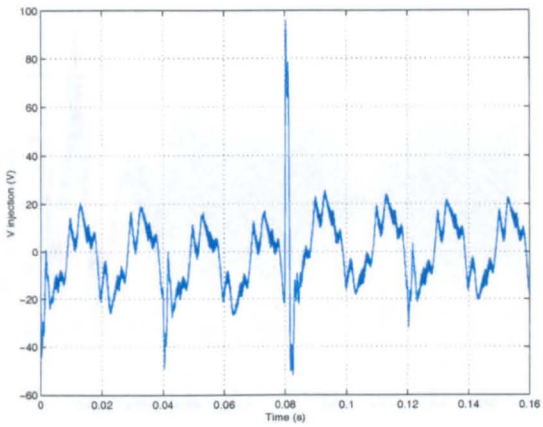

(b) Voltage transient.

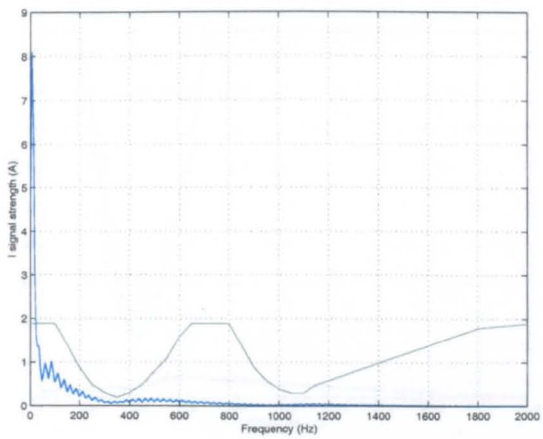

(c) Current spectrum.

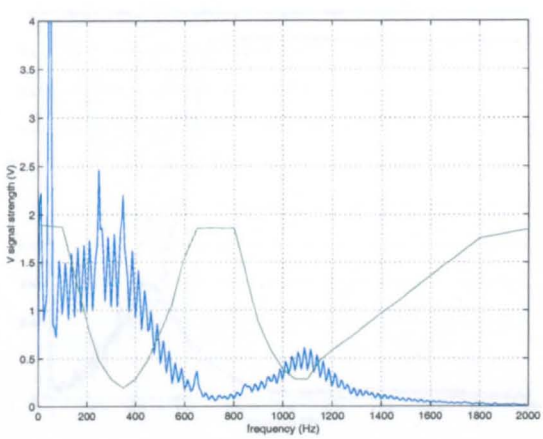

(d) Voltage spectrum.

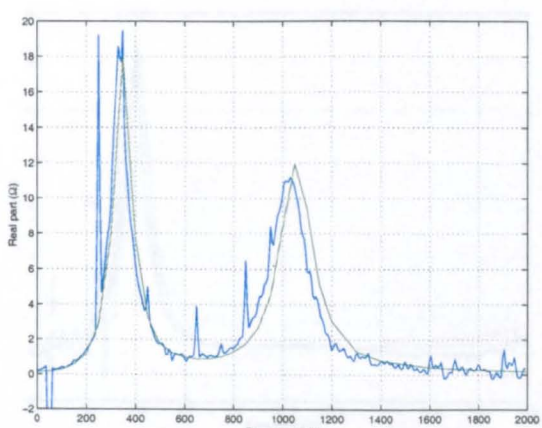

(e) Real impedance.

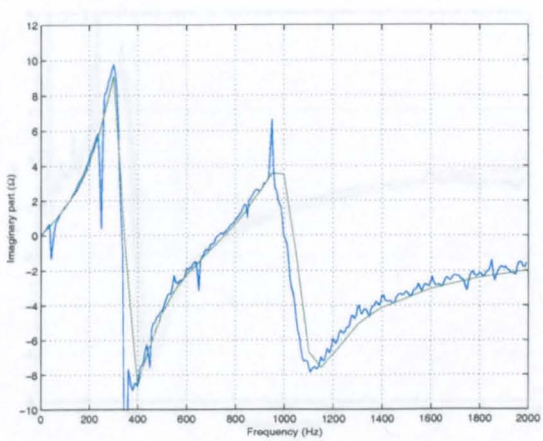

(f) Imaginary impedance.

Figure 5.21: Medium term injection results: c5

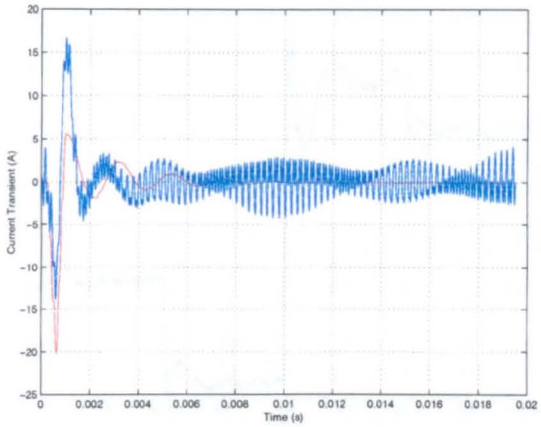

(a) Current transient.

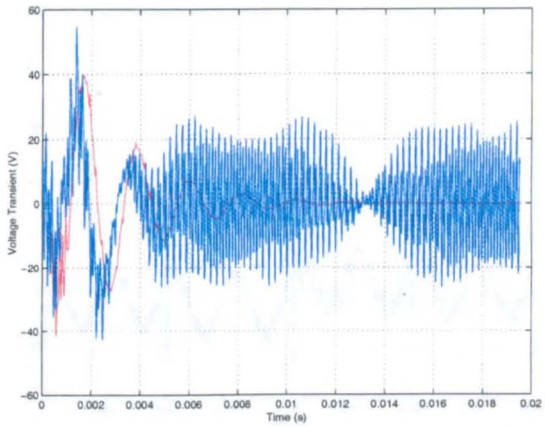

(b) Voltage transient.

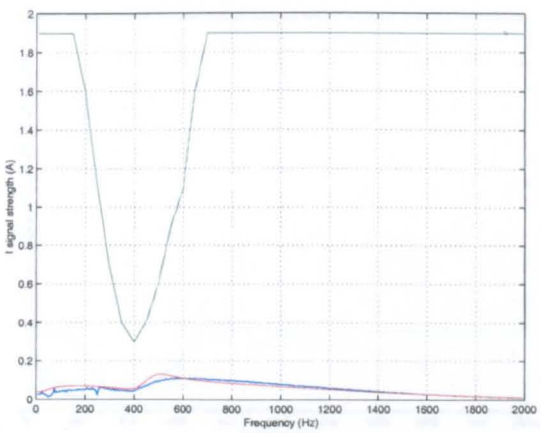

(c) Current spectrum.

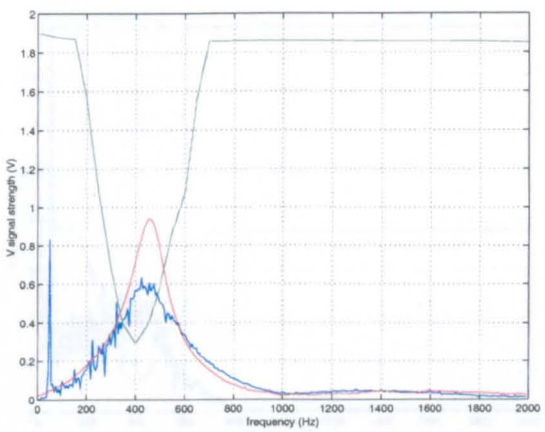

(d) Voltage spectrum.

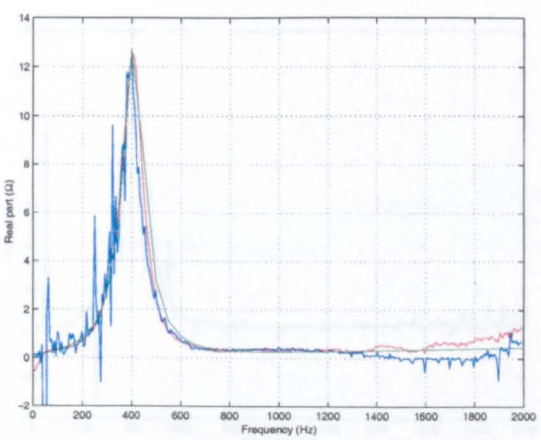

(e) Real impedance.

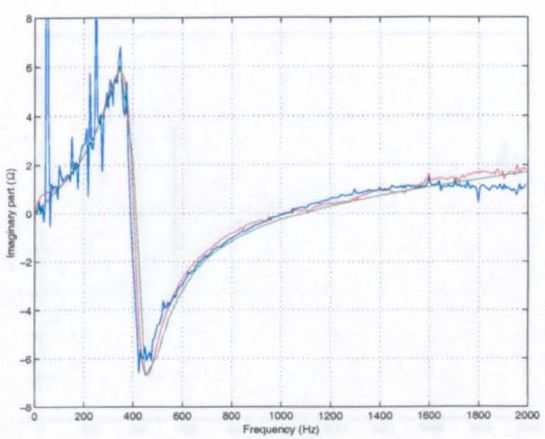

(f) Imaginary impedance.

Figure 5.22: Short term injection results: c6

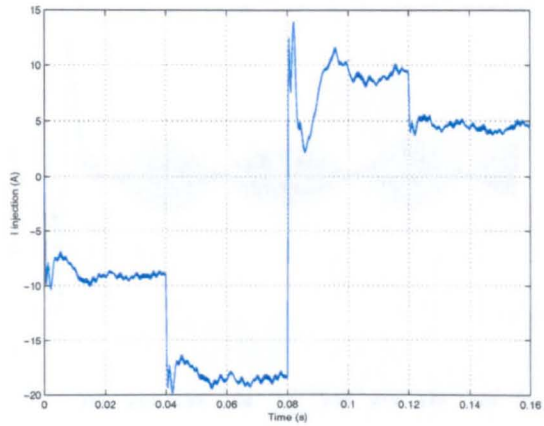

(a) Current transient.

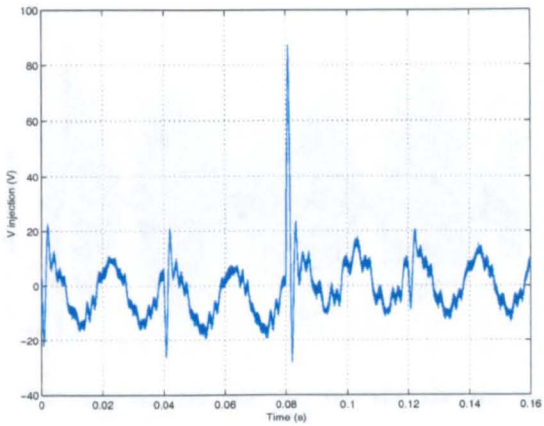

(b) Voltage transient.

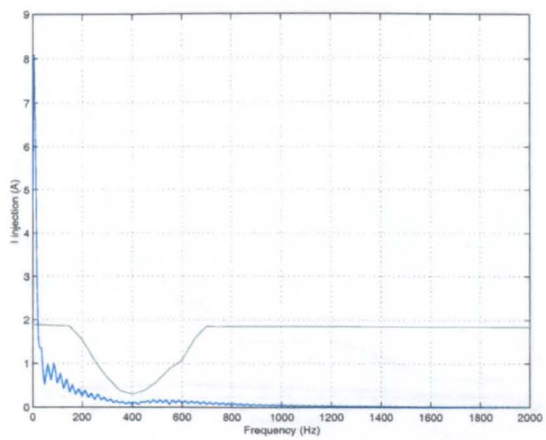

(c) Current spectrum.

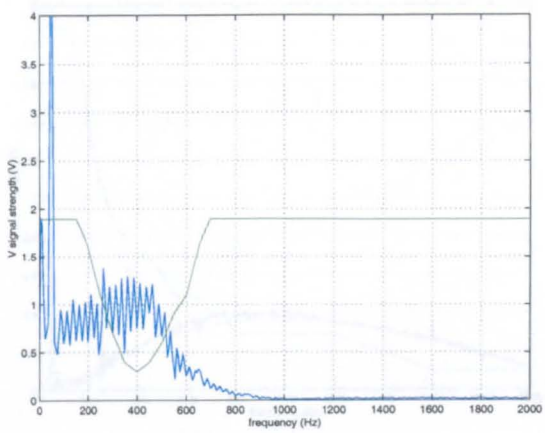

(d) Voltage spectrum.

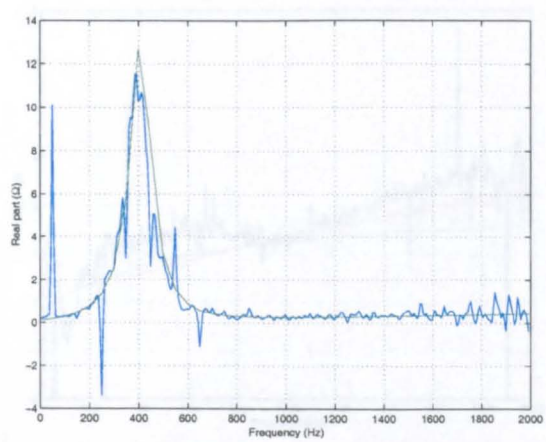

(e) Real impedance.

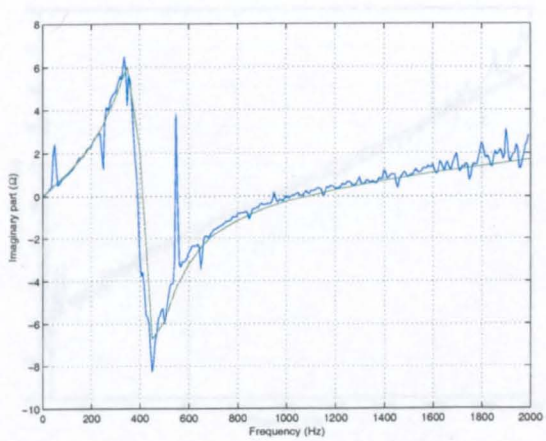

(f) Imaginary impedance.

Figure 5.23: Medium term injection results: c6

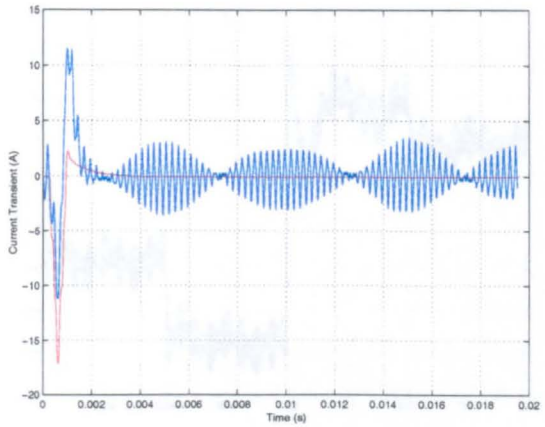

(a) Current transient.

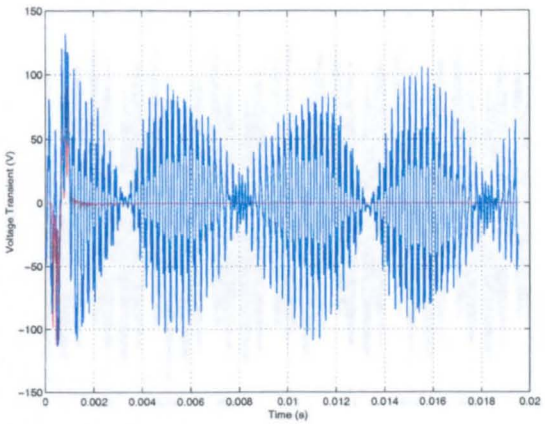

(b) Voltage transient.

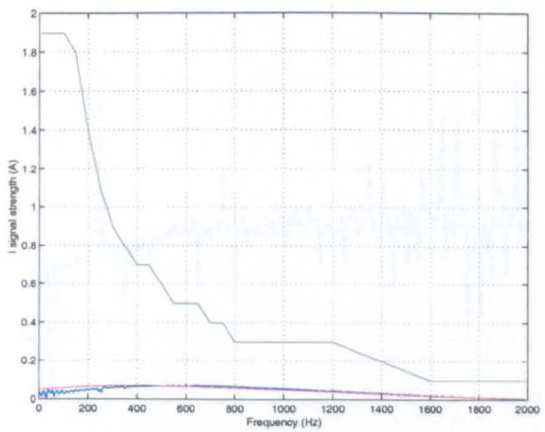

(c) Current spectrum.

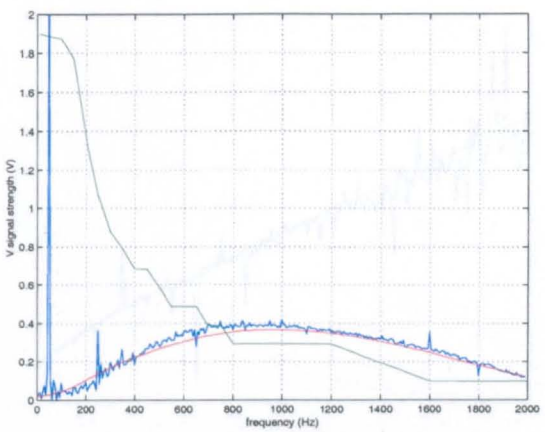

(d) Voltage spectrum.

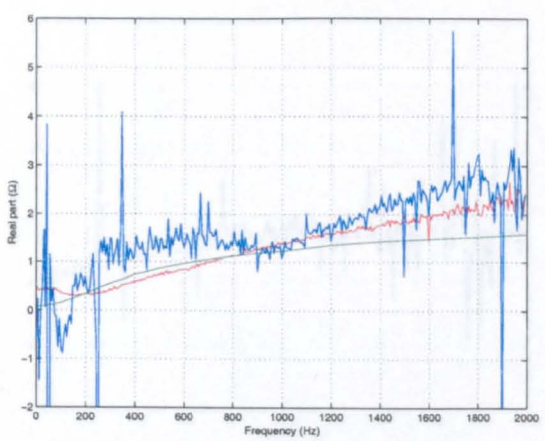

(e) Real impedance.

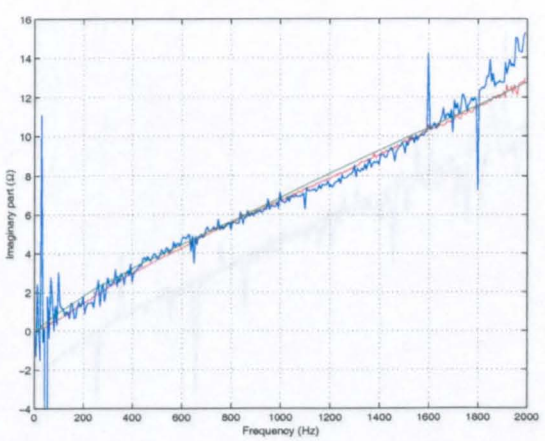

(f) Imaginary impedance.

Figure 5.24: Short term results: c7

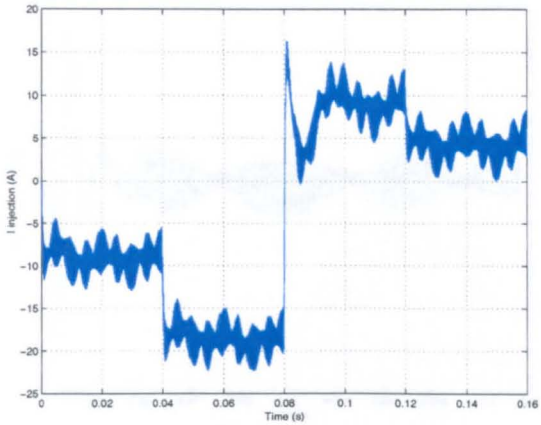

(a) Current transient.

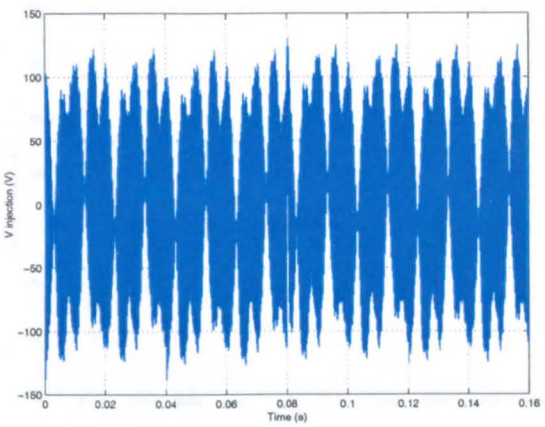

(b) Voltage transient.

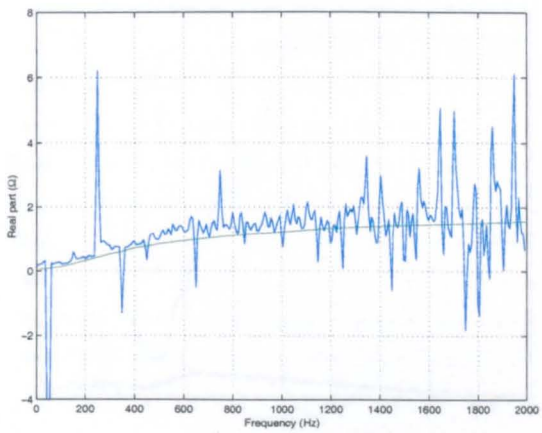

(c) Current spectrum.

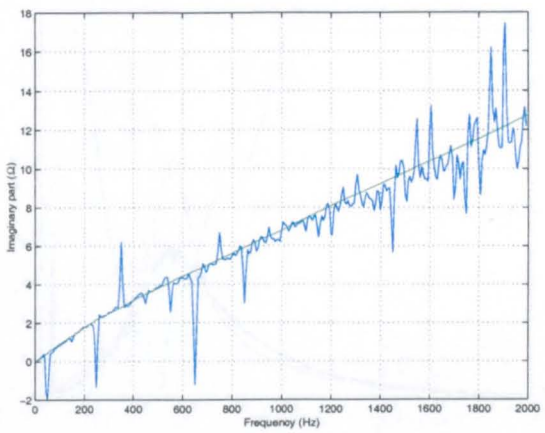

(d) Voltage spectrum.

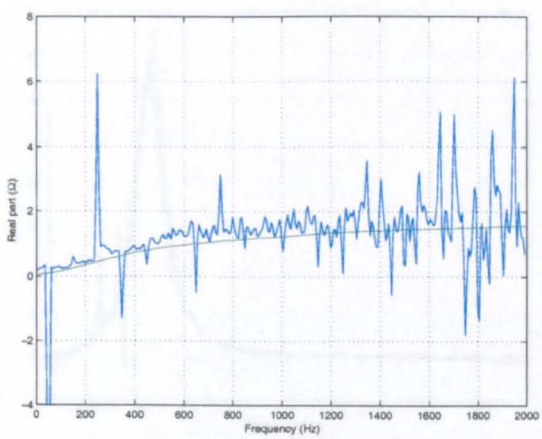

(e) Real impedance.

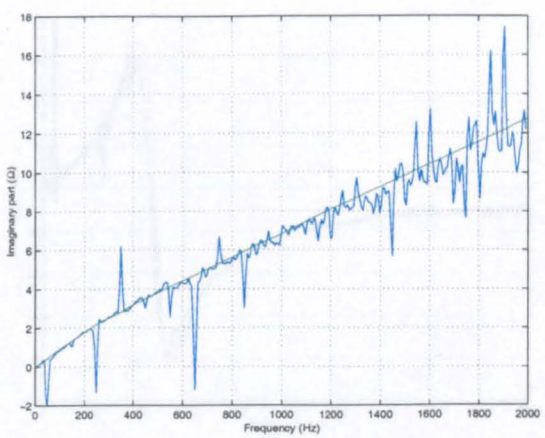

(f) Imaginary impedance.

Figure 5.25: Medium term injection results: c7

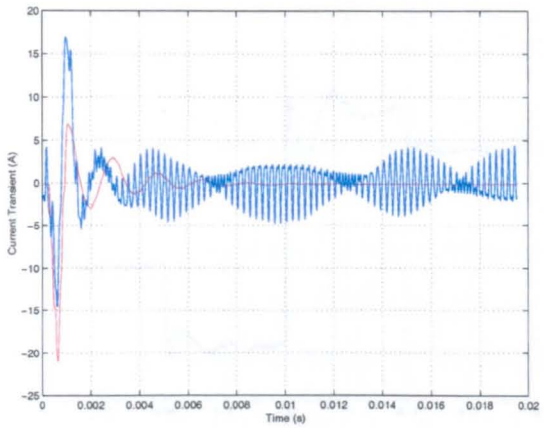

(a) Current transient.

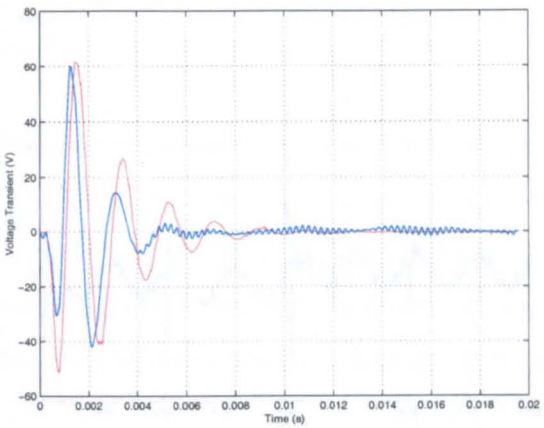

(b) Voltage transient.

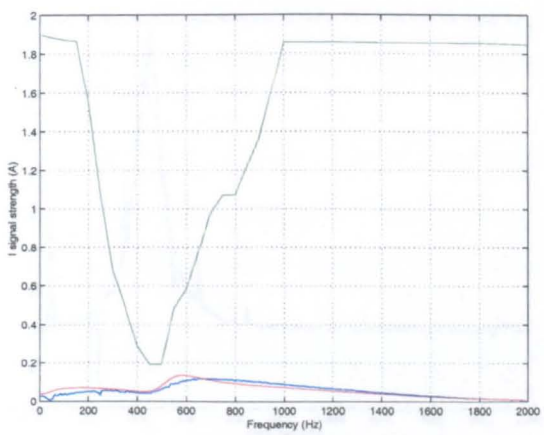

(c) Current spectrum.

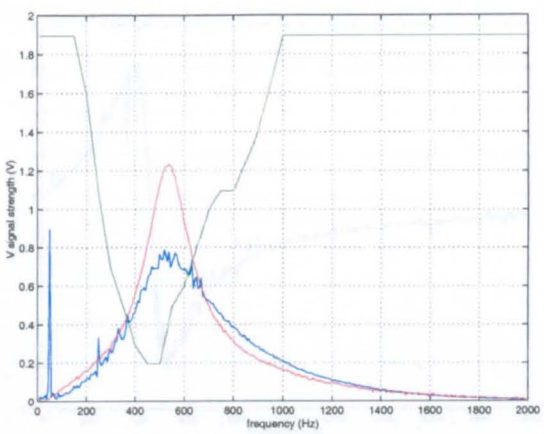

(d) Voltage spectrum.

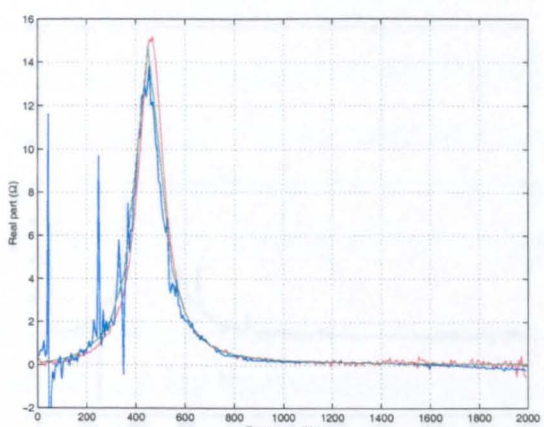

(e) Real impedance.

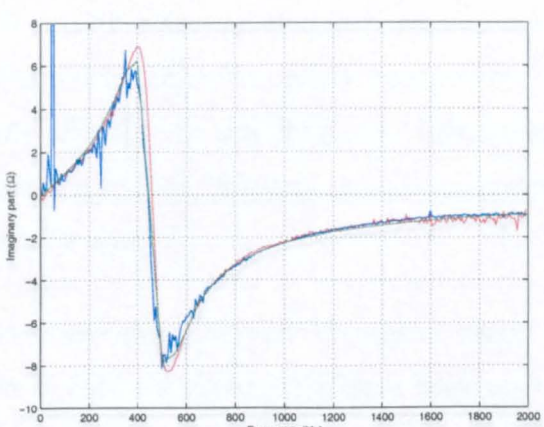

(f) Imaginary impedance.

Figure 5.26: Short term injection results: c8

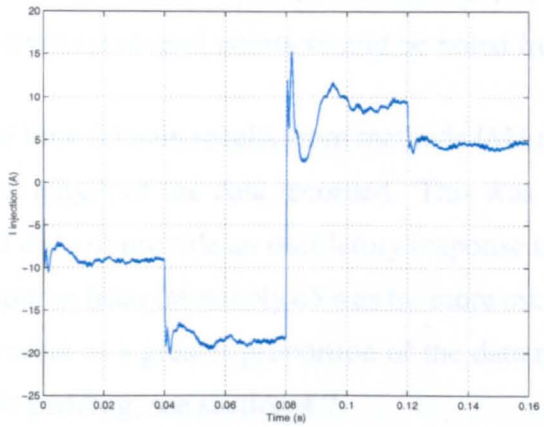

(a) Current transient.

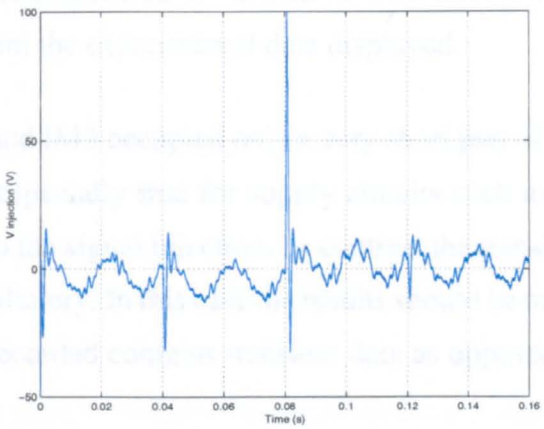

(b) Voltage transient.

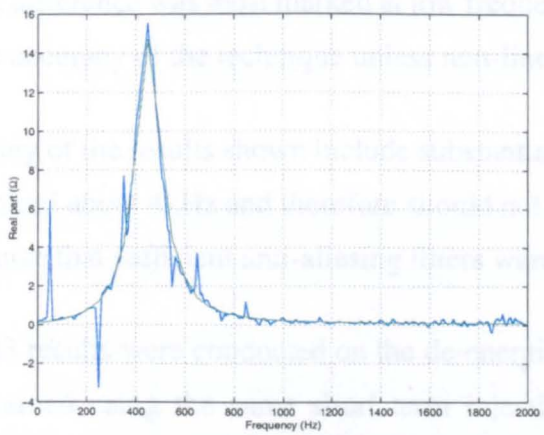

(c) Current spectrum.

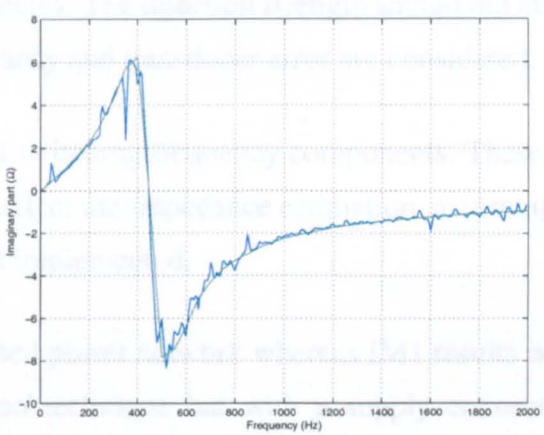

(d) Voltage spectrum.

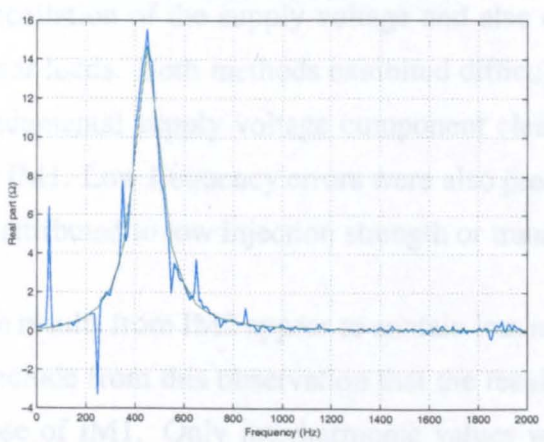

(e) Real impedance.

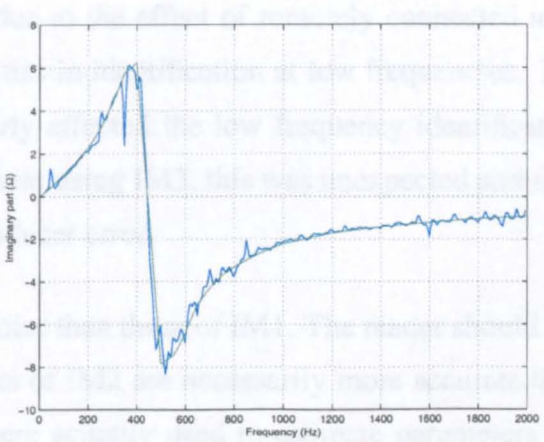

(f) Imaginary impedance.

Figure 5.27: Medium term injection results: c8

Parameter estimation from these results will be considered in the next section. Before such an analysis several points should be noted from the experimental data displayed.

The time domain results from methods IM1 and IM3 occupied only a very short part of the total length of the data recorded. This was especially true for supply circuits such as c1 that did not provide an oscillatory response to the signal injection. In contrast the transient response from the supply c5 was far more oscillatory. In this case the results should be more accurate as a greater proportion of the data recorded contains transient data as opposed to zero padding, see section 4.7.

The medium term injection strength applied was greater than the short term injection and the difference was most marked at low frequencies. The injection strength should not affect the accuracy of the technique unless non-linearity and transducer error are considered.

Many of the results shown include substantial switching frequency components. These are centred about 4kHz and therefore should not affect the impedance estimation, assuming of course that sufficient anti-aliasing filters were implemented.

IM3 results were conducted on the de-energised power network whereas IM1 results were obtained using the same short term injection technique but with a supply connection present. The effect of the supply can thus be seen. There was a considerable difference in the noise components especially at harmonic frequencies. This was due to imperfect cancellation of the supply voltage and also due to the effect of remotely connected non-linear loads. Both methods exhibited difficulties in identification at low frequencies. The fundamental supply voltage component clearly affected the low frequency identification for IM1. Low frequency errors were also present using IM3, this was unexpected and may be attributed to low injection strength or transducer error.

The results from IM2 appear to contain less noise than those of IM1. The reader should not conclude from this observation that the results of IM2 are necessarily more accurate than those of IM1. Only interharmonic values were actually used to estimate parameters for the different supplies, these may not be affected by the apparently high noise component present in the IM1 results. The smooth appearance of the IM2 impedance estimates was

due to the application of a Hanning window during the processing of the results.

The results for circuits c7 and c8 were very similar to those of c1 and c3 respectively. This was expected and shows that steady state current cancellation was successful in both cases.

5.4.2 Parameter estimation from experimental results

Using the results obtained in the previous section it was possible to complete the remaining part of the impedance estimation techniques. Appropriate interharmonic values were selected, as discussed in the previous chapter, in the frequency range between d.c. and 1kHz. These values were used in order to formulate a linear transfer function for each supply impedance configuration. Figures are shown over the following pages to illustrate this process.

Impedance estimation figures are shown for each supply circuit and for both injection techniques IM1 and IM2. Interharmonic values are shown in each case, these were chosen according to the method outlined for each technique in the previous chapter. These values were then used to calculate linear transfer functions for the supply impedance in each case. A third order transfer function was assumed in all cases. These impedance calculated from these functions was also displayed in the figures. Finally the impedance measured from IM3 was again plotted for comparison.

Trace	Description	Trace colour
IM1	Short term injection method Interharmonic values chosen Frequencies are:$25(2n+1), 0 \leq n \leq 19$	Blue
IM2	Medium term injection method Interharmonic values chosen Frequencies are:$25(2n+1)+6.25, 0 \leq n \leq 19$	Blue
IM3	Discrete frequency injection No supply connection	Green
Curve fit	Output from curve fitting algorithm Points plotted at 6.25Hz intervals	Red

Table 5.2: Legend for Curve fitting results figures

Blue	Short term injection (IM1) interharmonics for curve fitting algorithm.
Blue	Medium term injection (IM2) interharmonics for curve fitting algorithm.
Green	Discrete frequency injection (IM3) values - no supply connection.
Red	Impedance estimate generated from the curve fitting algorithm.

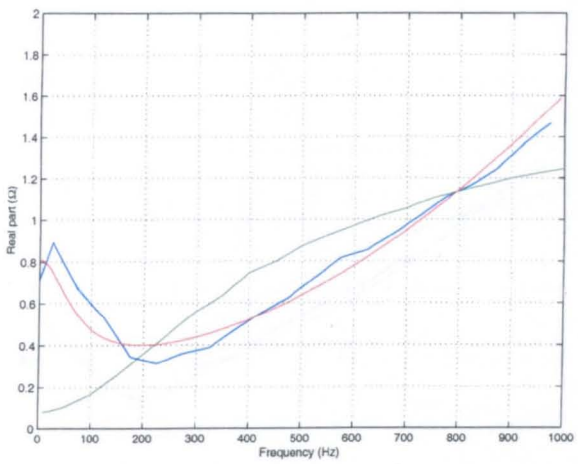

(b) Real impedance (IM1).

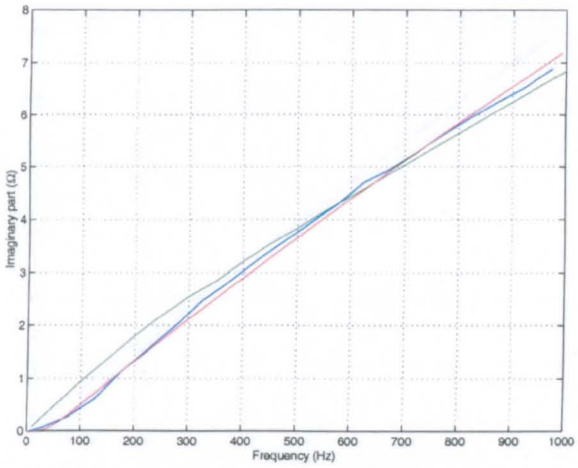

(c) Imaginary impedance (IM1).

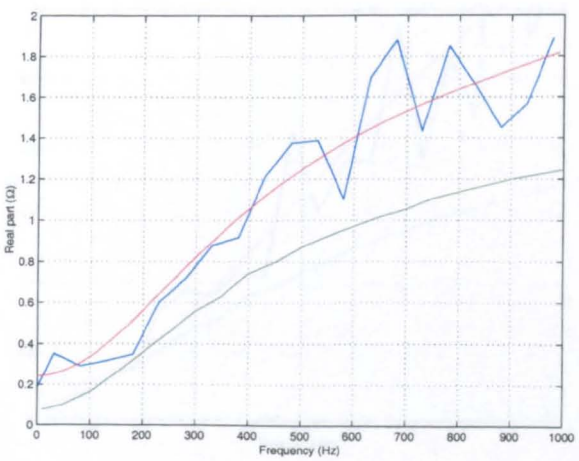

(d) Real impedance (IM2).

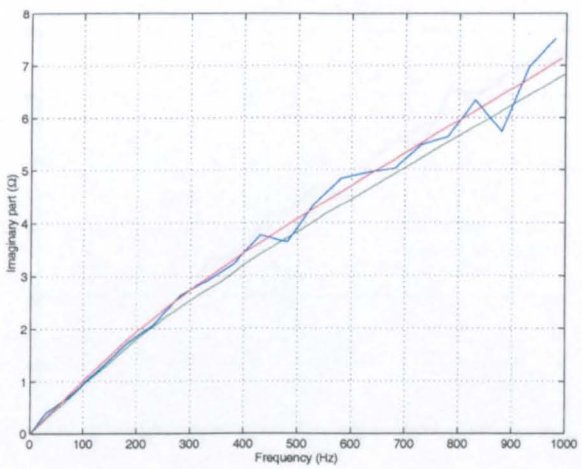

(e) Imaginary impedance (IM2).

Figure 5.28: Parameter estimation from experimental results: c1

Blue	Short term injection (IM1) interharmonics for curve fitting algorithm.
Blue	Medium term injection (IM2) interharmonics for curve fitting algorithm.
Green	Discrete frequency injection (IM3) values - no supply connection.
Red	Impedance estimate generated from the curve fitting algorithm.

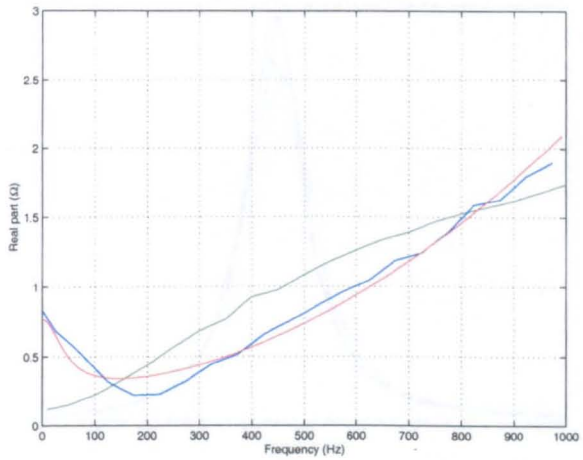

(b) Real impedance (IM1).

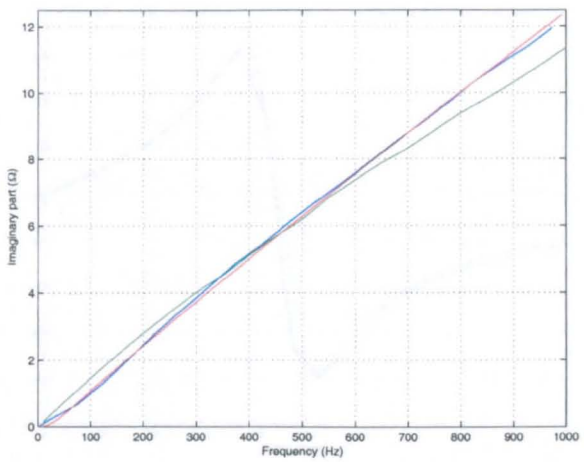

(c) Imaginary impedance (IM1).

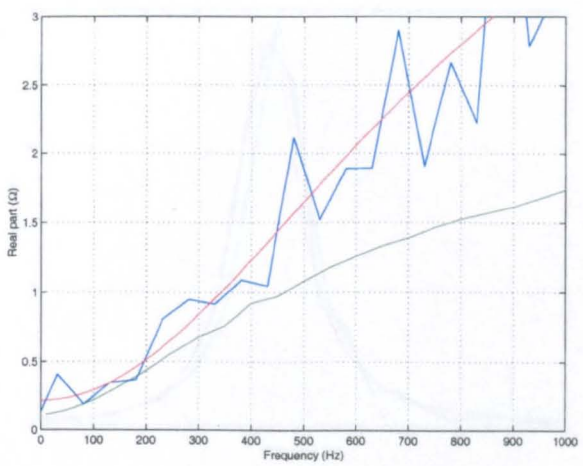

(d) Real impedance (IM2).

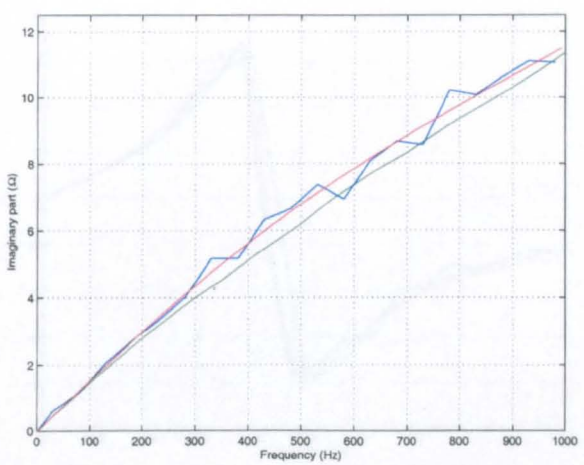

(e) Imaginary impedance (IM2).

Figure 5.29: Parameter estimation from experimental results: c2

Blue	Short term injection (IM1) interharmonics for curve fitting algorithm.
Blue	Medium term injection (IM2) interharmonics for curve fitting algorithm.
Green	Discrete frequency injection (IM3) values - no supply connection.
Red	Impedance estimate generated from the curve fitting algorithm.

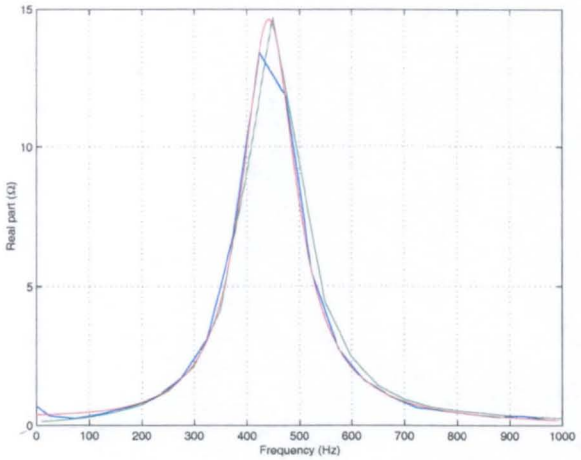

(b) Real impedance (IM1).

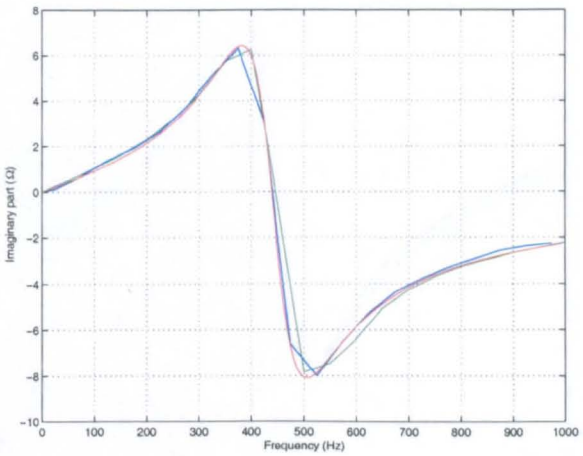

(c) Imaginary impedance (IM1).

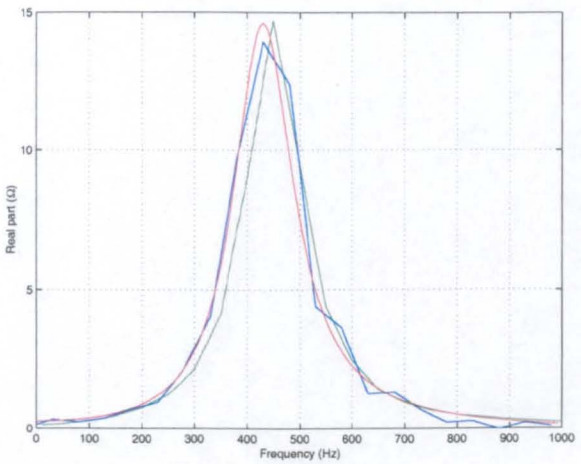

(d) Real impedance (IM2).

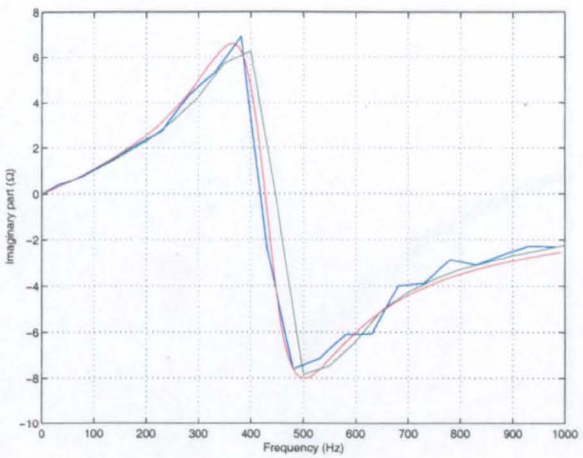

(e) Imaginary impedance(IM2).

Figure 5.30: Parameter estimation from experimental results: c3

Blue	Short term injection (IM1) interharmonics for curve fitting algorithm.
Blue	Medium term injection (IM2) interharmonics for curve fitting algorithm.
Green	Discrete frequency injection (IM3) values - no supply connection.
Red	Impedance estimate generated from the curve fitting algorithm.

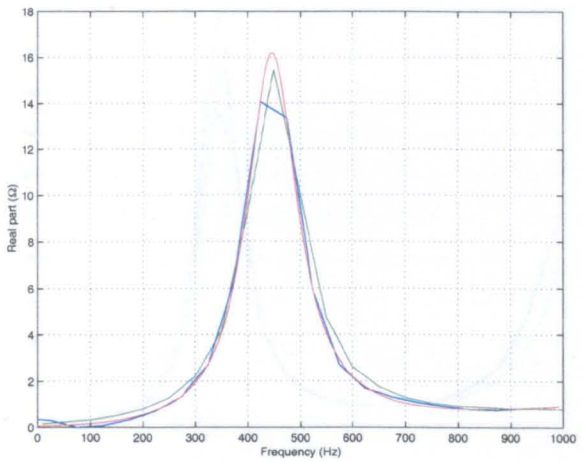

(b) Real impedance (IM1).

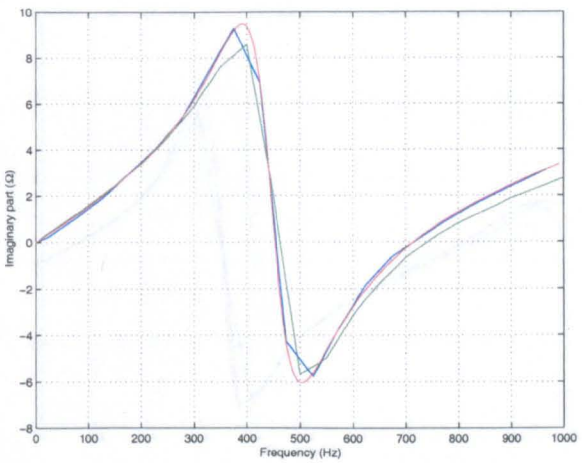

(c) Imaginary impedance (IM1).

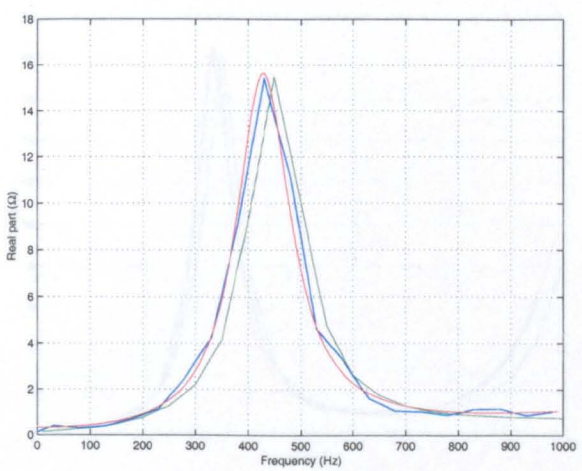

(d) Real impedance (IM2).

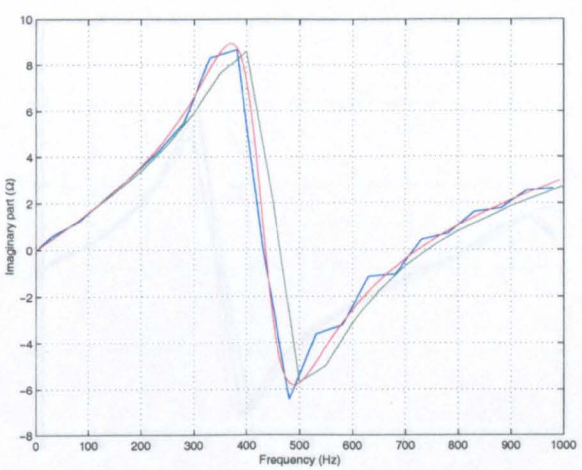

(e) Imaginary impedance (IM2).

Figure 5.31: Parameter estimation from experimental results: c4

Blue	Short term injection (IM1) interharmonics for curve fitting algorithm.
Blue	Medium term injection (IM2) interharmonics for curve fitting algorithm.
Green	Discrete frequency injection (IM3) values - no supply connection.
Red	Impedance estimate generated from the curve fitting algorithm.

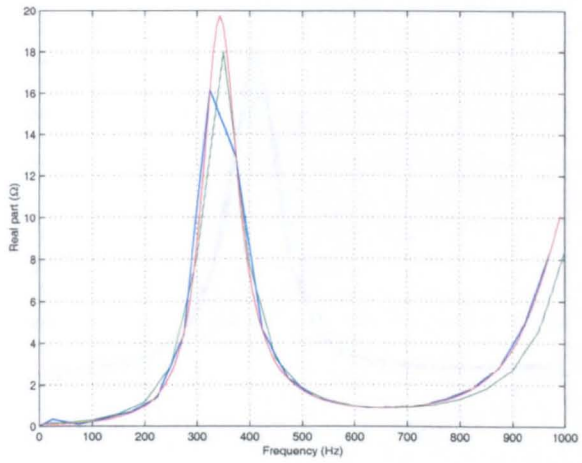

(b) Real impedance (IM1).

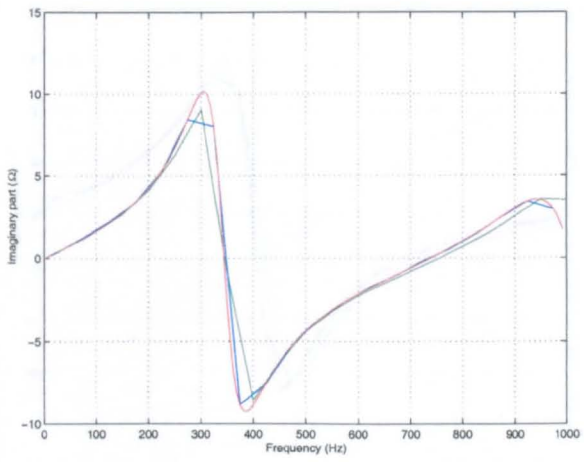

(c) Imaginary impedance (IM1).

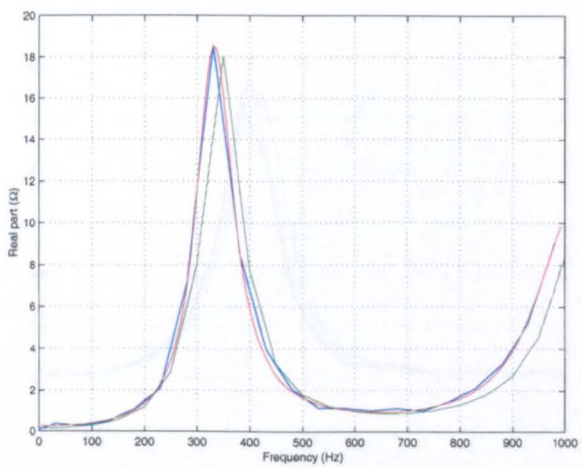

(d) Real impedance (IM2).

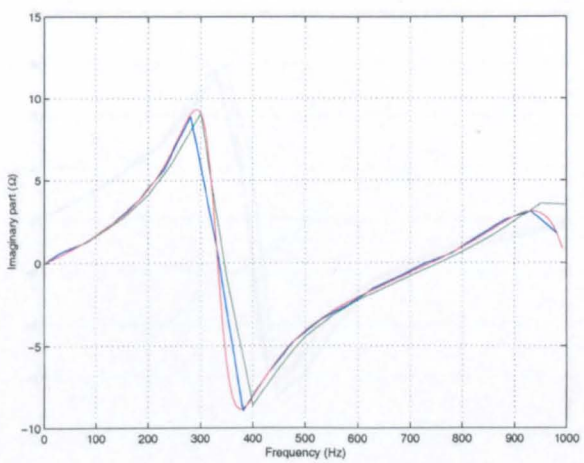

(e) Imaginary impedance (IM2).

Figure 5.32: Parameter estimation from experimental results: c5

Blue	Short term injection (IM1) interharmonics for curve fitting algorithm.
Blue	Medium term injection (IM2) interharmonics for curve fitting algorithm.
Green	Discrete frequency injection (IM3) values - no supply connection.
Red	Impedance estimate generated from the curve fitting algorithm.

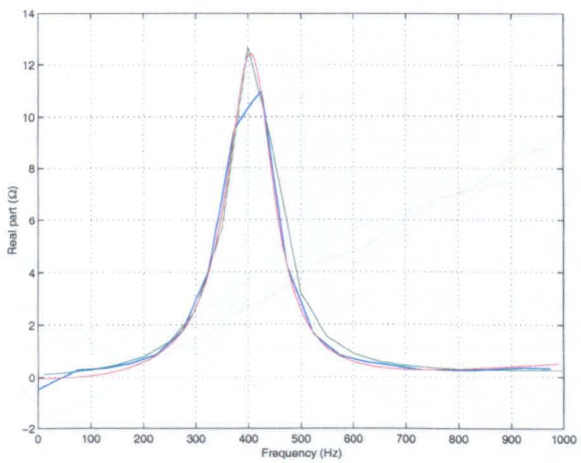

(b) Real impedance (IM1).

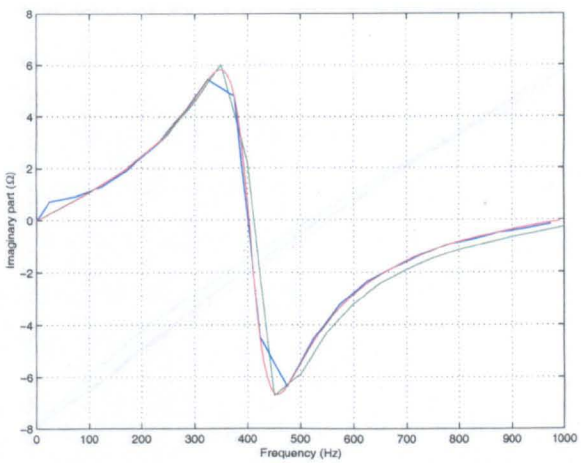

(c) Imaginary impedance (IM1).

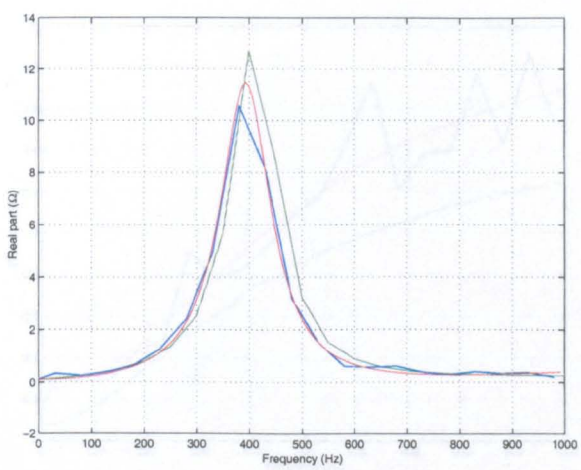

(d) Real impedance (IM2).

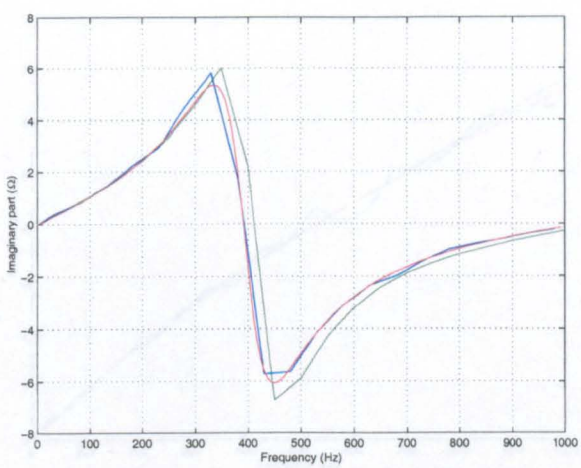

(e) Imaginary impedance (IM2).

Figure 5.33: Parameter estimation from experimental results: c6

Blue	Short term injection (IM1) interharmonics for curve fitting algorithm.
Blue	Medium term injection (IM2) interharmonics for curve fitting algorithm.
Green	Discrete frequency injection (IM3) values - no supply connection.
Red	Impedance estimate generated from the curve fitting algorithm.

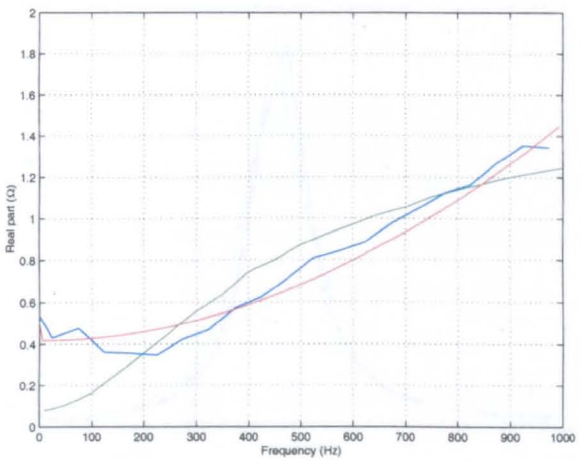

(b) Real impedance (IM1).

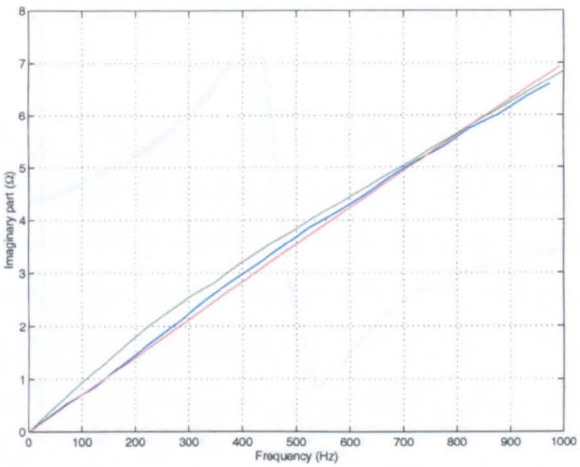

(c) Imaginary impedance (IM1).

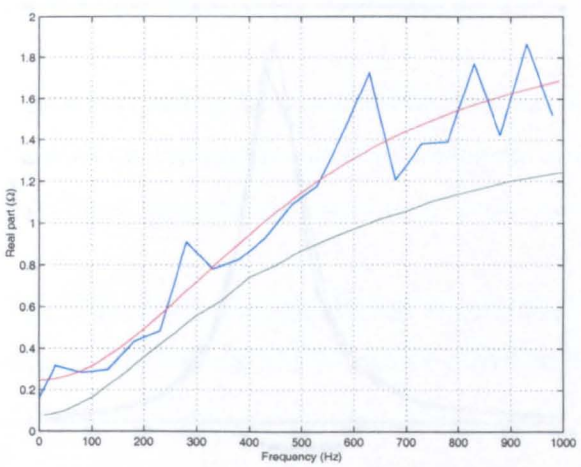

(d) Real impedance (IM2).

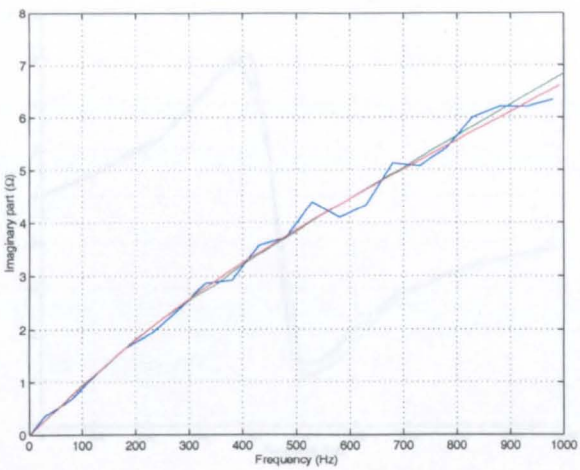

(e) Imaginary impedance (IM2).

Figure 5.34: Parameter estimation from experimental results: c7

Blue	Short term injection (IM1) interharmonics for curve fitting algorithm.
Blue	Medium term injection (IM2) interharmonics for curve fitting algorithm.
Green	Discrete frequency injection (IM3) values - no supply connection.
Red	Impedance estimate generated from the curve fitting algorithm.

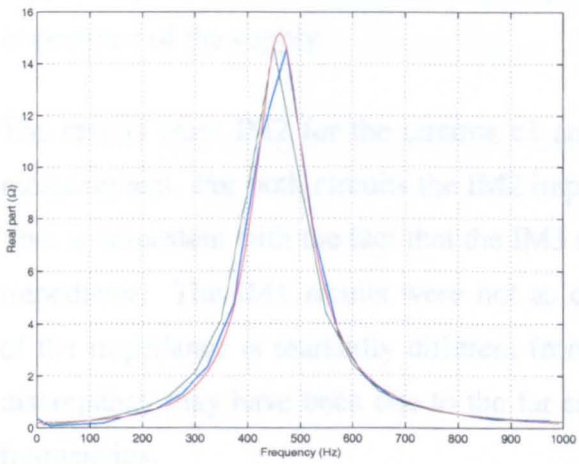

(b) Real impedance (IM1).

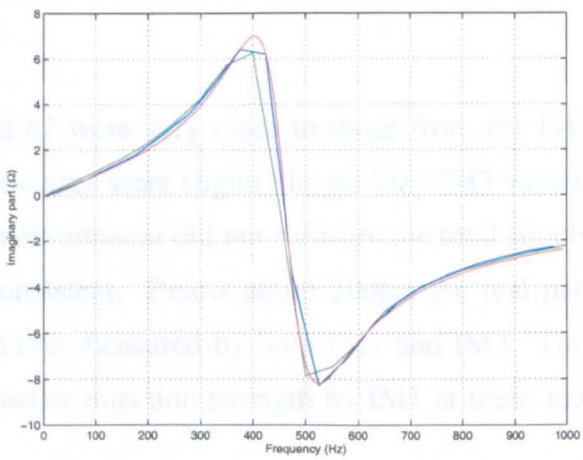

(c) Imaginary impedance (IM1).

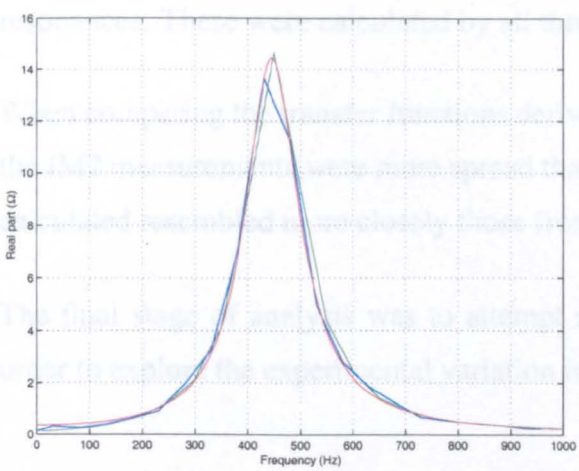

(d) Real impedance (IM2).

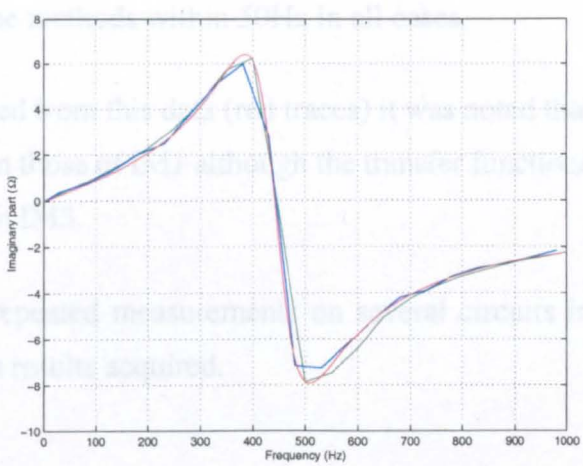

(e) Imaginary impedance (IM2).

Figure 5.35: Parameter estimation from experimental results: c8

From the preceding figures it is clear that both the short term and medium term injection techniques were able to provide excellent measurements of the supply impedance. Noise components due to the supply voltage were practically eliminated and the curve fitting routine was able to provide transfer functions that fitted the experimental data. It was not strictly correct to compare the impedance estimates derived from IM1 and IM2 with the calibrator derived measurement of IM3 as the latter method does not consider the total supply impedance. Nevertheless this impedance was the closest available to the actual impedance of the supply.

The results from IM2 for the circuits c1 and c2 were very close to those from the IM3 measurement. For both circuits the IM2 impedances were slightly larger than IM3 values. This is consistent with the fact that the IM3 measurement did not measure the total supply impedance. The IM1 results were not as consistent. Below about 200Hz the real part of the impedance is markedly different from that measured by both IM1 and IM3. This discrepancy may have been due to the far smaller injection strength by IM1 at these low frequencies.

In the test circuits that included resonances both IM1 and IM2 were able to identify the resonances. These were calculated by all three methods within 50Hz in all cases.

When comparing the transfer functions derived from this data (red traces) it was noted that the IM2 measurements were more spread than those of IM1 although the transfer functions calculated resembled more closely those from IM3.

The final stage of analysis was to attempt repeated measurements on several circuits in order to explore the experimental variation in results acquired.

5.4.3 Statistical variation of experimental results

Repeated measurements were made using both IM1 and IM2 on circuits c1, c3 and c6. These circuits were chosen as being representative of common supply circuits. Thirty measurements were made by each method for each circuit chosen. The mean impedance has been plotted in the following figures. Furthermore, error bars indicating errors at one standard deviation have been shown to give an indication of the variability of the impedance estimates obtained using these techniques.

The twenty interharmonic values in the range between 0 and 1kHz have been plotted.

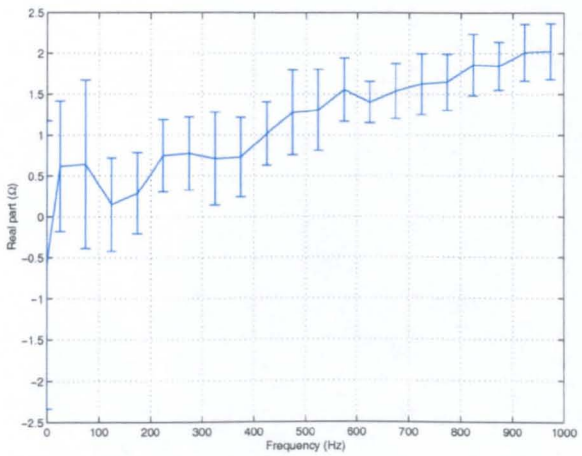

(a) Real impedance (IM1).

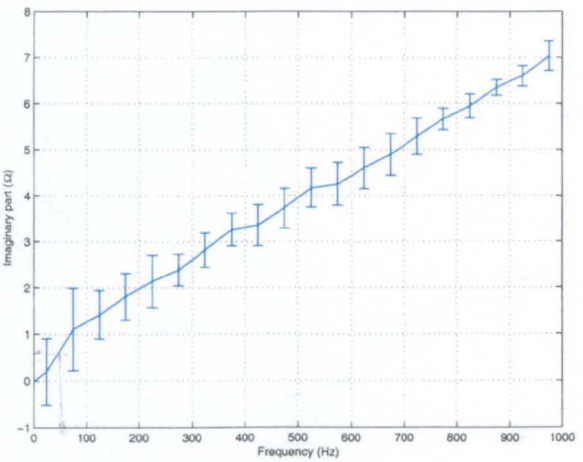

(b) Imaginary impedance (IM1).

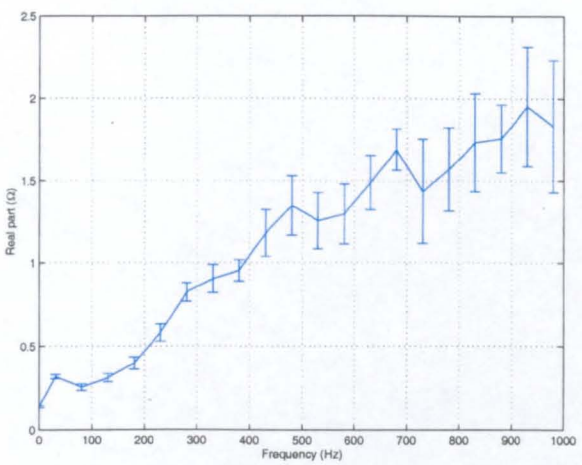

(c) Real impedance (IM2).

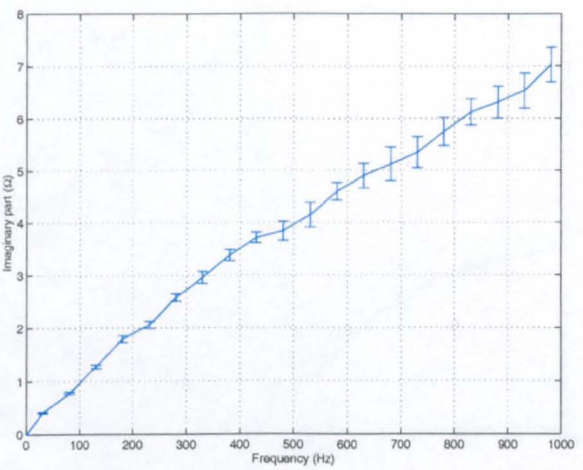

(d) Imaginary impedance (IM2).

Figure 5.36: Mean and standard deviation of experimental results: c1

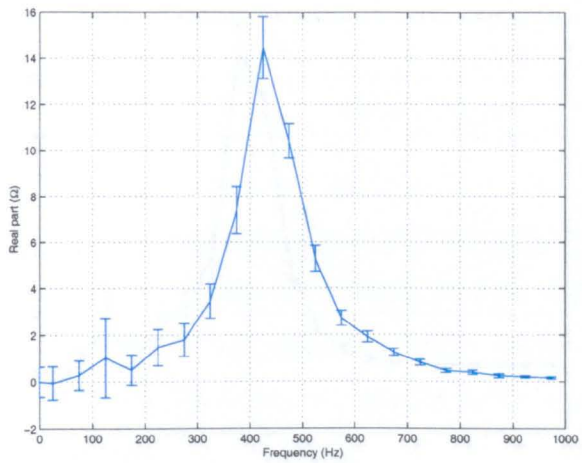

(a) Real impedance (IM1).

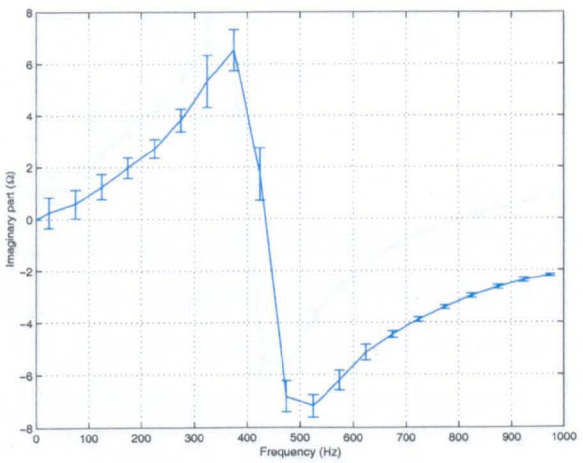

(b) Imaginary impedance (IM1).

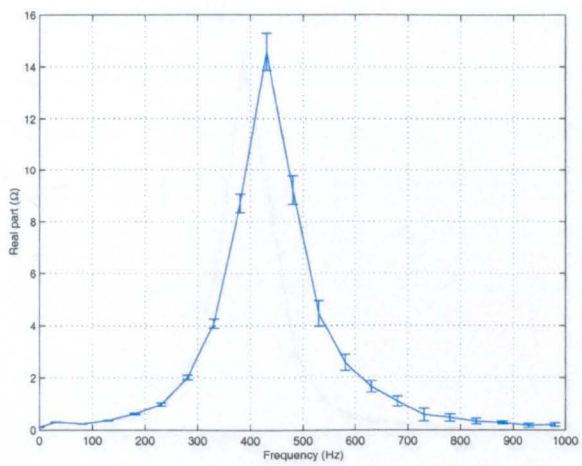

(c) Real impedance (IM2).

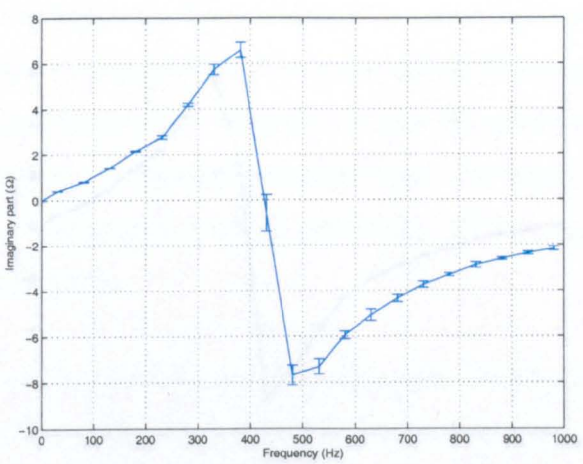

(d) Imaginary impedance (IM2).

Figure 5.37: Mean and standard deviation of experimental results: c3

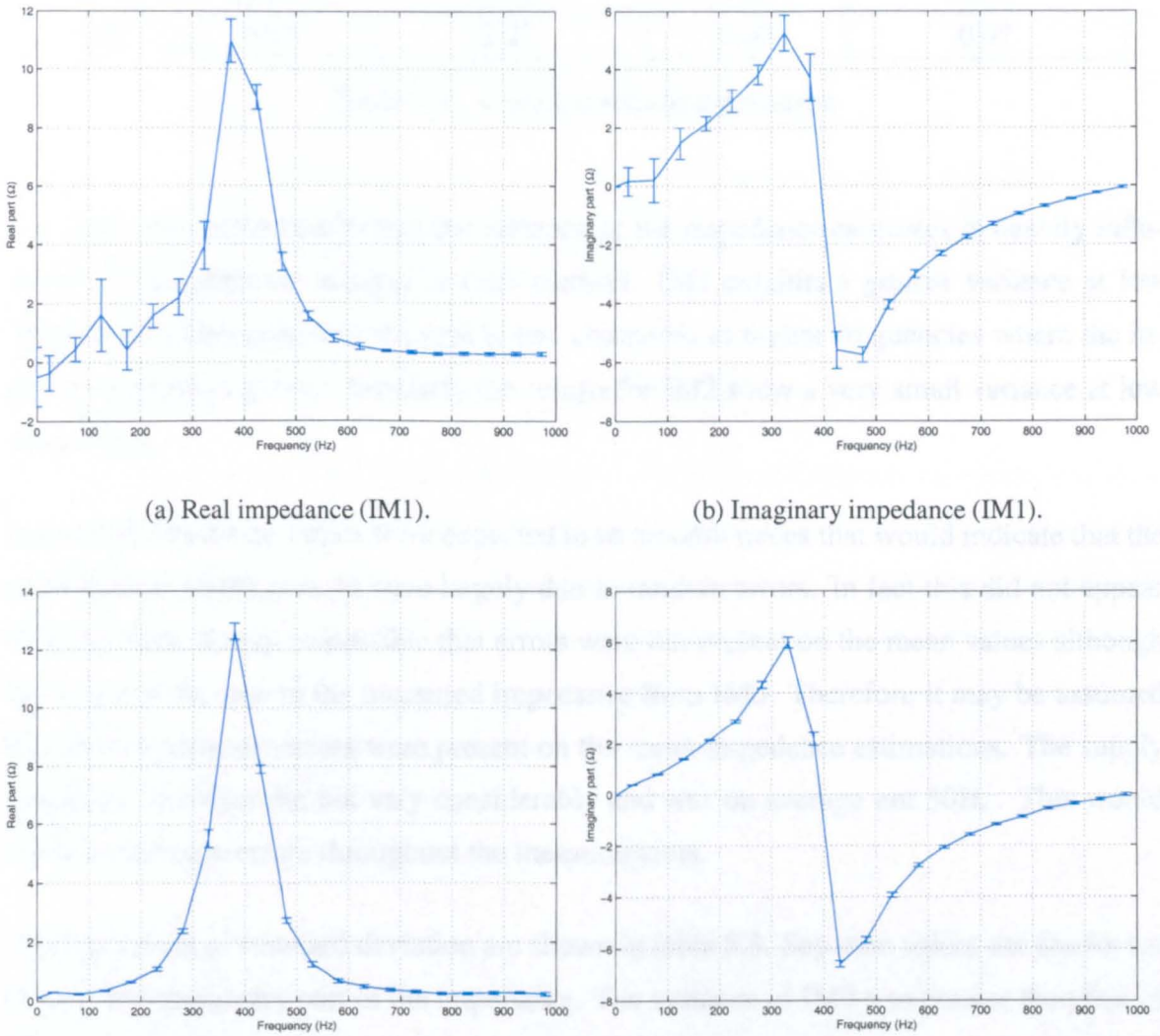

(a) Real impedance (IM1).

(b) Imaginary impedance (IM1).

(c) Real impedance (IM2).

(d) Imaginary impedance (IM2).

Figure 5.38: Mean and standard deviation of experimental results: c6

Circuit	Injection method			
	Short term (IM1)		Medium term (IM2)	
	Real part (Ω)	Imaginary part (Ω)	Real part (Ω)	Imaginary part (Ω)
c1	0.53	0.41	0.15	0.17
c3	0.54	0.38	0.19	0.16
c6	0.38	0.27	0.07	0.07

Table 5.3: Averaged standard deviation

It is clear from these results that the variance of the impedance estimates is heavily influenced by the injection strength of each method. IM1 exhibits a greater variance at low frequencies where injection strength is low compared to higher frequencies where the injection strength is greater. Similarly the results for IM2 show a very small variance at low frequencies.

The mean impedance values were expected to be smooth traces that would indicate that the measurement errors present were largely due to random errors. In fact this did not appear to be the case. It may be possible that errors were not present on the mean values although this was not the case in the measured impedance from IM3. Therefore it may be assumed that some systematic errors were present on the mean impedance estimations. The supply frequency therefore did not vary considerably and was on average not 50Hz. This would result in common errors throughout the measurements.

Average values of standard deviation are shown in table 5.3. Separate values are shown for the real and imaginary part of the impedance. The variance of IM2 was greater than that of IM1 as expected from a comparison of injection strengths.

5.4.4 Conclusions from experimental results

The experimental results given in this chapter have verified the measurement techniques described in the previous chapter. Performance was shown to be excellent although was

mainly dependent on the injection strength of each method at each frequency of interest.

It may be possible to improve the performance of both methods with more accurate steady state cancellation. This could be achieved with a phase locked loop (PLL) identifying the exact supply frequency. This would further reduce the signal processing requirements of each method. It may be possible to also use the same PLL within the ASF to gain an accurate knowledge of the supply frequency and to ensure that a certain number of samples are made each fundamental cycle. In this case the ASF transducers could also be used for system impedance identification as the sampling rate would not need to be as high.

5.5 Summary

This chapter has successfully demonstrated the two proposed impedance estimation techniques and the signal processing algorithms associated with each. All analysis has so far ignored the interaction of NLLs connected close to the point of measurement. It is the aim of the next chapter to investigate how both techniques are affected by a locally connected NLL.

Chapter 6

Measurement results in the presence of non-linear loads

6.1 Introduction

The aim of this chapter was to investigate the performance of the two proposed measurement techniques in the presence of NLLs. In practice a measurement of supply impedance may be required at a point where a NLL is connected. For example, a consumer may intend to install an active or passive filter to compensate for such a load. It is therefore necessary to establish the performance of the techniques when a NLL is connected at the point of measurement. It is obviously not desirable to disconnect the load for such a measurement.

In the previous chapter linear estimates of the supply impedance were successfully made even though many NLLs were inadvertently connected to the laboratory supply, within other experimental systems. This did not significantly affect the impedance estimates obtained. In this chapter NLLs connected at the POM were considered in order to determine whether the measurement procedure would affect the NLLs in such a way as to influence the interharmonic impedance estimates.

6.2 Experimental circuits

Three experimental systems were utilized to study the performance of each measurement technique described. The experimental circuits employed are shown in figure 6.1. The circuits are referred to as circuits A, B and C. No *a priori* knowledge of the non-linear loads was used for identification as such information will not be readily available in practical situations. Circuit A is a CS-NLL load, circuit B is a VS-NLL load and C is a combined VS-NLL and CS-NLL, as defined in chapter 2. The third circuit was implemented experimentally to either represent a VS-NLL connected remotely from the point of measurement or a VS-NLL with smoothing inductors connected to reduce the harmonic current output of such a load.

In order to verify the measurement techniques, readings were taken for both categories of NLL using the medium and short term techniques. Only supply circuits C1 and C3 were used in the interest of brevity. The medium term injection technique performance was considered initially followed by the short term injection performance. Injection results are displayed for each technique followed by a discussion of the measurement results.

6.3 Medium term injection

The medium term injection technique was applied to circuits A, B and C. In each case both supply circuits c1 and c3 were used. Typical measurement results are shown in figures 6.2 to 6.7. A discussion of these measurements follows the figures. Figures 6.2 and 6.3 show measurement results using circuit A for c1 and c3 respectively. Figures 6.4 and 6.5 show measurements for circuit B for c1 and c3. Finally, figures 6.6 and 6.7 show measurement results for circuit C, also for c1 and c3.

6.3.1 Medium term injection results

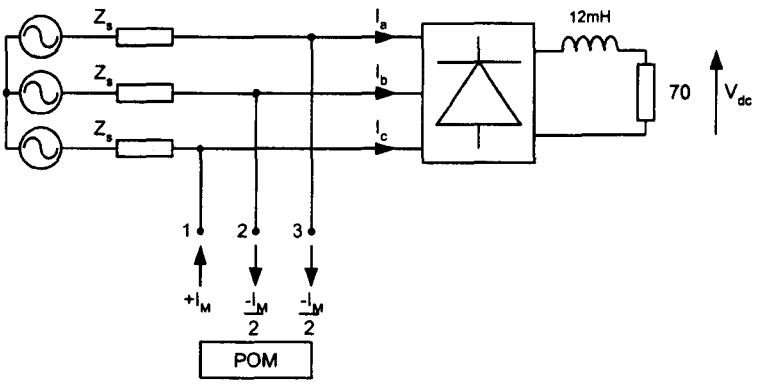

(a) Circuit A: CS-NLL.

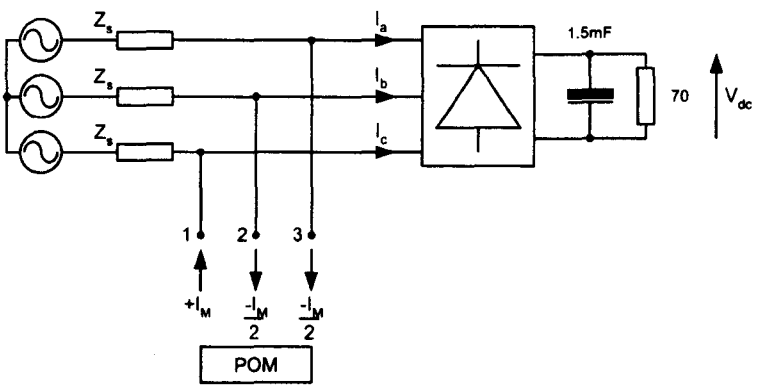

(b) Circuit B: VS-NLL.

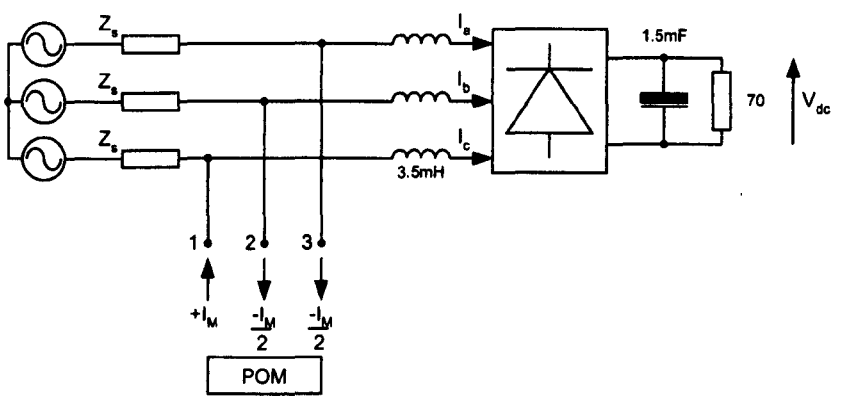

(c) Circuit C: Combined NLL.

Figure 6.1: Experimental circuits

Blue	Medium term injection (IM2) data before curve fitting.
Red	Interharmonic values used for the curve fitting algorithm.
Green	Calibrator measurements (IM3) with supply and NLL disconnected.

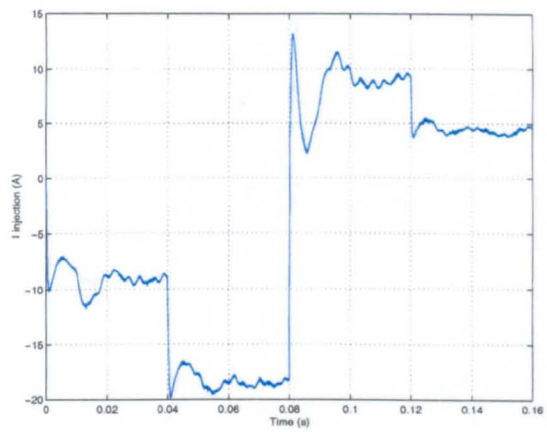

(b) Current transient.

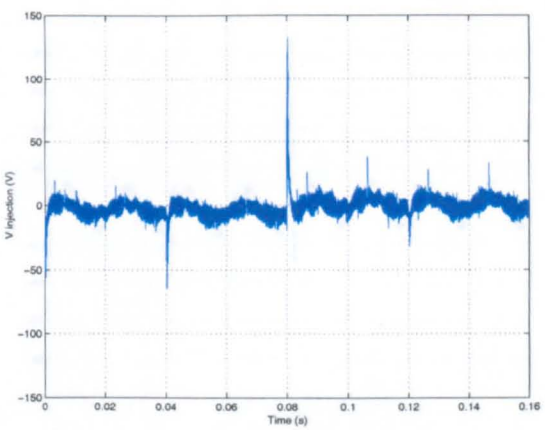

(c) Voltage transient.

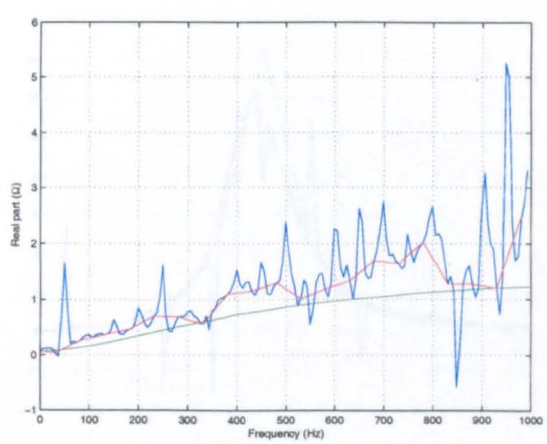

(d) Real impedance.

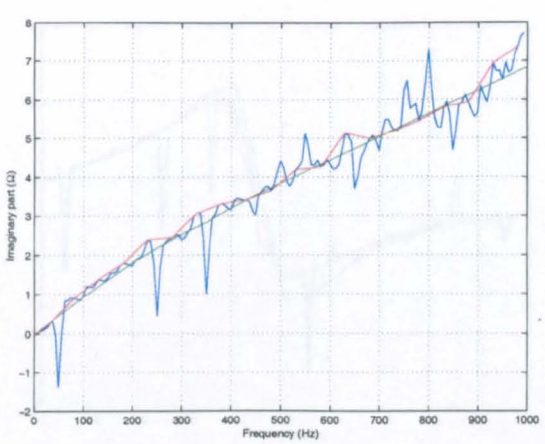

(e) Imaginary impedance.

Figure 6.2: Medium term injection for circuit A (CS-NLL) and supply c1

Blue	Medium term injection (IM2) data before curve fitting.
Red	Interharmonic values used for the curve fitting algorithm.
Green	Calibrator measurements (IM3) with supply and NLL disconnected.

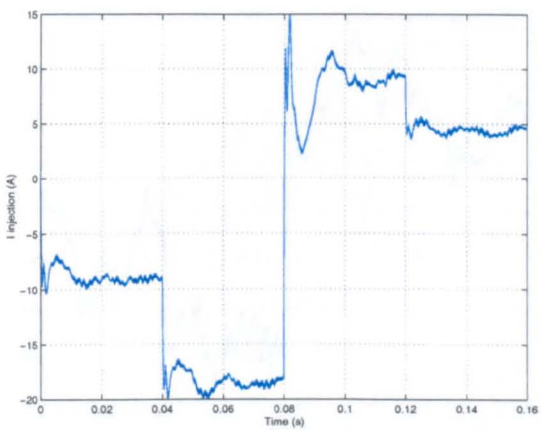

(b) Current transient.

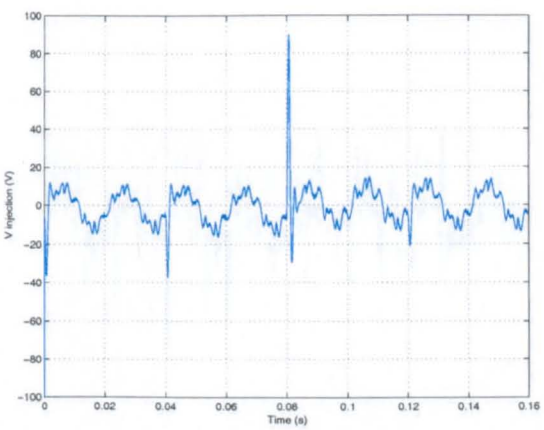

(c) Voltage transient.

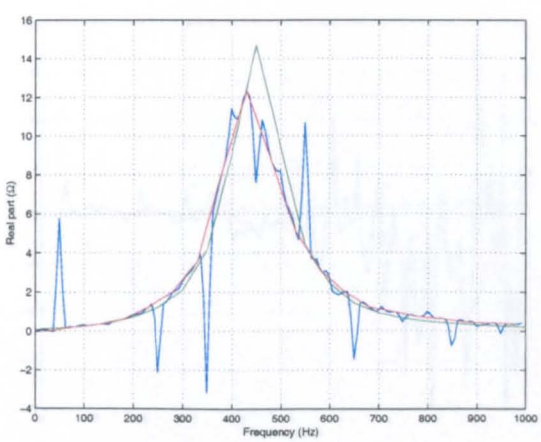

(d) Real impedance.

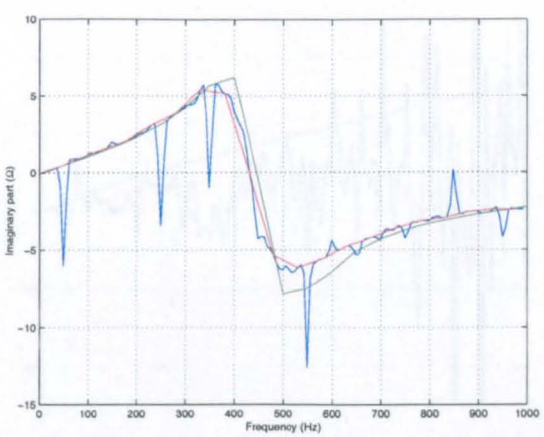

(e) Imaginary impedance.

Figure 6.3: Medium term injection for circuit A (CS-NLL) and supply c3

Blue	Medium term injection (IM2) data before curve fitting.
Red	Interharmonic values used for the curve fitting algorithm.
Green	Calibrator measurements (IM3) with supply and NLL disconnected.

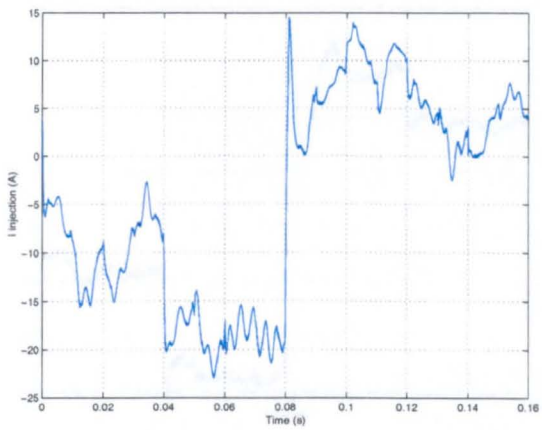

(b) Current transient.

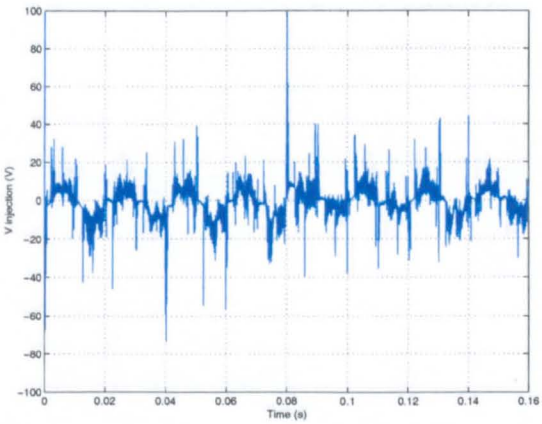

(c) Voltage transient.

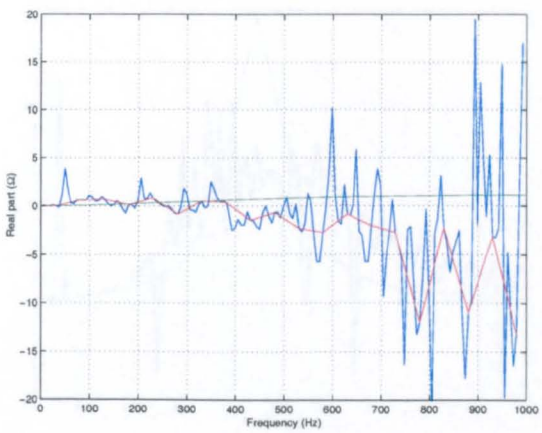

(d) Real impedance.

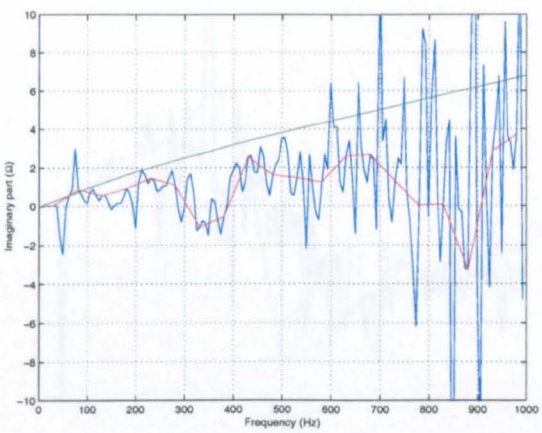

(e) Imaginary impedance.

Figure 6.4: Medium term injection for circuit B (VS-NLL) and supply c1

Blue	Medium term injection (IM2) data before curve fitting.
Red	Interharmonic values used for the curve fitting algorithm.
Green	Calibrator measurements (IM3) with supply and NLL disconnected.

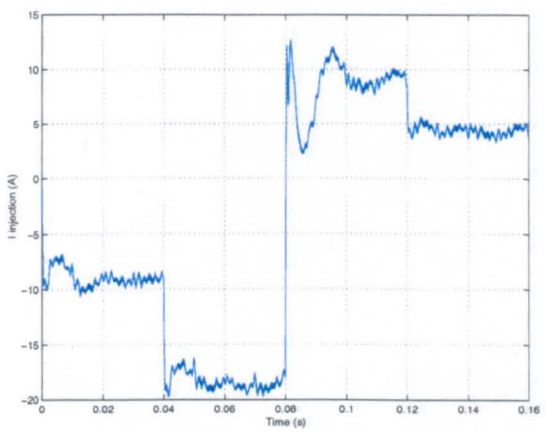

(b) Current transient.

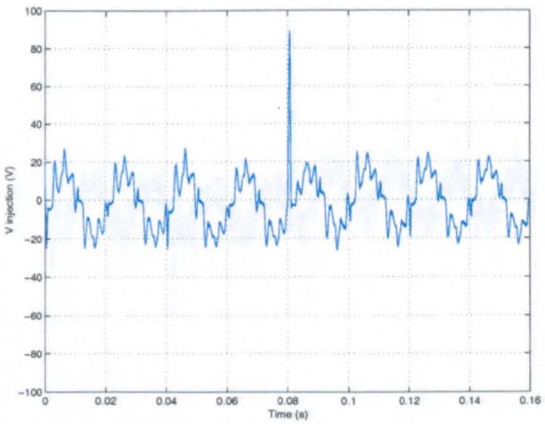

(c) Voltage transient.

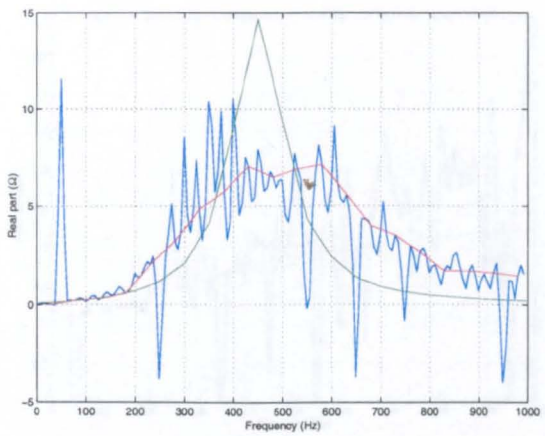

(d) Real impedance.

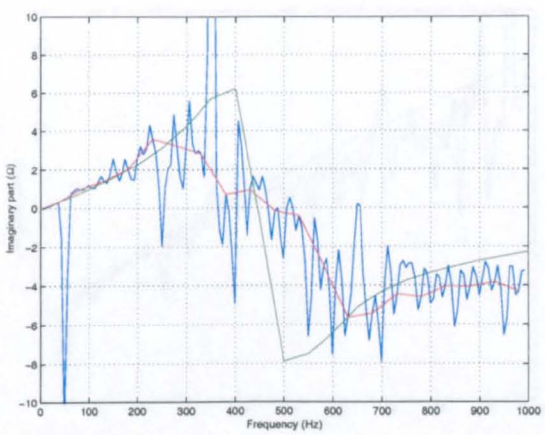

(e) Imaginary impedance.

Figure 6.5: Medium term injection for circuit B (VS-NLL) and supply c3

Blue	Medium term injection (IM2) data before curve fitting.
Red	Interharmonic values used for the curve fitting algorithm.
Green	Calibrator measurements (IM3) with supply and NLL disconnected.

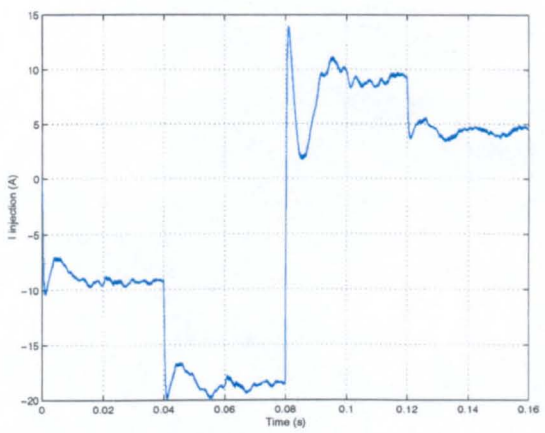

(b) Current transient.

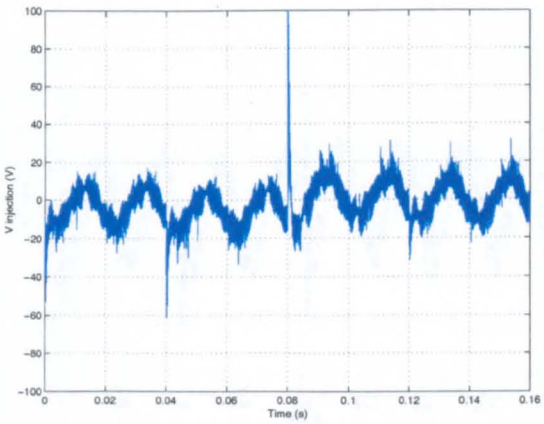

(c) Voltage transient.

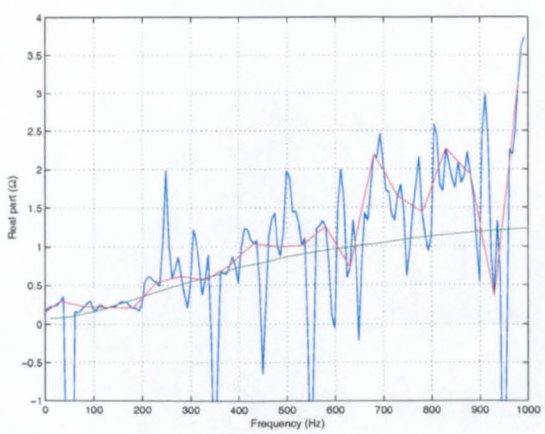

(d) Real impedance.

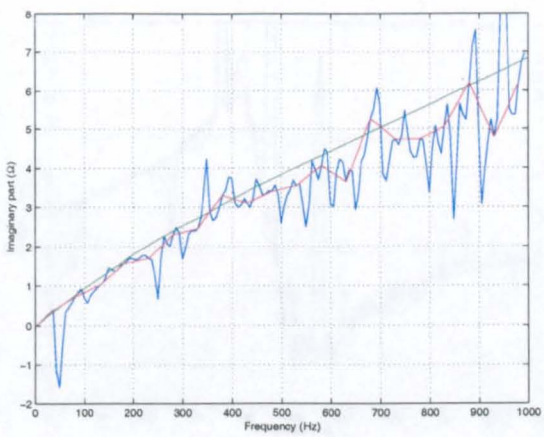

(e) Imaginary impedance.

Figure 6.6: Medium term injection for circuit C (combined NLL) and supply c1

Blue	Medium term injection (IM2) data before curve fitting.
Red	Interharmonic values used for the curve fitting algorithm.
Green	Calibrator measurements (IM3) with supply and NLL disconnected.

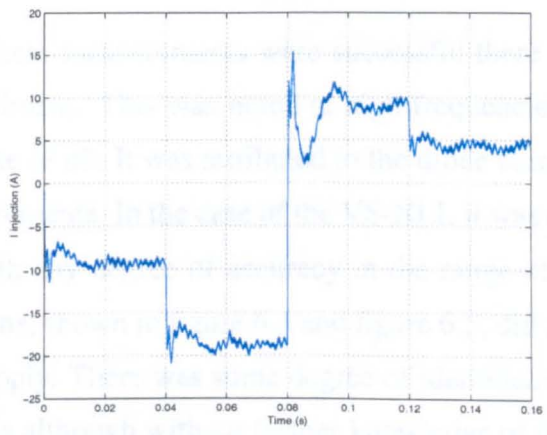

(b) Current transient.

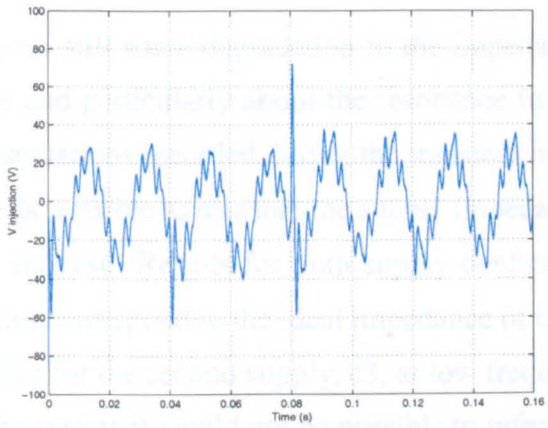

(c) Voltage transient.

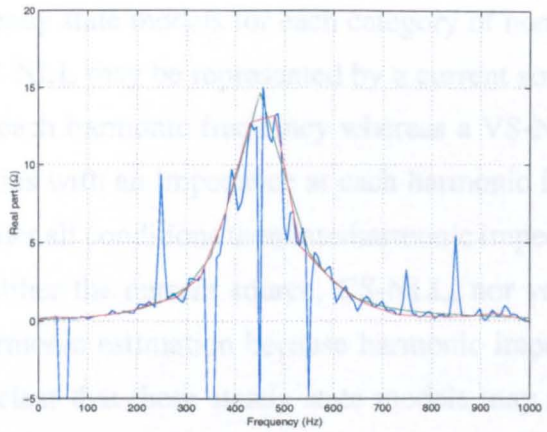

(d) Real impedance.

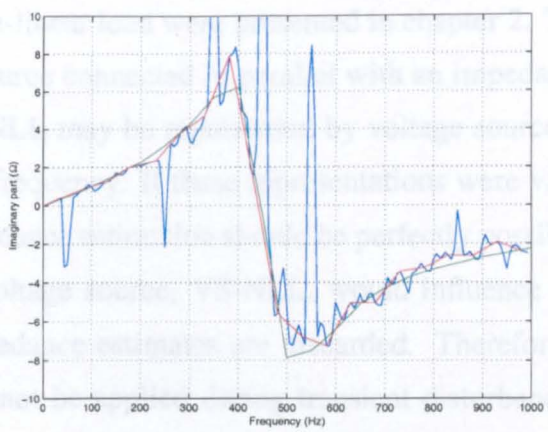

(e) Imaginary impedance.

Figure 6.7: Medium term injection for circuit C (combined NLL) and supply c3

6.3.2 Discussion of medium term injection results

From the results presented it was clear that the medium term injection technique was able to successfully estimate the supply impedance in the presence of the CS-NLL. In the second case, a VS-NLL connected, the measurement was unsuccessful and clearly the NLL had affected the impedance estimation greatly. In the final case, a VS-NLL with additional input inductors, it was again possible to estimate the supply impedance.

Where measurements were successful there was still some degradation in the impedance estimate. This was noted at high frequencies and particularly about the resonance in the case of c3. It was attributed to the diode commutations recorded during the transient measurements. In the case of the VS-NLL it was not possible to measure the supply impedance with any degree of accuracy in the range of interest. Results for both supply configurations, shown in figure 6.4 and figure 6.5, did not correspond to the ideal impedance of each supply. There was some degree of identification for the second supply, c3, at low frequencies although without further knowledge of the system it would not be possible to infer the actual supply impedance.

Steady state models for each category of non-linear load were presented in chapter 2. The CS-NLL may be represented by a current source connected in parallel with an impedance at each harmonic frequency whereas a VS-NLL may be represented by voltage source in series with an impedance at each harmonic frequency. If these representations were valid under all conditions then interharmonic impedance estimation should be perfectly possible. Neither the current source, CS-NLL, nor voltage source, VS-NLL, would influence the harmonic estimation because harmonic impedance estimates are discarded. Therefore it is clear that these steady state models may not be applied during transient disturbances, this is especially true for the VS-NLL. The physical characteristics of each NLL must be considered to explain the performance of the measurement techniques in this situation.

The output of the CS-NLL does not vary to a significant degree during the transient disturbance. The points of diode commutation are largely unaffected due to the fact that only a small fraction of the injected current will actually flow into the CS-NLL. This is in turn

due to the magnitude of the passive impedance connected. This passive load, consisting of a large smoothing inductor, L_{load}, and load resistance, R_{load}, has a very high impedance in comparison to the supply impedance. In normal operation it is only the d.c. impedance of the passive load that is important as the diode rectifier and smoothing inductor are present. In all CS-NLL loads of this nature the impedance of the passive load will be large at all non-d.c. frequencies.

During the transient injection a wideband disturbance is applied. Very little injection current will actually flow into the CS-NLL as ($Z_s \ll Z_{load}$). This may not be true in all instances such as at frequencies where a supply impedance resonance exists. In this situation the supply impedance may be large and of the same order of magnitude as the passive impedance, in this case it should be expected that the measurement accuracy about the resonance will be affected.

Figure6.8 shows the impedance of both supplies used and the impedance of the passive load connected to the rectifier.

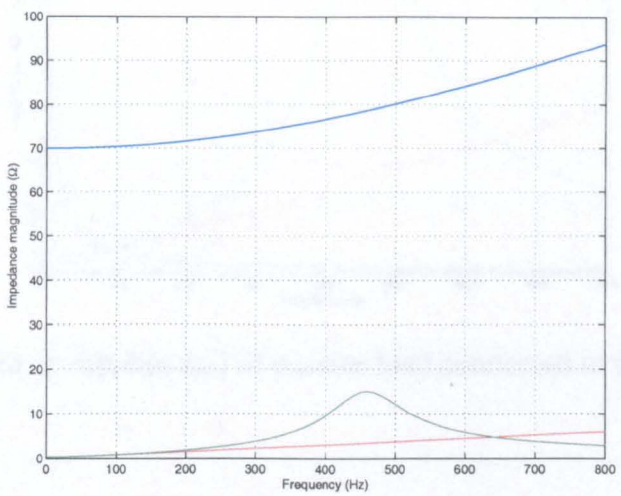

Figure 6.8: Impedance of supplies and of passive load connected to the rectifier output for circuit A

From figure 6.8 it is clear that, irrespective of the diode conduction state, very little injection current will flow into the CS-NLL. If the power output of the CS-NLL were increased the resistive part of the load would be reduced although a larger smoothing inductor would be

required. Hence in most practical situations the amount of injection current flowing into the CS-NLL will be small and measurement of the supply impedance will not be affected significantly.

In contrast to the CS-NLL the output of the VS-NLL will be greatly affected by the transient disturbance. It is this correlation between the output of the NLL and the injected current waveform that greatly affects the measurement performance in such a network. This correlation invalidates the assumption made in chapter 4 assuming that a linear system was under consideration. The ratio of supply impedance to passive load impedance connected after the diode bridge may again be used to explain the measurement performance. Figure6.9 shows the relative impedance values for both supplies and the passive load connected to the VS-NLL rectifier output.

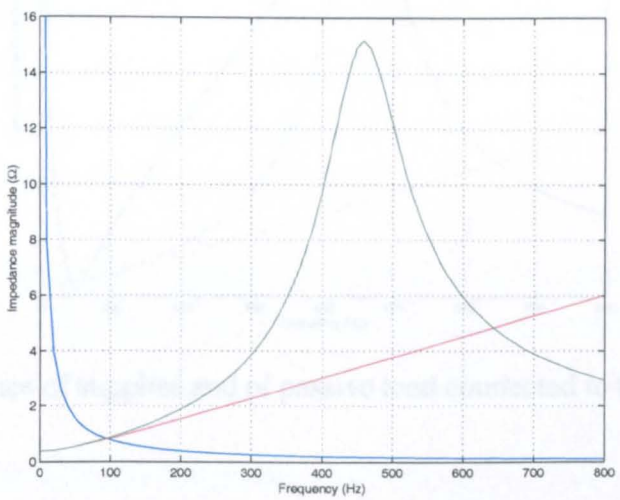

Figure 6.9: Impedance of supplies and of passive load connected to the rectifier output for circuit B

For the VS-NLL the supply impedance shall only be significantly smaller than the passive load impedance at very low frequencies. As a consequence the measurement will only identify the supply impedance at these low frequencies. At higher frequencies the passive load impedance will be much less than the supply impedance. Hence injection current will flow through the rectifier when the diodes are appropriately biased. This will affect the diode commutations which will in turn alter the operating point of the NLL. Therefore the

medium term injection technique will not adequately identify the supply impedance in the presence of this VS-NLL. It should be noted that the scale of the VS-NLL is not of great importance, in this case the VS-NLL only supplies 3kW of power. The impedance of the passive part of the NLL that is important as well as the effect that the disturbance has upon the diode switching positions that determines how successful the measurement will be.

In the final test circuit, circuit C, additional 3.5mH line inductors were connected at the input of the VS-NLL. Figure 6.9 is redrawn to include the additional load impedance, this is shown as figure 6.10.

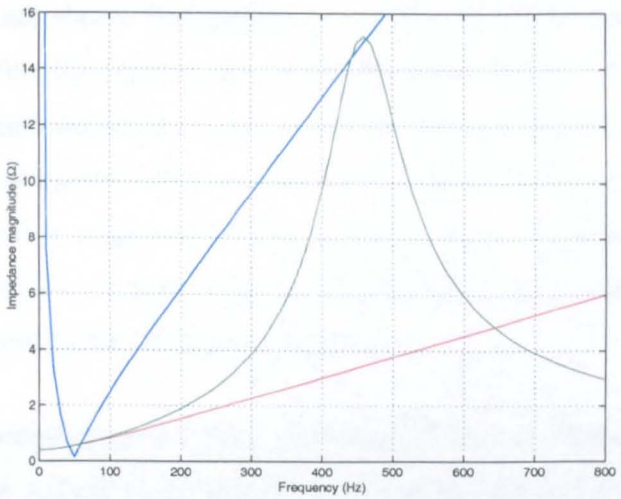

Figure 6.10: Impedance of supplies and of passive load connected to the rectifier output for circuit C

The additional load impedance means that less of the injected measurement current flows into the NLL. Hence the measurement of the supply impedance will have improved accuracy. Measurement accuracy will be lowest at the frequencies where the load impedance is small compared to the supply impedance. Therefore the results should be affected most around 50Hz for both supplies and about the resonant point, 450Hz, in the case of supply c3.

Results for this final circuit show that remotely connected NLLs will generally have little influence upon measurement accuracy assuming that there is considerable impedance, relative to the supply impedance, between the POM and the NLL in question. This was also

verified in the previous chapter. NLLs connected to the laboratory supply had no noticeable influence upon the measurement process, these were separated electrically from the POM by the experimental rig supply transformer.

6.4 Short term injection

The performance of the short term injection technique was also investigated. Measurements were taken for circuits A, B and C. The results are shown in figures 6.12 to 6.22. Three measurement results are shown for supply c1 with the CS-NLL connected. In each case the short term injection was applied at a different point in the voltage cycle. The first measurement is commenced while current is flowing through phase 1 into the rectifier. The second measurement is started when no current is flowing from phase 1 into the rectifier. The third measurement is triggered so that a diode commutation takes place during the transient injection. For the c1 supply figure 6.11(a) shows the steady state voltage V_{12} at the POM and the current in the NLL in each phase.

This series of measurements is repeated using the c3 supply. Similarly, Figure 6.11(b) shows the steady state voltage V_{12} at the POM and the current in the NLL in each phase.

6.4.1 Short term injection results

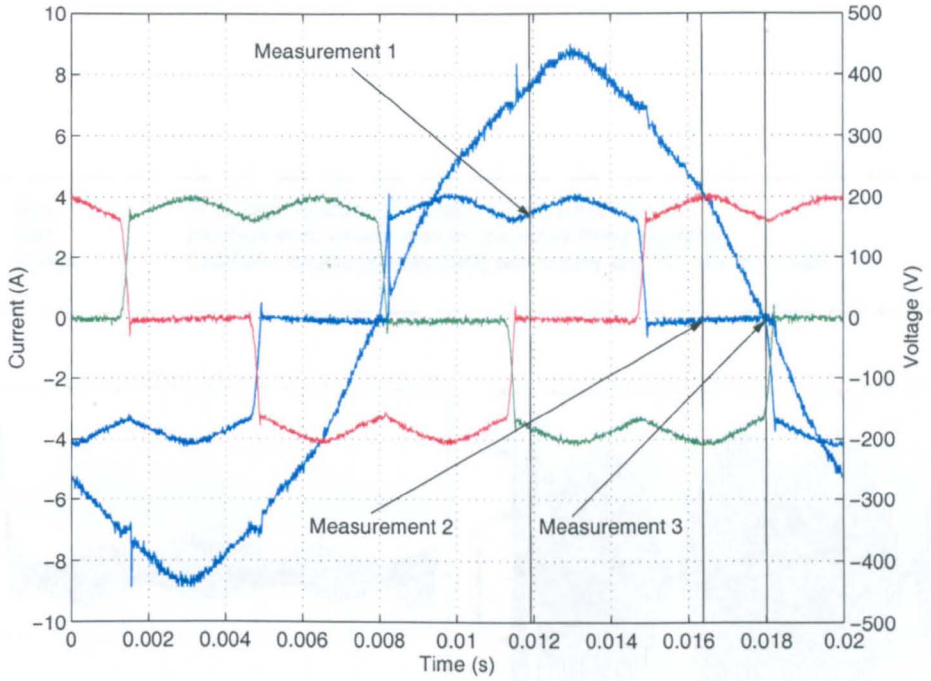

(a) Supply circuit c1

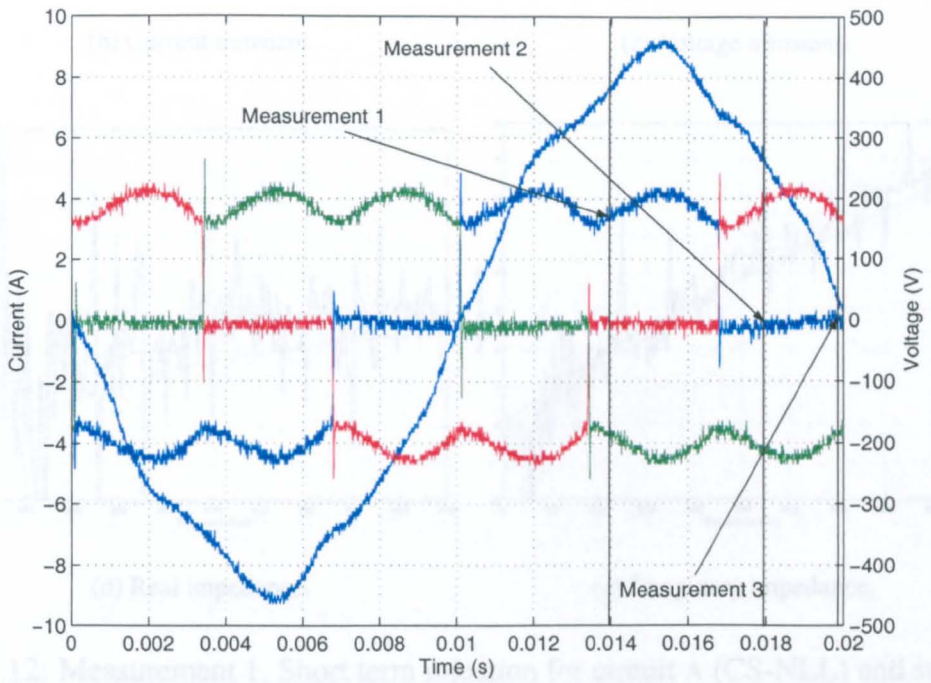

(b) Supply circuit c3

Figure 6.11: CS-NLL measurements. Phase 1 current: Blue. Phase 2 current: Red. Phase 3 current: Green

Blue	Short term injection (IM1) data before curve fitting.
Red	Interharmonic values used for the curve fitting algorithm.
Green	Calibrator measurements (IM3) with supply and NLL disconnected.

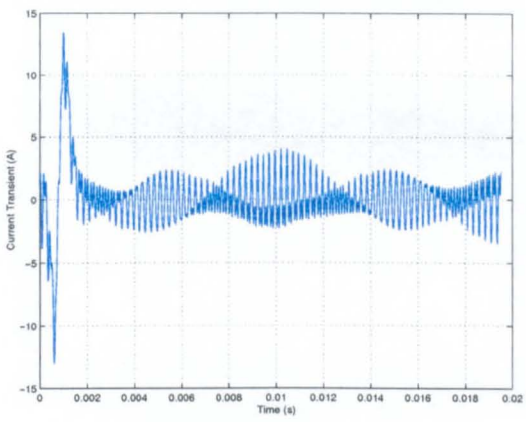

(b) Current transient.

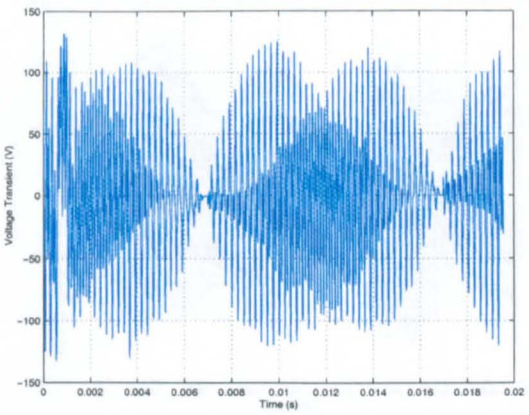

(c) Voltage transient.

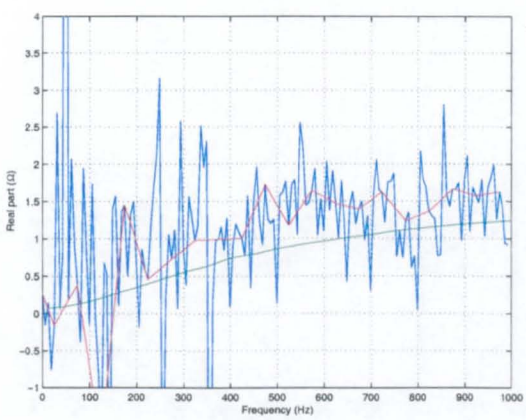

(d) Real impedance.

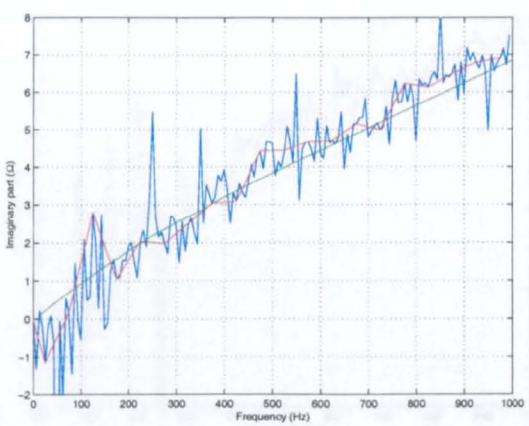

(e) Imaginary impedance.

Figure 6.12: Measurement 1. Short term injection for circuit A (CS-NLL) and supply c1.

Blue	Short term injection (IM1) data before curve fitting.
Red	Interharmonic values used for the curve fitting algorithm.
Green	Calibrator measurements (IM3) with supply and NLL disconnected.

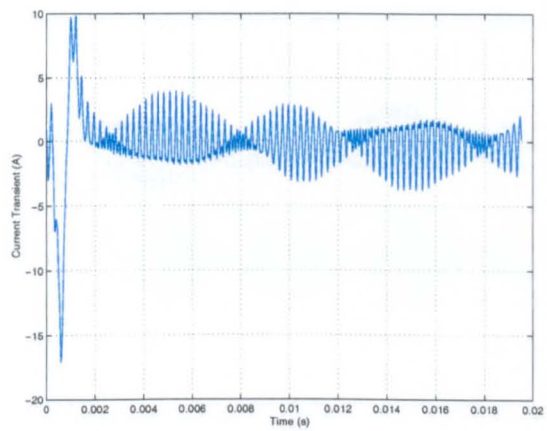

(b) Current transient.

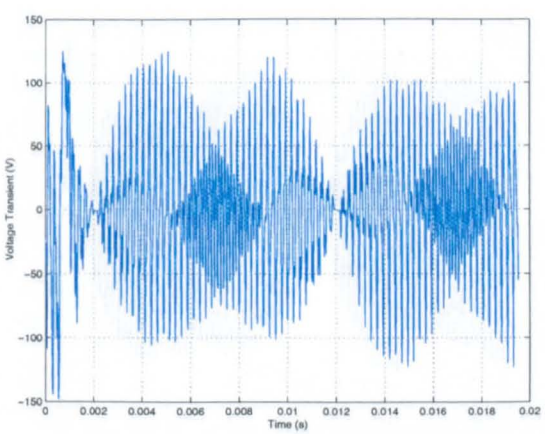

(c) Voltage transient.

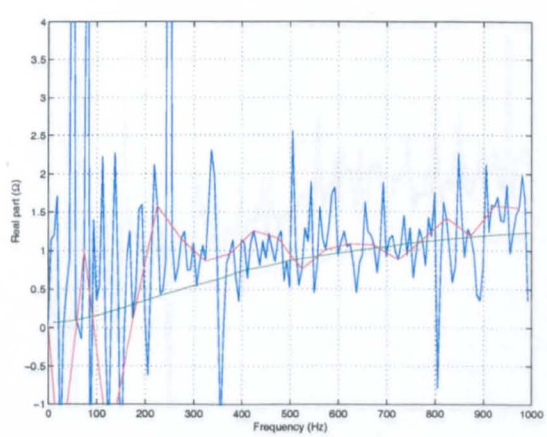

(d) Real impedance.

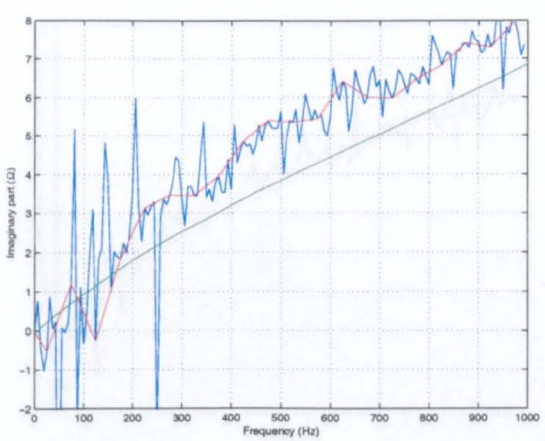

(e) Imaginary impedance.

Figure 6.13: Measurement 2. Short term injection for circuit A (CS-NLL) and supply c1

Blue	Short term injection (IM1) data before curve fitting.
Red	Interharmonic values used for the curve fitting algorithm.
Green	Calibrator measurements (IM3) with supply and NLL disconnected.

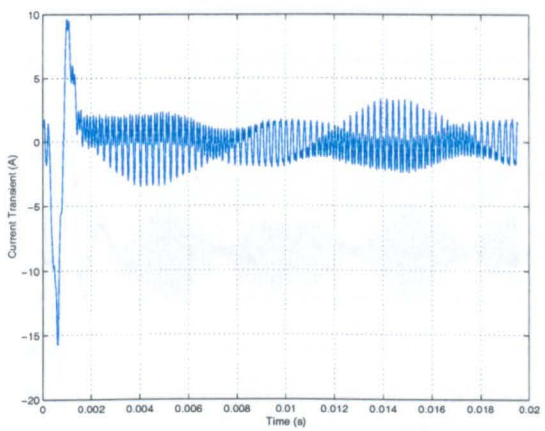

(b) Current transient.

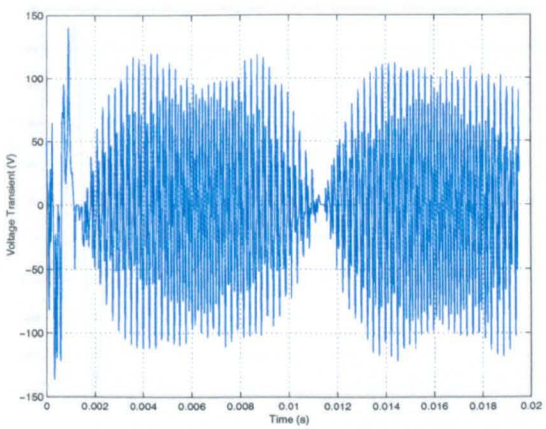

(c) Voltage transient.

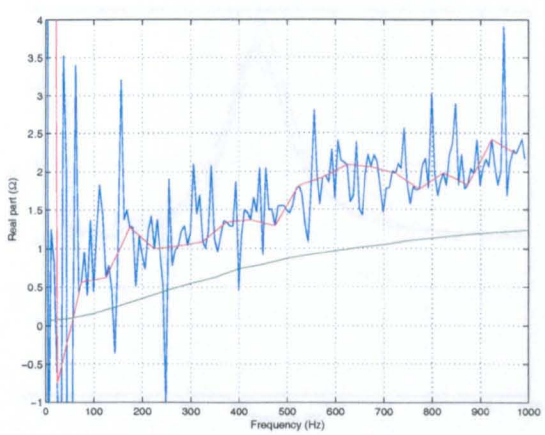

(d) Real impedance.

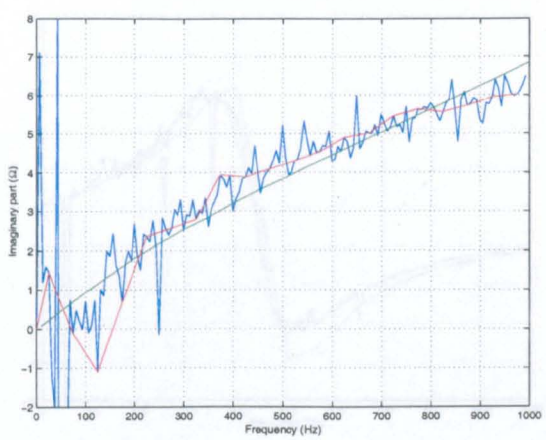

(e) Imaginary impedance.

Figure 6.14: Measurement 3. Short term injection for circuit A (CS-NLL) and supply c1

Blue	Short term injection (IM1) data before curve fitting.
Red	Interharmonic values used for the curve fitting algorithm.
Green	Calibrator measurements (IM3) with supply and NLL disconnected.

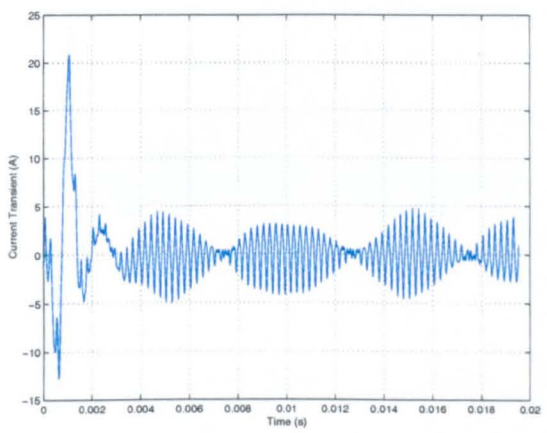

(b) Current transient.

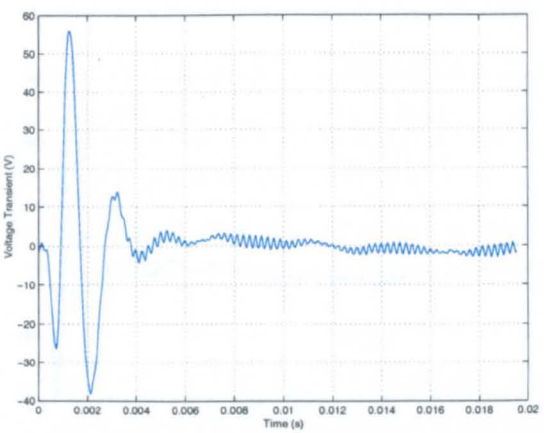

(c) Voltage transient.

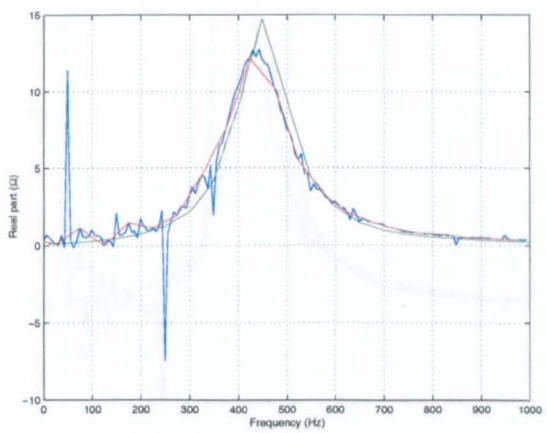

(d) Real impedance.

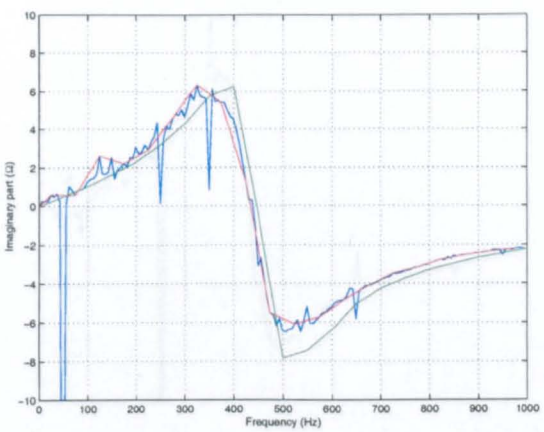

(e) Imaginary impedance.

Figure 6.15: Measurement 1. Short term injection for circuit A (CS-NLL) and supply c3

Blue	Short term injection (IM1) data before curve fitting.
Red	Interharmonic values used for the curve fitting algorithm.
Green	Calibrator measurements (IM3) with supply and NLL disconnected.

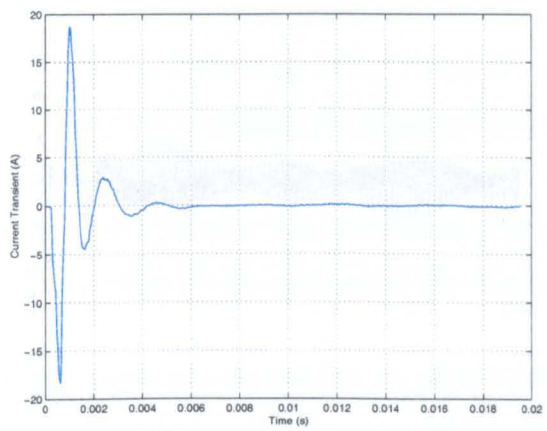

(b) Current transient.

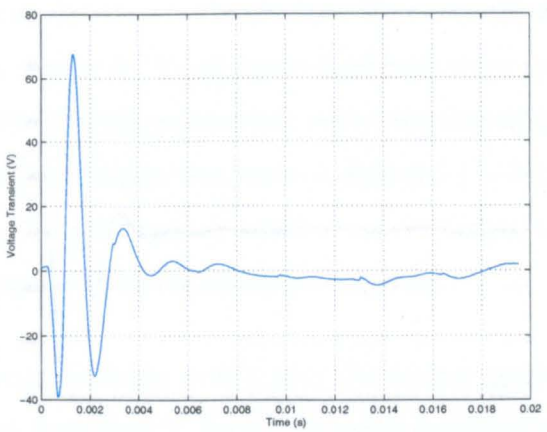

(c) Voltage transient.

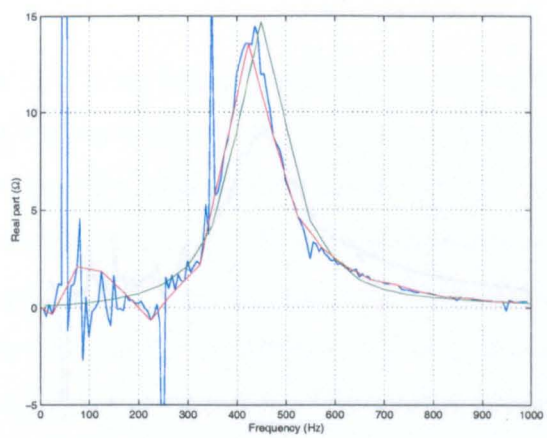

(d) Real impedance.

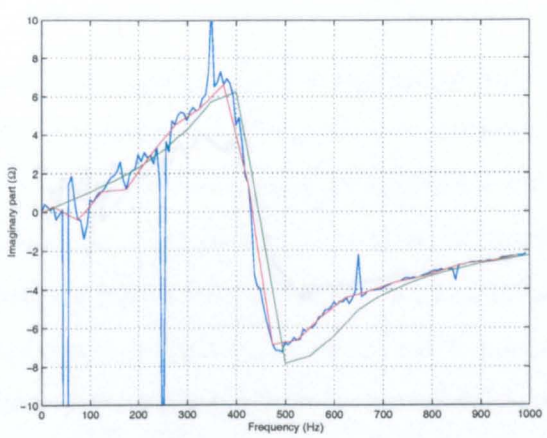

(e) Imaginary impedance.

Figure 6.16: Measurement 2. Short term injection for circuit A (CS-NLL) and supply c3

Blue	Short term injection (IM1) data before curve fitting.
Red	Interharmonic values used for the curve fitting algorithm.
Green	Calibrator measurements (IM3) with supply and NLL disconnected.

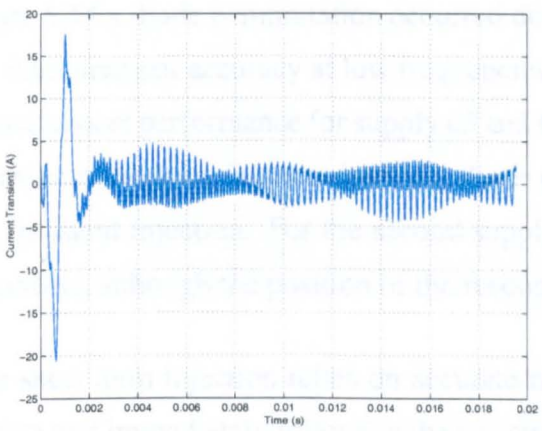

(b) Current transient.

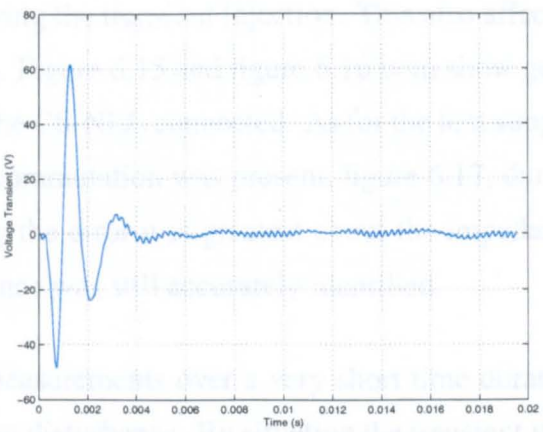

(c) Voltage transient.

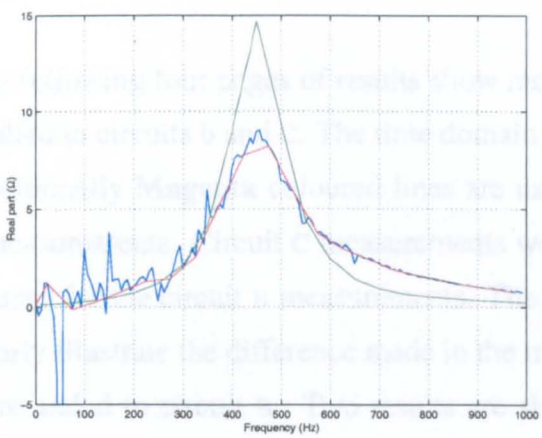

(d) Real impedance.

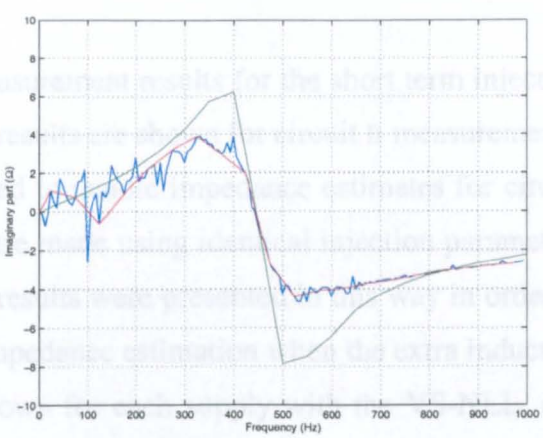

(e) Imaginary impedance.

Figure 6.17: Measurement 3. Short term injection for circuit A (CS-NLL) and supply c3

6.4.2 Discussion of circuit A results

The short term injection had some success in identifying the supply impedance with the CS-NLL connected. In figures 6.12 and 6.13 the c1 supply was measured although some discrepancies were noted at the low frequencies. The first of these measurements was conducted with the short term injection positioned such that current was flowing in phase 1, the second measurement was such that no current was flowing in phase 1. In the case of figure 6.14 a diode commutation occurred during the transient injection. This also affected the measurement accuracy at low frequencies. Figure 6.15 and figure 6.16 both show good measurement performance for supply c3 and the CS-NLL connected. As for the first supply, measurement errors increased when a diode commutation was present, figure 6.17, during the transient injection. For the second supply the error was greatest about the impedance resonance although the position of the resonance was still accurately identified.

The short term injection relies on accurate measurements over a very short time duration during and immediately following the transient disturbance. By situating the transient very close to a diode commutation the accuracy is affected and degrades the impedance estimation.

The following four pages of results show measurement results for the short term injection applied to circuits b and C. The time domain results are shown for circuit B measurements. Additionally **Magenta** coloured lines are used to denote impedance estimates for circuit c measurements. Circuit C measurements were made using identical injection parameters as used for the circuit B measurements. The results were presented in this way in order to clearly illustrate the difference made in the impedance estimation when the extra inductors were added to circuit B. Two results are shown for each supply with the VS-NLL, one measurement takes place that does not affect the diode commutation and one measurement is made that does alter the diode switching instants. Figures 6.18(a) and 6.18(b) show the injection positions for supplies c1 and c3 respectively.

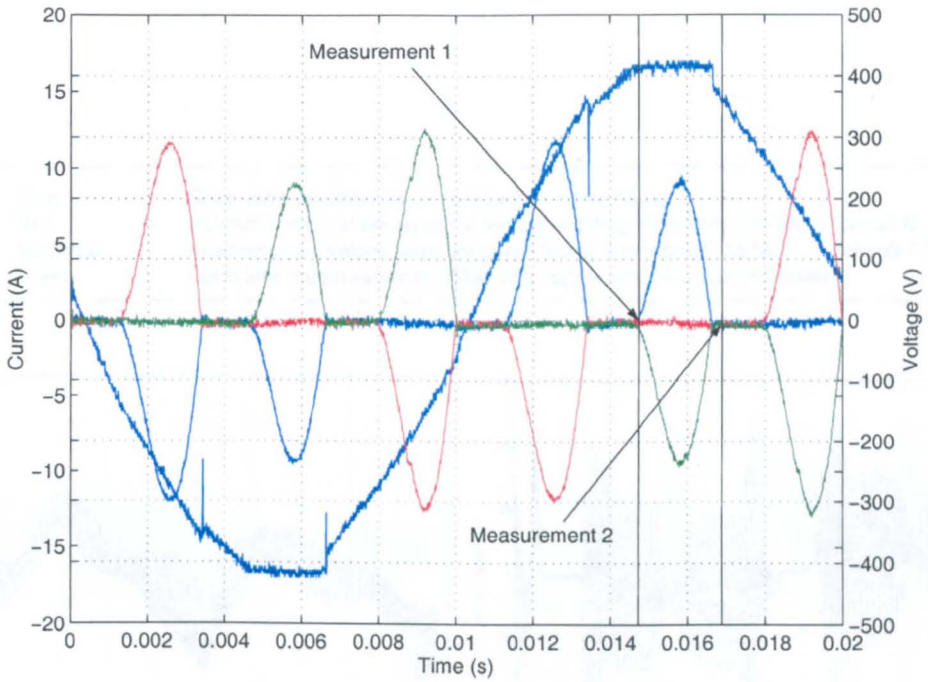

(a) Supply circuit c1

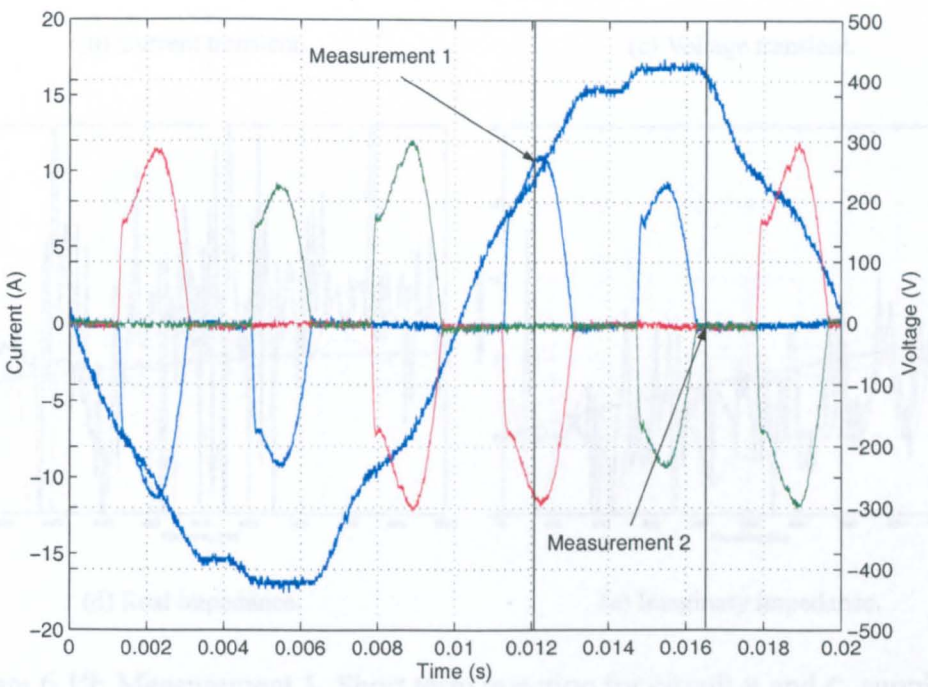

(b) Supply circuit c3

Figure 6.18: VS-NLL measurements. Phase 1 current: Blue. Phase 2 current: Red. Phase 3 current: Green

Blue	Short term injection (IM1) data before curve fitting.
Red	Interharmonic values used for the curve fitting algorithm (VS-NLL) (circuit B).
Magenta	Interharmonic values used for curve fitting from combined NLL (circuit C).
Green	Calibrator measurements (IM3) with supply and NLL disconnected.

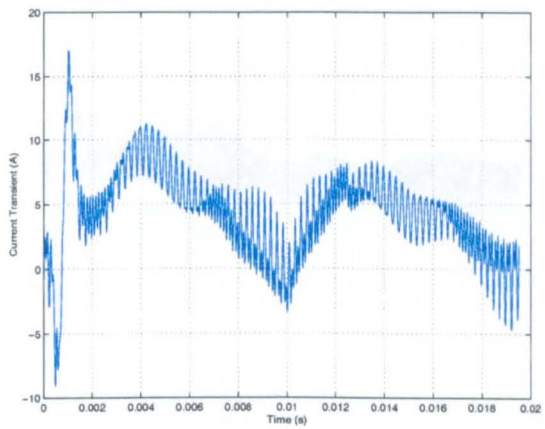

(b) Current transient.

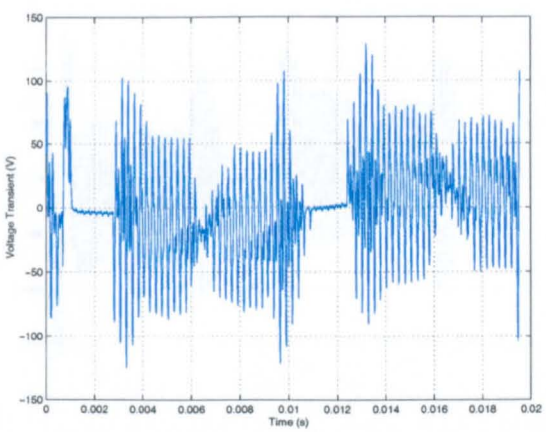

(c) Voltage transient.

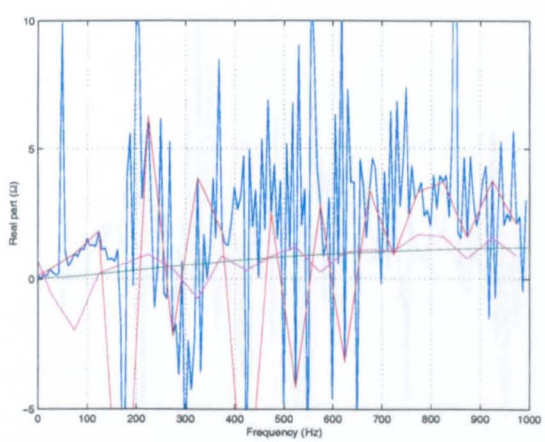

(d) Real impedance.

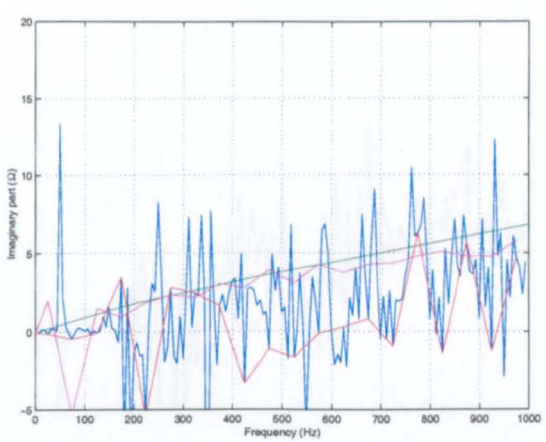

(e) Imaginary impedance.

Figure 6.19: Measurement 1. Short term injection for circuit B and C, supply c1

Blue	Short term injection (IM1) data before curve fitting.
Red	Interharmonic values used for the curve fitting algorithm (VS-NLL) (circuit B).
Magenta	Interharmonic values used for curve fitting from combined NLL (circuit C).
Green	Calibrator measurements (IM3) with supply and NLL disconnected.

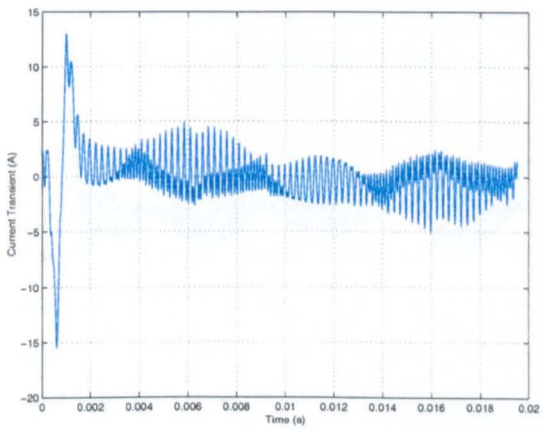

(b) Current transient.

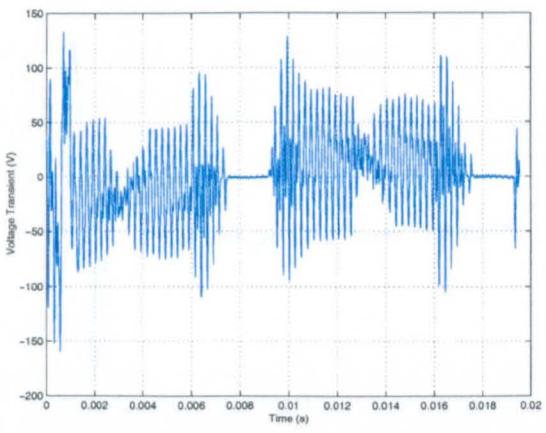

(c) Voltage transient.

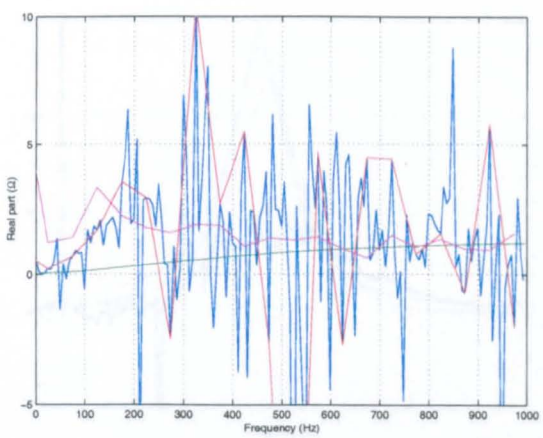

(d) Real impedance.

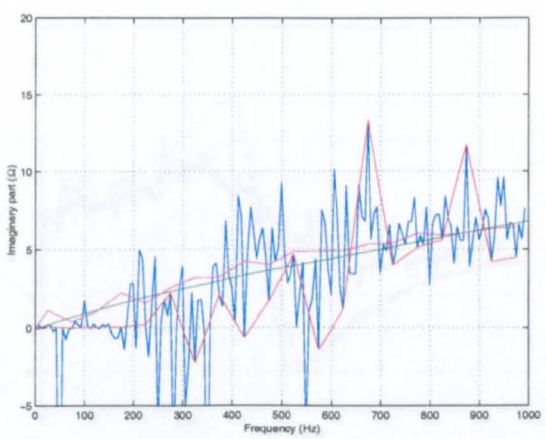

(e) Imaginary impedance.

Figure 6.20: Measurement 2. Short term injection for circuit B and C, supply c1

Blue	Short term injection (IM1) data before curve fitting.
Red	Interharmonic values used for the curve fitting algorithm (VS-NLL) (circuit B).
Magenta	Interharmonic values used for curve fitting from combined NLL (circuit C).
Green	Calibrator measurements (IM3) with supply and NLL disconnected.

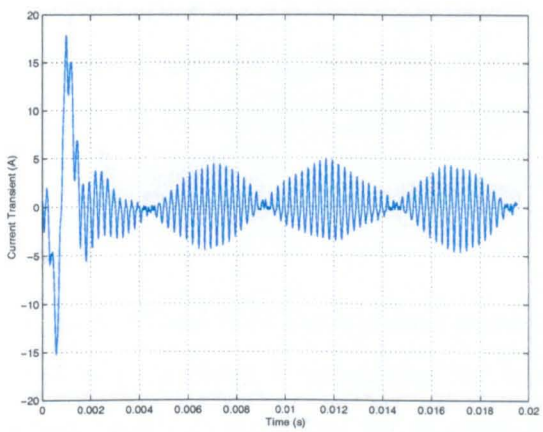

(b) Current transient.

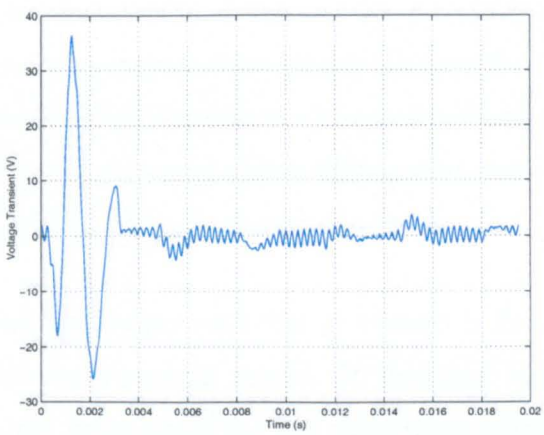

(c) Voltage transient.

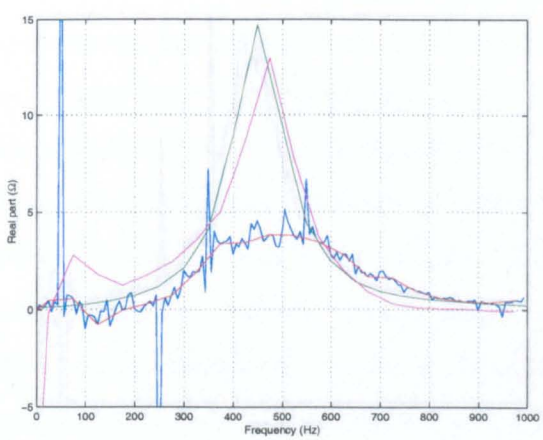

(d) Real impedance.

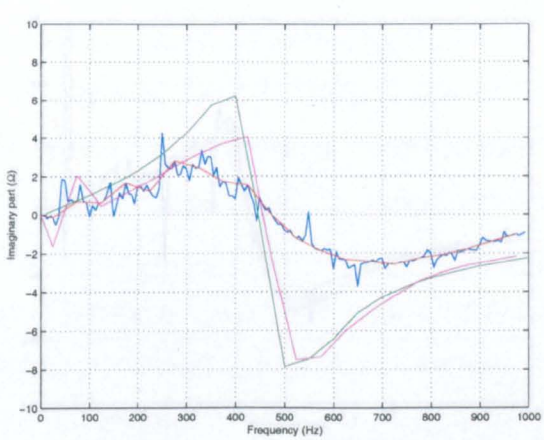

(e) Imaginary impedance.

Figure 6.21: Measurement 1. Short term injection for circuit B and C, supply c3

Blue	Short term injection (IM1) data before curve fitting.
Red	Interharmonic values used for the curve fitting algorithm (VS-NLL) (circuit B).
Magenta	Interharmonic values used for curve fitting from combined NLL (circuit C).
Green	Calibrator measurements (IM3) with supply and NLL disconnected.

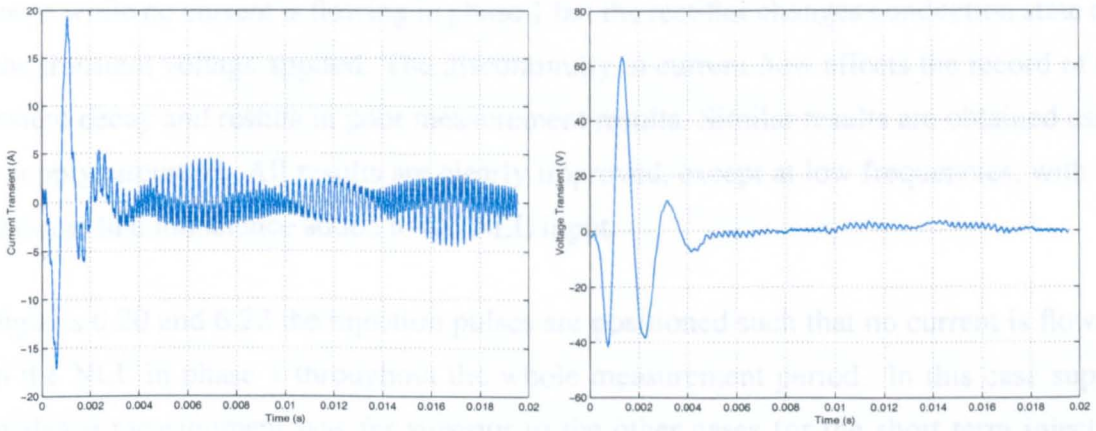

(b) Current transient. (c) Voltage transient.

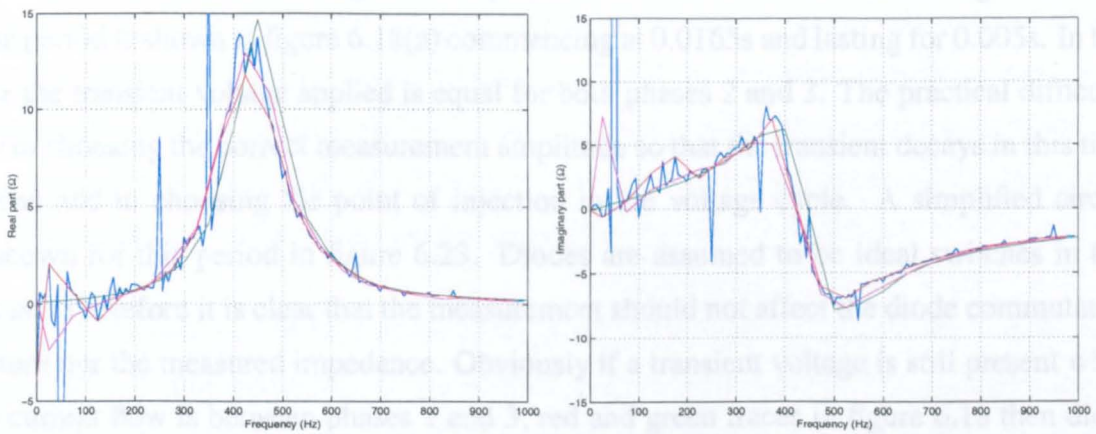

(d) Real impedance. (e) Imaginary impedance.

Figure 6.22: Measurement 2. Short term injection for circuit B and C, supply c3

6.4.3 Discussion of short term injection results

The results obtained using the short term injection were highly dependent upon the point of transient injection. In figure 6.19 it is clear that the transient injection current is affecting the normal operation of the VS-NLL. A significant proportion of the measurement input current flows through the rectifier and the connected passive load. This severely affects the measurement accuracy, as seen in figure 6.19(c) and 6.19(d). The transient input commences while no current is flowing in phase 1 but the rectifier changes conduction state due to the transient voltage applied. The discontinuity in current flow affects the record of the transient decay and results in poor measurement results. Similar results are obtained using the supply circuit c3. All results are clearly improved, except at low frequencies, with the additional line inductance added to the NLL input.

In figures 6.20 and 6.22 the injection pulses are positioned such that no current is flowing into the NLL in phase 1 throughout the whole measurement period. In this case supply impedance measurement was far superior to the other cases for the short term injection method. Ideally the injection should be positioned in time such that the transient voltage is applied when current is flowing between phases 2 and 3, or no current is flowing at all. This time period is shown in figure 6.18(a) commencing at 0.0165s and lasting for 0.005s. In this case the transient voltage applied is equal for both phases 2 and 3. The practical difficulty lies in choosing the correct measurement amplitude so that the transient decays in this time period and in choosing the point of injection in the voltage cycle. A simplified circuit is shown for this period in figure 6.23. Diodes are assumed to be ideal switches in this circuit. Therefore it is clear that the measurement should not affect the diode commutation pattern nor the measured impedance. Obviously if a transient voltage is still present when the current flow is between phases 1 and 3, red and green traces in figure 6.18 then diode commutation may still be affected resulting in a degraded impedance estimation. This argument only applies to the balanced three phase case.

The short term injection measurement results were seriously affected by the presence of a VS-NLL at the point of measurement.

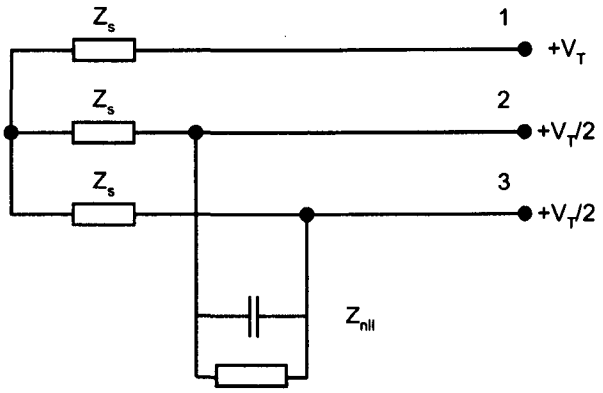

Figure 6.23: Conduction between phases 2 and 3

6.5 Improved measurement using Prony method

Work was undertaken in order to improve the short term identification of system impedance in the presence of VS-NLL loads. A numerical technique has been used in order to overcome some of the problems introduced by the non-linear elements. The time domain extended Prony method was used to estimate the transient signals from very few sampled data points. Using this method the continuous section of the transients may be extrapolated as if the diode conduction positions did not change. The work presented here is for simulation results only. Some experimental verification has been undertaken but the system has not been refined to provide consistent identification. An intelligent system shall be developed in order to automatically implement the algorithm used.

The Prony method is a technique for fitting a sum of complex exponentials to a series of data points. A full discussion of the method is described in [76]. The sum of complex exponentials forms a solution to a homogeneous differential equation [86]. The general solution is shown in equation 6.1.

$$f(t) = f(n\delta t) = \sum_{i=0}^{P-1} C_i \mu_i^n \quad \text{where} \quad \mu_i = e^{s_{pi}\delta t} \tag{6.1}$$

n represents the time step, P represents the number of poles in the system, C_i is the residual of the i'th pole and s_{pi} is the complex frequency of the i'th pole.

The Prony method is used to calculate values of both C_i and s_{pi} given the order of the system, P. This is in fact a non-linear problem with no simple solution. The Prony method provides a sub-optimal solution to this problem by solving for the coefficients using a linear process. The basic Prony technique [87] uses $2P$ points of data in order in order to calculate coefficients for P poles. This version is particularly influenced by signal noise [88] [76]. When more than $2P$ data points are available a least squares solution may be applied in order to reduce the influence of the noise, this improved version is known as the extended Prony method.

When applying the method three calculation steps are necessary. The first stage involves finding the inverse of a $((P-1) \times N)$ matrix, the second requires solving a polynomial of order N and, finally, the last step requires a another $((P-1) \times N)$ matrix inversion. Clearly the process is very computationally intensive. The other difficulty is that a system order, P, must be chosen. If the system order is not known, as is the case in this work, a means is required to estimate the correct order. Automatic approaches are possible [88] but in this work a method using a high degree of over-determination is implemented [89]. If N data points are used then a system order of $\left(\frac{N}{3}\right)$ is initially assumed [90]. A solution is then computed. Many of the poles calculated in this manner merely model the measured noise in the measurement data. In order to identify the system and not the measurement noise these extra poles must be eliminated. A simple method is employed that identifies the poles with frequencies below 4kHz and with high magnitude residuals. These poles are retained.

Alternative implementations have been developed. Dowling used the total least squares (TLS) approach [91] and the linearly constrained TLS approach [92]. Pre-processing filters have also been tried [93] [94]. In practice these did not provide a significant improvement over the ordinary least squares solution using singular value decomposition (SVD) [78].

For this work the Prony method is used in order to extrapolate a transient signal such that

the final response is as if the NLL was not connected. The process used was:

1. The short term transient measurement was applied. The disturbance was injected at a point in the voltage cycle where the VS-NLL was not conducting.
2. The point of VS-NLL diode commutation was detected and the data prior to this event and after the initial injection was extracted.
3. The prony method was applied to the extracted data segment. In practice this was between 80 and 150 samples.
4. New transient signals were generated using the initial recorded data and the extrapolated data generated from the Prony method.
5. System identification was carried out using the newly generated transient signals.

This method is used for the short term injection technique in the presence of a VS-NLL. The first part of this section uses simulation results for a single phase system, as in figure 6.24. This work was still applicable in the balanced three phase case as long as the injection was completed when either no current was flowing in the NLL or when current was flowing between phases 2 and 3.

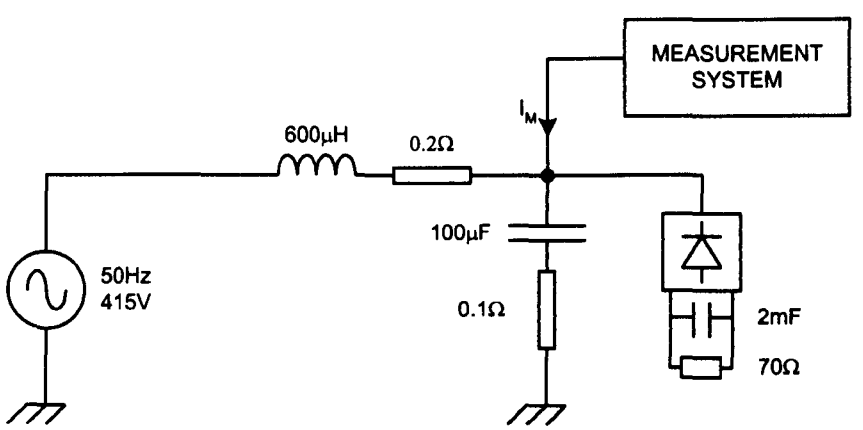

Figure 6.24: Simulation circuit used for demonstration of Prony technique

In order to clearly describe the possible application of this technique ideal simulations have initially been utilized. A supply frequency of exactly 50Hz is used, no noise is applied to the measured signals and a sampling rate of 51.2kHz is used. At the end of this section the method will be demonstrated on noised simulation data and in an experimental setting.

6.5.1 Short term injection time

Input current and voltage for the uncontrolled non-linear load are shown in figure 6.25. A successful injection measurement using the short term technique would be positioned such that the whole transient event takes place in the region where no current flows into the distorting load. It is not sufficient to use the switching times shown in this figure for that means directly as the injection may alter these times. The best chance of successful measurement occurs if the injection strength is very low and is positioned so that no injection current flows into the load.

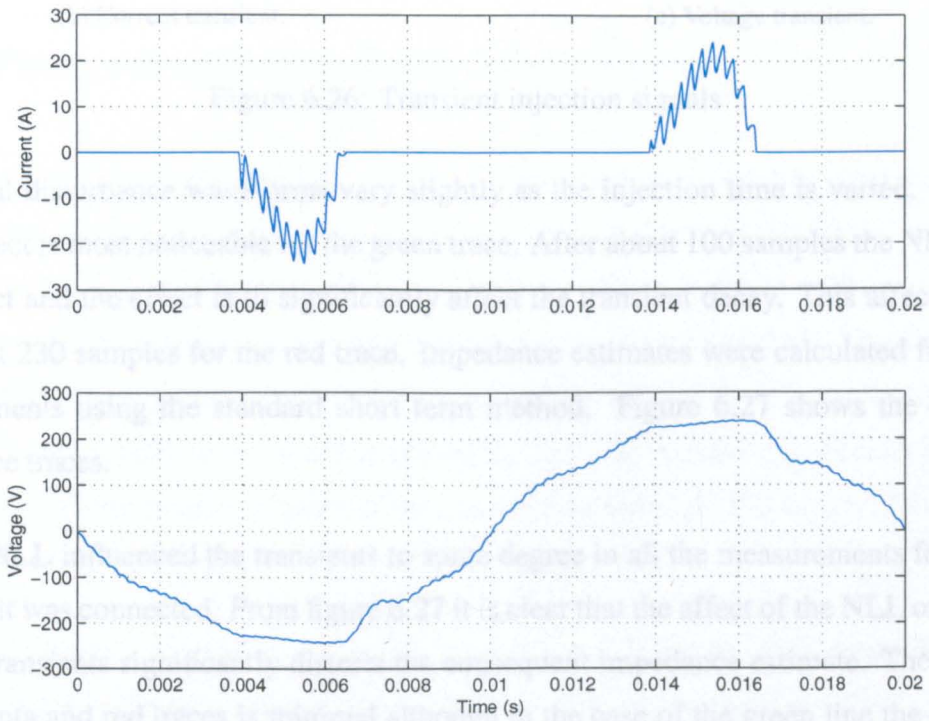

Figure 6.25: Rectifier input current and voltage

Injections, using the same strength injection as in chapter 4, were conducted over a range of injection points. The current and voltage transient signals are shown in figure 6.26.

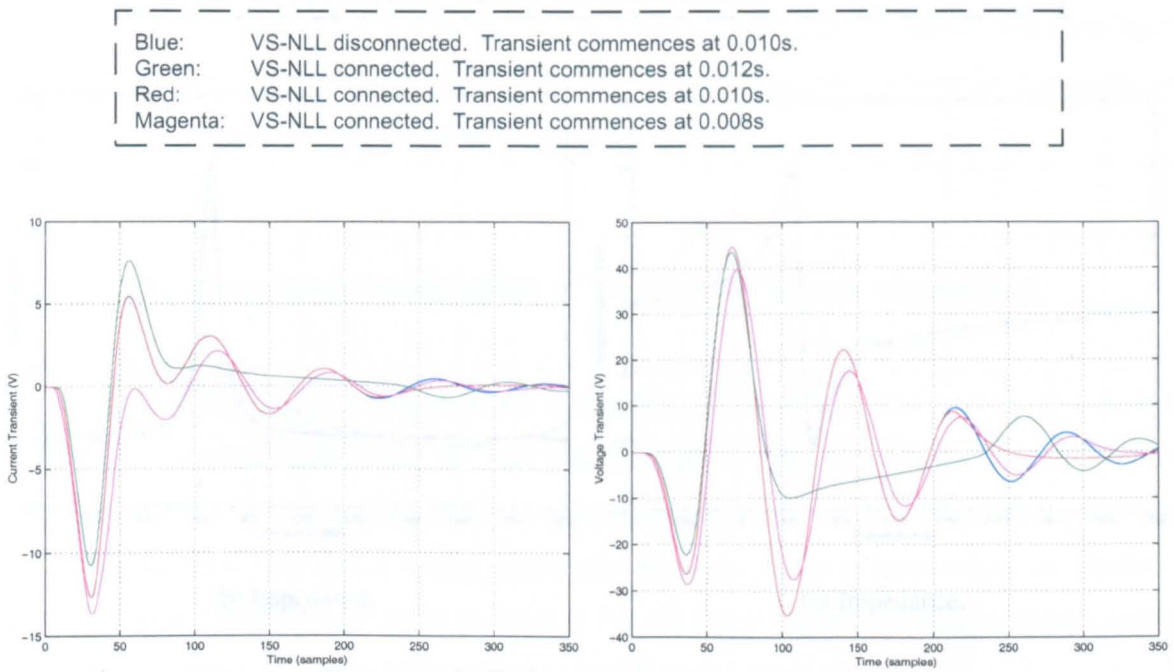

(b) Current transient.

(c) Voltage transient.

Figure 6.26: Transient injection signals

The initial disturbance waveforms vary slightly as the injection time is varied. The non-linear effect is most noticeable for the green trace. After about 100 samples the NLL begins to conduct and the effect is to significantly affect the transient decay. This affect can also be seen at 230 samples for the red trace. Impedance estimates were calculated from these measurements using the standard short term method. Figure 6.27 shows the estimated impedance traces.

The VS-NLL influenced the transients to some degree in all the measurements for circuits in which it was connected. From figure 6.27 it is clear that the affect of the NLL on the time domain transients significantly distorts the consequent impedance estimate. The affect on the magenta and red traces is minimal although in the case of the green line the measured impedance is distorted significantly.

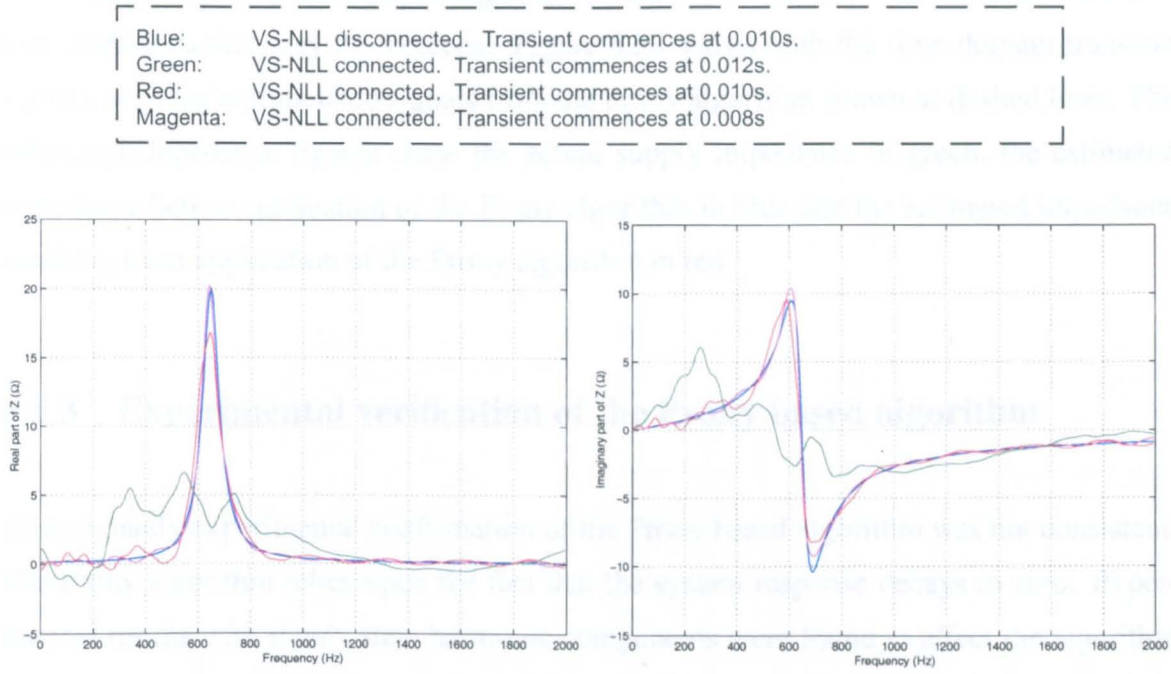

(b) Impedance. (c) Impedance.

Figure 6.27: Estimated supply impedance

6.5.2 Prony extrapolation of time domain signals

It is possible to use the extended time domain Prony method in order to improve the measurement results in some circumstances. Consider injection measurements commenced at 0.010s and at 0.011s. The time domain records are shown in figure 6.28 as solid traces. The Prony algorithm developed was applied to these time domain records. The dashed lines show the Prony extrapolated section of data. (a) and (b) refer to the injection at 0.010s and figures (c) and (d) refer to the injection at 0.011s. The time domain signals calculated from the extended Prony method algorithm may be used to calculate the supply impedance in the same way as before. These results are shown in figure 6.28.

The same process was carried out for the second simulation, the most demanding of the two previous simulations, using more realistic conditions. Noise was added to both the measured signals at the same level as used in the first simulations, in section 4.12.1. Furthermore the sampling rate was 51.151kHz, the practical rate used in experimental work.

The supply frequency was also changed to 50.1Hz to provide the least favourable simulation conditions that may be foreseen. Figure 6.30 shows both the time domain transient signals, with the extrapolated signals from the Prony algorithm shown as dashed lines. The estimated impedance figures show the actual supply impedance in green, the estimated impedance before application of the Prony algorithm in blue and the estimated impedance resulting from application of the Prony algorithm in red.

6.5.3 Experimental verification of the Prony based algorithm

Unfortunately experimental confirmation of the Prony based algorithm was not consistent. The Prony algorithm relies upon the fact that the system response decays to zero. Experimental results with steady state harmonic components were found to affect the algorithm in many instances. This led to wildly inaccurate estimates of the system response. Furthermore, it was not possible to detect whether or not the Prony algorithm would be successful prior to its application. This work is therefore still in progress.

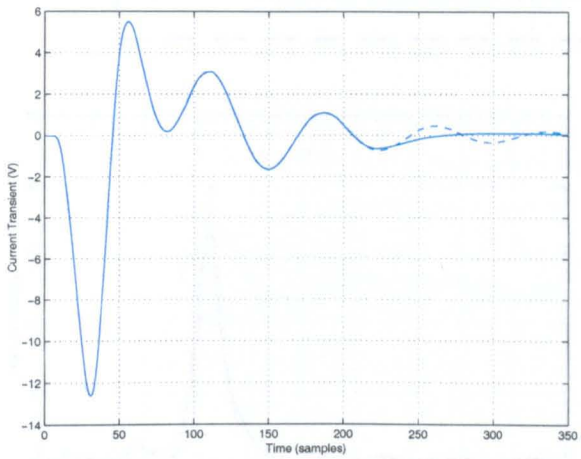

(a) Current transient for injection at 0.010s.

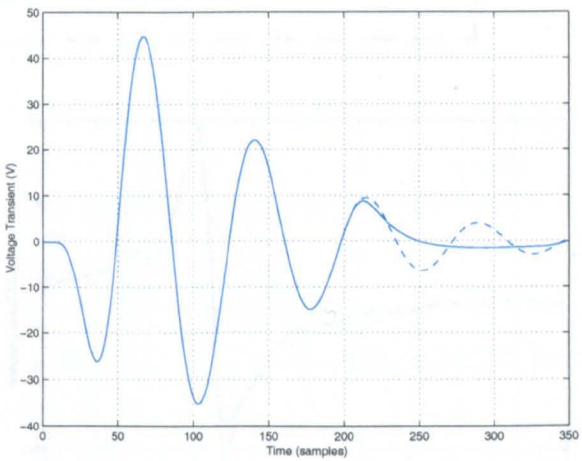

(b) Voltage transient for injection at 0.010s.

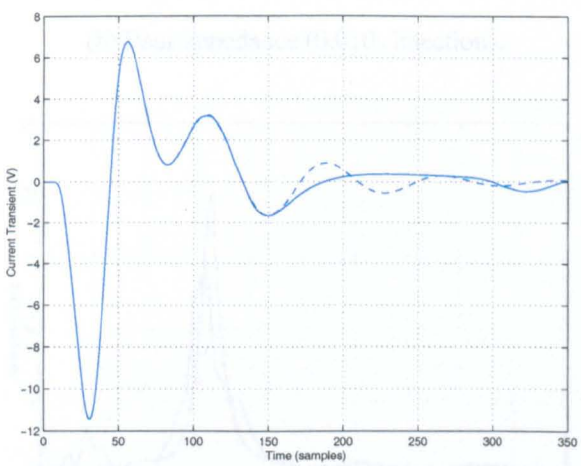

(c) Current transient for injection at 0.011s.

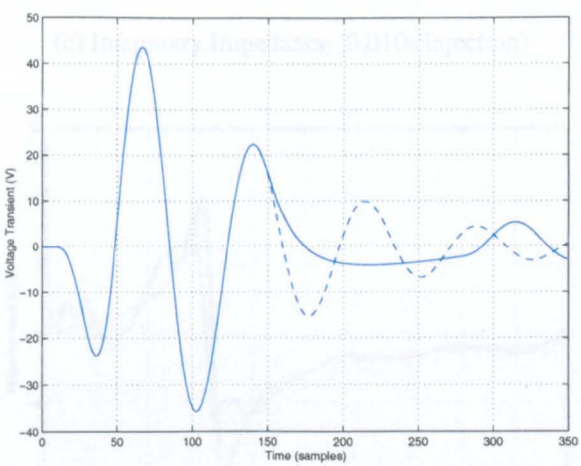

(d) Voltage transient for injection at 0.011s.

Figure 6.28: Injection signals and extraploated signals using the Prony algorithm.

Green: Ideal impedance.
Blue: Impedance estimate before application of the Prony algorithm.
Red: Impedance estimate after application of the Prony algorithm.

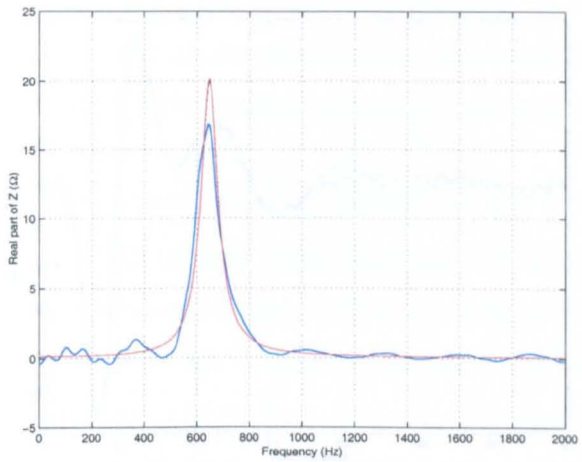

(b) Real impedance (0.010s injection).

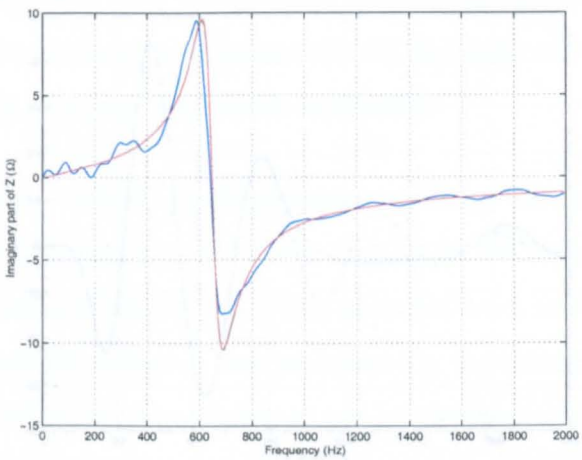

(c) Imaginary Impedance (0.010s injection).

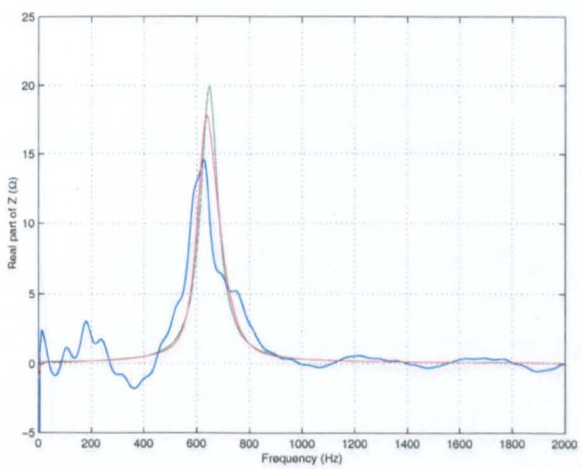

(d) Real Impedance (0.011s injection).

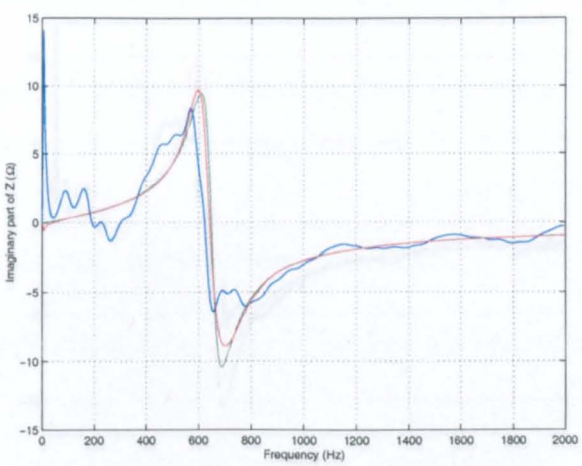

(e) Imaginary Impedance (0.011s injection).

Figure 6.29: Estimated supply impedance after Prony extrapolation

Green: Ideal impedance.
Blue: Impedance estimate before application of the Prony algorithm.
Red: Impedance estimate after application of the Prony algorithm.

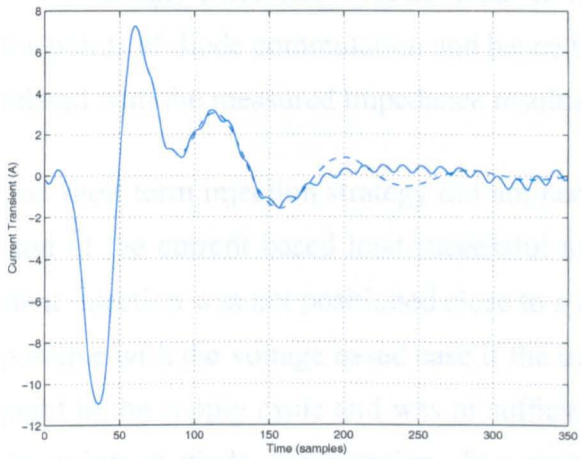

(b) Current transient.

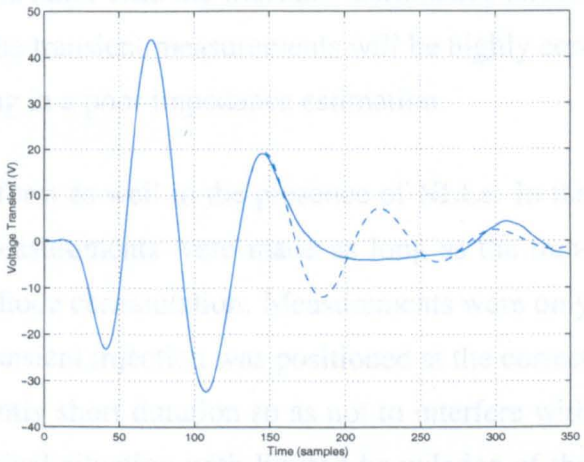

(c) Voltage transient.

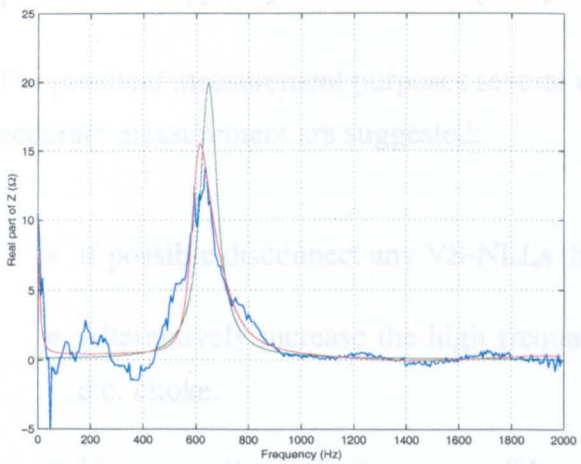

(d) Real impedance.

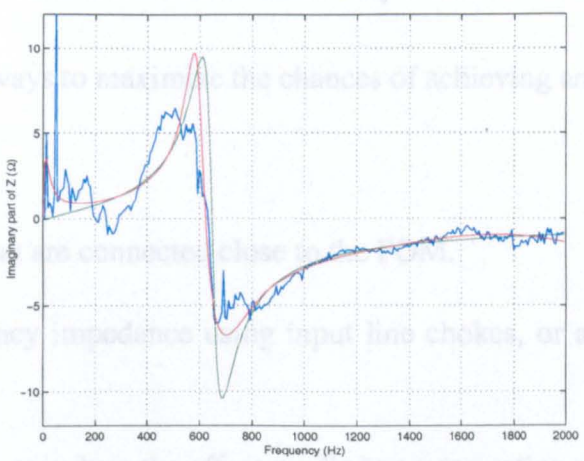

(e) Imaginary impedance.

Figure 6.30: Application of the Prony based algorithm on realistic simulation data

6.6 Conclusion

The medium term injection was able to identify the supply impedance even with a locally connected CS-NLL. This method was not able to measure the supply impedance in the presence of a VS-NLL with any accuracy. In the former case the transient measurement does not affect the times of diode commutation significantly. Therefore the measurement is not strongly correlated with the load. In the latter case the transient disturbance affects the points of diode commutation and hence the transient measurements will be highly correlated with the measured impedance resulting in a poor impedance estimation.

The short term injection strategy did not perform as well in the presence of NLLs. In the case of the current based load successful measurements were made as long as the transient injection was not positioned close to a diode commutation. Measurements were only possible with the voltage based case if the transient injection was positioned at the correct point in the supply cycle and was of sufficiently short duration so as not to interfere with the points of diode commutation. In a practical situation with limited knowledge of the network behaviour it will be unable to commence transient injection at the most suitable point in the supply cycle and so the quality of measured results will be very variable.

For practical measurement purposes several ways to maximize the chances of achieving an accurate measurement are suggested:

- If possible disconnect any VS-NLLs that are connected close to the POM.
- Alternatively increase the high frequency impedance using input line chokes, or a d.c. choke.
- Use as small an injection as possible so as reduce the affect on diode commutations.
- In the short term injection case, position the injection in the time domain away from diode commutations. Also position the injection such that current flow in the NLL occurs between phases 2 and 3 with respect to the measurement phase definitions.

A numerical algorithm, employing the extended Prony method, was also investigated. The aim of this work was to extrapolate recorded transient data to ignore switching effects due to the presence of NLLs. This area of research requires further work.

Chapter 7

Using impedance estimates for prediction of load current

7.1 Introduction

The aim of this chapter is to use experimentally derived impedance estimates and voltage measurements in order to predict the harmonic current drawn by a load. The chapter is split into two sections. In the first section impedance estimates from chapter 5 are used to predict the current drawn by a harmonic producing NLL. In the second section a voltage feedback ASF is implemented using the existing hardware.

7.2 Load current prediction

Voltage measurements were used in conjunction with a supply impedance estimate in order to predict the current demand of an example load. The predicted current was compared with the measured current to determine whether this is a feasible method of deriving references for an active filter.

A NLL was connected to the balanced experimental supply. This load was operated such that a fundamental current of approximately 15A was drawn. During this operation the line voltage v_{12} and the line current i_{12} were recorded. The experimental system is shown in figure 7.1

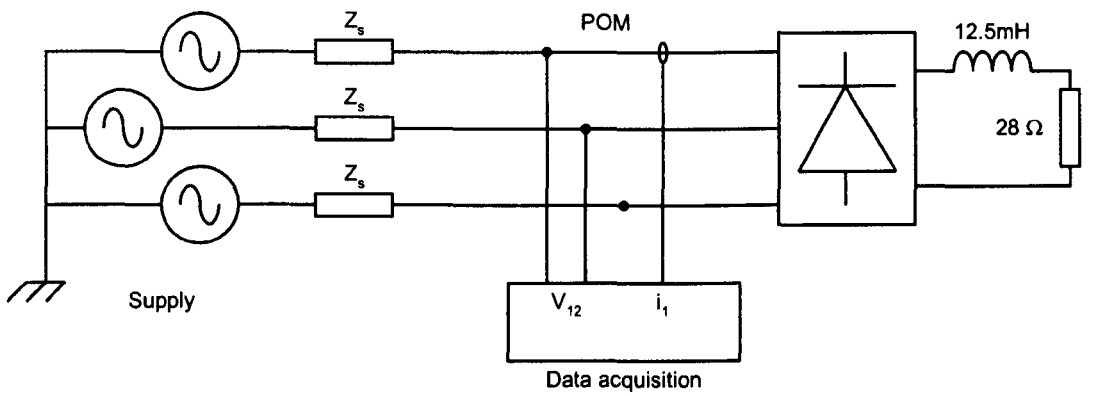

Figure 7.1: Experimental system

The standard laboratory supply was connected to the harmonic producing load. It was necessary to record steady state voltage waveforms before connection of the load so that background distortion of the supply may be taken into consideration. Supply configurations c1 and c3 were considered. c3 was used as the additional capacitors had the effect of amplifying the 7th harmonic voltage distortion. A linear transfer function, derived from the experimental measurement data in chapter 5, was used to calculate the supply impedance at the harmonic frequencies of interest. Current prediction was restricted to the 5th, 7th, 11th, 13th, 17th and 19th harmonics. These harmonics are the most significant harmonics below 1kHz in a balanced three phase system. Transducer error in measuring the voltage distortion became more significant at higher harmonic orders, thus degrading the accuracy of the results.

Unfortunately it was not possible to measure the steady state (no load) distortion at the same time as the load was connected due to the topology of the experimental circuit. Waveforms recorded at different times were thus used for the two voltage measurements. Fluctuations were present on these measurements that significantly affected the harmonic compo-

nents. To reduce this effect 100 fundamental supply cycles were recorded in each state. These were averaged in order reduce the level of noise. The correct phase relationship was achieved by using a separate, un-loaded, supply for triggering purposes.

Figure 7.2 shows two fundamental cycles of the recorded data. The loaded and unloaded voltage waveforms are shown as well as a phase current.

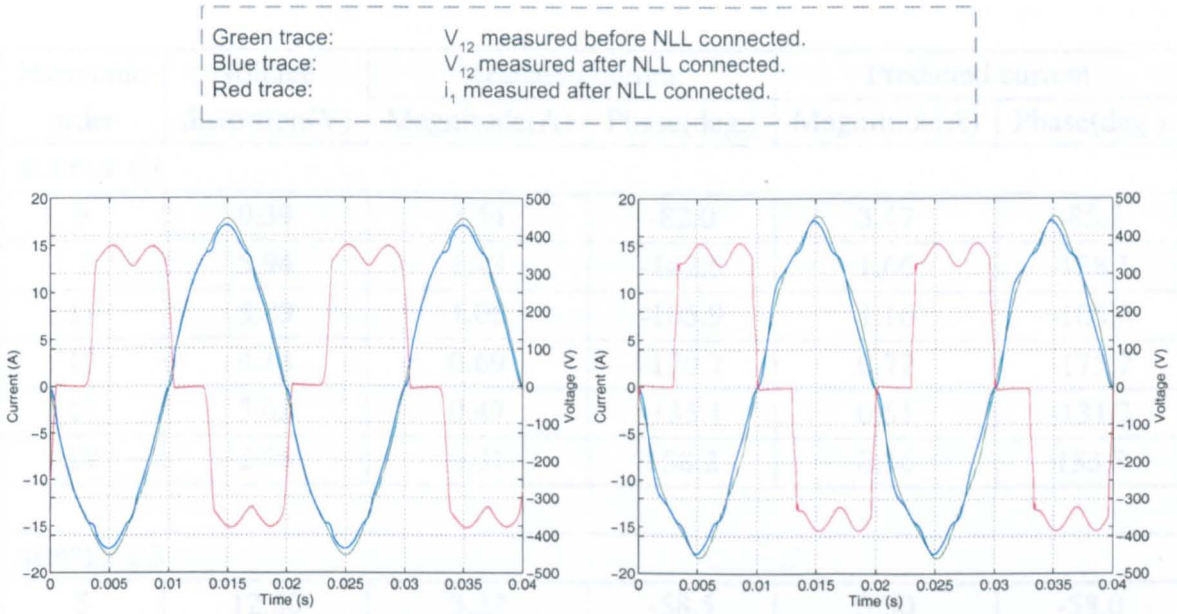

(b) c1 voltage and current measurements

(c) c3 voltage and current measurements

Figure 7.2: Predicted current distortion results.

Table 7.1 shows the results for the described experiment. Measured and predicted current is displayed for each of the harmonics of interest. The magnitude of the voltage distortion is also shown to give an indication of the level of distortion present for each harmonic order. The harmonic voltage signals were very small and so there is considerable scope for both magnitude and phase errors. The data for table 7.1 was captured using a LeCroy digital storage oscilloscope. The oscilloscope utilised 8 bit A/D converters. On the voltage channel this gave a precision of 3.9V and on the current channel a precision of 0.15A. If the effect of the A/D converters was treated as random noise then the effect of averaging 100 samples would be to reduce the standard deviation of this noise by a factor of 10.

Harmonic order	Voltage distortion(V)	Measured current		Predicted current	
		Magnitude(A)	Phase(deg.)	Magnitude(A)	Phase(deg.)
SUPPLY C1					
5	9.39	3.54	-82.0	3.47	-85.7
7	5.94	1.43	-142.6	1.66	-138.1
11	5.89	1.06	-105.9	1.16	-105.2
13	4.14	0.69	-170.7	0.72	-175.7
17	3.62	0.47	-135.1	0.51	-131.2
19	2.76	0.31	158.2	0.36	153.8
SUPPLY C3					
5	12.80	3.52	-58.5	3.30	-58.0
7	19.76	2.76	-75.5	2.68	-78.7
11	7.12	1.14	-12.5	1.07	-4.8
13	4.07	0.93	-62.9	0.87	-66.5
17	1.85	0.62	12.7	0.63	11.67
19	1.15	0.48	-38.6	0.46	-53.6

Table 7.1: Current prediction results using laboratory supply

7.3 Current prediction summary

The two prediction tests undertaken clearly demonstrate that it is possible to derive the current drawn from the example load using a voltage measurement and the supply impedance. Small errors were present in the comparative table, possible explanations for such errors are:

- Measurement errors due to transducer inaccuracy, truncation error and noise pickup in the voltage and current signals.
- Error in the impedance measurement. This may include error due to the fact that the system is not perfectly balanced and natural fluctuations that are present due to the connection and disconnection of remote loads.
- Impedance values of the supply at harmonic frequencies are based upon the assumption of a linear system. The curve fitting algorithm was applied using interharmonic impedance values. This assumption of linearity is clearly not true at the harmonic frequencies although the actual effect is hard to quantify.
- The supply voltage harmonic content varying between measuring V_{12} before, and after, the connection of the NLL. The harmonic content of the supply voltage will vary with time depending upon remotely connected NLLs.

7.4 Voltage detection active power filters

The remainder of this chapter is devoted to the demonstration of an ASF based upon voltage feedback and knowledge of the supply impedance. A brief description of active filter reference generation is given and a derivation provided that enables reference currents to be calculated using a linear transfer function representation of the supply impedance. The active filter control scheme is described briefly. Finally experimental results are shown to demonstrate an ASF in use using the experimentally measured impedance measurements. The ASF was also operated using incorrect impedance to show how this may affect the system stability.

An active filter is used to provide some form of compensation for the harmonic currents drawn by non-linear loads connected to a power system. Three important features may be used to describe an active filter system:

- Active filter circuit topology.
- Reference generation scheme.
- Control scheme.

An active shunt filter (ASF) was chosen as a continuation of active filtering work using this topology [19]. The reference current generation scheme used in this work extended previous generation methods that sought to use supply impedance data. Measured data was used, in the form of a linear transfer function, as provided by the impedance measurement part of this work. This is considered in the following section.

The control scheme employed by the ASF was a state of the art multiple rotating reference frame controller that is described further in section 7.7. This form of controller is used to compensate for the distortion created at particular harmonic frequencies. The number of harmonic frequencies that may be compensated for by the ASF is determined by the processing power of the controller and the order of these harmonics is limited by the switching frequency of the voltage source inverter. In this work it was possible to compensate for the

5th and 7th harmonic distortion at the same time. It was also possible to compensate for the 11th and 13th harmonics although it was only possible to compensate at two frequencies in total.

7.5 Active shunt filter reference generation

Figure 7.3 shows a simplified diagram of a power network. An ASF has been connected, to provide some form of harmonic compensation, by injecting a current I_{ASF} into the system at PCC. The actual current injected will depend upon both the effectiveness of the ASF circuit control and the reference current passed to the controller. In this section the generation of the reference current is of concern. Section 7.7 contains details of the actual control method used experimentally.

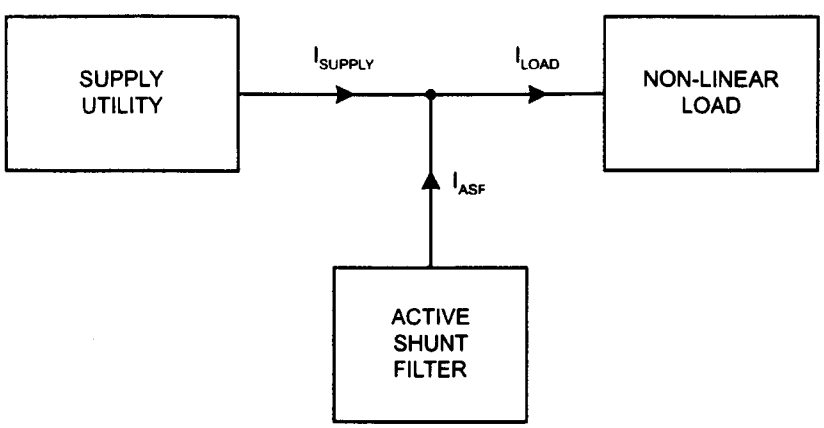

Figure 7.3: Active filter connection

The active filter output current is I_{ASF}. Several means have been adopted for calculating this as a reference for the controller [95]. each method providing the filter circuit with different characteristics. The most common methods are:

1. Measurement of I_{LOAD}.
2. Measurement of I_{SUPPLY}.

3. Using knowledge of the load.

4. Measurement of V_{PCC} and knowledge of supply impedance.

The first method measures the load current,I_{LOAD}. The ASF reference current is made equal to the harmonic part of I_{LOAD}[95]. This approach is used to cancel the harmonic current produced by a single NLL or many NLLs connected at the PCC. Therefore the harmonic current drawn from the supply should be zero. This technique may not be used in order to cancel the harmonic voltage distortion present at the PCC. The advantage of this method lies in its simplicity. One disadvantage is that separate transducers are required to measure I_{LOAD} as well as I_{ASF}.

The second method measures the harmonic content of the supply to derive the reference [96] [97]. Only the supply current need be measured in this case. The disadvantage of this method is that current control is made very difficult as no measure of I_{ASF} is made. The average current mode technique is used in both cases. If I_{ASF} is also measured then this technique is effectively the same as the previous one.

If the active filter is providing compensation for a single load it may be possible to provide information from the load to the ASF. This is the basis of the third method. For example, in [98] a neural network takes information from a motor drive, the d.c. link voltage and current in this case. This information is processed by the trained neural network to provide suitable reference currents for the ASF.

The final method, the voltage feedback ASF, is designed to cancel voltage distortion at the PCC. Such a method may be used to create a clean supply at the PCC or on a small power network, such as on offshore oil platforms [20], where network losses must be minimized. This approach may also be applicable for use by a utility for reducing network distortion [99]. Installation of such an ASF is simplified as only V_{PCC} and I_{ASF} are measured, thus no transducers are required externally from the ASF. This solution may not be suitable for use by a consumer when compensating for a single NLL on a network with high voltage distortion. A consumer that is not experiencing problems due to distortion effects is more likely to install an active filter that corrects for the users own injected harmonic currents

specifically. This is the method used by the experimental ASF in this work and that shall be demonstrated in this chapter.

7.6 Active filters using supply impedance within reference generation

Previous attempts to implement this type of control made various assumptions as to the supply impedance at the PCC. In [100] the supply was assumed to be comprised of an inductor in series with a resistor although it is unclear how these quantities were calculated. In [101] the supply impedance was taken to be the impedance of the transformer at the PCC. Brogan [20] implemented an ASF using short circuit ratings of the supply connection. Akagi [102] proposed a control strategy based on voltage detection for damping of harmonic propagation in distribution systems. Network impedances were also calculated from short circuit ratings. In [103] a similar active filter was proposed that emulated a tuned LC filter at harmonic frequencies. The authors in [103] accept that knowledge of the supply impedance is required for the correct design of their active filter. Grady et al. [29] put forward a minimization procedure for voltage distortion to be corrected by an active power line conditioner (APLC). It was stated that the APLC is provided with voltage distortion measurements around the network and an impedance matrix for the network is known. Finally, in [104], an ASF was proposed for the suppression of harmonic voltage distortion. In this work a neural network was used to estimate a controller gain parameter. This parameter was essentially an estimate of the supply impedance. The author's technique is shown to provide good suppression results. This technique could alternatively use a measured impedance estimate for the control gain parameter.

In [99] an active filter controller was derived using the method proposed in [102]. The active filter was designed to emulate a tuned passive filter at harmonic frequencies. It is interesting to note that the stability of such a filter using impedance values and voltage measurements was shown to be more stable than an active filter based upon reference generation using load current measurement, described in the previous section.

It can be seen that various means of impedance estimation have been used although none have measured the supply impedance using on-line measurements from the active filter. It is therefore necessary to formulate a means of using the measured impedance estimates for reference current calculation.

7.6.1 Reference generation using supply impedance transfer function

Figure 7.4 shows a generalized power system with the ASF connected. Linear loads are included in the Thevenin equivalent of the supply and all non-linear loads have been represented as two individual loads, those connected at the PCC and those connected remotely.

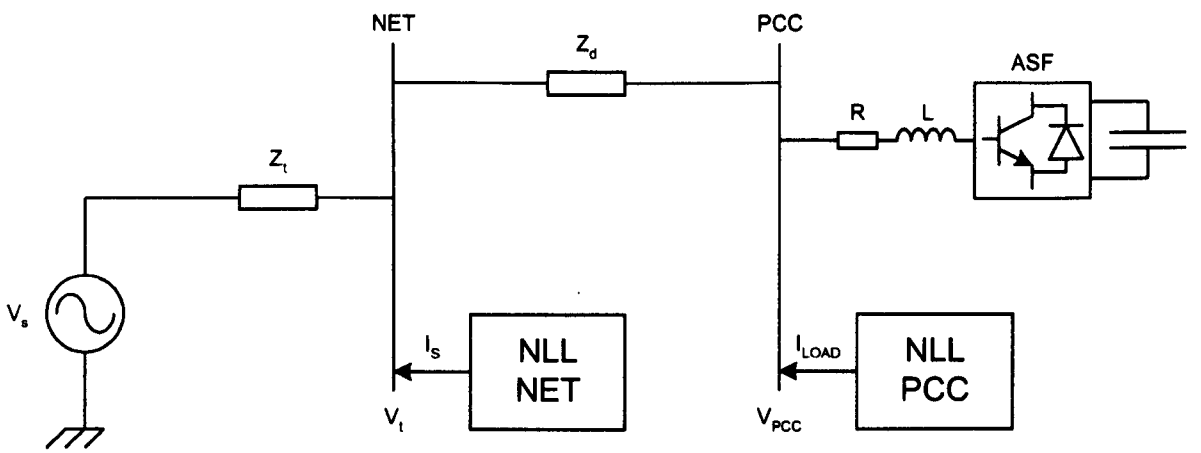

Figure 7.4: Power system with ASF

Using certain assumptions it is possible to take the power system of figure 7.4 and to create an equivalent circuit. From this equivalent the harmonic reference currents for the ASF controller shall be derived. The equivalent circuit is shown in figure 7.5.

Consider the power system at a harmonic frequency at which the ASF is operating. V_s is a fundamental source only. NLL-NET, in figure 7.4, is assumed to be of the CS-NLL form. This may be assumed for NLL-NET, with respect to the ASF point of connection, if there is significant impedance between PCC and the connection of background VS-NLL loads. Clearly remotely connected converters conforming to the CS-NLL model may be

shown in this manner. Converters connected at the PCC are also assumed to be CS-NLLs. This assumption is generally necessary for shunt connected filters [39] [40] [20] [105]. It is equivalent to stating that injected harmonic current from the ASF must flow in the direction of the supply and not of the load. Magoarou et al. [105] investigate the stability of power system with an ASF connected at the same point as a power converter using an uncontrolled rectifier and a capacitively smoothed load (VS-NLL). The authors encountered stability problems and suggested the addition of line inductors between the ASF and the load, hence changing the load to behave as a CS-NLL.

A simplified model of a CS-NLL is adopted, represented by a current source at each harmonic. A linear impedance has not been included to account for power flow at harmonic frequencies. In the steady state, with the ASF cancelling all voltage distortion at the PCC, all power flow will be at the fundamental frequency. Therefore no linear impedance term is required to correctly model NLL-PCC.

In [55] a CS-NLL was considered connected to an inductive supply. The authors conclude that at low order harmonics such a load offers minimal damping and hence an impedance that is of much greater magnitude than the supply impedance. At higher order harmonics, from the 17th and above, such a load may provide considerably less impedance at harmonic frequencies. From this it was deduced that at higher harmonics the NLL may provide some damping to the power system response. This effect may be more prevalent at a lower frequency if a resonance exists in the linear impedance function for the power system. Therefore this is further justification that at low harmonic orders it is sufficient to assume that all power flow occurs at the fundamental frequency and so no harmonic impedance terms are necessary. Figure 7.5 shows the final equivalent circuit that was used for derivation of the current references.

Using figure 7.5 equation 7.1 may be stated to quantify the voltage distortion V_{hc} at harmonic h.

$$V_{hc} = I_{hs}Z_t + (I_{af} + I_{hl})(Z_t + Z_d) \tag{7.1}$$

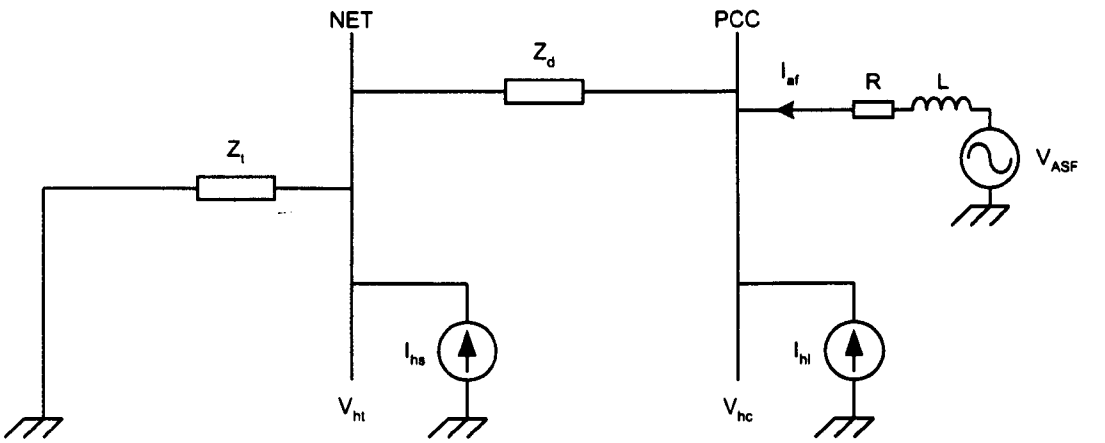

Figure 7.5: ASF equivalent connection

In order to remove all voltage distortion at the ASF PCC for harmonic h, $V_{hc} = 0$. Reference quantities are denoted with an asterisk, thus the ASF reference current is I^*_{af}. If the voltage distortion has been forced to zero then the actual ASF harmonic current will be equal to the harmonic reference current, $I_{af} = I^*_{af}$. Equation 7.2 describes this state.

$$I^*_{af} = \left(\frac{-Z_t}{Z_t + Z_d}\right) I_{hs} - I_{hl} \tag{7.2}$$

Combining equations 7.1 and 7.2 to determine a reference current in terms of voltage distortion, when this distortion has not been fully cancelled.

$$I^*_{af} = I_{af} - \left(\frac{V_{hc}}{Z_t + Z_d}\right) \tag{7.3}$$

Alternatively a current error may be defined as the difference between the reference current and the actual active filter current at a particular instant. This error is shown as equation 7.4.

$$I_{err} = \left(\frac{-V_{hc}}{Z_t + Z_d}\right) \tag{7.4}$$

Therefore for each harmonic controller it is necessary to measure the voltage distortion and the supply impedance $(Z_t + Z_d)$ in order to calculate an error quantity for the input to some form of controller. The supply impedance measured in the previous chapters of this thesis is equal to this supply impedance, $Z_s = Z_t + Z_d$. If the supply impedance is represented as a second order linear system it may be written as shown in equation 7.5. The impedance could be represented by a transfer function of higher order but in an attempt to maintain clarity it shall be restricted to a second order system.

$$Z_s = \frac{B_2 s^2 + B_1 s + B_0}{A_2 s^2 + A_1 s + A_0} \tag{7.5}$$

The system considered will in fact be a balanced three phase system. Vector notation is thus introduced at this point to include all three phases. New variables, **i** and **v**, are introduced. **v** is merely voltage distortion at the PCC but **i** is defined such that equation 7.3 may be written in the simple form:

$$\mathbf{v} = \mathbf{Z_s}(t)\mathbf{i}$$

i, **v** and $\mathbf{Z_s}$ are defined in equations 7.6 to 7.8.

$$\mathbf{i} = \begin{pmatrix} i_{af1} - i^*_{af1} \\ i_{af2} - i^*_{af2} \\ i_{af3} - i^*_{af3} \end{pmatrix} \tag{7.6}$$

$$\mathbf{v} = \begin{pmatrix} v_{hc1} \\ v_{hc2} \\ v_{hc3} \end{pmatrix} \tag{7.7}$$

$$\mathbf{Z} = \begin{pmatrix} Z_s & 0 & 0 \\ 0 & Z_s & 0 \\ 0 & 0 & Z_s \end{pmatrix} \tag{7.8}$$

A differential equation may then be written in the time domain, equation 7.9.

$$B_2\frac{d^2\mathbf{i}}{dt^2} + B_1\frac{d\mathbf{i}}{dt} + B_0\mathbf{i} = A_2\frac{d^2\mathbf{v}}{dt^2} + A_1\frac{d\mathbf{v}}{dt} + A_0\mathbf{v} \tag{7.9}$$

The ASF control was developed using dq axis controllers [19] [106]. The three phase currents and voltages were first transformed into $\alpha\beta$ coordinates and then into a dq reference frame. A separate rotating frame of reference was used for each harmonic controller. Once the quantities were converted into $\alpha\beta$ coordinates the dq transformation was conducted using equation 7.10. ω is the appropriate angular frequency for each harmonic controller. Appendix C contains details of the transformations, details of how the dq reference frame controllers are derived and a complete derivation of the reference currents.

$$v_{dq} = \frac{2}{3\sqrt{2}}(v_\beta + jv_\alpha)e^{j\omega t} \tag{7.10}$$

Equation 7.10 was substituted into equation 7.9. Exponential terms were then cancelled and a Laplace transform was applied to the result. Real and imaginary terms were equated, yielding equations 7.11 for the real parts and equation 7.12 for the imaginary parts.

$$\begin{aligned} &I_q\left(-B_2\omega^2 + B_2s^2 + B_1s + B_0\right) + I_d\left(2B_2\omega s + B_1\omega\right) \\ &= V_q\left(-A_2\omega^2 + A_2s^2 + A_1s + A_0\right) + V_d\left(2A_2\omega s + A_1\omega\right) \end{aligned} \tag{7.11}$$

$$\begin{aligned} &I_d\left(-B_2\omega^2 + B_2s^2 + B_1s + B_0\right) + I_q\left(-2B_2\omega s - B_1\omega\right) \\ &= V_d\left(-A_2\omega^2 + A_2s^2 + A_1s + A_0\right) + V_q\left(-2A_2\omega s - A_1\omega\right) \end{aligned} \tag{7.12}$$

Equations 7.11 and 7.12 are redefined for convenience as equations 7.13 and 7.14.

$$FI_q + GI_d = XV_q + YV_d \tag{7.13}$$

$$FI_d - GI_q = XV_d - YV_q \tag{7.14}$$

where $F, G, X,$ and Y are:

$$F = -B_2\omega^2 + B_2s^2 + B_1s + B_0 \tag{7.15}$$

$$G = 2B_2\omega s + B_1\omega \tag{7.16}$$

$$X = -A_2\omega^2 + A_2s^2 + A_1s + A_0 \tag{7.17}$$

$$Y = 2A_2\omega s + A_1\omega \tag{7.18}$$

Equation 7.13 and 7.14 form a pair of simultaneous equations that may be solved for I_d and I_q. The solution is shown in equations 7.19 and 7.20.

$$I_d = \left(\frac{GY + FX}{F^2 + G^2}\right) V_d + \left(\frac{GX - FY}{F^2 + G^2}\right) V_q \tag{7.19}$$

$$I_q = \left(\frac{FY - GX}{F^2 + G^2}\right) V_d + \left(\frac{FX + GY}{F^2 + G^2}\right) V_q \tag{7.20}$$

The solution to the simultaneous equations yields two distinct admittance terms. These are:

$$Y_{dd} = Y_{qq} = \left(\frac{GY + FX}{F^2 + G^2}\right) \tag{7.21}$$

$$Y_{dq} = -Y_{qd} = \left(\frac{GX - FY}{F^2 + G^2}\right) \tag{7.22}$$

If the ASF controllers are sufficiently slow then the references may be considered in the steady state, therefore $s \rightarrow 0$. In this case the parameters F, G, X and Y will be reduced to the forms shown in equations 7.23 to 7.26.

$$F' = -B_2\omega^2 + B_0 \tag{7.23}$$

$$G' = -B_3\omega^3 + B_1\omega \tag{7.24}$$

$$X' = -A_2\omega^2 + A_0 \tag{7.25}$$

$$Y' = -\omega^3 + A_1\omega \tag{7.26}$$

From this section it can be seen that the supply impedance transfer functions may be used to calculate the admittances Y_{dd} and Y_{dq}. Using these quantities I_d and I_q can be calculated. Finally the reference currents can be calculated, equation 7.6 indicates the final step in this process. The d and q references are shown in equations 7.27 and 7.28.

$$I^*_{afd} = I_{afd} - I_d \tag{7.27}$$

$$I^*_{afq} = I_{afq} - I_q \tag{7.28}$$

7.7 Control of the ASF

The overall aim of the ASF control is to control the current flowing in the line inductors. This is achieved by controlling the output voltage of the inverter. The control hardware measures the line inductor current, the voltage at the PCC and receives reference inputs calculated according to the previous section.

The ASF uses a control strategy that employs three dq rotating frames of reference. The first controller uses a fundamental rotating reference frame. The second two controllers are such that each operates at a different harmonic frequency. Normally these operate at the 5th and 7th harmonic frequencies although a test was conducted at the end of this chapter using

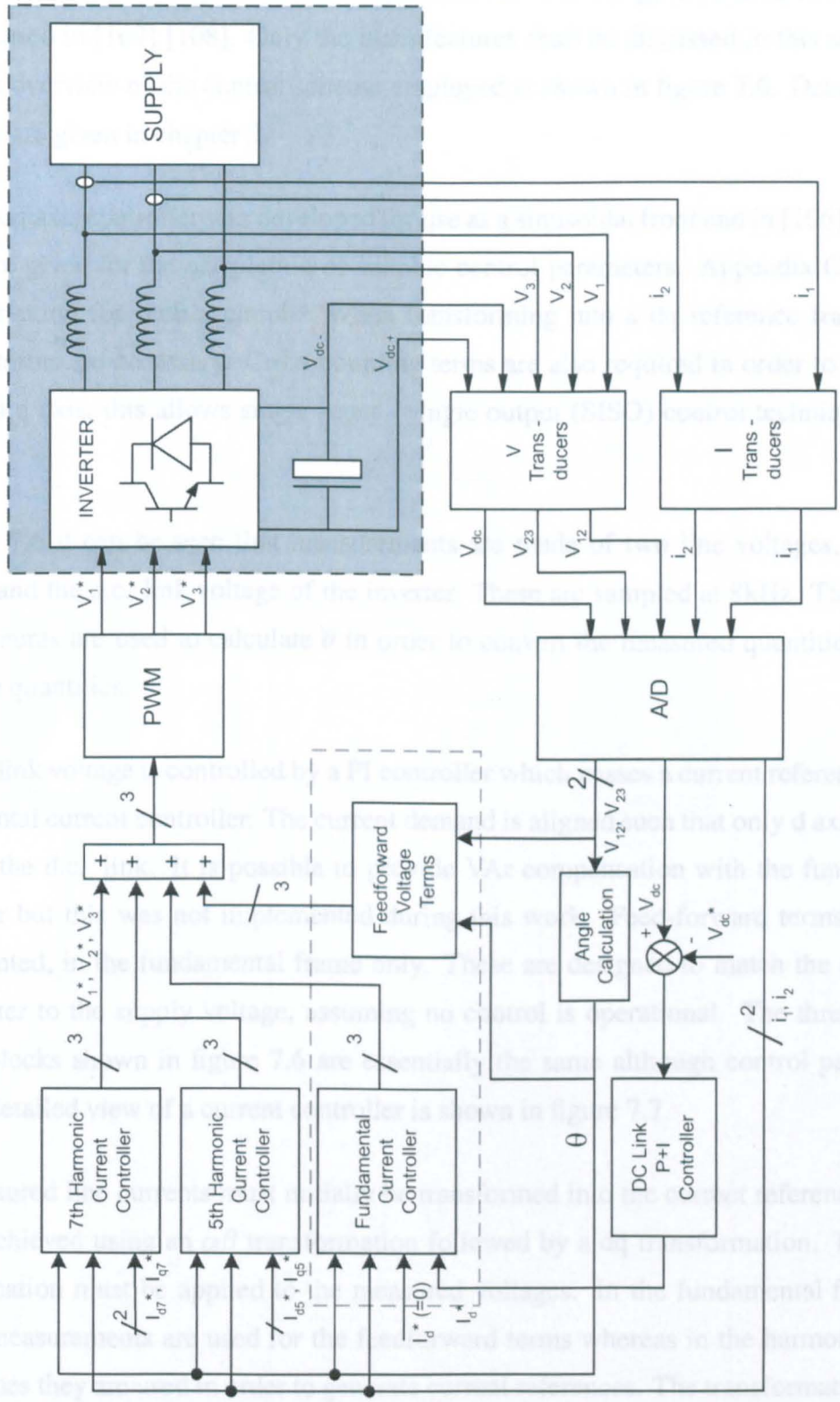

Figure 7.6: ASF control scheme in dq reference frame

a 7th harmonic and 11th harmonic controller. This control strategy is detailed in full in [19] and also used in [107] [108]. Only the main features shall be discussed in this section. A complete overview of the control scheme employed is shown in figure 7.6. Details of the hardware are given in chapter 3.

A single dq axis controller was developed for use as a sinusoidal front end in [106] in which details are given for the calculation of suitable control parameters. Appendix C details a brief derivation for such a circuit. When transforming into a dq reference frame feed-forward terms are necessary. Cross coupling terms are also required in order to decouple the d and q axis, this allows single input - single output (SISO) control techniques to be applied.

In figure 7.6 it can be seen that measurements are made of two line voltages, two line currents and the d.c. link voltage of the inverter. These are sampled at 8kHz. The voltage measurements are used to calculate θ in order to convert the measured quantities into dq reference quantities.

The d.c. link voltage is controlled by a PI controller which passes a current reference to the fundamental current controller. The current demand is aligned such that only d axis current supplies the d.c. link. It is possible to provide VAr compensation with the fundamental controller but this was not implemented during this work. Feed-forward terms are also implemented, in the fundamental frame only. These are designed to match the output of the inverter to the supply voltage, assuming no control is operational. The three current control blocks shown in figure 7.6 are essentially the same although control parameters vary. A detailed view of a current controller is shown in figure 7.7.

The measured line currents must initially be transformed into the correct reference frame. This is achieved using an $\alpha\beta$ transformation followed by a dq transformation. The same transformation must be applied to the measured voltages. In the fundamental frame the voltage measurements are used for the feedforward terms whereas in the harmonic reference frames they are used in order to generate current references. The transformation angle for the 5th frame is calculated from $\theta_5 = -5\theta$ as the frequency is 5 times greater than the

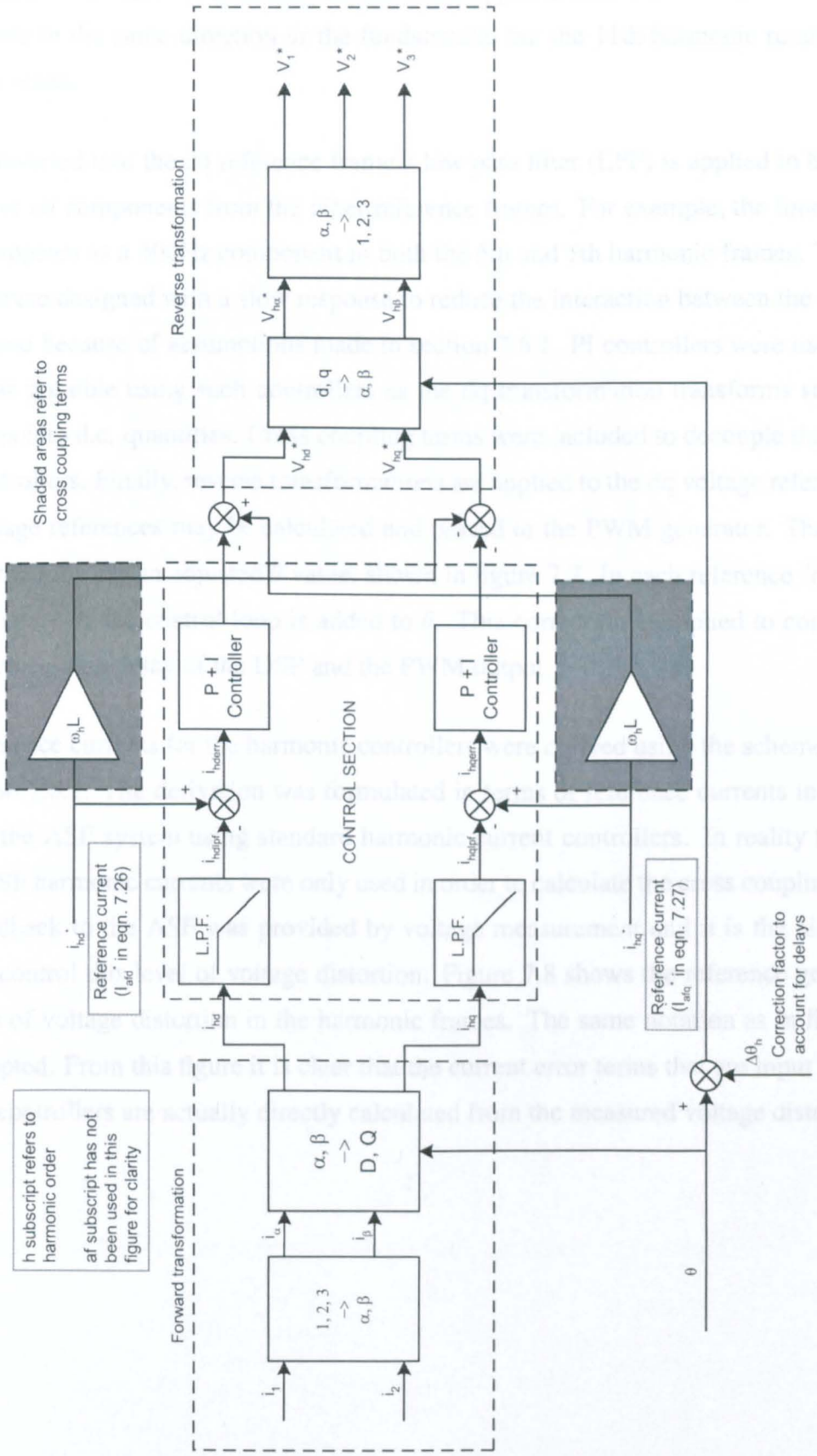

Figure 7.7: ASF harmonic controller

fundamental frame and the 5th frame rotates in the opposite sense. The 7th and 13th frames both rotate in the same direction as the fundamental but the 11th harmonic rotates in the opposite sense.

Once converted into the dq reference frame a low pass filter (LPF) is applied to both axes to remove all components from the other reference frames. For example, the fundamental current appears as a 300Hz component in both the 5th and 7th harmonic frames. The controllers were designed with a slow response to reduce the interaction between the different frames and because of assumptions made in section 7.6.1. PI controllers were used. Zero error was possible using such controllers as the dq transformation transforms sinusoidal quantities into d.c. quantities. Cross coupling terms were included to decouple the d and q axis controllers. Finally, reverse transformations are applied to the dq voltage references so that voltage references may be calculated and passed to the PWM generator. The reverse transformations use an adjusted θ value, shown in figure 7.7. In each reference frame, the angular delay of the control loop is added to θ. This correction is applied to compensate for the processing delay of the DSP and the PWM output.

The reference currents for the harmonic controllers were derived using the scheme derived in section 7.6.1. The derivation was formulated in terms of reference currents in order to explain the ASF system using standard harmonic current controllers. In reality the measured ASF harmonic currents were only used in order to calculate the cross coupling terms. The feedback to the ASF was provided by voltage measurement and it is the aim of the ASF to control this level of voltage distortion. Figure 7.8 shows the reference generation in terms of voltage distortion in the harmonic frames. The same notation as in figure 7.7 was adopted. From this figure it is clear that the current error terms that are input to the PI current controllers are actually directly calculated from the measured voltage distortion.

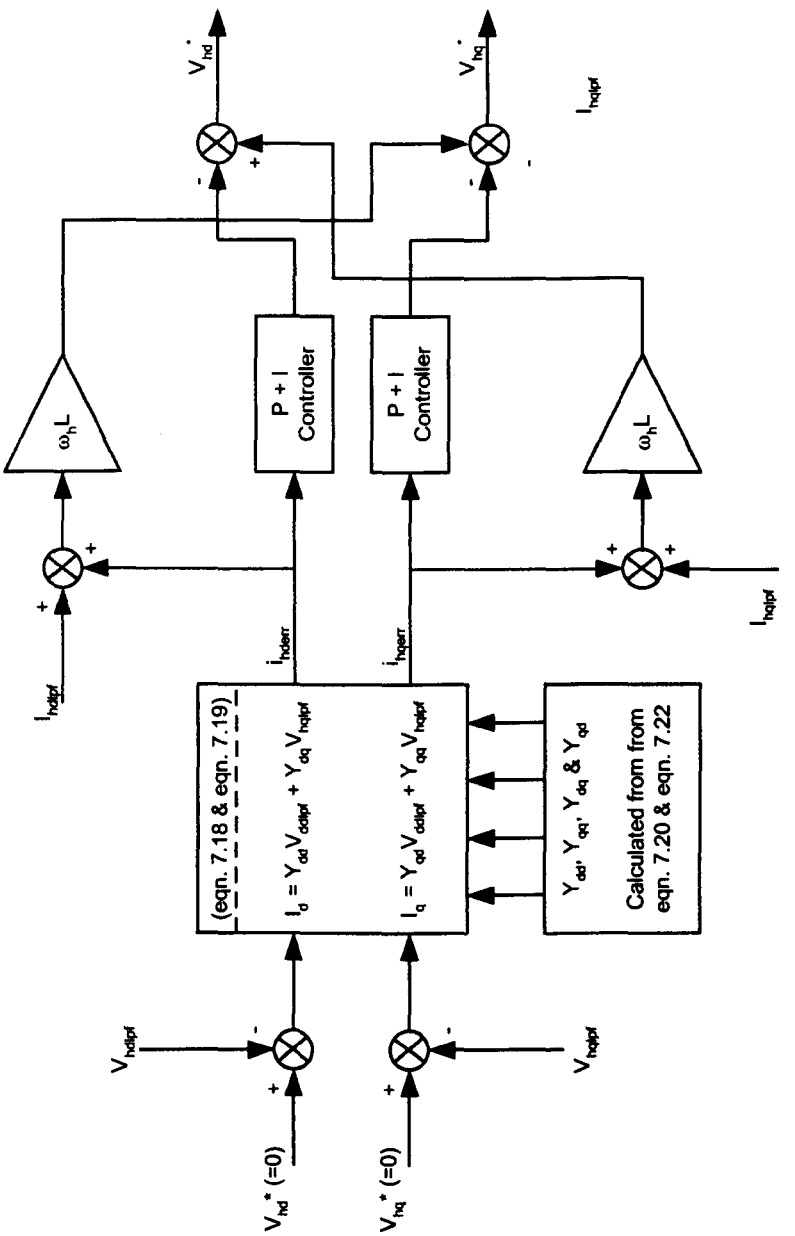

Figure 7.8: Voltage feedback for current error generation

7.7.1 Control parameter design

Harmonic control design is simplified greatly due to the application of the dq transformation and decoupling of the subsequent d and q axes by cross coupling terms. Figure 7.9 shows a single axis controller. In total there are six such controllers.

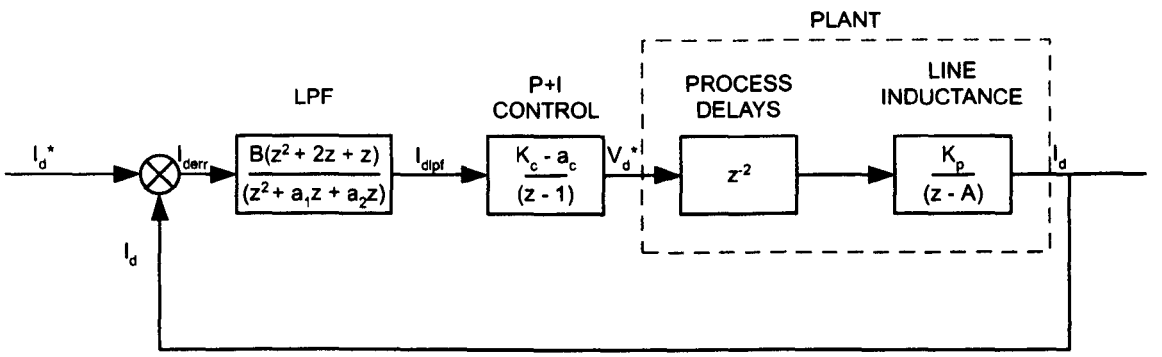

Figure 7.9: Single axis controller

The control parameters were designed in the z domain [109]. A second order Butterworth digital LPF was implemented. The process delays were included to account for the 125μs DSP processor delay, delays in the gate driver and dead time circuitry. These were modelled by two process delays. The plant is merely the line inductance, with a small resistive component. In the s domain this is

$$H(s) = \frac{1}{Ls + R}$$

This was converted to the z domain using the Tustin transformation [109]. Table 7.2 shows the filter cut off frequencies and the bandwidth of the different controllers. Low bandwidth controllers were utilized in order to reduce the coupling between controller operating at different harmonic frequencies. The fundamental controller was operated at a much higher bandwidth to the harmonic controllers as it was important for the ASF to track the fundamental supply voltage. The impedance of the line inductors was much less at the fundamental frequency compared to the harmonic frequencies of interest. Therefore a small error in the control at this frequency resulted in large currents flowing in the ASF circuit.

Controller	LPF 3dB frequency (Hz)	Control bandwidth (Hz)
Fundamental	80	20
Fifth harmonic	20	5
Seven harmonic	20	3

Table 7.2: Control parameters

7.8 Experimental results

Three experimental demonstrations were conducted to illustrate the operation of the ASF with a voltage feedback controller. Figure 7.10 shows the experimental system constructed for this purpose although the first demonstration was conducted with the load disconnected.

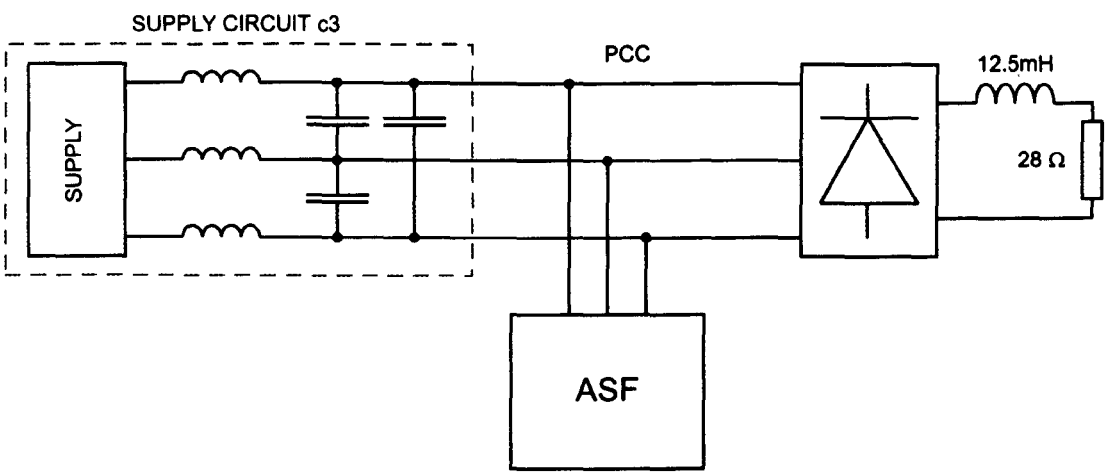

Figure 7.10: Experimental circuit

The three tests carried out were:

- **Voltage distortion compensation with no load.**
- **Voltage distortion compensation with load connected.**
- **Voltage distortion compensation with incorrect parameters.**

The first two tests were designed to demonstrate the successful operation of the ASF using measurements of voltage distortion with the values of supply admittance calculated from previous measurement work. The third test was designed to show the operation of the ASF when incorrect admittance coefficients were used by the control.

7.8.1 Voltage distortion compensation with no load

The harmonic controllers act to compensate for the voltage distortion at the fifth and seventh harmonics without any load connected at the PCC. Ideally all the fifth and seventh harmonic voltage distortion should be cancelled. V_{d5lpf} and V_{q5lpf} represent the voltage distortion within the controller for the fifth harmonic. The same notation is used at the seventh harmonic. Therefore the success of the control scheme may be ascertained by looking at both the actual line voltage harmonics and at the dq axis voltage distortion within the controller. In order to control the fifth harmonic voltage distortion to zero both V_{d5lpf} and V_{q5lpf} must be controlled to zero.

The impedance of supply c3 is shown in figure 7.11. It can be seen that both the fifth and seventh harmonics lie before the resonant peak at roughly 450Hz.

Figure 7.11 was calculated using the transfer function derived from experimental results, see section 5. This transfer function was estimated as a second order function in order to test the derivation shown earlier in this chapter for admittance calculation.

$$Z_s = \frac{-0.14s^2 + 1.2 \times 10^4 s + 6.3 \times 10^6}{s^2 + 1.3 \times 10^3 s + 7.3 \times 10^6}$$

The transfer function shown cannot represent a realizeable passive impedance network as the second order numerator coefficient is negative. In fact, this impedance would be better modelled as a first order system. The required admittance terms were then calculated according to equations 7.21 and 7.22. These terms are shown in table 7.3

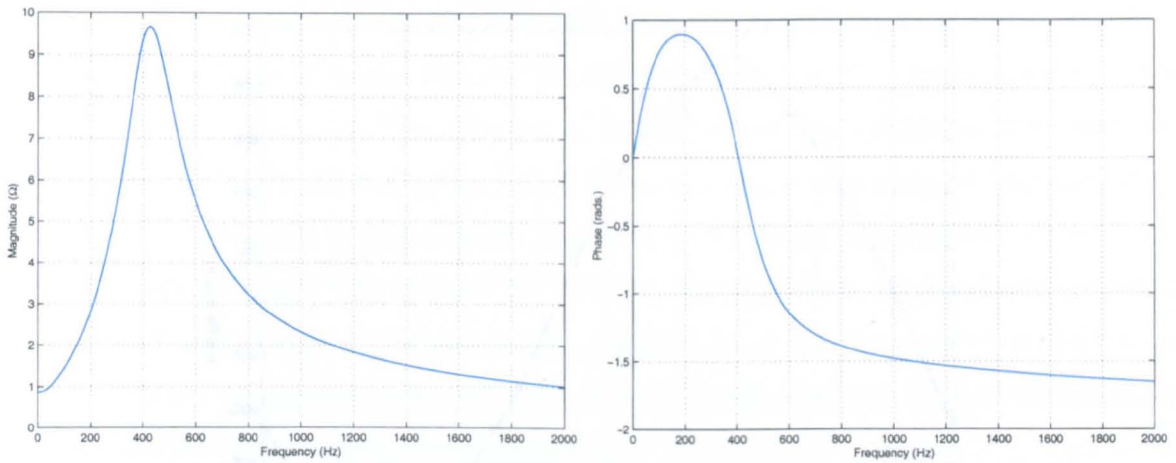

(a) Impedance magnitude

(b) Impedance phase

Figure 7.11: Supply impedance for c3 (per phase)

Harmonic order	Admittance (S)	
	Y_{dd}	Y_{dq}
5	0.26	0.29
7	0.18	0.09

Table 7.3: Admittance terms for calculation of current references

The ASF was initially operated with zero current control references, that is, no harmonic current was injected into the system. The control references were then enabled and the control was used to cancel the fifth and seventh harmonic voltage distortion at the PCC. Figure 7.12 shows the measured line voltage, V_{12} before distortion compensation in blue. The line voltage is shown again, in red, once steady state operation of the compensating control was reached. The harmonic content of the waveforms in figure 7.12 is shown in figure 7.13, using the same trace colours as for figure 7.12. The third and ninth harmonics were also plotted to show that the system was not completely balanced and hence not all the assumptions made in the control design and impedance measurement were fully justified.

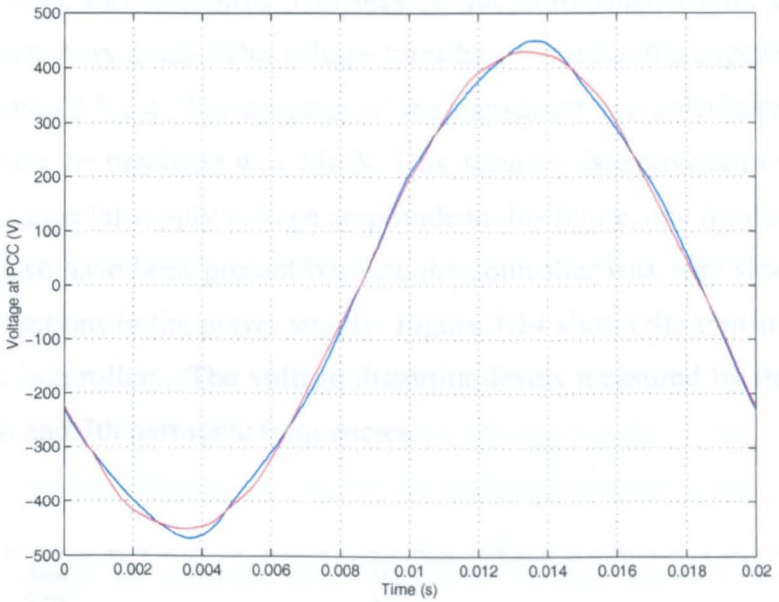

Figure 7.12: Line voltage distortion before(blue) and after(red) controllers turned on

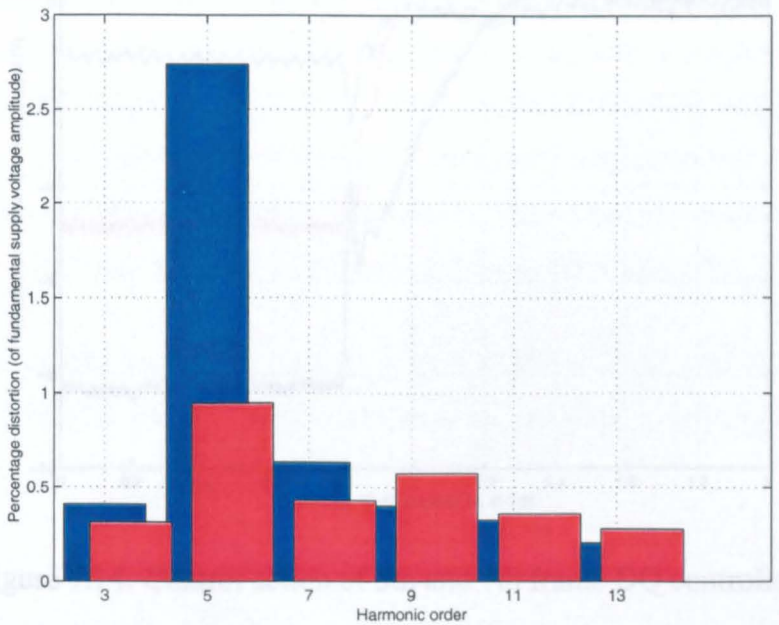

Figure 7.13: Line voltage harmonics before(blue) and after(red) controllers activated

Figure 7.13 shows that the harmonic voltage levels were reduced considerably. A small amount of distortion still remained. This may be due to transducer error as the harmonic voltage levels were very small. The voltage transducers used in the experimental rig were described in section 3.2.2.4. The accuracy of the transducer was calculated to be approximately 0.8V while the precision was 24mV. This accuracy is equivalent to approximately 0.2% of the fundamental supply voltage amplitude in this figure, and figures 7.15 and 7.20. The error may also have been present because the controller was very slow and unable to track small fluctuations in the power supply. Figure 7.14 shows the transient performance of the harmonic controllers. The voltage distortion levels measured by the controller are shown at the 5th and 7th harmonic frequencies.

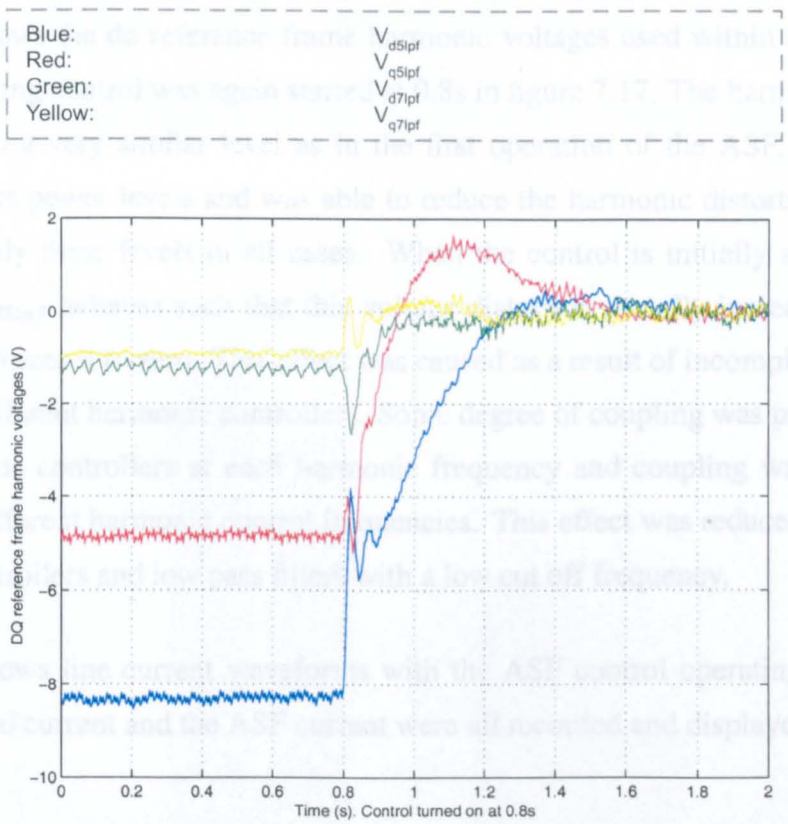

Figure 7.14: Control action of 5th and 7th frame DQ controllers

The distortion compensating control was activated at 0.8s. Prior to this time figure 7.14 shows that voltage distortion existed at both frequencies. Once the control was activated

and its output reached steady state it can clearly be seen that all four harmonic voltage components were controlled to zero. The transient response was slow but the system was designed to demonstrate the technique and the controllers were not optimized for transient performance.

7.8.2 Voltage distortion compensation with load connected

A load was then connected at the PCC in order to increase the levels of harmonic distortion and to test the ASF with a load connected at the same point. Figure 7.15 shows the measured line voltage and figure 7.16 shows the harmonic content of the line voltage.

Figure 7.17 shows the dq reference frame harmonic voltages used within the controllers. The compensating control was again started at 0.8s in figure 7.17. The harmonic distortion was reduced to a very similar level as in the first operation of the ASF. The ASF was tested at various power levels and was able to reduce the harmonic distortion at the PCC to approximately these levels in all cases. When the control is initially activated it can be seen that V_{d5lpf} behaves such that this voltage distortion actually increases before the control action forces it to zero. This effect was caused as a result of incomplete decoupling between the different harmonic controllers. Some degree of coupling was present between the d and q axis controllers at each harmonic frequency and coupling was also present between the different harmonic control frequencies. This effect was reduced by using low bandwidth controllers and low pass filters with a low cut off frequency.

Figure 7.18 shows line current waveforms with the ASF control operating. The supply current, the load current and the ASF current were all recorded and displayed.

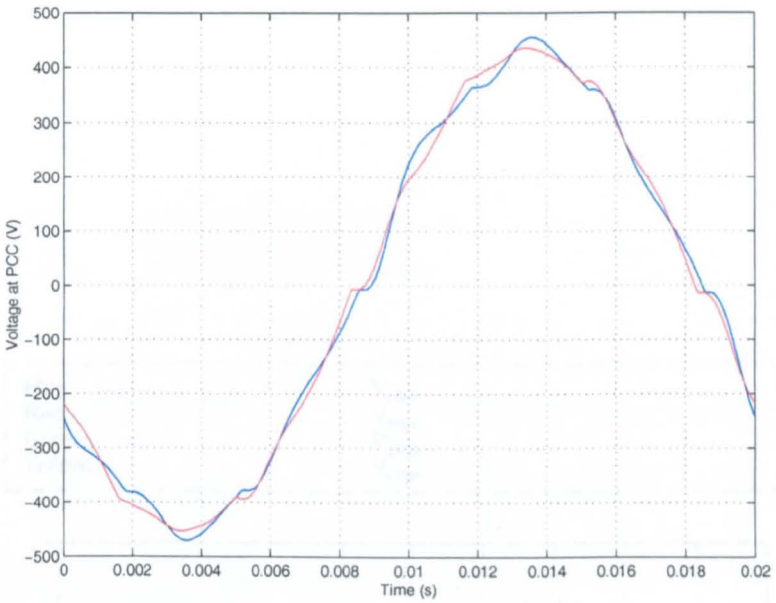

Figure 7.15: Line voltage distortion before(blue) and after(red) control action

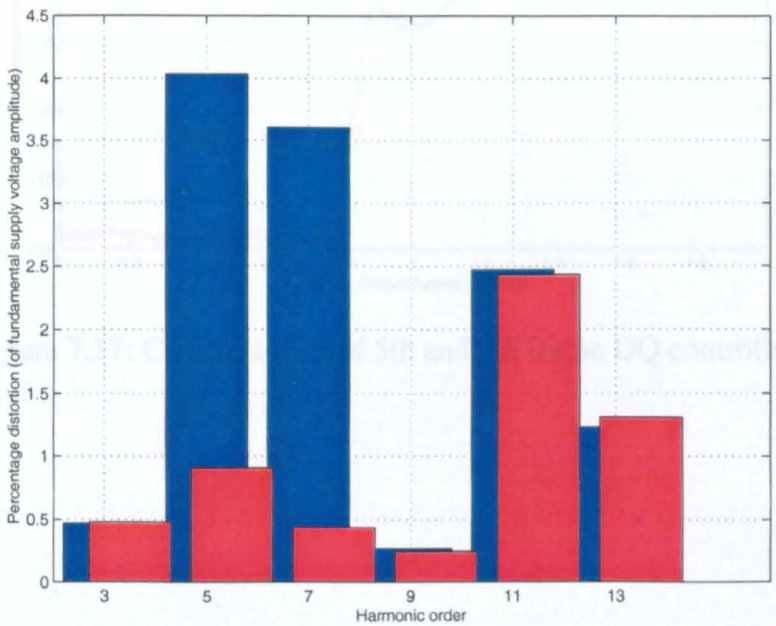

Figure 7.16: Line voltage harmonics before(blue) and after(red) control action

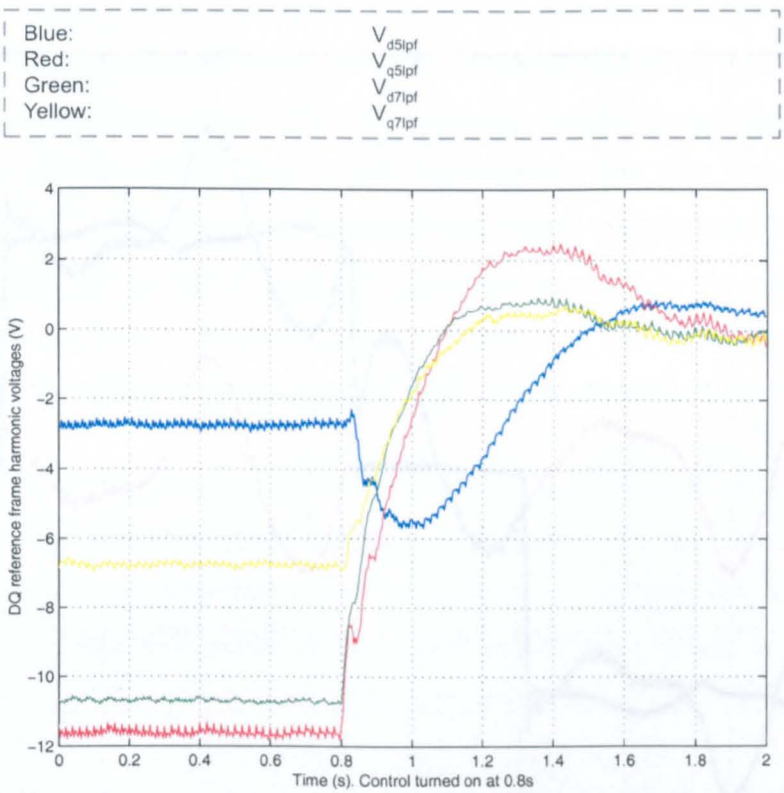

Figure 7.17: Control action of 5th and 7th frame DQ controllers

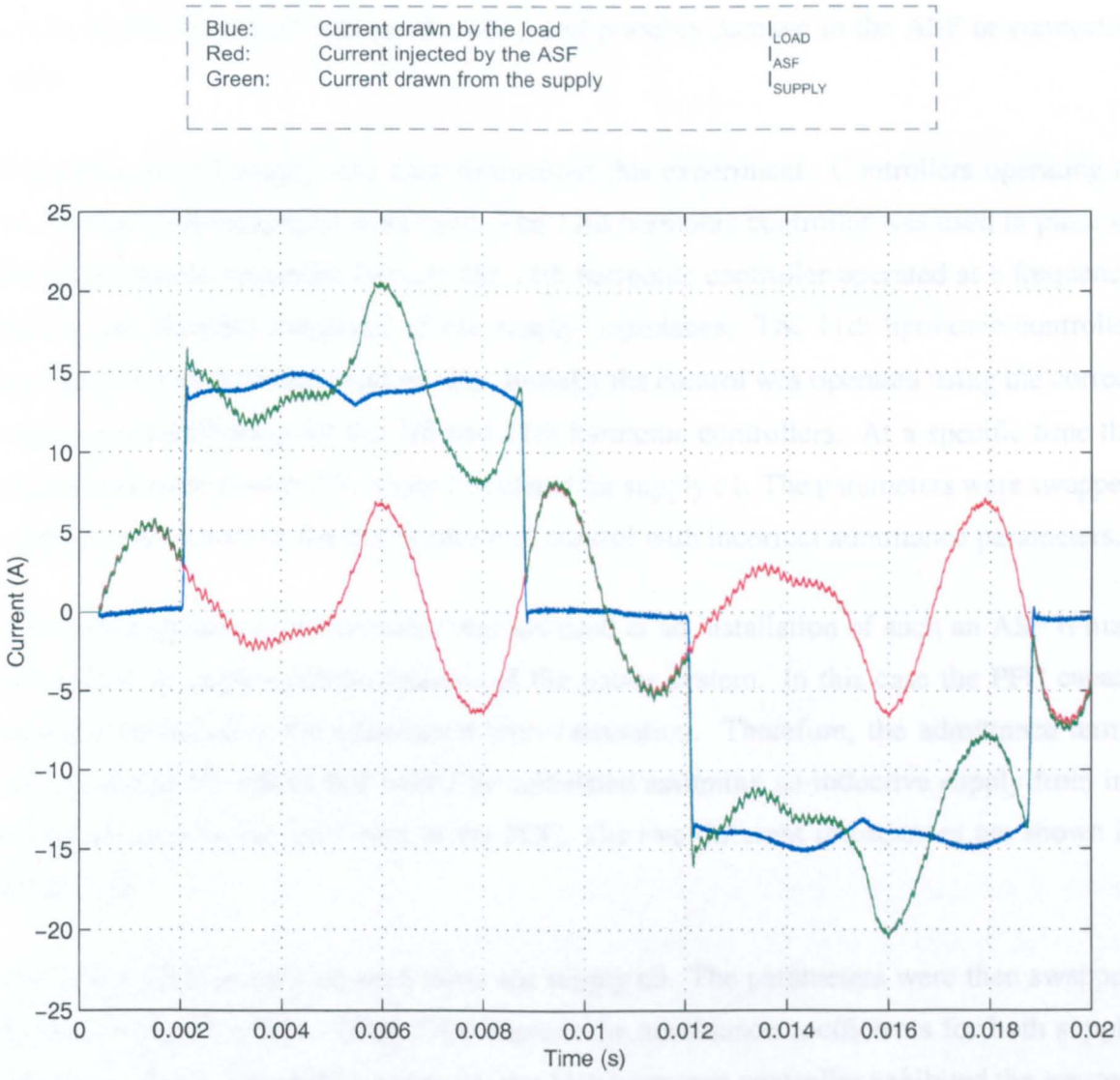

Figure 7.18: Line current waveforms during ASF operation

7.8.3 Voltage distortion compensation with incorrect parameters

The final demonstration to be carried out using the ASF was to test the control scheme with an incorrect supply impedance estimate. The aim of this section was to investigate the stability of the ASF in a situation when the supply impedance is not known. Instability would lead to increased voltage distortion and possibly damage to the ASF or connected loads.

Physically, the c3 supply was used throughout this experiment. Controllers operating at the 7th and 11th harmonics were used. The 11th harmonic controller was used in place of the 5th harmonic controller because the 11th harmonic controller operated at a frequency beyond the resonant frequency of the supply impedance. The 11th harmonic controller was designed with a bandwidth of 3Hz. Initially the control was operated using the correct admittance coefficients for the 7th and 11th harmonic controllers. At a specific time the coefficients were swapped for those calculated for supply c1. The parameters were swapped in order to demonstrate the performance of control with incorrect admittance parameters.

If on-line impedance measurement was not used at an installation of such an ASF it may be possible to neglect certain features of the power system. In this case the PFC capacitors are neglected in the admittance term calculation. Therefore, the admittance terms were swapped for values that would be calculated assuming an inductive supply from information such as the fault level at the PCC. The two different impedances are shown in figure 7.19.

The initial parameters used were those for supply c3. The parameters were then swapped for the c1 supply values. Table 7.4 compares the admittance coefficients for both supply situations. The Y_{dq} admittance term for the 11th harmonic controller exhibited the greatest change, changing from -0.19 to +0.28. Clearly, for the same voltage distortion the generated reference current was very different.

The ASF was initially operated in a stable manner with the correct parameters. The level of harmonic distortion in the supply voltage is shown in figure 7.20. The blue trace shows

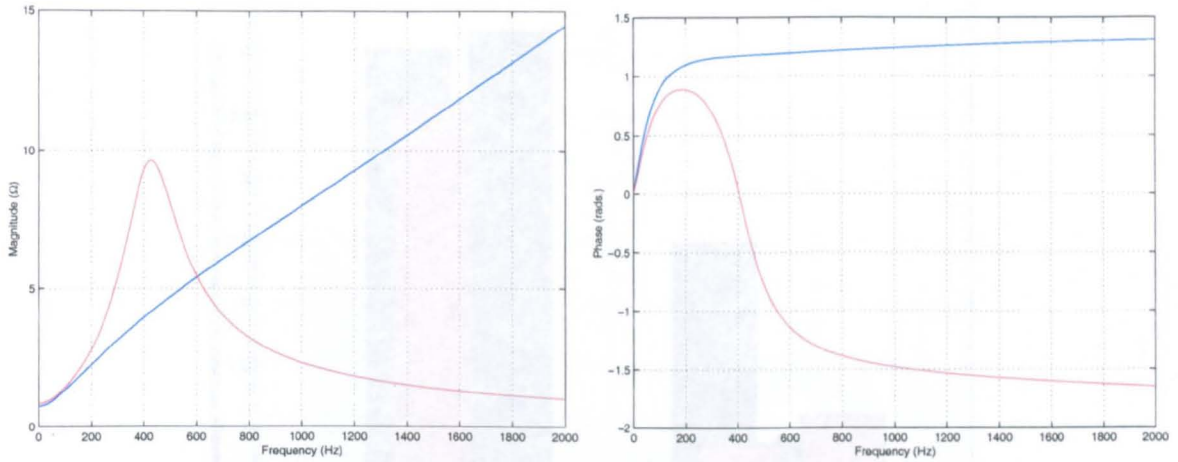

(a) Impedance magnitude (b) Impedance phase

Figure 7.19: Supply impedance for c1 and c3, blue: c1, red: c3

Harmonic order	Admittance (S)			
	c1		c3	
	Y_{dd}	Y_{dq}	Y_{dd}	Y_{dq}
7	0.16	0.39	0.18	0.09
11	0.12	0.28	0.12	-0.19

Table 7.4: Admittance terms for calculation of current references

the distortion before compensation control and the red trace shows the distortion in steady state compensation operation. This clearly shows that the ASF was capable of cancelling the distortion at both the 7th and 11th harmonics. The performance at the 11th harmonic was good even though it was not using an optimized controller. The performance of this controller may also be limited due to the switching frequency of the inverter, 4kHz.

The final figure, figure 7.21, shows the controller voltages V_{d11lpf}(blue) and V_{q11lpf}(red). Before 0.8s the control was operating using the correct admittance parameters. At 0.8s the parameters were changed to those for the c1 supply circuit.

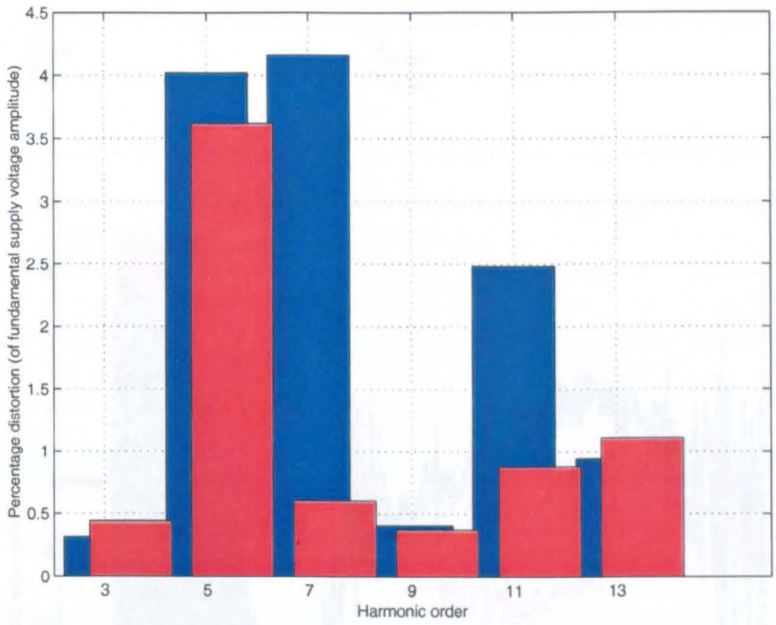

Figure 7.20: Line voltage harmonics before(blue) and after(red) control action

Before the parameter swap the ASF operation is stable but at 0.8s, time of parameter swap, the controller began to go unstable. In fact the ASF tripped at the end of the time period shown as the total line current exceeded 50A, the software OVERCURRENT trip level. Therefore it is clear that the controllers must be given impedance information that is correct for the supply. The phase difference between the impedance of the two different supplies at the 11th harmonic frequency was approximately 130 degrees. A comprehensive stability analysis has not been completed for this system although it is clear that the current reference demand will be far from that which is necessary to cancel the voltage distortion.

The accuracy of the magnitude estimate of the impedance is not critical for this application. It will affect the transient response of the ASF and in cases of extreme inaccuracy may cause instability or alternatively give rise to an exceptionally slow transient response. The phase of the impedance estimate is of greater importance, in particular it it essential to know of any resonant frequencies in the impedance transfer function. If these are not known then it is possible that the current reference input may be completely out of phase with the actual reference required for cancellation of voltage distortion.

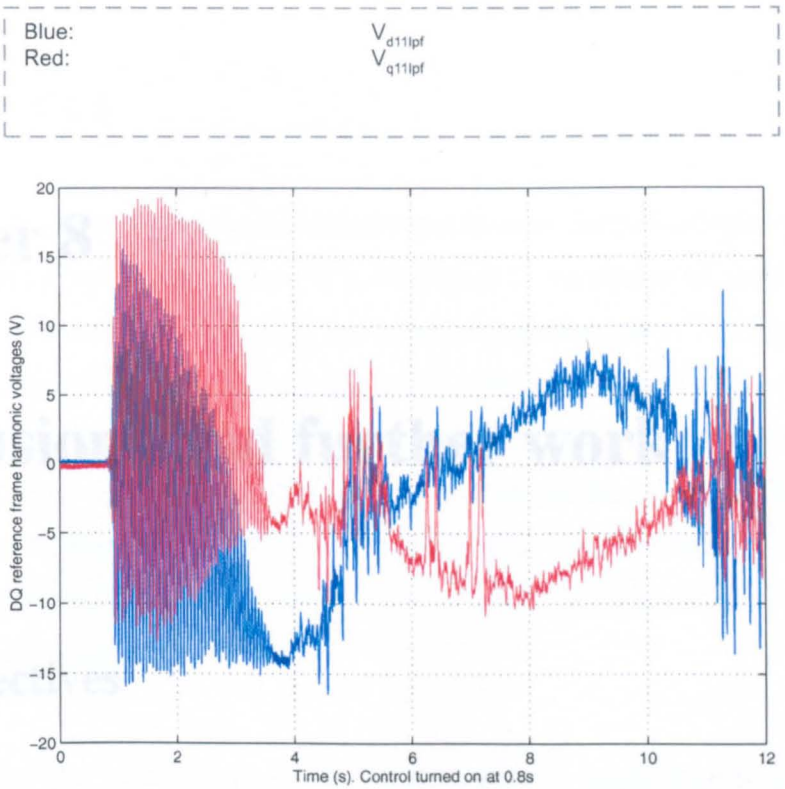

Figure 7.21: Control action of 11th harmonic dq frame controllers.

7.9 Summary

This chapter has demonstrated the use of the impedance measurement results to predict current drawn by harmonic producing NLLs. Impedance measurement was used to calculate reference currents for an ASF harmonic controller. This led to a fully functioning ASF based upon voltage feedback in order to compensate for the harmonic voltage distortion present at the PCC. Furthermore it was possible to demonstrate that an incorrect impedance estimate may lead to unstable ASF control.

Chapter 8

Conclusions and further work

8.1 Objectives

This thesis has described work undertaken to investigate potential methods for the on-line measurement of system impedance. The objectives of the project were set out in Chapter 1:

- To develop impedance measurement techniques specifically designed to be embedded in an existing piece of power electronic equipment such as an active filter.
- To determine whether it is possible to make power system impedance measurements in a real power network in the presence of many locally connected pieces of power electronic equipment.
- To experimentally demonstrate power quality improvement using knowledge of the system impedance.

These objectives have been addressed within the thesis. In this chapter the main conclusions shall be summarised.

8.2 Conclusions

8.2.1 Objective 1

Knowledge of the power system impedance is invaluable for power system modelling including harmonic propagation studies. It is important in the design of passive filters, especially at points of connection with high levels of voltage distortion. Traditionally, the fault level would be used to estimate the impedance at a point of connection. This estimate would be made at the fundamental frequency. Assumptions are then required as to the nature of the connection if this value is to be used in order to estimate the impedance at harmonic frequencies. Alternatively an on-line measurement may be used in order to provide accurate impedance information over a wide range of frequencies. On-line measurement techniques were split into two categories:

- Operating point impedance. In this case the system impedance is measured at harmonic frequencies. These impedance values are dependent upon the operating point of the system and may not be used to infer the impedance at other frequencies or under different operating conditions.
- Absolute interharmonic impedance. In this case interharmonic impedance values are estimated. These are absolute values that may be used to infer other interharmonic impedance values. Strictly speaking, these interharmonic values should not be used to infer harmonic impedance values if non-linear loads are present.

The second option was chosen as the most appropriate for this application. An absolute measurement technique was therefore developed for interharmonic values.

In chapter 4 two possible methods were proposed for the on-line system impedance measurement. Both the short term injection method and the medium term injection method were designed to be embedded into the normal operation of an active shunt filter. Simulation results confirmed that, in theory, both methods were capable of accurate measurement

of a linear system impedance model in the frequency range between 0 and 1kHz. Total measurement time for both methods was 16 fundamental supply cycles, 0.32s. A balanced three phase system was assumed throughout this development although a generalized approach for an unbalanced system was described.

The short term injection used a very short duration current impulse disturbance. This type of injection had been employed by previous researchers at the transmission level using existing uncontrolled sources of disturbance. In this case the active filter was used in order to provide the disturbance. The system provided control over the amplitude and injection time of the injected transient, thereby allowing much greater control of the measurement process. Such an approach was not previously described in the research literature.

The medium term injection again employed a wideband disturbance signal although this was injected by the active filter over 8 fundamental supply cycles. This means of disturbance had not previously been discussed in the literature. This method has advantages over the short term injection in that the disturbance is less severe in amplitude and the recorded transient disturbance was of greater duration allowing more accurate signal processing. It also possesses advantages when compared to injection methods that inject current disturbances at single frequencies. The measurement period is far shorter which is beneficial for an embedded measurement. It also allows greater accuracy as the network is less likely to change state during a measurement.

In chapter 5 both proposed methods were tested experimentally. The measurement techniques were experimentally verified in a laboratory under realistic conditions. The mains supply was used which exhibited frequency variation and a significant number of power electronic loads were also operated in the vicinity. Both injection techniques provided excellent identification of the 8 different supply test circuits constructed. From the results it was clear that the accuracy of identification at each frequency is directly dependent upon the strength of the disturbance at that frequency. There is thus clearly a trade off between the accuracy of identification and possible disruption of the normal network operation if a large disturbance is applied. The medium term injection method provided more accurate low frequency identification as the injection strength was heavily biased towards the low

frequency region.

The most challenging supply circuit that was identified was the experimental supply transformer alone (supply c1). When a transient disturbance was applied to this circuit there was no oscillatory transient response. Therefore the transient signals recorded for the short term injection technique were particularly short. Reasonably accurate identification was still possible in this case although greater errors were present in the real part of the identification compared to the other supply circuits. Both injection techniques were able to identify resonant points in the supply impedance with a high degree of accuracy.

The impedance results showed that large errors were present in the estimated impedance at harmonic frequencies. These errors were primarily due to poor cancellation of the steady state voltage at the point of measurement. Even in measurement cases where steady state cancellation appeared to be almost exact errors were still present in the impedance estimates at harmonic frequencies. Very little inaccuracy in this cancellation gave rise to large errors in the harmonic frequency impedance. This suggests that it would always be necessary to apply some form of interpolation or curve fitting about the harmonic frequencies. The curve fitting algorithm was applied using only interharmonic impedance estimates as input data. Consequently the steady state cancellation errors were eliminated. The disadvantage of this approach was that discontinuities in the impedance at harmonic frequencies could not be identified.

Both methods were designed to provide fast measurements of system impedance suitable for use by an active filter. Further work is under progress in order to utilize the Prony method for the short term injection technique so that data acquisition time may be reduced. If this is possible then the method may be more suited to implementation within an active filter.

The first objective of this project has been accomplished with the development of the short term and medium term injection techniques.

8.2.2 Objective 2

In chapter 5 measurements were successfully made in the laboratory. Many power electronic non-linear loads were operational during the experimental work, of both the current source and voltage source categories of load. These loads were all separated from the point of measurement by the experimental supply transformer. As this transformer was the major source of impedance measured these remotely connected loads did not significantly affect the measurement results. In chapter 6 the performance of both techniques was investigated in the presence of locally connected non-linear loads. The term locally connected load was used to refer to a load that was connected to the point of measurement with a connection impedance much smaller than the system impedance. Experimentally, the non-linear loads employed were connected at the point of measurement.

Successful identification was possible with locally connected non-linear loads in certain cases. The success of the measurement was dependent upon the nature of the local non-linear load. Successful operation of the medium term injection was demonstrated in the presence of the current source category of load (CS-NLL). Results were seriously degraded in the presence of the voltage source category of non-linear load (VS-NLL). In the latter case the non-linear load acts as a voltage source that is influenced by the transient disturbance. This correlation between the output of the harmonic producing load and the transient disturbance means that the act of measurement affects the state of the network. It was therefore not possible to achieve satisfactory identification in this case. The same identification constraints were necessary for the short term injection method. That is, it was possible to measure system impedance in the presence of the CS-NLL but not with a VS-NLL connected. Due to power system frequency variation and noise the Prony method based extension to the short term injection measurement was implemented with limited success. Therefore a solution to impedance identification with a VS-NLL connected at the point of measurement is still required.

Further measurements were made using the VS-NLL load with additional input inductance. This inductance may represent input filters, a supply transformer or a significant length of cabling to the converter load. In this case the identification was much improved. The tran-

sient disturbance did not significantly alter the state of the VS-NLL and therefore improved measurement results were possible.

This section of work has shown that it is possible to measure the system impedance in the presence of non-linear loads. The main constraint is that loads that may be described as voltage source non-linear loads should not be connected at the same point of connection as the measurement apparatus. In fact an impedance significantly greater than the supply impedance should be present between the two points for accurate identification of the supply impedance. The capacitively smoothed diode bridge rectifier is the most common example of this type of load. If the measurement techniques were to be embedded into a piece of dedicated measurement equipment then this restriction must be considered when making an impedance measurement. This constraint also applies to the previous methods reviewed. Alternatively, the measurement technique would be embedded into an active filter control algorithm. In this case stability issues described in section 7.6.1 demand that an active shunt filter should not be connected at the point of connection of a VS-NLL without significant line inductance at the input to the VS-NLL. Therefore, in any real implementation of an active shunt filter, the measurement techniques will operate successfully.

This concludes the second objective of this work. It has been shown that on-line impedance measurements were possible in a real environment with power electronic loads operating and in the presence of power system noise and frequency variation. The operating limits of the techniques were defined in terms of the non-linear loads connected in the network.

8.2.3 Objective 3

Power quality improvement with the aid of impedance measurement was demonstrated in chapter 7. An active shunt filter was developed using voltage feedback. Previous active filtering techniques were reviewed that used supply impedance values. In these cases the impedance was assumed to be known. In this work the measured supply impedance was used in order to calculate reference currents for the harmonic controllers. A generalized approach was developed that so that an impedance transfer function, taken directly from

the measurement algorithm, could be used in the harmonic reference current generation. This approach was novel as it did not assume any knowledge of the supply.

The active filter reference generation used measurements of the voltage at the point of connection and the supply impedance transfer function. These were used in order to calculate references to cancel the voltage distortion at the point of connection of the active filter. This type of active filter would be particularly suited to operation in a number of scenarios. This active filter could be used in order to reduce the voltage distortion at a point where sensitive equipment is connected. In such a situation this may lead to a reduction in nuisance tripping. Alternatively this active filter could be implemented by a utility in order to provide harmonic compensation on its distribution network. Voltage distortion compensation would provide a general filtering to compensate for all harmonic current drawn from the point of connection. If connected in this manner all customer connected VS-NLLs will be connected via distribution transformers. Therefore these loads will appear as CS-NLLs and will not affect the measurement techniques. Finally, this control scheme would also be suitable for direct compensation of a large non-linear load in an isolated network. Offshore oil platforms have been suggested as an example of this type of network [20]. In this case if a high power non-linear load is operated from a sinusoidal supply then the voltage feedback active filter will directly compensate for the load current drawn without the need for load current transducers to be installed.

Operation of the active filter was verified experimentally. The voltage distortion at the point of connection was reduced dramatically by the use of the active filter. The distortion was almost completely eliminated both before and after the connection of a load at the point of connection. Compensation was conducted for both the 5th and 7th harmonic frequencies. It was also possible to compensate at the 11th harmonic frequency although the limited processing power meant that only two compensation frames could be implemented. Successful operation was demonstrated in the presence of a supply impedance resonance. A 5th harmonic controller and an 11th harmonic controller were implemented in this case. The resonant point of the impedance lay between the operating frequencies of the two controllers. The final demonstration was used to show the operation of the active filter when the resonance was not anticipated. The active filter operation quickly became

unstable clearly indicating the need for supply impedance knowledge for this power quality enhancing apparatus.

8.3 Suggestions for further work

The suggestions for further work are split into two categories. The first category are those suggestions for refinement to the present system and the second category are suggestions as to the future direction of this work.

Possible improvements to the present experimental work are:

- A more extensive investigation of the medium term injection method should be undertaken. It would be desirable to test the technique on a variety of real network connections to further confirm the validity of this method. In order to achieve this some parts of the experimental rig will have to be redesigned. It will be necessary to remove the experimental supply transformer so that measurements of the actual power network may be taken. One of the primary reasons for using the step down supply transformer was that the d.c. link voltage rating in the experimental inverter was 800V. If the rig transformer is removed then it may also be necessary to increase the voltage rating of the d.c. link. Furthermore the voltage ratings of the IGBT switches, 1200V at present, should also be assessed. Once these measures are complete it will be possible to take power system measurements directly on the laboratory supply.

- On completion of the first suggested improvement it would then be feasible to embed the injection technique into a purpose built impedance measurement instrument. This could be used at various points of connection in order to map the impedances in an industrial network. Such information would be useful for harmonic propagation studies. With such information it may be possible to redistribute sensitive loads in a systematic manner to improve the power quality of the network.

- The measurement technique could be embedded into the normal operation of the active filter. The measurement technique has already been implemented during active filter operation and successful active filter operation was demonstrated using the measured supply impedance. In order to automate the process some form of management strategy must be devised. Its' purpose would be to manage the periodic measurement of the supply impedance and update the reference currents accordingly. Supply impedance measurement could be determined at set intervals or alternative means could be devised to decide when to update the impedance estimate. If the measurement is to be truly integrated into the filter control then it may also be possible to reduce the amount of data acquisition required. A phase locked loop (PLL) could be implemented to track the supply frequency. This would firstly benefit the active filter control. Secondly it could also be used to reduce spectral leakage in the impedance measurement operation. If the improvement in steady state cancellation was sufficient the impedance measurement sampling frequency could be reduced. It should then be possible to use the existing active filter measurements for the impedance estimation. As a result the dedicated impedance measurement hardware would no longer be required.

- Knowledge of the system impedance may also prove equally useful, if not more so, in alternative active filter control strategies. It is therefore suggested that other control strategies are reviewed to ascertain whether knowledge of the supply impedance may improve other strategies.

- Knowledge of the system impedance should also be of benefit to power system protection and control strategies. A review of these benefits should be carried out.

Further work is to be undertaken on the Prony extrapolation work described in chapter 6. Simulation showed that the short term injection technique could potentially be used to measure the supply impedance even when heavily influenced by the interaction of locally connected non-linear loads. Further investigation of the numerical techniques employed is required to improve noise immunity and to compensate for the practical reality of imperfect steady state cancellation. It is hoped that this work will lead to a short term measurement

technique with a much smaller measurement time and good performance in the presence of harmonic producing loads.

Impedance measurement techniques may also be suited for applications other than described in this work. Areas where an on-line measurement of impedance may prove beneficial are protections systems and embedded generation control. The problem of islanding in embedded generation control is one area where such a measurement may prove useful. Small scale embedded generation units must either be isolated or turned off in the event of a distribution failure so that protection mechanisms have a chance to clear the fault and so that a loss of synchronism does not occur. Measurement of the impedance may provide useful information as to the state of the distribution system. Exporting power to the distribution system is often uneconomic due to the scale of the generation and the price paid for exported units. Therefore such systems are often controlled to so that there is no power flow between the customer and the distribution system. In this case islanding and distribution system faults are particulary difficult to identify.

References

[1] I. P. Burdon, "Gas and the current generation mix in england and wales," IEE *Power engineering journal*, vol. 14, pp. 61–67, April 2000.

[2] B. M. Weedy, *Electric Power Systems*, vol. 1. John Wiley and Sons Ltd., 3 ed., 1987.

[3] S. Williamson, "The induction motor - a state of the ark technology," *Power engineering journal*, vol. 10, pp. 190–200, August 1996.

[4] T. A. Short, "Harmonics and IEEE519. www.pti-us.com/pti/consult/dist/papers/harmonics/harmonics.htm," 1992.

[5] R. C. Dugan, M. F. McGranaghan, and H. W. Beaty, *Electrical Power Systems Quality*. McGraw Hill, 1 ed., 1996.

[6] A. E. Emanuel, "Harmonics in the early years of electrical engineering: a brief review of events, people and documents," in *Ninth international conference on harmonics and quality of power (ICHQP)*, vol. 1, (Florida, USA), pp. 1–7, IEEE, 2000.

[7] R. Yacamini, "Overview of harmonic distortion," in *Colloquium on sources and effects of harmonic distortion in power systems*, vol. 1, (London), IEE, 1997.

[8] N. Mohan, T. M. Undeland, and W. P. Robbins, *Power electronics: converters, applications and design*, vol. 1. John Wiley & sons, 2nd ed., 1989.

[9] R. Dugan, "Distributed generation," IEEE *Industry applications magazine*, vol. 8, pp. 19–25, April 2002.

[10] M. E. Fraser, C. D. Manning, and B. M. Wells, "Transformerless four-wire pwm rectifier and its application in ac-dc-ac converters," *IEE Proceedings on electrical power applications*, vol. 142, no. 6, pp. 397–400, 1995.

[11] F. Z. Peng, G. W. Ott, and D. J. Adams, "Harmonic and reactive power compensation based on the generalized instantaneous reactive power theory for three phase four wire systems," IEEE *Transactions on power electronics*, vol. 13, no. 6, pp. 1174–1181, 1998.

[12] E. I. Carroll, "Power electronics for very high power applications," *Power engineering journal*, vol. 13, pp. 81–87, April 1999.

[13] H. Fujita, "The unified power quality conditioner: the integration of series and shunt active filters," IEEE *Transactions on power electronics*, vol. 13, no. 2, pp. 315–322, 1998.

[14] R. M. Davis, *Power diode and thyristor circuits*, vol. 1. IEE, 1986.

[15] J. W. Kolar, H. Ertl, and F. C. Zach, "A comprehensive design approach for a three phase high-frequency single switch discontinuous mode boost power factor corrector based on analytically derived normalized converter component ratings," IEEE *Transactions on Industry Applications*, vol. 31, no. 3, 1995.

[16] A. W. Green, J. T. Boys, and G. F. Gates, "3 phase voltage sourced reversible rectifier," *IEE proceedings on electric power applications*, vol. 135 B, no. 6, pp. 362–370, 1988.

[17] H. Akagi, Y. Kanazawa, and A. Nabae, "Instantaneous reactive power compensators comprising switching devices without energy storage elements," IEEE *Transactions on industry applications*, vol. 20, no. 3, pp. 625–630, 1984.

[18] S. Bhattacharya, T. M. Frank, D. M. Divan, and B. Banerjee, "Active filter system implementation," IEEE *Industry applications magazine*, vol. 4, pp. 47–63, September 1998.

[19] D. Butt, *An investigation of harmonic correction techniques using active filtering*. PhD thesis, University of Nottingham, 1999.

[20] P. B. Brogan, *An active filter based on voltage feedback.* PhD thesis, University College Cork, 1999.

[21] F. Kamran and T. G. Habetler, "Combined deadbeat control of a series-parralel converter combination used as a universal power filter," IEEE *Transactioons on power electronics*, vol. 13, no. 1, 1998.

[22] L. Malesani, P. Mattavelli, and P. Tomasin, "High performance hysteresis modulation technique for active filters," IEEE *Transactions on Power electronics*, vol. 12, no. 5, pp. 752–759, 1998.

[23] Y. T. Ying, "Fuzzy tuning current vector control of a three phase pwm inverter for high performance a.c. drives," IEEE *transactions on industrial electronics*, vol. 45, no. 5, pp. 782–791, 1998.

[24] V. Cardenas, N. Vazquez, and C. Hernandez, "Sliding mode control applied to a 3 phase shunt active power filter using compensation with instantaneous reactive power theory," in *Power electronics specialists conference (PESC)*, pp. 236–241, 1998.

[25] "IEEE recommended practices and requirements for harmonic control in electrical power systems," IEEE STD. 519-1992, IEEE Standards board, January 1993.

[26] "Planning levels for harmonic voltage distortion and the connection of non-linear equipment to transmission systems and distribution networks in the united kingdom," G5/4, Electricity Association, February 2001.

[27] "Limitation of emission of harmonic currents in low voltage power supply systems for equipment with rated current greater than 16a," BS IEC 61000-3-4:1998, British Standards, 1998.

[28] G. T. Heydt, D. J. Kish, F. Holcomb, and Y. Hill, "A methodology for assessment of harmonic impact and compliance with standards for distribution systems," *IEEE Transactions on Power Delivery*, vol. 6, no. 4, pp. 1748–1754, 1991.

[29] W. M. Grady, M. J. Samotyj, and A. H. Noyola, "Minimizing network harmonic voltage distortion with an active power line conditioner," *IEEE Transactions on Power Delivery*, vol. 6, no. 4, pp. 1690–1697, 1992.

[30] A. A. Girgis, W. H. Quaintance, J. Qiu, and E. B. Makram, "A time domain three phase power system impedance modeling approach for harmonic filter analysis," *IEEE Transactions on Power Delivery*, vol. 8, no. 2, pp. 504–510, 1993.

[31] L. S. Czarnecki, "Effect of minor harmonics on the performance of resonant harmonic filters in distribution systems," *IEE Proceedings: Electric Power Applications*, vol. 144, no. 5, pp. 349–356, 1997.

[32] K. Smith, P. Brogan, and I. Wilson, "Measurements and simulation of d.c. drive harmonics on an interconnected offshore system with long cables," in *EPE97*, vol. 4, pp. 946–951, 1997.

[33] P. M. Hart, "An experimental study of short-circuit currents on a low-voltage system.," *IEEE Transactions on Industry Applications*, vol. 24, no. 5, pp. 940–946, 1988.

[34] Y. Du and J. Burnett, "Experimental investigation into harmonic impedance of low-voltage cables," *IEE Proceedings: Generation, Transmission and Distribution*, vol. 147, no. 6, pp. 322–328, 2000.

[35] J. Arrillaga, *Power system harmonics*. John Wiley & Sons, 1985.

[36] W. P. Baker, "The measurement of the system impedance at harmonic frequencies," in *International conference on harmonics in power systems*, vol. 1, (Manchester, England), pp. 141–158, 1981.

[37] A. E. Emanuel, J. Janczak, D. J. Pileggi, E. M. Gulachenski, C. E. Root, M. Breen, and T. J. Gentile, "Voltage distortion in distribution feeders with nonlinear loads," *IEEE Transactions on Power delivery*, vol. 9, no. 1, pp. 79–87, 1994.

[38] A. R. Wood and J. Arrillaga, "The frequency dependent impedance of an hvdc converter," *IEEE transactions on power delivery*, vol. 10, no. 3, pp. 1635–1641, 1995.

[39] F. Z. Peng, "Application issues of active power filters," *IEEE industry applications magazine*, vol. 4, pp. 21–30, September/October 1998.

[40] F. Z. Peng, "Harmonic sources and filtering approaches," *IEEE industry applications magazine*, vol. 7, pp. 18–25, July/August 2001.

[41] M. Sakui, H. Fujita, and M. Shioya, "A method for calculating harmonic currents of a three phase bridge uncontrolled rectifier with dc filter," *IEEE Transactions on Industrial Electronics*, vol. 36, no. 3, pp. 434–440, 1989.

[42] M. Lemoine, "Methods of measuring harmonic impedances," in *International conference on electricity distributuion*, vol. 1, (London, UK), pp. 5–7, IEE, 1977.

[43] A. Oliveira, J. C. Oliveira, J. W. Resende, and M. S. Miskulin, "Practical approaches for ac system harmonic impedance measurements," *IEEE Transactions on Power Delivery*, vol. 6, no. 4, pp. 1721–1726, 1991.

[44] D. Crevier and A. Mercier, "Estimation of higher frequency network equivalent impedances by harmonic analysis of natural waveforms," *IEEE Transactions on Power Apparatus and Systems*, vol. PAS-97, no. 2, pp. 424–431, 1978.

[45] L. S. Czarnecki and Z. Staroszczyk, "On line measurement of equivalent parameters of distribution system and its load for harmonic frequencies," in *IEEE instrumentation and measurement technology conference (IMTC95)*, (Naltham, MA, USA), pp. 692–698, 1995.

[46] L. S. Czarnecki and Z. Staroszczyk, "On line measurement of equivalent parameters for harmonic frequencies of a power distribution system and load," *IEEE Transactions on Instrumentation and Measurement*, vol. 45, no. 2, pp. 467–472, 1996.

[47] Z. Staroszczyk, "Accuracy problems in on line one phase distibution/load system identification task," in *IEEE international symposium on industrial electronics (ISIE96)*, vol. 1, (Warsaw, Poland), pp. 354–357, 1996.

[48] E. Ahmed, W. Xu, and X. Liu, "Application of modal transformations for power system harmonic impedance measurement," *Electrical Power and Energy Systems*, vol. 23, pp. 147–154, 2001. pdf, related to 3 phase transient paper.

[49] E. Duggan and R. E. Morrison, "A non-invasive technique for the measurement of power system harmonic impedance," in *CIRED. 11th International Conference on Electricity Distribution 1991*, vol. 2, (Liege, Belgium), pp. 2.1–2.5, 1991.

[50] Y. Xiao, J.-C. Maun, H. Mahmoud, T. Detroz, and S. Do, "Harmonic impedance measurement using voltage and current increments from disturbing loads.," in *Ninth International Conference on Harmonics and Quality of Power* (A. Domijan, ed.), vol. 1, (Orlando, FL, USA), pp. 220–225, IEEE, 2000.

[51] A. S. Morched and P. Kundur, "Identification and modelling of load characteristics at high frequencies," *IEEE Transactions on Power Systems*, vol. PWRS-2, no. 1, pp. 153–160, 1987.

[52] A. A. Girgis and R. B. McManis, "Frequency domain techniques for modelling distribution or transmission networks using capacitor switching induced transients," *IEEE Transactions on Power Delivery*, vol. 4, no. 3, pp. 1882–1890, 1989.

[53] E. W. Palmer and G. F. Ledwich, "Three phase harmonic modelling of power system loads," *IEE Proceedings, Part C: Generation, Transmission and Distribution*, vol. 140, no. 3, pp. 206–212, 1993.

[54] M. Nagpal, W. Xu, and J. Sawada, "Harmonic impedance measurement using three phase transients," *IEEE Transactions on Power Delivery*, vol. 13, no. 1, pp. 272–277, 1998.

[55] M. J. Bridgemann, N. MacLeod, S. B. Tennakoon, and R. E. Morrison, "The resonance damping effect associated with linear shunt loads and single-phase converters.," in *Ninth International Conference on Harmonics and Quality of Power* (A. Domijan, ed.), vol. 2, (Orlando, FL, USA.), pp. 535–540, IEEE, 2000.

[56] W. C. Beattie and S. R. Matthews, "Measurement of harmonic impedance from analysis of transients generated by capacitors," in *3rd International Conference on Advances in Power System Control, Operation and Management*, vol. 1, (Hong Kong), pp. 97–102, IEE, 1995.

[57] C. Xie, S. Tennakoon, R. Langella, D. Gallo, A. Testa, and A. Wixon, "Harmonic impedance measurement of 25 kv single phase ac supply systems.," in *Ninth International Conference on Harmonics and Quality of Power.* (A. Domijan, ed.), vol. 1, (Orlando, FL, USA.), pp. 214–219, IEEE, 2000.

[58] J. F. Hauer, "Application of prony analysis to the determination of modal content and equivalent models for measured power system response," *IEEE Transactions on Power Systems*, vol. 6, no. 3, pp. 1062–1068, 1991.

[59] G. M. Jenkins and D. G. Watts, *Spectral analysis and its applications.* Time series analysis, San Francisco: Holden-Day, first ed., 1969.

[60] Z. Staroszczyk, "Time dependant power systems impedance - interpretation and measuring problems," in *IEEE instrumentation and measurement technology conference (IMTC99): Measurements for the new millenium*, vol. 2, (Venice, Italy), pp. 795–800, 1999.

[61] H. Barnes, L. C. Campbell, S. J. Kearley, and R. D. Kendon, "Predicted and measured values of harmonic impedance at uk substations," in *CIRED 1985: 8th international conference on electricity distribution*, (Brighton, England), pp. 87–91, IEE, 1985.

[62] B. Harris, A. W. Kelley, J. P. Rhode, and M. E. Baran, "Instrumentation for measurement of line impedance," in *IEEE Applied Power Electronics Conference and Exposition - APEC*, vol. 2, pp. 887–893, IEEE, 1994. same as Rhode paper.

[63] J. P. Rhode, A. W. Kelley, and M. E. Baran, "Line impedance measurement: A nondisruptive wideband technique," in *IAS Annual Meeting*, vol. 3, (Orlando, Florida, USA), pp. 2233–2240, IEEE, 1995.

[64] J. P. Rhode, A. W. Kelley, and M. E. Baran, "Complete characterization of utilization-voltage power system impedance using wideband measurement," *IEEE Transactions on industry applications*, vol. 33, no. 6, pp. 1472–1479, 1997.

[65] M. Tsukamoto, S. Ogawa, Y. Natsuda, Y. Minowa, and S. Nishimura, "Advanced technology to identify harmonics characteristics and results of measuring.," in *Ninth*

International Conference on Harmonics and Quality of Power (A. Domijan, ed.), vol. 1, (Orlando, FL, USA), pp. 341–346, IEEE, 2000.

[66] L. E. Banta, G. J. Cokkinides, and A. P. Meliopoulos, "Distribution system impedance measurement techniques," in *International conference on harmonics in power systems*, (Worcester polytechnic institute), pp. 220–224, 1984.

[67] Z. Staroszczyk, "Problems in real time wide band identification of power systems," in *IEEE Instumentation and Measurement Technology Conference*, (St. Paul, Minnesota, USA), 1998.

[68] "ID9001-II series instruction manual," tech. rep., Heenan Drives Limited.

[69] K. Griffiths, "A vector controlled 50kw motor drive," tech. rep., School of Electrical and Electronic Engineering, 1996.

[70] TMS320C4X *Users guide*. Texas Instruments, 1992.

[71] "QPC/C40 user documentation," tech. rep., Blue Wave Systems.

[72] M. Sumner, *Vector controlled induction motor drive using transputer parallel processors*. PhD thesis, University of Nottingham, 1990.

[73] N. Teske, *Sensorless position control of induction machines using high frequency signal injection*. PhD thesis, University of Nottingham, 2001.

[74] M. Bienert, "Development of hardware for high dynamic control of induction machines using a dsp," tech. rep., School of Electrical and Electronic Engineering, September 1998 1998.

[75] J. Paul, D. W. P. Thomas, and M. Sumner, "Time-domain simulation of line admittance measurement using current injection," internal report, University of Nottingham, Department of Electrical and Electronic Engineering, 1999.

[76] S. M. Kay, "Spectrum analysis - a modern perspective," *Proceedings of the IEEE*, vol. 69, no. 11, pp. 1380–1419, 1981.

[77] M. L. Van Blaricum and R. Mittra, "Problems and solutions associated with prony's method for processing transient data," *IEEE Transactions on Antennas and Propagation*, vol. AP-26, no. 1, pp. 174–182, 1978.

[78] S. L. Marple, *Digital Spectral Analysis with Applications*. Prentice Hall, 1987.

[79] A. V. Oppenheim, R. W. Schafer, and J. R. Buck, *Discrete-time signal processing*. Prentice-Hall Inc., 2 ed., 1999.

[80] "Report to the director of the office of gas and electricity markets 2000 - 2001," tech. rep., National Grid, May 2001.

[81] E. C. Levi, "Complex curve fitting," *IRE Transactions on automatic control*, vol. 4, pp. 37–44, 1959.

[82] J. E. Dennis and R. B. Schnabel, *Numerical methods for unconstrained optimization and non-linear equations*. Prentice Hall, 1983.

[83] E. Kreyszig, *Advanced engineering mathematics*. John Wiley & Sons, 6th ed., 1988.

[84] J. J. Grainger and W. D. Stevenson, *Power System Analysis*. McGraw-Hill, 1994.

[85] R. E. Walpole, *Introduction to Statistics*, vol. 1. New York: Collier Macmillan, 3rd ed., 1982.

[86] G. Smyth, "Prony estimation (www.maths.uq.edu.au/ gks/research/prony.html)," 2000.

[87] F. Hildebrand, *Introduction to Numerical Analysis*, vol. 1. New York: Dover Publications, 2 ed., 1987.

[88] D. A. Van Den Eijkel and D. A. Marshall, "The simulation and measurement of system harmonic impedance," in *CIGRE. Proceedings of the 33rd Session. International Conference on Large High Voltage Electric Systems*, vol. 2, (Paris, France), pp. 1–4, 1990.

[89] S. Braun and Y. M. Ram, "Determination of stuctural modes via the prony model: System order and noise induced poles," *Journal of the acoustical society of America*, vol. 81, no. 5, pp. 1447–1459, 1987.

[90] W. M. Steedly, C. J. Ying, and R. L. Moses, "A modified tls-prony method using data decimation," *IEEE Transactions on Signal Processing*, vol. 42, no. 9, pp. 2292–2303, 1994.

[91] E. M. Dowling, R. D. DeGroat, and D. A. Linebarger, "Transient analysis with the linearly constrained tls prony method," in *IEEE International Symposium on Electromagnetic Compatibility*, (Dallas, Texas, USA), pp. 265–269, IEEE, 1993.

[92] E. M. Dowling, R. D. DeGroat, and D. A. Linebarger, "Exponential parameter estimation in the presence of known components and noise," *IEEE Transactions on Antennas and Propagation*, vol. 42, no. 5, pp. 590–599, 1994.

[93] N. H. Younan and C. D. Taylor, "On using the SVD-prony method to extract poles of an em system from its transient response," *Electromagnetics*, vol. 11, no. 2, pp. 223–233, 1991.

[94] T. H. Friddell, J. A. Ritcey, and D. Haynor, "Data pre-conditioning for improved performance of the prony method," in *23rd Asilomar conference on signals, systems and computers*, vol. 1, (Pacific Grove, California, USA), pp. 360–364, Maple Press, 1989.

[95] H. Akagi, "New trends in active filters," in *EPE 95*, (Seville), pp. 17–26, 1995.

[96] F. Pottker and I. Barbi, "Power factor correction of non-linear loads employing a single phase active power filter: control strategy, design methodology and experimentation," in *Power electronics specialists conference (PESC)*, vol. 1, pp. 104–109, 1997.

[97] P. Delarue and R. Bausiere, "New control method for active power filter needing line current measurement only," in *EPE95*, vol. 1, (Seville, Spain), pp. 914–919, 1995.

[98] J. H. Marks and T. C. Green, "Predictive control of active power filters," in *Power electronics and variable speed drives*, vol. 1, (London, UK), pp. 18–23, IEE, 2000.

[99] H. Akagi, H. Fujita, and K. Wada, "A shunt active filter based on voltage detection for harmonic termination of a radial power distribution line," *IEEE Transactions on Industry Applications*, vol. 35, no. 3, pp. 638–645, 1999.

[100] C. Lott, O. Lapierre, and H. Pouliquen, "High-power voltage source pwm active filter with low switching effect," in *EPE95*, vol. 1, (Seville, Spain), pp. 908–913, 1995.

[101] H. Pouliquen, P. Lemerle, and E. Plantive, "Voltage harmonics source compensation using a shunt active filter," in *EPE'95*, vol. 1, (Seville, Spain), pp. 117–122, 1995.

[102] H. Akagi, "Control stategy and site selection of a shunt active filter for damping of harmonic propagation in power distribution systems," *IEEE Transactions on Power Delivery*, vol. 12, no. 1, pp. 354–363, 1997.

[103] Y. Sato, T. Kawase, M. Akiyama, and T. Kataoka, "A control strategy for general purpose active filters based on voltage detection," in *IEEE Industrial Applications Society Annual Meeting*, vol. 1, (Phoenix, Arizona, USA), pp. 471–478, 1999.

[104] A. Kumamoto, T. Hikihara, Y. Hirane, K. Oku, O. Nakamura, S. Tada, K. Mizuki, and Y. Ogihara, "Suppression of harmonic voltage distortion by neural network controlled active filter," in *IEEE Industrial Applications Society Annual Meeting*, vol. 1, pp. 754–761, 1992.

[105] F. Le Magoarou and F. Monteil, "Influence of the load characteristics and the line impedance on the stability of an active power filter," in *Fifth international conference on power electronics and variable-speed drives*, vol. 1, (London, UK), pp. 175–180, IEE, 1994.

[106] R. S. Pena-Guinez, *Vector control stategies for a doubly-fed induction generator driven by a wind turbine*. PhD thesis, University of nottingham, 1996.

[107] M. Bojrup, P. Karlsson, M. Alakula, and L. Gertmar, "A multiple rotating integrator controller for active filters," in *EPE99*, vol. CD-ROM, (Lausanne, Switzerland), 1999.

[108] P. Brogan and R. Yacamini, "An active filter based on voltage feedback," in *Power electronics and variable speed drives (PEVD98)*, vol. 1, (London, UK), pp. 1–4, IEE, 1998.

[109] G. F. Franklin, J. D. Powell, and M. L. Wohrman, *Digital control of dynamic systems*. Addison-Wesley, 1990.

Appendix A

Impedance relationships

The impedance of an unbalanced three phase three wire load may be represented by an impedance matrix, as defined in equation A.1. This matrix relates the phase voltage to the current in each phase.

$$\begin{pmatrix} v_1 \\ v_2 \\ v_3 \end{pmatrix} = \begin{pmatrix} Z_{11} & Z_{12} & Z_{13} \\ Z_{21} & Z_{22} & Z_{23} \\ Z_{31} & Z_{32} & Z_{33} \end{pmatrix} \begin{pmatrix} i_1 \\ i_2 \\ i_3 \end{pmatrix} \tag{A.1}$$

An alternative version using line voltages instead of phase voltages is also possible. This relationship is given in equation A.2.

$$\begin{pmatrix} v_{12} \\ v_{23} \\ v_{31} \end{pmatrix} = \begin{pmatrix} \tilde{Z}_{11} & \tilde{Z}_{12} & \tilde{Z}_{13} \\ \tilde{Z}_{21} & \tilde{Z}_{22} & \tilde{Z}_{23} \\ \tilde{Z}_{31} & \tilde{Z}_{32} & \tilde{Z}_{33} \end{pmatrix} \begin{pmatrix} i_1 \\ i_2 \\ i_3 \end{pmatrix} \tag{A.2}$$

In the particular case of a balanced impedance the conversion between the impedance ma-

trices in equation A.1 and equation A.2 is simple as all the self impedance terms, Z_{11}, Z_{22} and Z_{33}, are equal. In an unbalanced system a unique transformation between the two forms does not exist without a further constraint. This constraint is provided by the fact that the mutual coupling between two phases is the same irrespective of the point of measurement. Therefore in equation A.1 $Z_{12} = Z_{21}$, $Z_{13} = Z_{31}$ and $Z_{23} = Z_{32}$. Only six independent impedance terms are thus present in equation A.1. A similar equivalency does not exist for equation A.2.

The transformation between the two impedance matrices may be described by a transformation matrix **T**, this is given in equation A.3.

$$\tilde{\mathbf{Z}} = \mathbf{TZ} \tag{A.3}$$

This matrix, **T** to convert the impedance matrix coefficients of the two relationships above is given for reference in equation A.4.

$$\begin{pmatrix} \tilde{Z}_{11} \\ \tilde{Z}_{12} \\ \tilde{Z}_{13} \\ \tilde{Z}_{21} \\ \tilde{Z}_{22} \\ \tilde{Z}_{23} \\ \tilde{Z}_{31} \\ \tilde{Z}_{32} \\ \tilde{Z}_{33} \end{pmatrix} = \begin{pmatrix} 1 & -1 & 0 & 0 & 0 & 0 \\ 0 & 1 & 0 & -1 & 0 & 0 \\ 0 & 0 & 1 & 0 & -1 & 0 \\ 0 & 1 & -1 & 0 & 0 & 0 \\ 0 & 0 & 0 & 1 & -1 & 0 \\ 0 & 0 & 0 & 0 & 1 & -1 \\ -1 & 0 & 1 & 0 & 0 & 0 \\ 0 & -1 & 0 & 0 & 1 & 0 \\ 0 & 0 & -1 & 0 & 0 & 1 \end{pmatrix} \begin{pmatrix} Z_{11} \\ Z_{12} \\ Z_{13} \\ Z_{22} \\ Z_{23} \\ Z_{33} \end{pmatrix} \tag{A.4}$$

An inverse transformation is also possible, $\mathbf{T}^{\mathrm{p}}$, equation A.5

$$\mathbf{Z} = \mathbf{T}^p \tilde{\mathbf{Z}} \tag{A.5}$$

The inverse transformation matrix, $\mathbf{T}^p$, was calculated using the pseudo-inverse of matrix $\mathbf{T}$ [83]. This is shown in equation A.6.

$$\begin{pmatrix} Z_{11} \\ Z_{12} \\ Z_{13} \\ Z_{22} \\ Z_{23} \\ Z_{33} \end{pmatrix} = \frac{1}{36} \begin{pmatrix} 15 & 5 & 4 & 0 & -1 & 1 & -15 & -4 & -5 \\ -7 & 7 & 0 & 8 & 1 & 3 & -1 & -8 & -3 \\ 1 & 3 & 8 & -8 & -3 & -1 & 7 & 0 & -7 \\ -5 & -15 & -4 & 4 & 15 & 5 & 1 & 0 & -1 \\ -3 & -1 & -8 & 0 & -7 & 7 & 3 & 8 & -5 \\ -1 & 1 & 0 & -4 & -5 & -15 & 5 & 4 & 15 \end{pmatrix} \begin{pmatrix} \tilde{Z}_{11} \\ \tilde{Z}_{12} \\ \tilde{Z}_{13} \\ \tilde{Z}_{21} \\ \tilde{Z}_{22} \\ \tilde{Z}_{23} \\ \tilde{Z}_{31} \\ \tilde{Z}_{32} \\ \tilde{Z}_{33} \end{pmatrix} \tag{A.6}$$

Appendix B

Simulation schematics for impedance measurement

SIMULINK schematics are shown for the impedance measurement simulations.

Figure B.1 shows the overall simulated system.

Figure B.2 shows the data acquisition system employed for the impedance measurement.

Figure B.3 shows a simplified active filter that was used for simulation work. The steady state current used to compensate for harmonic producing loads is not included in the simulation. This current will not change during the impedance measurement as the reference current is fixed and the current controllers have slow response times with respect to the duration of the measurement process. Therefore this current will be not be present in the measurement data once steady state cancellation has been conducted.

Figure B.4 shows the injected voltage waveforms for both the short term injection technique and for the medium term injection technique.

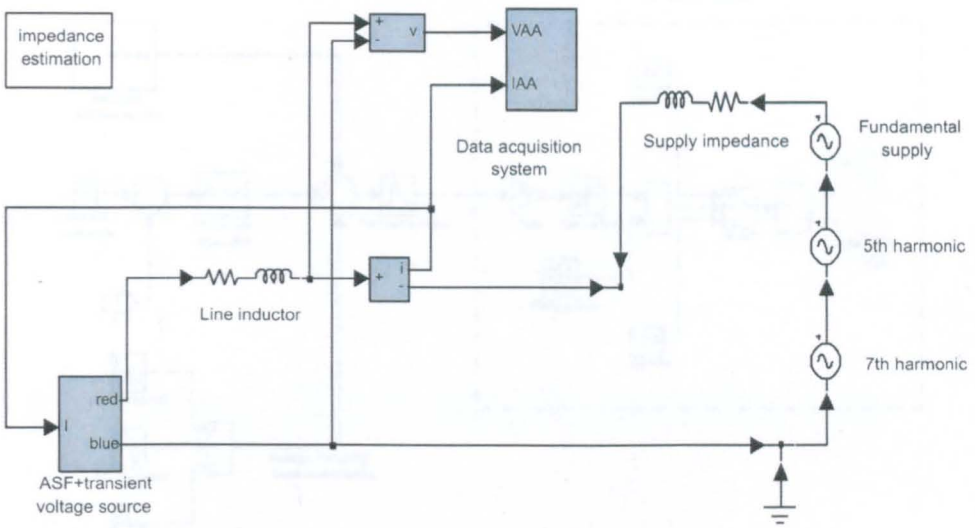

Figure B.1: Simulated single phase system

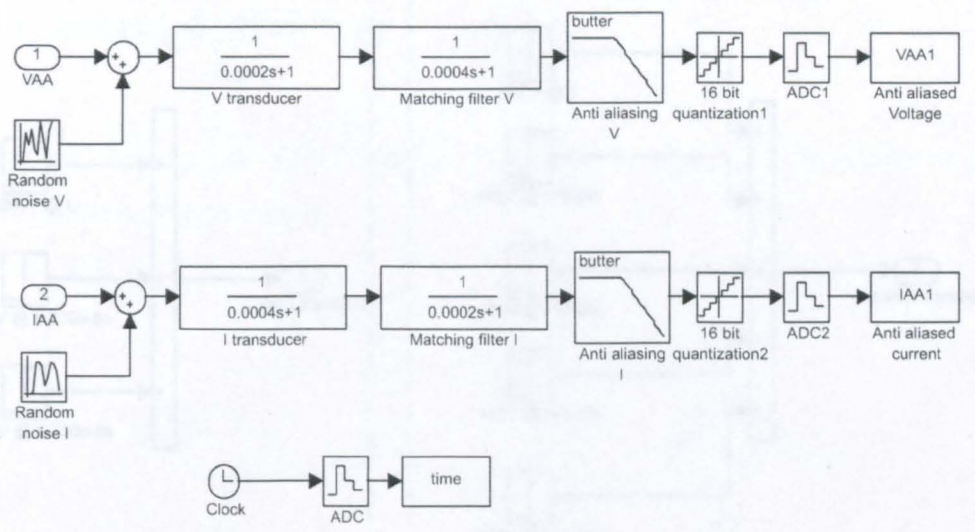

Figure B.2: Data acquisition system for impedance estimation

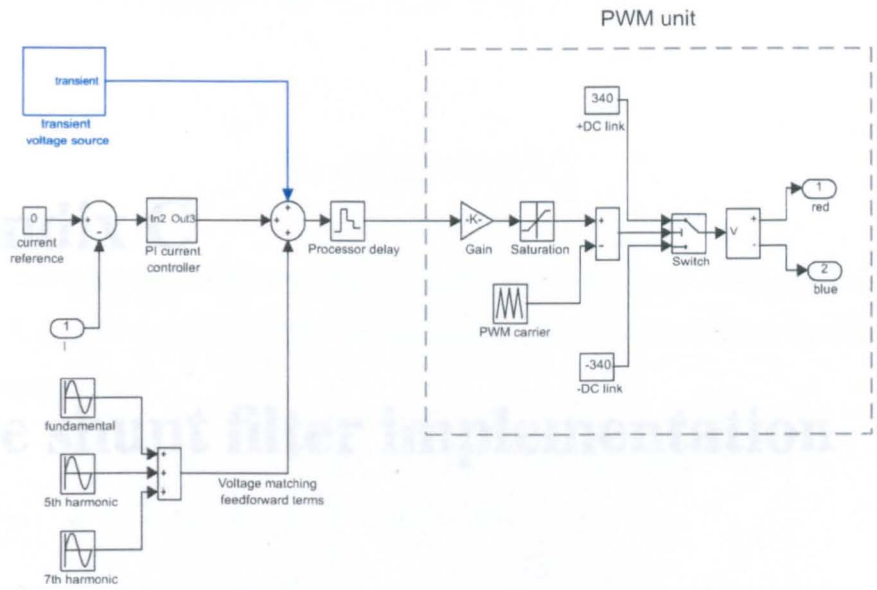

Figure B.3: Active shunt filter

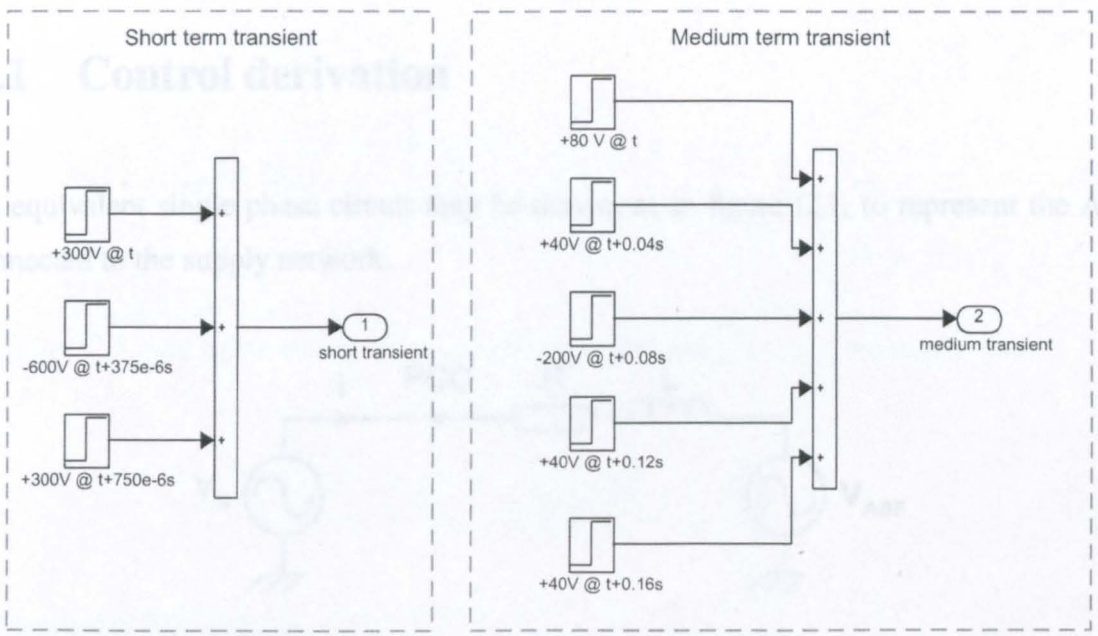

Figure B.4: Transient sources for short term and medium term injection

Appendix C

Active shunt filter implementation

This appendix contains details of the ASF implementation. The transformations required by the control algorithm are shown. Experimental results are also shown in order to demonstrate the ASF harmonic controllers in both transient conditions and in the steady state.

C.1 Control derivation

An equivalent single phase circuit may be drawn, as in figure C.1, to represent the ASF connected to the supply network.

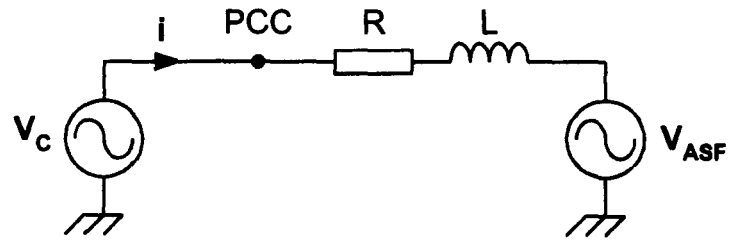

Figure C.1: Single phase equivalent of the ASF connection

The ASF is represented as a controlled voltage source. The ASF supply voltage is repre-

sented by v_c. The control algorithm used assumes a balanced three phase system. Equation C.1 shows a vector equation for the circuit in figure C.1.

$$\mathbf{V_c} = \mathbf{V_{asf}} + \mathbf{iR} + \mathbf{L}\frac{d\mathbf{i}}{dt} \tag{C.1}$$

R and **L** are matrices that represent the resistance and inductance of the ASF input chokes in terms of R, L_s and L_m. These are the resistance, self inductance and mutual inductance per phase respectively.

$$\mathbf{R} = \begin{pmatrix} R & 0 & 0 \\ 0 & R & 0 \\ 0 & 0 & R \end{pmatrix} \quad \text{and} \quad \mathbf{R} = \begin{pmatrix} L_s & L_m & L_m \\ L_m & L_s & L_m \\ L_m & L_m & L_s \end{pmatrix}$$

A transformation is applied to the equation C.1 so that it is transformed into an $\alpha\beta$ set of coordinates. This transformation, **T**, is shown in equation C.2 for the transformation of measured currents to currents in the $\alpha\beta$ set of coordinates.

$$\mathbf{i}_{\alpha\beta} = \mathbf{T}\mathbf{i}_{123} \quad , \quad \begin{pmatrix} i_\alpha \\ i_\beta \end{pmatrix} = \begin{pmatrix} \frac{3}{2} & 0 & 0 \\ 0 & \frac{\sqrt{3}}{2} & \frac{-\sqrt{3}}{2} \end{pmatrix} \begin{pmatrix} i_1 \\ i_2 \\ i_3 \end{pmatrix} \tag{C.2}$$

Equation C.1 may be rewritten as equation C.3 on applying the $\alpha\beta$ transformation.

$$\mathbf{V}_{c\alpha\beta} = \mathbf{V}_{asf\alpha\beta} + \mathbf{R}_{\alpha\beta}\mathbf{i}_{\alpha\beta} + \mathbf{L}_{\alpha\beta}\frac{d\mathbf{i}_{\alpha\beta}}{dt} \tag{C.3}$$

In equation C.3 $\mathbf{R}_{\alpha\beta}$ and $\mathbf{L}_{\alpha\beta}$ are:

$$\mathbf{R}_{\alpha\beta} = \begin{pmatrix} R & 0 \\ 0 & R \end{pmatrix} \quad \text{and} \quad \mathbf{L}_{\alpha\beta} = \begin{pmatrix} L_s - L_m & 0 \\ 0 & L_s - L_m \end{pmatrix} = \begin{pmatrix} L & 0 \\ 0 & L \end{pmatrix}$$

Finally, a *dq* transformation is applied. The angular frequency of the *dq* transformation is ω. The complex transformation used is shown in equation C.4.

$$v_{dq} = \frac{2}{3\sqrt{2}}(v_\beta + jv_\alpha)e^{\omega t} \tag{C.4}$$

Equation C.4 is substituted into equation C.3. Cancel exponential terms and equate as real and imaginary parts.

$$(V_{cq} + jV_{cd})\,e^{-j\theta} = (V_{asfq} + jV_{asfd})\,e^{-j\theta} = R\,(i_q + ji_d)\,e^{-j\theta} + L\frac{d\left((i_q + ji_d)\,e^{-j\theta}\right)}{dt} \tag{C.5}$$

$$\text{Real}: \quad V_{cq} = V_{asfq} + i_q R + L\frac{di_q}{dt} + L\omega i_d \tag{C.6}$$

$$\text{Imaginary}: \quad V_{cd} = V_{asfd} + i_d R + L\frac{di_d}{dt} - L\omega i_q \tag{C.7}$$

Equations C.6 and C.7 describe the ASF in the *dq* reference frame. These equations may then be developed into the control scheme described in chapter 7. Cross coupling between the d and q axes is eliminated by the use of cross coupling feed forward terms to compensate for the final term in each of the equations above. Feed forward terms are also utilised

C.2 ASF controller performance

The ASF controller performance in the steady state was recorded in order to demonstrate the operation of the controllers. The ASF was connected to the supply but there was no load connected at the PCC. Harmonic references were set at fixed values. Several figures are shown, these are:

- Figure C.2 shows 5th harmonic current injection.
- Figure C.3 shows 7th harmonic current injection.
- Figure C.4 shows 5th and 7th harmonic current injection.

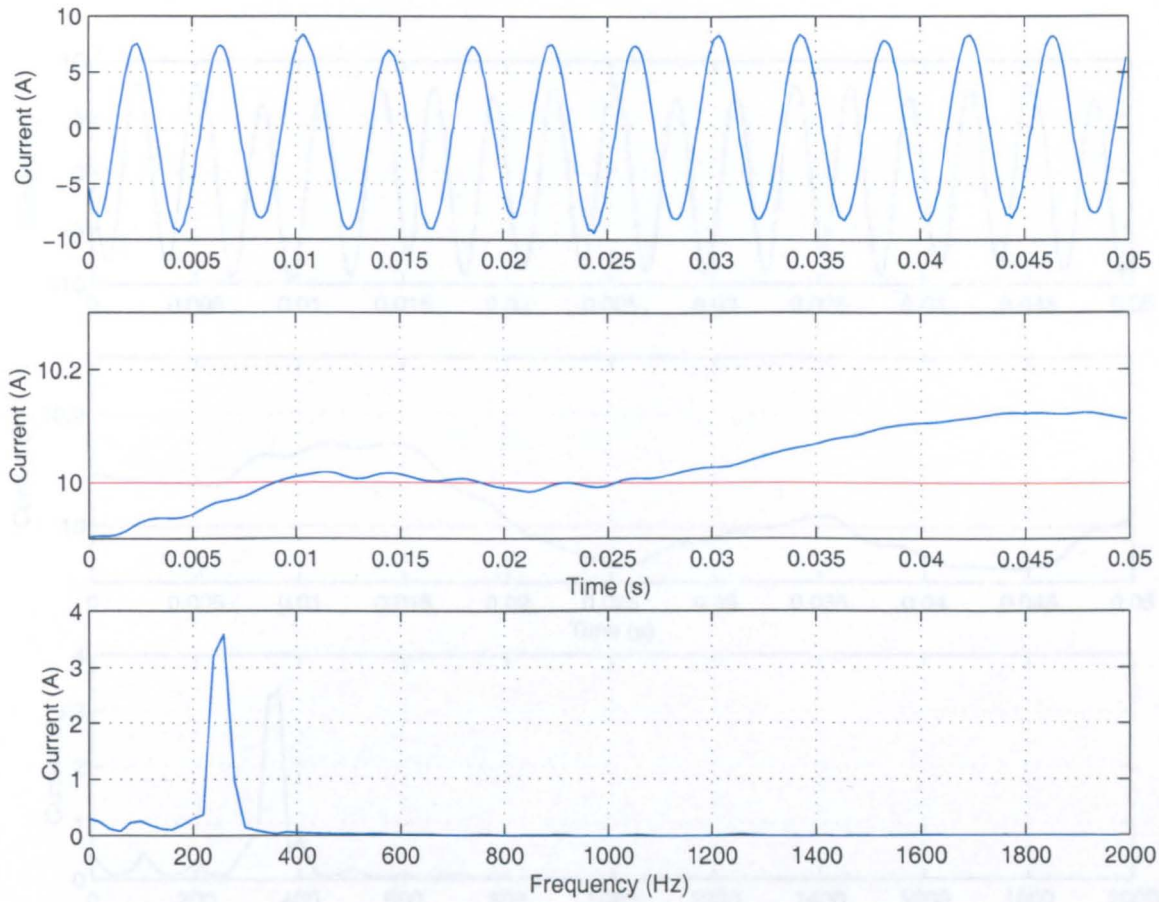

Figure C.2: Steady state 5th harmonic injection. (a) Line current. (b) controller output, reference is 10. (c) Line current in the frequency domain.

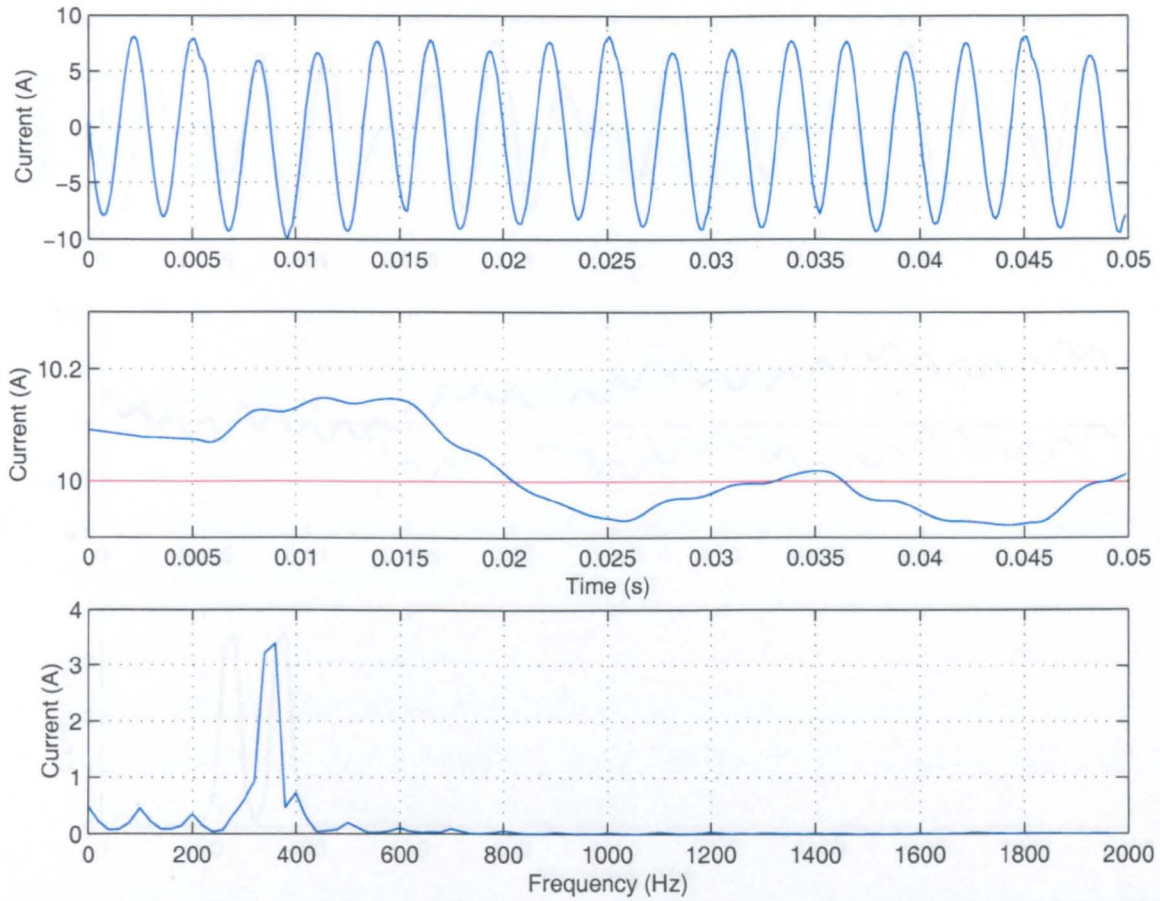

Figure C.3: Steady state 7th harmonic injection. (a) Line current. (b) controller output, reference is 10. (c) Line current in the frequency domain.

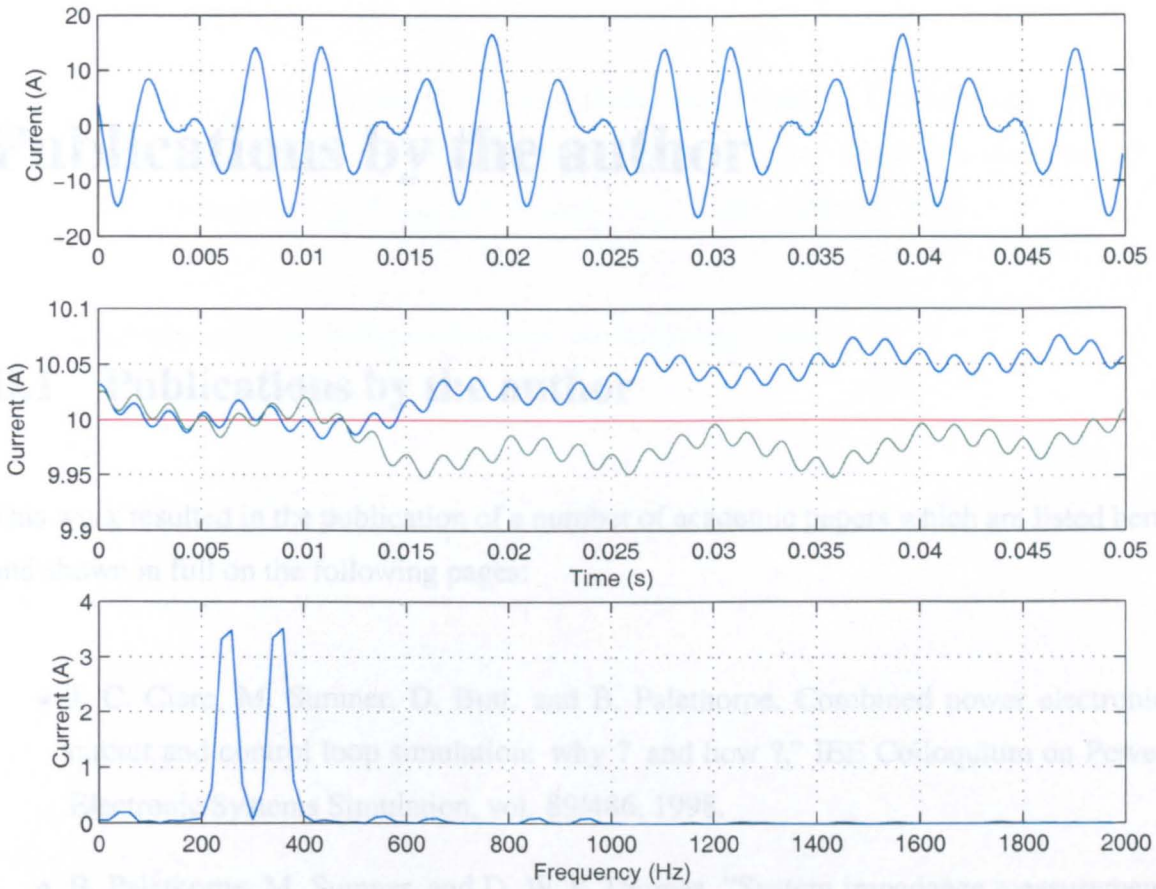

Figure C.4: Steady state 5th and 7th harmonic injection. (a) Line current. (b) controller output, reference is 10. (c) Line current in the frequency domain.

Appendix D

Publications by the author

D.1 Publications by the author

This work resulted in the publication of a number of academic papers which are listed here and shown in full on the following pages:

- J. C. Clare, M. Sumner, D. Butt, and B. Palethorpe, Combined power electronic circuit and control loop simulation: why ? and how ?," IEE Colloquium on Power Electronic Systems Simulation, vol. 89/486, 1998.
- B. Palethorpe, M. Sumner, and D. W. P. Thomas, "System impedance measurement for use with active Filter control " in Eighth international conference on Power Electronics and Variable Speed Drives, vol. 1, (London, UK), pp. 24-28, IEE, 2000.
- B. Palethorpe, M. Sumner, and D. W. P. Thomas, "Power system impedance measurement using a power electronic converter" in Ninth international conference on Harmonics and Quality of Power (A. Domijan, ed.), vol. 1, (Florida, USA), pp. 208-213, IEEE, 2000.
- B. Palethorpe, M. Sumner, and D. W. P. Thomas, "A power supply impedance mea-

surement technique for use with a power electronic inverter" in Ninth European conference on Power Electronics and Applications, (Graz, Austria), CD-ROM, EPE, 2001.

- M. Sumner, B. Palethorpe, D. Thomas, P. Zanchetta, and M. C. Di Piazza, "Estimation of power supply harmonic impedance using a controlled voltage disturbance" in 32'nd annual Power Electronics Specialists Conference, (Vancouver, Canada), CD-ROM, IEEE, 2001.

- M. Sumner, B. Palethorpe, D. Thomas, P. Zanchetta, and M. C. Di Piazza, "Estimation of power supply harmonic impedance using a controlled voltage disturbance" , IEEE Transactions on Power Electronics, vol. 17, no. 2, March 2002.

The published papers are shown in full over the following pages.

Combined power electronic circuit and control loop simulation: why? And how?

J C Clare, M Sumner, D Butt and B Palethorpe

Power Electronics, Machines and Control Group

School of Electrical and Electronic Engineering

The University of Nottingham, Nottingham, NG7 2RD

1 Introduction

Power electronic systems provide a considerable challenge to CAD packages due to their strong non-linearities and widely varying time constants. This is particularly so if an attempt is made to simulate the entire system including the power circuit, load characteristics, control loops and thermal effects. Due to the lack of available tools and desktop computing power it has been normal practice to study each of these aspects independently. This has limited the effectiveness of CAD for power electronic systems since important interactions are inevitably either overlooked or simplified to the point that they are unrealistic. In addition, considerable ingenuity has been required on the part of the user to partition the problem in such a way that meaningful results are obtained in a reasonable computation time.

The situation is however changing and tools are now becoming available which enable us to get closer to a "complete system" simulation. In this paper we concentrate on combined simulations of power electronic circuits (including representations for the load and supply) and their control systems principally for the purpose of control system design and validation prior to prototyping. The need for a combined approach is illustrated with reference to the design of an active filter system. A "wish list" of desirable features for a CAD package is outlined. Some commonly used programs are compared and our experiences in applying them to this problem are discussed.

2 Combined simulation: Why?

The need for a combined approach is best illustrated with a specific example. A problem we have been concerned with recently is the control design for a shunt active power filter (APF) application. The principle of the system is conceptually very simple as shown in Figure 1. An active filter is connected in parallel with a non-linear load (such as a rectifier) and injects a current which exactly balances the harmonic current drawn by the load so as to improve the distortion factor (and hence power factor) of the current drawn from the utility. In practice the non-linear load can be a combination of many loads such as variable speed drives for example.

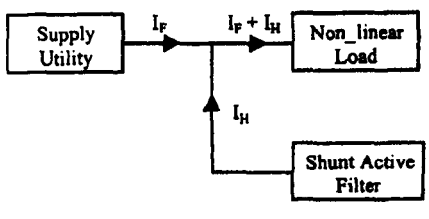

Figure 1 Active power filter principle

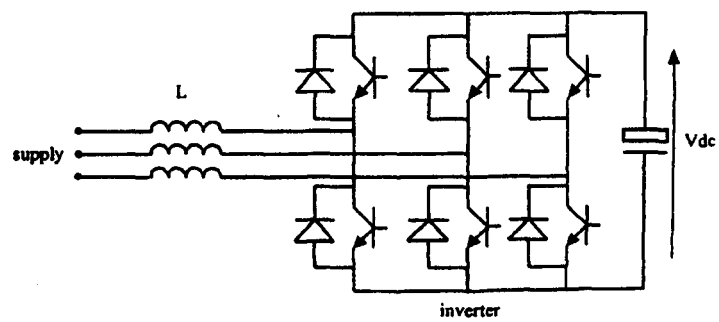

Figure 2 Practical realisation of shunt filter

For example, in the control structure shown in Figure 3 the measured supply voltage is injected into the current control loop after the current controller. Despite the fact that the current control loop bandwidth is 400Hz (to adequately follow a 7th harmonic reference) its rejection to disturbances at this point is very poor. Consequently any inappropriate 5th or 7th harmonic components injected at this point due to voltage distortion produce uncontrolled harmonic currents. The APF thus becomes a source of distortion rather than a sink. Inverter interlock produces similar effects. Supply distortion can also affect the reference angle for the 3-phase to 2-axis transformations. PWM processing delays introduce phase errors which are important in this application since the voltage across the line inductors is small in comparison to the supply voltage and PWM converter terminal voltage. Small phase errors can thus cause large current errors. Switching frequency limitations mean that the current control loops must be designed using discrete sampled data (z-domain) techniques to achieve the required bandwidth.

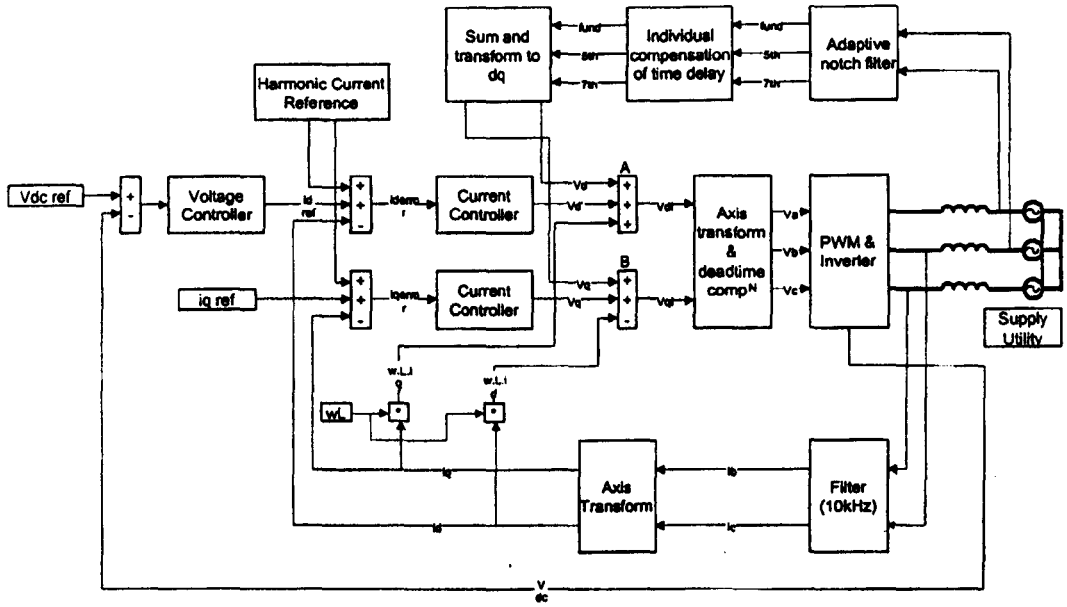

Figure 4 Improved control structure

An improved control structure that overcomes these problems using feed-forward techniques and interlock compensation is shown in Figure 4. In arriving at this structure and designing its practical implementation, we have made extensive use of computer simulation using various packages and simulation techniques. Without discussing the control in further detail it should be apparent that any simulation model which hopes to accurately predict the performance of this system must include a representation of the supply, the power circuit and a detailed representation of the control loop including the effects of discrete control and the time delays inherent in the PWM process.

A "wish list" of what we would like to be able to do with a CAD tool for this and similar problems is as follows:

- enter the power electronic circuit, supply and load as circuit elements in a topological description using components from a library if possible,
- have a choice of different levels of sophistication for switching device modelling,
- enter the control system in standard control terms as one of the following or a combination of these,
  - control block diagrams,
  - transfer functions,
  - control equations (ie difference equations for a digital controller),
- port control algorithm directly from a simulation directly to a target hardware controller ,
- have efficient simulation so that interactive CAD is possible.

modulation as well. The model is however useful for looking at aspects of the control design and we can study the effects of supply distortion, PWM calculation time and inverter interlock in an approximate way by injecting error signals at the appropriate points. Results illustrating these points are given later.

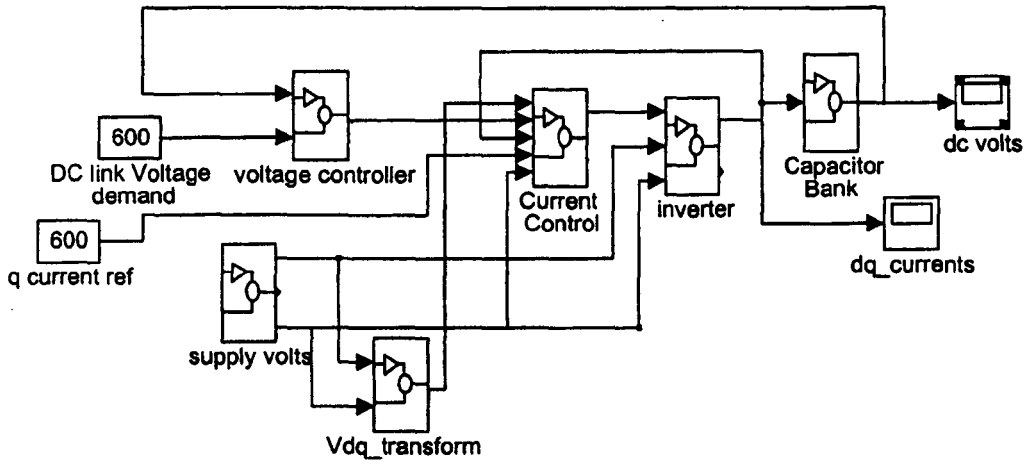

Figure 5 Simulink model of APF

Saber

Saber is a circuit simulation based package with very extensive features. It is generally run on workstations. Electrical networks are input via a schematic capture front end. There are extensive libraries of models for a wide range of components including power devices, power converters, electrical machines and mechanical systems. We have generally found it more convenient however to make our own representations of converters/machines etc from the low level models rather than use those provided. The control system can be input in a number of ways for example:

- using electrical component models (generally inconvenient except for simple systems),
- in terms of s-domain or z-domain transfer functions,
- as control equations using the MAST language provided in Saber,
- as a combination of the above.

The flexibility exists to implement complex control systems and to incorporate them within an electrical network description of the system. However for control studies alone our experience shows that a block diagram orientated package such as Simulink is probably easier to use and will lead to faster development of simulation models.

A Saber model of the APF system is shown in Figure 6 where its correspondence to the electrical network is obvious. Unlike the Simulink model, the equations governing the behaviour of the network are automatically generated from this topological description and do not have to be derived for input to the model. Simple variable resistance models of the inverter switching devices which respond to a logical input are used. These could be replaced with more complex device models and a representation of the gate drive hardware at the expense of simulation runtime. A single control block "CONTROL" implements the control algorithms and mimics as closely as possible the code which runs on the target microcontroller hardware. This block has available to it all the necessary electrical variables and a clock signal which controls the sampling process. The sampling process must be accurately modelled since the exact point of sampling in relation to the inverter switching critically affects the quality of the sampled waveforms. The outputs from this block are the logical PWM signals for the 6 inverter devices. The control block implements the following functions:

```
#       Fundamental, idf current control
#
        if(time < 595m){
           idferror = idfref - idf
           vdfslash = lastvdfslash +0.1*(idferror -
0.98*lastidferror)

           last2vdfslash= lastvdfslash
           lastvdfslash = vdfslash
           last2idferror=lastidferror
           lastidferror = idferror
#
```

Figure 7 Segment of control code in Saber model

The simulation described above incorporates all of the practical effects outlined in Section 2 and can be used to develop control code in virtually its final form with confidence. It is important to realise however that a simulation of this complexity can only be put together once significant work has already been done on developing the control methodology and structure. For this purpose the Simulink model is more convenient.

4 Comparison of simulation results

Figure 8 shows a simulation from the Simulink model for the d-axis current control loop performance to step control reference demands in the presence of supply voltage distortion. The 6 times supply frequency ripple transforms to 5th and 7th harmonic distortion in the a,b,c reference frame. Figure 9 shows the response for the same conditions when feedforward compensation of the supply voltage ripple is incorporated. The Simulink model is not able to represent inverter interlock and the effects of PWM calculation times on the control loop. Figure 10 shows a simulation result from the Saber model which incorporates feedforward compensation of the supply voltage distortion but without inverter interlock compensation. The severe deterioration in performance seen here is completely missed by the Simulink model. Figure 11 shows a result from the Saber model where the control algorithm is improved to include feedforward compensation for the supply voltage distortion and inverter interlock compensation. Finally Figure 12 shows some results from the practical rig illustrating the effect of interlock compensation on the harmonic performance.

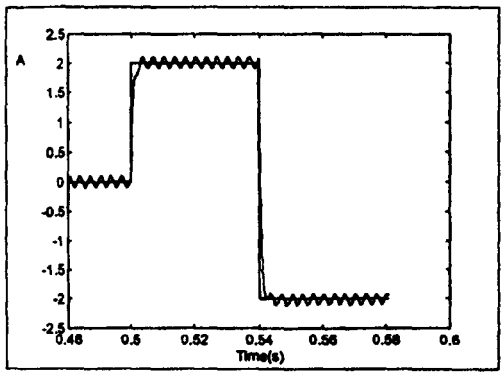

Figure 8 Simulink model results without feedforward compensation

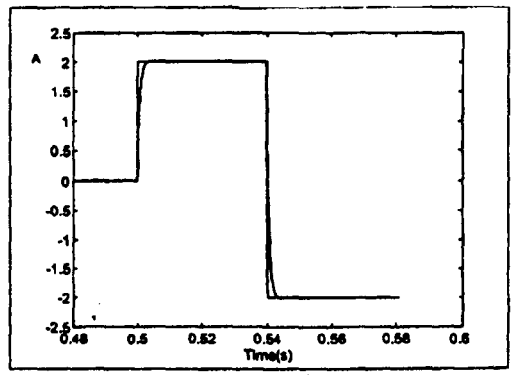

Figure 9 Simulink model results with feedforward compensation

SYSTEM IMPEDANCE MEASUREMENT FOR USE WITH ACTIVE FILTER CONTROL

B Palethorpe, M Sumner and D W P Thomas

The University of Nottingham, UK

ABSTRACT

This paper describes a method for on-line measurement of power system impedance to source. The method employs a power electronic circuit to inject a small current disturbance onto the energised power network, and the measurements of the disturbance current and resultant voltage transient are used to identify impedance. Simulation results demonstrate the effectiveness of the technique for identification of the impedance of transmission lines and linear loads. An alternative data processing technique is introduced in order to address the measurement problems associated non-linear loads. This technique is also illustrated using simulation.

INTRODUCTION

Power electronic loads such as switch mode power supplies and variable speed drives draw high levels of harmonic currents from the supply utility. These harmonic currents lead to supply voltage distortion and a whole host of associated problems. Transmission losses increase and so a higher rated distribution network is needed. Losses in transformers and motors also increase when supplied from a non-sinusoidal source resulting in extra heating and required derating. Other problems associated with a non-sinusoidal supply include false circuit breaker tripping, interference to sensitive electrical equipment and metering problems [1].

There are several means by which the harmonic currents drawn may be reduced. The harmonic current drawn by each power electronic load may be reduced with the addition of line inductors or by using a more elaborate rectifier topology, such as a twelve pulse rectifier or a sinusoidal front end. These solutions are not practical due to the cost of altering existing equipment. Passive filters connected in the transmission system can be used to successfully damp current harmonics although a further set of problems are introduced. Passive filters can introduce system resonances that amplify some harmonics and hence make the situation worse [1]. These filters are also bulky, lossy and particularly hard to design for power systems with high voltage distortion [2]. The most promising alternative - active filters - offer the opportunity to compensate for harmonic currents drawn by a particular load network in an efficient manner without creating additional resonances or affecting existing equipment. The most widely

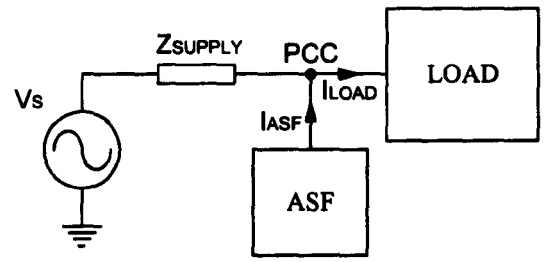

Figure 1: Active Shunt Filter

used active filter topology is the Active Shunt Filter (ASF), shown in figure 1. The ASF is controlled to act as an ideal current source. The injected current, I_{ASF} , is controlled in order to directly cancel the harmonic part of the load current I_L.

It is clear that no matter which technique is chosen to mitigate supply current harmonics, for proper design and system performance an accurate knowledge of the supply system impedance is required. Passive filter designs must be correctly chosen to avoid setting up system resonances. Active filter control stability can be severely influenced by the supply impedance, particularly if it varies. This work has therefore concentrated on investigating techniques for supply impedance measurement.

SYSTEM IMPEDANCE MEASUREMENT

System impedance values are invaluable for power system modelling and simulation. In particular the supply impedance is important for many calculations such as fault current and cable ratings [3]. If the system impedance structure for a particular plant is known then it may be possible to alleviate voltage distortion within that plant by simply redistributing sensitive loads to points of low harmonic distortion, or moving non-linear loads accordingly, thus reducing the need for extra equipment. Alternatively, passive filters can be designed such that the filter resonant peaks avoid

Power Electronics and Variable Speed Drives, 18-19 September 2000, Conference Publication No. 475 IEE 2000

further harmonic problems [2]. As mentioned earlier, active filter control can also be improved, particularly with regards to its dynamic performance. Indeed it may also be possible to create the ASF reference currents from this information, i.e.

$$I_{ref} = \frac{V_{pcc}}{Z_{system}} \quad (1)$$

thus limiting the instrumentation required for ASF control simply to that provided within the unit itself: ASF current and PCC voltage measurement. Several techniques have been proposed for system impedance measurement. Most of these strategies employ the use of special electrical and measurement circuitry to derive a one-off estimate. The approach described in this paper provides the potential for embedding the impedance measurement into the structure of the ASF itself, so that on-line control optimisation can be maintained. This clearly provides many advantages

ONLINE IMPEDANCE MEASUREMENT OVERVIEW

Several techniques have been tried in recent years in order to measure impedance whilst the network is energised. Particular attention has been paid to measuring the supply impedance at customer connections.

Active on-line methods involve injecting some form of disturbance onto the energised network. The response of the network to the injected signal is used to calculate the impedance with respect to the disturbance. Two distinct measurement methods have proved most effective. The first method involves systematically injecting a small sinusoidal current signal over the frequency range of interest, as in [3]. By measuring the phase and amplitude of the voltage and current at the injection point the impedance may be measured over the frequency injection range. The second method involves injecting a narrow current spike onto the network. This impulse like signal must have sufficient spectral content over the frequency range of interest. The resulting voltage transient is recorded and the impedance at that point may be calculated in the frequency domain by equation 2, $\mathcal{F}$ being the Fourier transform.

$$Z(f) = \frac{\mathcal{F}(V(t))}{\mathcal{F}(I(t))} \quad (2)$$

With both methods there is clearly a trade off between disturbing the system sufficiently for measurement purposes and interfering with the network equipment operation. The latter active method is more suited to a real time control application as the injection and transient recording times are shorter than for the former method. Current spike injection has been used at the transmission level for impedance measurement as in [4], [5], [6]. In these papers distribution feeder capacitor bank switching is used to induce the required transient. Much smaller transients have also been injected using thyristor switched resistive loads so that the network is not adversely affected [7]. This work has shown some success for linear impedance measurement.

PROPOSED IMPEDANCE MEASUREMENT SYSTEM

There are two impedance measurement requirements within this project: (1) to develop a stand-alone on-line impedance measurement system and (2) to incorporate the system as part of an ASF control scheme. The work described here has concentrated on the first objective and will be embedded into an ASF control scheme in the near future.

The current impulse injection technique is employed. In this approach a hardware structure similar to an IGBT based ASF has been simulated, as shown in figure 2. The DC link voltage is switched across filter inductor L_F in order to create a current spike of 625μs duration. The amplitude of the spike is approximately 60 - 100A. Both the transient voltage disturbance and the input current signal are recorded and an impedance estimate is calculated according to equation 2. Figure 2 shows the system simulated for evaluation of the supply impedance measurement method. The frequency range of interest was between DC and 2kHz.

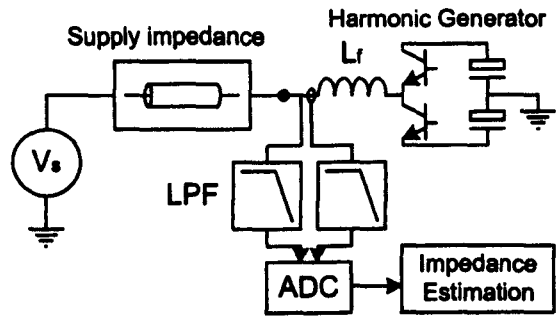

Figure 2: Supply impedance measurement

4th order Butterworth anti-aliasing filters were used with a cut off frequency of 2.4kHz. A sampling rate of 13 kHz was used with a Hamming window applied to the sampled data. The high sampling

rate was used in order to sample sufficient data points within the injected current pulse. 8 bit A/D quantization was used to account for measurement noise levels present in a real system.

In order to negate the effect of the 50Hz supply from the impedance spectrum a differential method was used to remove the supply and its harmonics. 160ms (8 mains cycles) of voltage and current data was recorded immediately prior to the injection. A further 160ms of data was recorded with sampling commencing at the start of the current injection. By subtracting the first set of data from the second the supply can be removed from all measurements. Figure 3 shows an example of a supply impedance network; this impedance was used within simulation for illustration of the injection technique.

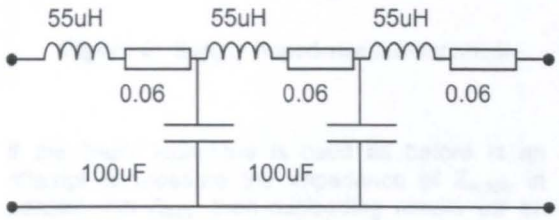

Figure 3: Supply impedance model

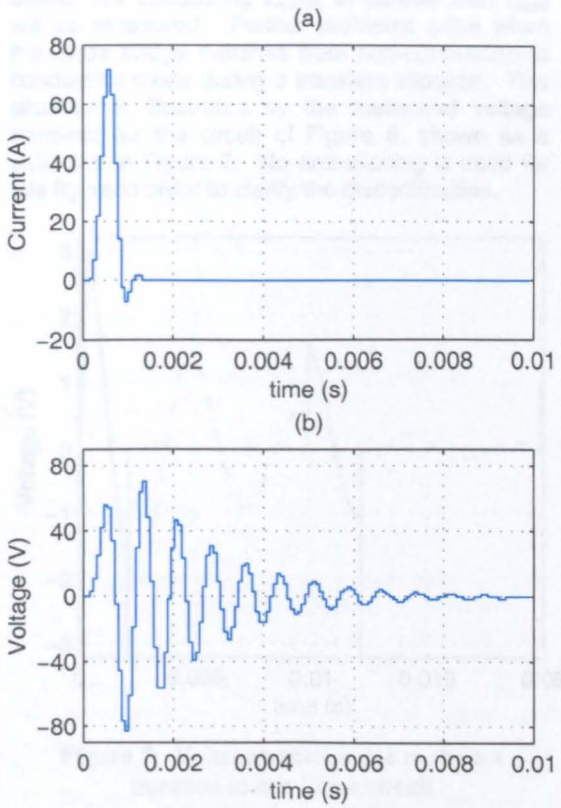

Figure 4: Current and Voltage transients for supply impedance measurements

Figures 4(a) and 4(b) show recorded data after the removal of the pre-transient current and voltage respectively.

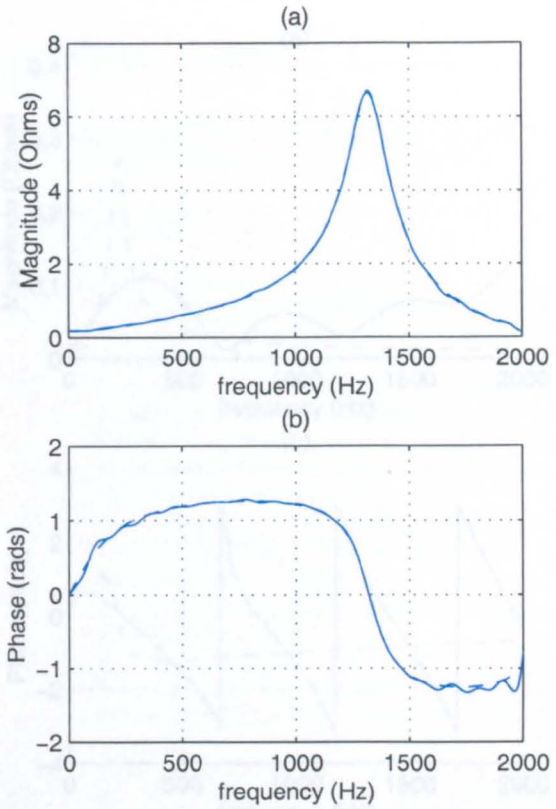

Figure 5: Supply impedance estimate

The impedance was then estimated using the Fourier transforms of the signals shown in figure 4(a) and 4(b), according to equation 2. This estimate is shown as magnitude and phase plots in figures 5(a) and 5(b). The solid lines indicate the estimated impedance and the dashed lines show analytic values.

It can be clearly seen from 5(a) and 5(b) that in the simulated ideal case the technique works very effectively in identifying passive impedances. Indeed, the technique has been tried on several more complex structures with a similar accuracy in measurement. Furthermore, if the measurement noise (simulated by poor A/D resolution) is increased certain correlation techniques, [4] [6], can be used in order to minimise the errors.

NON-LINEAR IMPEDANCE MEASUREMENT

Difficulties arise when non-linear elements are included within a network. The switching transitions of power electronic devices change the instantaneous impedance values and so render impedance estimates made with the previous method useless. For example, consider the non-linear circuit shown in figure 6

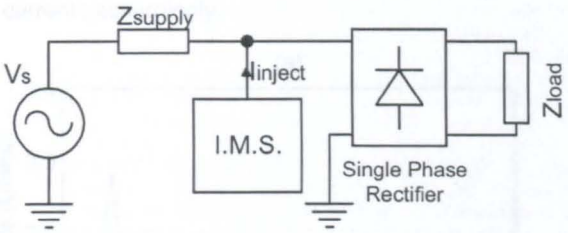

Figure 6: Supply impedance measurement

If the linear technique is used as before in an attempt to measure the impedance of Z_{supply} in parallel with Z_{load} then misleading results will be obtained. When the diodes are reverse biased then only Z_{supply} will be measured and when the diodes are conducting Z_{supply} in parallel with Z_{load} will be measured. Further problems arise when the diode bridge switches from non-conduction to conduction mode during a transient injection. This situation is illustrated by the measured voltage transient for the circuit of Figure 6, shown as a solid line in Figure 7. No anti-aliasing is used for this figure in order to clarify the discontinuities.

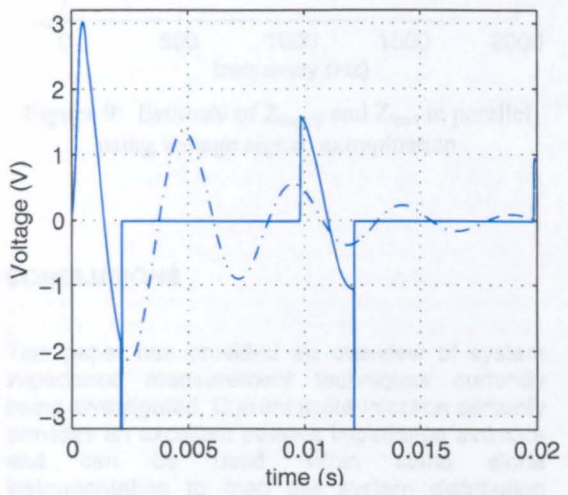

Figure 7: Voltage transient due to current injection in non linear circuit

If this transient data is used in order to estimate Z_{supply} in parallel with Z_{load} then impedance estimates are obtained that are shown in figure 8(a) and 8(b). The dashed line shows the

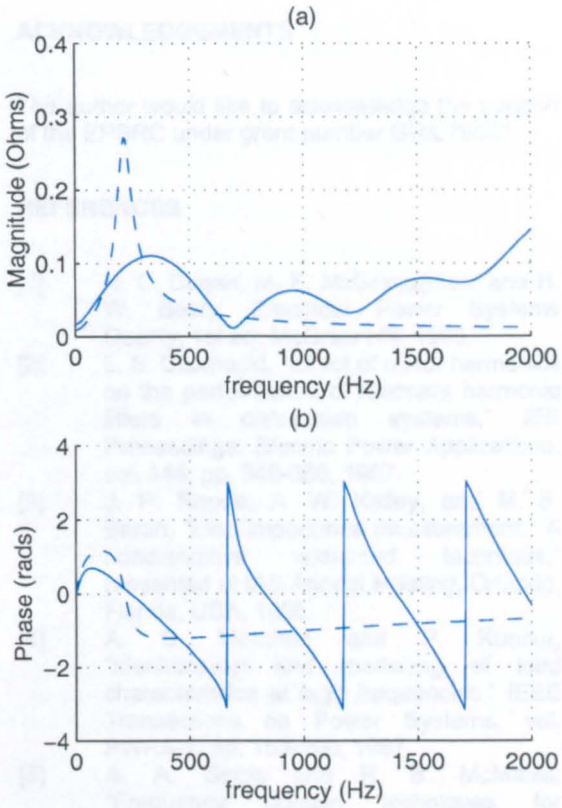

Figure 8: Initial estimate of Z_{supply} and Z_{load} in parralel

analytical impedance whereas the solid line shows the estimated impedance using the injection technique.

A numerical technique has been used in order to overcome some of the problems introduced by switching circuit elements. The time domain extended Prony method [8] can be used to estimate a transient signal in a linear circuit from very few sampled data points. Using this method the continuous section of the transient voltage in Figure 7 may be extrapolated as if the circuit were linear. This extrapolation is continued until the voltage decays to zero. This is shown in Figure 7 by the dashed line. Therefore impedance estimates can be made when the diodes are conducting and when the diodes are not conducting, simply by moving the position of the injected current spike in relation to the supply phase. During the conduction period Z_{supply} in parallel with Z_{load} will be estimated. Similarly when the diodes are reverse biased Z_{supply} will be

estimated. Figure 9 shows the impedance estimate for Z_{supply} in parallel with Z_{load}, as a solid line. The analytic impedance response is again shown as a dashed line. Z_{supply} is modelled as a simple inductive and resistive supply model and Z_{load} is a smoothing capacitor with a resistive load. With knowledge of the passive impedance behind a diode bridge rectifier, and the supply voltage to that rectifier it is possible to estimate the current harmonics drawn [9] and generate ASF reference currents accordingly.

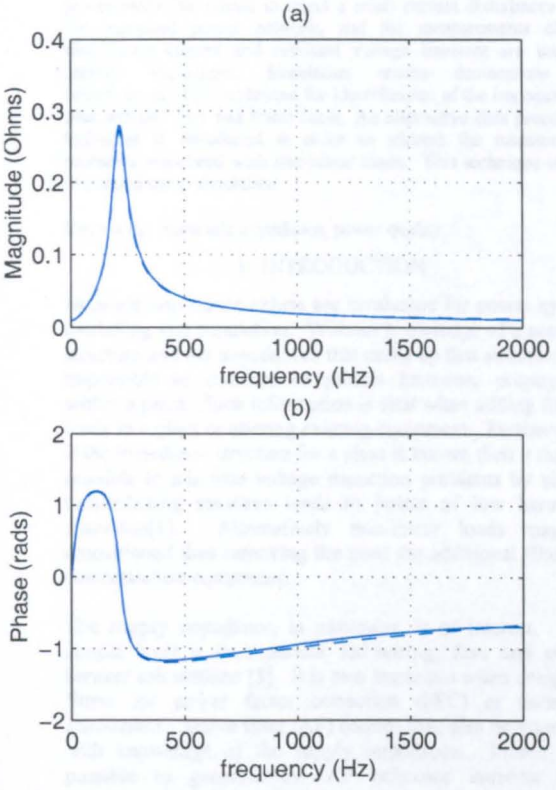

Figure 9: Estimate of Z_{supply} and Z_{load} in parallel using voltage signal extraploation

CONCLUSIONS

This paper has provided an overview of system impedance measurement techniques currently being investigated. Current spike injection certainly provides an excellent passive impedance estimate and can be used within stand alone instrumentation to map the system distribution impedance of a particular plant. This could prove extremely useful for aiding with harmonic reduction in offshore applications. The second technique employing Prony extrapolation provides a method for identifying non-linear load currents. Simulation results using capacitively smoothed diode bridge rectifiers have proved extremely encouraging. Experimental investigation of these techniques is now underway.

ACKNOWLEDGEMENTS

The author would like to acknowledge the support of the EPSRC under grant number GR/L76527

REFERENCES

[1] R. C. Dugan, M. F. McGranaghan, and H. W. Beaty, Electrical Power Systems Quality, 1st ed: McGraw Hill, 1996.

[2] L. S. Czarnecki, "Effect of minor harmonics on the performance of resonant harmonic filters in distribution systems," IEE Proceedings: Electric Power Applications, vol. 144, pp. 349-356, 1997.

[3] J. P. Rhode, A. W. Kelley, and M. E. Baran, "Line impedance measurement: A nondisruptive wideband technique," presented at IAS Annual Meeting, Orlando, Florida, USA, 1995.

[4] A. S. Morched and P. Kundur, "Identification and modelling of load characteristics at high frequencies," IEEE Transactions on Power Systems, vol. PWRS-2, pp. 153-160, 1987.

[5] A. A. Girgis and R. B. McManis, "Frequency domain techniques for modelling distribution or transmission networks using capacitor switching induced transients," IEEE Transactions on Power Delivery, vol. 4, pp. 1882-1890, 1989.

[6] M. Nagpal, W. Xu, and J. Sawada, "Harmonic impedance measurement using three phase transients," IEEE Transactions on Power Delivery, vol. 13, pp. 272-277, 1998.

[7] Z. Staroszczyk, "Accuracy problems in on line one phase distibution/load system identification task," presented at IEEE international symposium on industrial electronics (ISIE96), Warsaw, Poland, 1996.

[8] S. M. Kay, "Spectrum analysis - a modern perspective," Proceedings of the IEEE, vol. 69, pp. 1380-1419, 1981.

[9] A. Mansoor, W. M. Grady, R. S. Thallam, R. S. Doyle, S. D. Krein, and M. J. Samotyj, "Effect of supply voltage harmonics on the input current of single phase diode bridge rectifier loads," IEEE Transactions on Power Delivery, vol. 10, pp. 1416-1422, 1995.

-208-

Power System Impedance Measurement using a Power Electronic Converter

B. Palethorpe
School. of Electrical & Electronic Engineering
University of Nottingham
United Kingdom

M. Sumner
School of Electrical & Electronic Engineering
University of Nottingham
United Kingdom

D. W. P. Thomas
School of Electrical & Electronic Engineering
University of Nottingham
United Kingdom

Abstract: This paper describes a method for on-line measurement of power system impedance to source. The method employs a power electronic circuit to inject a small current disturbance onto the energised power network, and the measurements of the disturbance current and resultant voltage transient are used to identify impedance. Simulation results demonstrate the effectiveness of the technique for identification of the impedance of transmission lines and linear loads. An alternative data processing technique is introduced in order to address the measurement problems associated with non-linear loads. This technique is also illustrated using simulation.

Keywords: harmonic impedance, power quality

I. INTRODUCTION

Network impedance values are invaluable for power system modelling and simulation. Without knowledge of a network structure and the impedances that make up that structure it is impossible to simulate or predict harmonic propagation within a plant. Such information is vital when adding further loads to a plant or altering existing equipment. Furthermore, if the impedance structure for a plant is known then it may be possible to alleviate voltage distortion problems by simply redistributing sensitive loads to points of low harmonic distortion[1]. Alternatively non-linear loads may be repositioned thus removing the need for additional filters or compensation equipment.

The supply impedance, in particular, is of interest. At a simple level it is important for wiring, fuse and circuit breaker calculations [3]. It is also important when designing filters for power factor correction (PFC) or harmonic attenuation. Active filter (AF) control may also be improved with knowledge of the supply impedance. Indeed it is possible to generate the AF reference currents from measurements of voltage distortion and supply impedance. .

Several techniques have been proposed and demonstrated for on-line linear impedance measurement. Active methods involve disturbing an energised power network and then measuring the resultant transients. Impedance values over the frequency range of interest may then be inferred. In this paper one of these techniques has been demonstrated on example linear systems by both simulation and experiment. This measurement technique has also been applied to a system with non-linear circuit elements - in this case a capacitively smoothed diode rectifier. The discontinuous current of the non-linear load (NLL) seriously degrades the impedance estimate and therefore a signal processing technique is introduced to allow identification of the system impedance without the NLL, and the passive impedance of the NLL itself.

0-7803-6499-6/00/$10.00 2000IEEE

II. ON-LINE IMPEDANCE MEASUREMENT

Active on-line measurement methods involve injecting some form of disturbance onto the energised network. The response to such an injected signal is used to calculate the impedance of the network at the point of measurement. In networks with high voltage distortion in the frequency range of interest it may be possible to use methods that do not involve disturbance signals but this is not generally the case [2]. Two distinct measurement methods have proved most effective. The first method involves systematically injecting a small sinusoidal current signal at each frequency of interest, as in [3]. By measuring the phase and amplitude of the voltage and current at the point of injection the impedance may be calculated at each frequency. The second method involves injecting a narrow current spike onto the network. This impulse like signal must have sufficient spectral content over the frequency range of interest. Both the injected current and the resulting voltage transient are recorded and the impedance at the point of injection is calculated in the frequency domain by (1), F being the Fourier transform.

$$Z(f) = \frac{F(V(t))}{F(I(t))} \qquad (1)$$

This approach has been used at the distribution level as in [4], [5] and [6]. In these papers distribution feeder capacitor bank switching is used to induce the required transients. Transients for this method have also been injected by dedicated hardware as in [7].

With both methods there is clearly a trade off between disturbing the system sufficiently for measurement purposes and interfering with the network equipment operation.

III PROPOSED MEASUREMENT SYSTEM

A practical measurement system has been developed for current spike injection and the recording of the subsequent transients. This work has only focused on single phase impedance estimation. However, it is possible to extend the technique to three phase circuits, using the approach suggested in [6]. A hardware structure similar to an IGBT based active shunt filter (ASF) has been used as shown in fig. 1. The dc link voltage is switched across the inductor L_f in order to create a symmetrical triangular current spike of 625 µs duration. In the frequency domain this signal will provide a sinc function form of excitation. At 2kHz the

excitation strength will be approximately 50% of the dc excitation and at 3.2kHz the main lobe will decay to zero strength. The amplitude of the current spike is approximately 60-100A. Both the voltage disturbance and the input current are recorded over a 160ms period using dedicated hardware. The impedance estimate is calculated within the host PC according to (1). Fig. 1 shows the measurement system for evaluation of the network impedance at the point of common coupling (PCC).

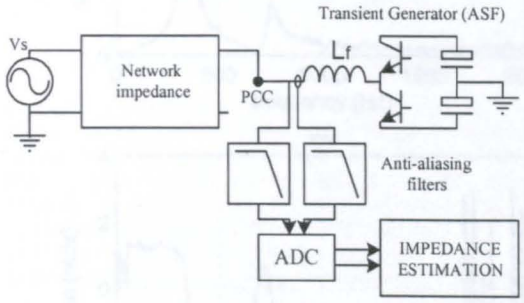

Fig. 1. The overall control scheme

4th order Butterworth anti aliasing filters were used with a cut off frequency of 2.4kHz. A sampling rate of 13 kHz was used with a Hamming window applied to the sampled data. The frequency of interest was between dc and 2kHz. The high sampling rate was used in order to sample sufficient data points within the injected current pulse. The experimental hardware was equipped with 16 bit A/D convertors although the simulations were conducted with 9 bit A/D quantization in order to emulate measurement noise levels present in a real system.

In order to negate the effect of the supply voltage from the impedance spectrum a two stage acquisition procedure was utilised. A data record of 160ms (8 * 50Hz mains cycles) of voltage and current data was taken immediately prior to the current injection. A further record of 160ms was taken with sampling commencing at the start of the current injection. By subtracting the first data set from the second the influence of the supply voltage, including its harmonics, can be removed from all measurements. 160ms of data allows a frequency resolution of 6.25Hz; the sampling window could be reduced if a lower resolution is sufficient.

IV. SIMULATION RESULTS FOR A LINEAR SYSTEM

In order to demonstrate the technique successfully on a linear system the procedure has been applied to the network shown in fig. 2. This network model has been designed to model a linear power network. The basic model includes a 1MVA transformer, a load with VAr compensating capacitor, a length of transmission line and a 45kW load - eg a heater. The network impedance was determined with respect to the PCC. Figs. (3(a)) and (3(b)) show recorded transient data after the removal of the pre-transient current and voltage measurements respectively.

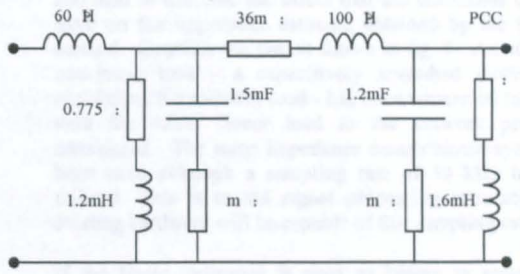

Fig. 2 example network

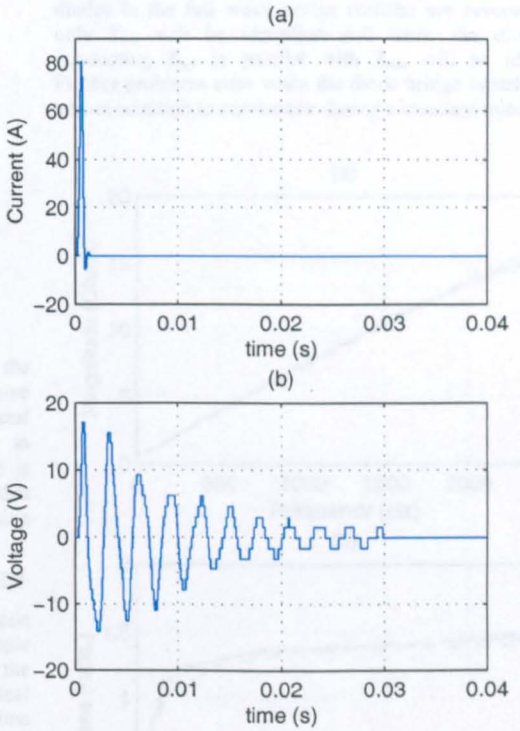

Fig3. Simulated current and voltage readings.

The impedance at the PCC was then calculated using (1). Figs. 4(a) and 4(b) show the magnitude and phase of the impedance estimate. The solid lines show the impedance estimate whereas the dotted lines show the theoretical impedance values. Note that 9 bit A/D quantization levels were used in order to emulate measurement noise within a real system.

-210-

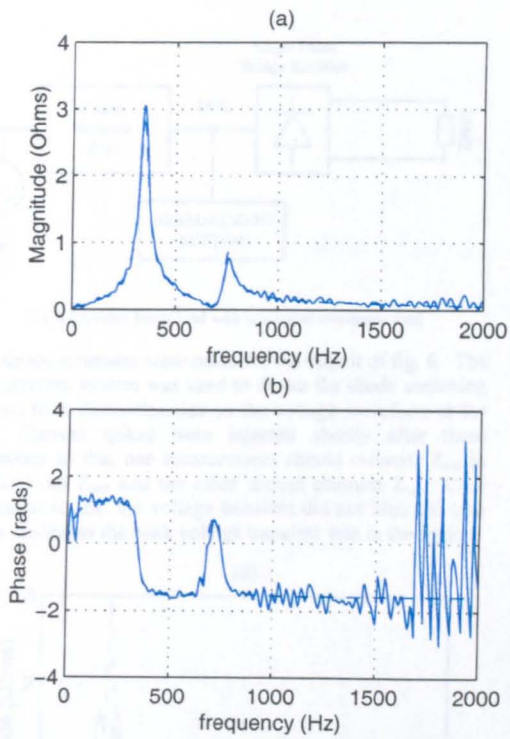

Fig. 4. Simulated impedance estimates

It can clearly be seen from figs. 4(a) and 4(b) that the technique works very effectively in identifying passive impedances. Indeed, the technique has been tried on several more complex structures with similar accuracy in measurement. Furthermore, if the measurement noise is increased there are correlation techniques, [4] and [5], that may be used in order to improve the identification performance.

V. EXPERIMENTAL RESULTS FOR LINEAR SYSTEM

The measurement method employed in the previous section has also been used to estimate the impedance of a simple load within the laboratory. Figs. 5(a) and 5(b) show the impedance estimate. The dashed line shows analytical impedance values taken from name plate data. The solid line shows the impedance estimate as an average of ten measurements; by averaging the impedance estimates random errors may be reduced. The impedance estimates are fairly good and further work is underway with more complicated circuit topologies.

VI. NON-LINEAR IMPEDANCE IDENTIFICATION

The vast majority of impedance estimation work to date has been concerned with linear systems. Identification problems due to non-linear loads were considered in [8] although no mathematical analysis was used to compensate. In [7] non-linear loads are again considered using the concept of running quantities. In this paper an approach shall be used in order to identify linear impedances within non-linear circuits and also to examine the effect that the non-linear elements have on the impedance estimate obtained by the previous method. Consider the circuit shown in fig. 6. An additional non-linear load – a capacitively smoothed diode bridge rectifier with a resistive load - has been connected in parallel with the 45kW linear load in the network previously considered. The same impedance measurement system has been used although a sampling rate of 50 kHz has been utilized. This is to aid signal processing accuracy. The existing hardware will be capable of this sampling rate.

If the linear technique is used as before to measure the impedance of Z_{net} (the linear network previously considered) in parallel with Z_{rect} (the passive impedance behind the diode bridge) then misleading results will be obtained. When the diodes in the full wave bridge rectifier are reverse biased only Z_{net} will be identified and when the diodes are conducting Z_{net} in parallel with Z_{rect} will be identified. Further problems arise when the diode bridge switches from non-conduction to conduction during a transient injection.

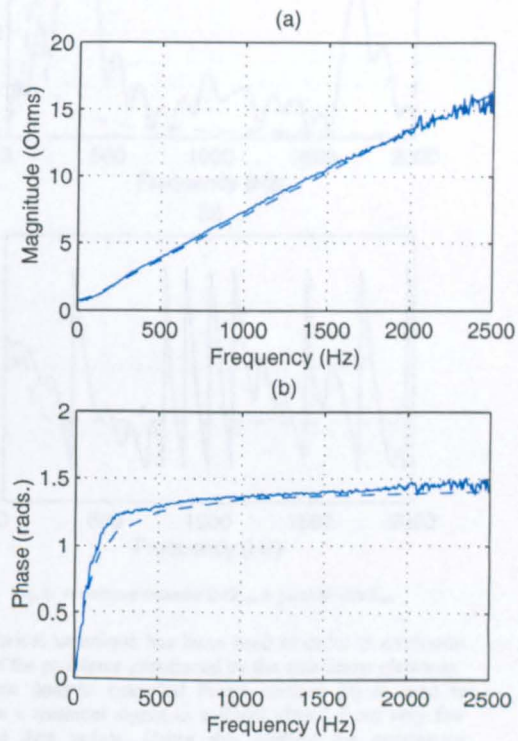

Fig. 5. Experimental impedance estimates.

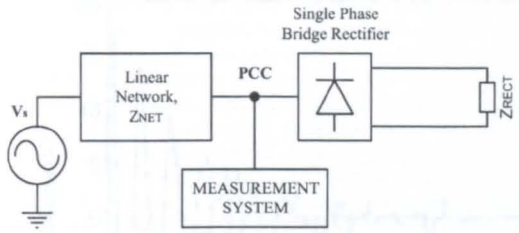

Fig. 6 Previous linear load with additional non-linear load

Impedance estimates were made for the circuit of fig. 6. The measurement system was used to detect the diode switching instants from discontinuities on the voltage waveform at the PCC. Current spikes were injected shortly after these transitions so that one measurement should estimate Z_{net} in parallel with Z_{rect} and the other should estimate Z_{net}. Care was taken so that the voltage transient did not alter the bias of the diodes, as the peak voltage transient was in the region

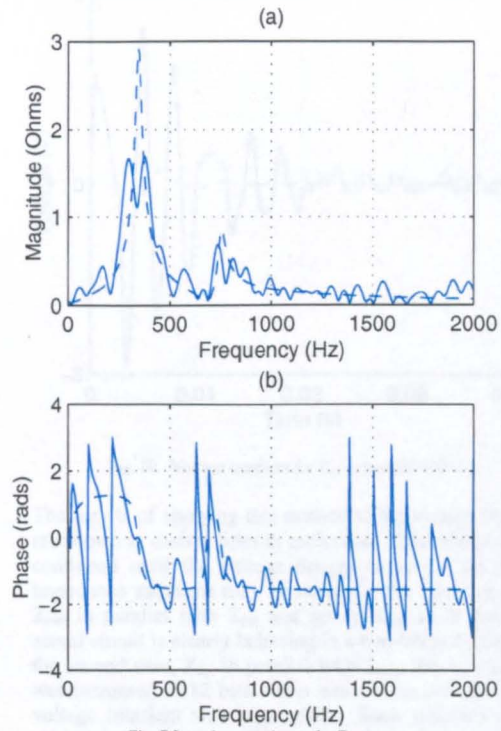

Fig. 7 Impedance estimate for Z_{net}

of 20V. Figs. 7(a) and 7(b) show the impedance estimate for Z_{net} and Z_{rect} in parallel whereas figs. 8(a) and 8(b) show the estimate for Z_{net}. In both sets of figures the solid lines show the impedance estimates made.

The dashed lines show the analytical impedance values. The magnitude estimate in fig. 7(a) does partially identify the two peaks although considerable errors are present. The phase identification is meaningless. The situation in figs. 8(a) and 8(b) is even worse and no valid identification could be drawn. This results from several factors including the strong discontinuities in the voltage waveform, and its lower amplitude reducing the signal to noise ratio.

VII NON-LINEAR IDENTIFICATION TECHNIQUE

In order to examine the poor performance of the identification technique it is worthwhile examining the transient voltage waveforms. The solid lines in Fig.10 and fig.11 show the voltage transients for the two cases.

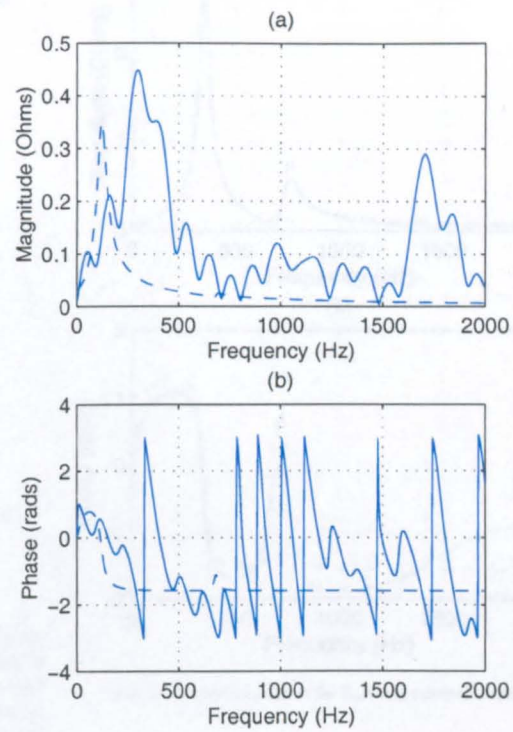

Fig. 8. Impedance estimate for Z_{rect} in parallel with Z_{net}

A numerical technique has been used in order to overcome some of the problems introduced by the non-linear elements. The time domain extended Prony method [9] is used to estimate a transient signal in a linear circuit from very few sampled data points. Using this method the continuous section of the transient voltage in figs 9 and 10 may be extrapolated as if the diode conduction positions did not switch.

-212-

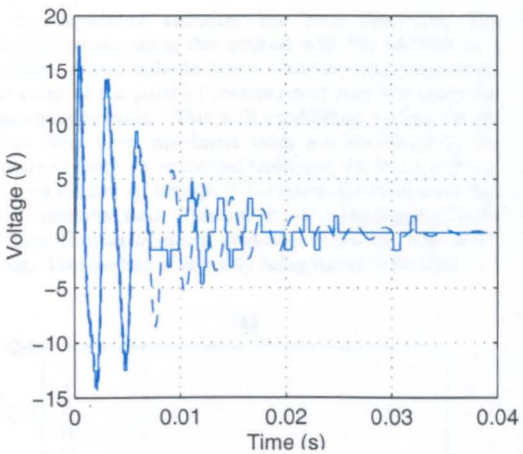

Fig. 9 Voltage transient for Z_{net} identification.

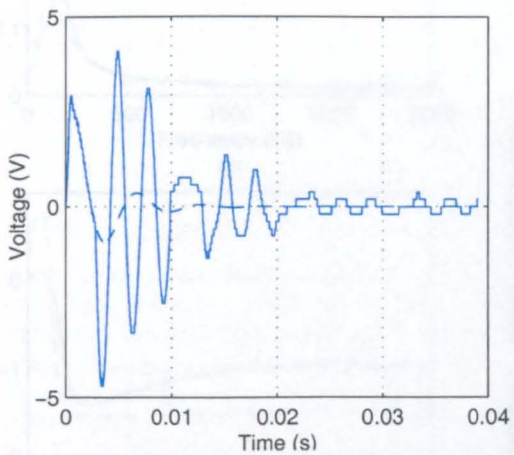

Fig. 10. Voltage transient for Z_{net} in parallel with Z_{rect} .

The results of applying this method to the voltage transients are shown as dashed lines in each case. This extrapolation is continued until the voltage decays to zero. As a result impedance estimates may be made for the linear quantities, Z_{rect} in parallel with Z_{net} and solely Z_{net}, even though the actual circuit is clearly behaving in a non-linear fashion. For the second case, Z_{net} in parallel with Z_{rect}, the A/D accuracy was increased to 12 bits. This was due to the fact that the voltage transient was very small. Such accuracy may be achieved by repeating the measurement many times and averaging the results. Alternatively a larger current injection could be applied. This problem is the subject of on going work. The Prony extrapolation method does require some additional information before the extrapolation may be completed. An estimate of the number of poles within the data must be supplied although this does not need to be exact. Methods are available for automatically deciding the number of poles within the data [10].

VIII. RESULTS FOR NON-LINEAR SYSTEM

The circuit impedances may be calculated once more using the extrapolated voltage sets. These results are shown in figs. 11 and 12. The dashed lines show the analytical impedance values and the solid lines show the new estimates. The impedance estimate for Z_{net} is a great improvement when compared to the impedance using the measured voltage signal, fig. 7. Although the impedance estimate in fig. 12 is still far from the analytic value it is superior to the estimate made in fig, 8 as the major peak in the magnitude has been identified.

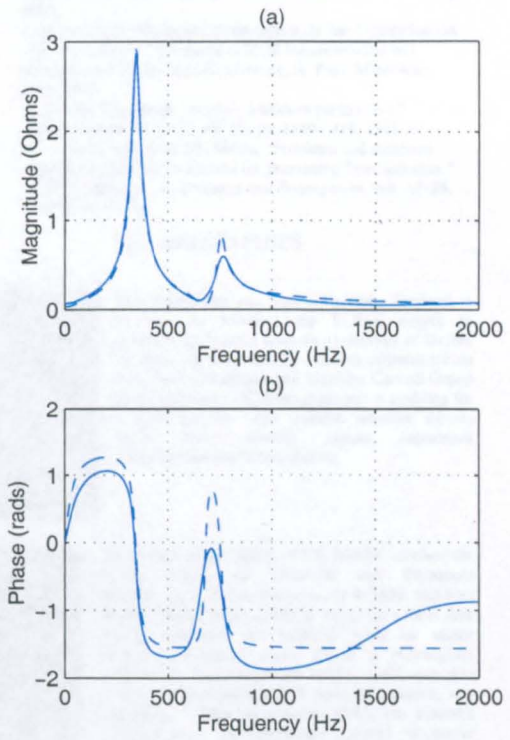

Fig. 11. Impedance estimate for Z_{net} using extrapolated transient

It is now possible to identify the linear loads within the non linear circuit. If prior knowledge of the circuit topology is known then it may be possible to calculate the harmonic currents drawn by the non-linear loads by analytical means. This could prove useful for harmonic generation identification and tariff problems.

IX. CONCLUSIONS

A successful linear impedance measurement technique has been demonstrated both practically and in simulation. A non-linear load was added to the simulated network and the effect

on the impedance estimates has been illustrated. The simulated results using this method with the addition of a non-linear circuit indicate that a relatively small non-linear load close to the point of measurement may invalidate the measurements made. This well established method clearly cannot cope when non-linear loads are introduced to the measured system. A numerical technique, the Prony method, has been used in an attempt to overcome the inaccuracy due to the additional load. This has shown promising results for the identification of linear elements within the non linear circuit. This method is currently being tested in practice

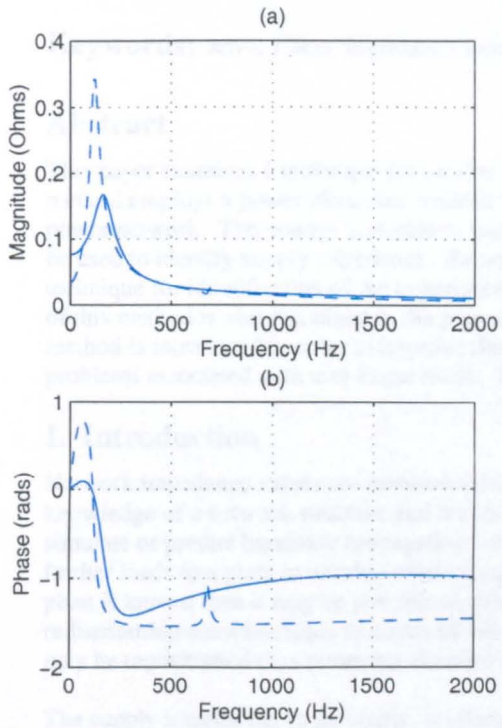

Fig. 12. Impedance estimate for Z_{net} in parallel with Z_{rect} using extrapolated transient

X. ACKNOWLEDGEMENTS

The author would like to acknowledge the support of the EPSRC under grant number GR/L76527. The author would also like to thank Dr. J.D. Paul for his help concerning the Prony extrapolation method.

XI. REFERENCES

[1] R. C. Dugan, M. F. McGranaghan, and H. W. Beaty, *Electrical Power Systems Quality*, 1 ed: McGraw Hill, 1996.

[2] A. Oliveira, J. C. Oliveira, J. W. Resende, and M. S. Miskulin, "Practical approaches for ac system harmonic impedance measurements," *IEEE Transactions on Power Delivery*, vol. 6, pp. 1721-1726, 1991.

[3] J. P. Rhode, A. W. Kelley, and M. E. Baran, "Line impedance measurement: A nondisruptive wideband technique," presented at IAS Annual Meeting, Orlando, Florida, USA, 1995.

[4] A. S. Morched and P. Kundur, "Identification and modelling of load characteristics at high frequencies," *IEEE Transactions on Power Systems*, vol. PWRS-2, pp. 153-160, 1987.

[5] A. A. Girgis and R. B. McManis, "Frequency domain techniques for modelling distribution or transmission networks using capacitor switching induced transients," *IEEE Transactions on Power Delivery*, vol. 4, pp. 1882-1890, 1989.

[6] M. Nagpal, W. Xu, and J. Sawada, "Harmonic impedance measurement using three phase transients," *IEEE Transactions on Power Delivery*, vol. 13, pp. 272-277, 1998.

[7] Z. Staroszczyk, "Time dependant power systems impedance - Interpretation and measuring problems," presented at IEEE instrumentation and measurement technology conference (IMTC99): Measurements for the new millenium, Venice, Italy, 1999.

[8] Z. Staroszczyk, "Problems in real time wide band identification of power systems," presented at IEEE Instumentation and Measurement Technology Conference, St. Paul, Minnesota, USA, 1998.

[9] S. M. Kay, "Spectrum analysis - a modern perspective," *Proceedings of the IEEE*, vol. 69, pp. 1380-1419, 1981.

[10] M. L. Van Blaricum and R. Mittra, "Problems and solutions associated with Prony's method for processing Transient data," *IEEE Transactions on Antennas and Propagation*, vol. AP-26, pp. 174-182, 1978.

XII. BIOGRAPHIES

Ben Palethorpe was born in Farnham, England, in 1974. He received the M.Eng. degree in Engineering Science from the University of Oxford in 1996. He is currently a research assistant within the Power Electronics and Machine Control Group at the University of Nottingham and is studying for a PhD. Degree. His research interests include active filter control, system impedance identification and power quality.

Dr Mark Sumner CEng, MIEE, MIEEE received the B.Eng degree in Electrical and Electronic Engineering from Leeds University in 1986. and then worked for Rolls Royce Ltd in Ansty for a short time before embarking on research work in vector controlled induction motor drives at Nottingham University. He received his PhD in 1990, and after working at Nottingham as a research assistant, was appointed lecturer in October 1992. His research interests cover microprocessor control of power electronic systems including advanced induction motor drives research, active shunt filters, system identification and the development of new converter topologies.

Dr David W P Thomas CEng, MIEE, MIEEE received the BSc degree in Physics from Imperial College of Science and Technology, the MPhil degree in Space Physics from Sheffield University, and the PhD degree in Electrical Engineering from Nottingham University, in 1981, 1987 and 1990 respectively. In 1990 he joined the School of Electrical and Electronic Engineering at the University of Nottingham as a Lecturer. His research interests are EMC, Protection and Simulation of Power Networks, Electrostatic Precipitation and High Voltage Insulation Testing.

A Power Supply Impedance Measurement Technique for use with a Power Electronic Inverter

Ben Palethorpe, Mark Sumner and David Thomas
School of Electrical and Electronic Engineering
University of Nottingham
Nottingham NG7 2RD, UK
Tel 0115 9515549
Fax 0115 9515616

Keywords: active filters, impedance measurement, power quality

Abstract

This paper examines a technique for on-line measurement of power system supply impedance. The method employs a power electronic inverter to apply a short duration transient onto the energised power network. The voltage disturbance and the consequent current transient are measured and may be used to identify supply impedance. Experimental results demonstrate the effectiveness of the technique for identification of the impedance of transmission lines and linear loads. The performance of this method is also examined in the presence of non-linear loads. An alternative data processing method is introduced in order to improve the technique and to compensate for the measurement problems associated with non-linear loads. This is also verified experimentally.

I. Introduction

Network impedance values are invaluable for power system modelling and simulation. Without knowledge of a network structure and the impedances that make up that structure it is impossible to simulate or predict harmonic propagation within a plant. Such information is vital when adding further loads to a plant or altering existing equipment. Furthermore, if the impedance structure for a plant is known then it may be possible to alleviate voltage distortion problems by simply redistributing sensitive loads to points of low harmonic distortion[1]. Alternatively non-linear loads may be repositioned thus removing the need for additional filters or compensation equipment.

The supply impedance, in particular, is of interest. At a simple level it is important for wiring, fuse and circuit breaker calculations [3]. It is also important when designing filters for power factor correction (PFC) or harmonic attenuation. Active Shunt Filter (ASF) control may also be improved with knowledge of the supply impedance. Indeed it is possible to generate the ASF reference currents from measurements of voltage distortion and supply impedance.

Several techniques have been proposed and demonstrated for on-line linear impedance measurement. Active methods involve disturbing an energised power network and then measuring the resultant behaviour of the network. Impedance values over the frequency range of interest may then be inferred. In this paper one of these techniques has been demonstrated experimentally on a practical system. An existing ASF connected to the supply is utilised to inject the disturbance at the point of common coupling (PCC).

This measurement technique has also been applied to a system with non-linear circuit elements – in this case a capacitively smoothed diode rectifier. The discontinuous current of the non-linear load (NLL) seriously degrades the impedance estimate and therefore a signal processing technique is introduced to allow identification of the supply impedance excluding the NLL.

II. On-Line Impedance Measurement

Active on-line measurement methods involve injecting some form of disturbance onto the energised network. The response to such an injected signal is used to calculate the impedance of the network at the point of measurement. In networks with high voltage distortion in the frequency range of interest it may be possible to use methods that do not involve disturbance signals but this is not generally the case [2]. Two distinct measurement methods have proved most effective. The first method involves systematically injecting a small sinusoidal current signal at each frequency of interest, as in [3]. By measuring the phase and amplitude of the voltage and current at the point of injection the impedance may be calculated at each frequency. The second method involves injecting a narrow current spike onto the network. This impulse like signal must have sufficient spectral content over the frequency range of interest. Both the injected current and the resulting voltage transient are recorded and the impedance at the point of injection is calculated in the frequency domain by (1), $\mathfrak{F}$ being the Fourier transform.

$$Z(f) = \frac{\mathfrak{F}(V(t))}{\mathfrak{F}(I(t))} \tag{1}$$

This approach has been used at the distribution level as in [4], [5] and [6]. In these papers distribution feeder capacitor bank switching is used to induce the required transients. Transients for this method have also been injected by dedicated hardware as in [7].

With both methods there is clearly a trade off between disturbing the system sufficiently for measurement purposes and interfering with the network equipment operation.

III. Experimental Measurement System

A practical measurement system has been developed for a short duration current injection and the recording of the subsequent transients. This work has been applied to both single phase and balanced three phase, three wire, systems. Single phase simulation results were presented in [8]. The work in this paper has focused on the balanced three phase, three wire system. It may be possible to extend the technique to the unbalanced three phase case by using the approach suggested in [6]. The measurement system comprises an IGBT based ASF and a separate data acquisition system. The ASF is utilised in order to apply the required disturbance to the supply. The overall system is shown in fig. 1.

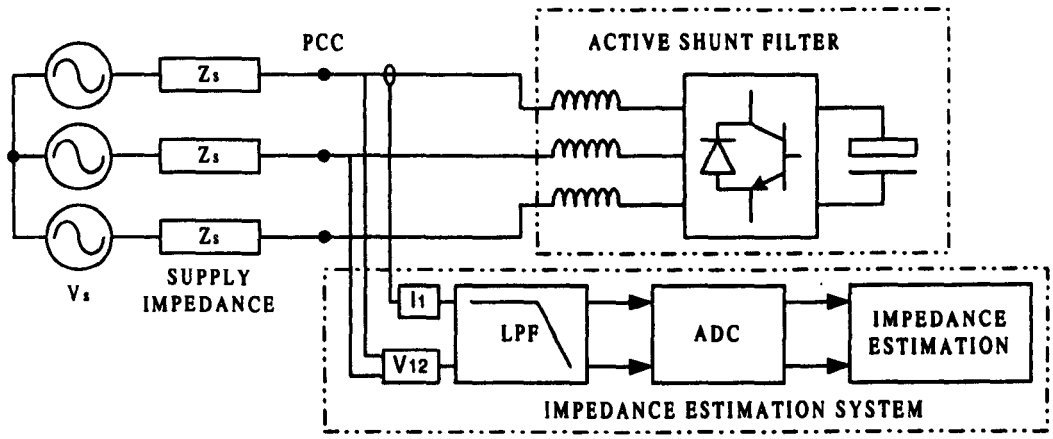

Fig. 1. The impedance estimation system

The ASF is controlled using a synchronously rotating frame of reference controller,[9]. Z_s is a Thevenin equivalent of the supply impedance. The impedance measurement system is made up of a current and voltage transducer, anti aliasing filters, a two channel A/D converter and a host PC for applying the data processing techniques to the experimental data.

As there are no other loads connected at the PCC the ASF draws only the current required to maintain the dc link voltage. The voltage across the ASF inductors is controlled so as to inject an approximately triangular current signal of 750μs duration. The amplitude of this current spike is limited by the voltage of the dc link and the ASF line inductance. Current injection amplitude has been limited to between 30-50A,well within the network rating. Both the voltage disturbance and the input current are recorded over a 160ms period using the dedicated hardware. The experimental hardware was equipped with 16 bit A/D converters with a sampling rate of 51.2 kHz. 2nd order Butterworth anti aliasing filters were used with a cut off frequency of 10 kHz. Such a high sampling rate was used in order to sample sufficient data points within the injected current pulse. The actual frequency of interest was between dc and 2kHz. The impedance estimate is calculated within the host PC according to (1). In order to negate the effect of the supply voltage from the impedance spectrum a two stage acquisition procedure was utilised. A data record of 160ms (eight cycles of 50Hz supply) of voltage and current data was taken immediately prior to the current injection. A further record of 160ms was taken with sampling commencing at the start of the current injection. By subtracting the first data set from the second the influence of the supply voltage, including its harmonics, can be removed from all measurements, the supply voltage is effectively short-circuited. The influence of any steady state current drawn is also removed. Certain assumptions have been made to justify this approach:

1. The supply impedance is balanced, linear and does not change during the data acquisition period.
2. The supply voltage amplitude and frequency are constant during the data acquisition period.

A balanced injection is applied so that the sum of the injected currents is zero. The injected current on phase 1 is $(+I_T)$ and the injected current on both phase 2 and phase 3 is $(-I_T/2)$. This technique will allow a minimum number of transducers and will reduce on-line data processing requirements. Fig. 2 shows the example supply system used for this work.

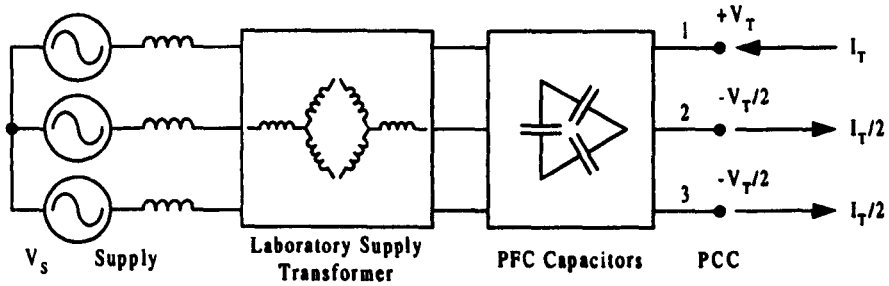

Fig. 2. Example supply system

The supply used is the standard 3 phase, 415 V, 50 Hz 100A laboratory supply. The experimental system is fed from a dedicated transformer with Power Factor Correction (PFC) capacitors connected to the supply in Delta formation. The experimental line voltage was 310 V and the ASF dc link voltage was controlled to be 680 V.

A single phase equivalent for this system may be derived. The voltages applied to both phase 2 and phase 3 at the PCC are identical and as a result a short circuit may be assumed. An approximate single phase equivalent of the laboratory supply is shown in fig. 3. The transformer and transmission

line have been modelled by a single series inductance and resistance. An impedance estimate from injection data may be used to identify the parameters in fig. 3. These values can be scaled appropriately to yield the three phase circuit parameters. It should be noted that this technique will only identify the positive sequence impedance terms of the supply.

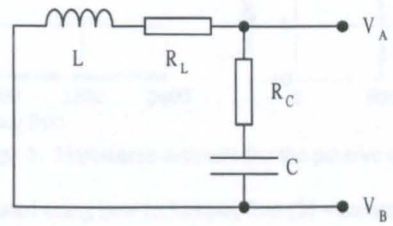

Fig. 3. Single phase equivalent of supply

IV. Experimental Results for the Linear System without Supply

In order to demonstrate the technique the procedure has been applied to the network shown in fig. 2. In order to correctly validate the technique an estimation of the impedance was initially made without the supply connected. The primary side of the transformer in fig. 2 was short-circuited in order to apply the estimation to a simple system without the supply connected. The dc link voltage of the ASF was separately supplied by an isolated source. The measured transients are shown in fig. 4.

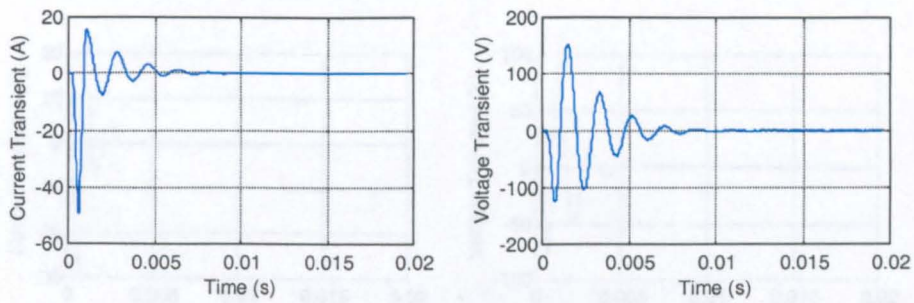

Fig. 4. Experimental transient waveforms for the passive system

In order to verify the method sinusoidal currents were injected into the system at frequencies up to 2kHz, using a WaveTek Datron Calibrator. Both V_{12} and i_1 were recorded over a number of complete cycles and hence the impedance could be plotted with frequency. Fig. 5 compares this measured impedance with the impedance estimated using the injection strategy. Line 1 (blue) shows the estimated impedance using the injection technique. Line 2 (red) shows the alternative estimate using sinusoidal injection at discrete frequency intervals.

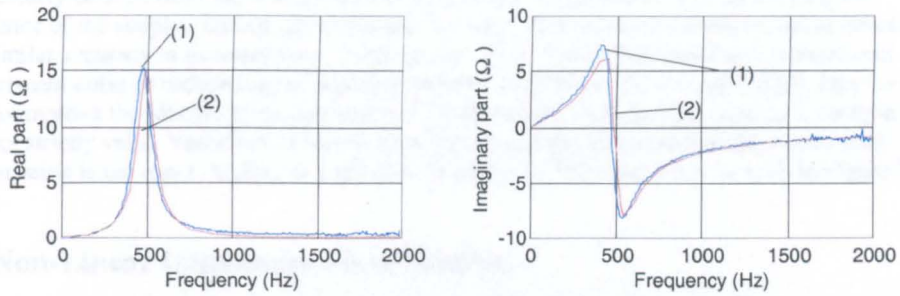

Fig. 5. Impedance estimate for the passive system

(Blue (1) – estimated using new technique, Red (2) – measured using calibrator)

V. Experimental Results for the Linear System with the Supply

The impedance estimation was repeated with the supply connected. Figure 6 shows the measured transient waveforms after the steady state data was subtracted. The supply impedance was estimated and is shown in fig. 7 as line 1 (blue). It was not possible to verify this result with an alternative measurement. The supply impedance should be dominated by the inductance of the transformer and the PFC capacitors. Hence the impedance of the supply should closely follow the impedance measured with the calibrator, as shown in fig. 5. Line 2 (red) in fig. 7 shows this impedance. There may be additional inductance associated with the supply and possibly some non-linear factors affecting the estimate.

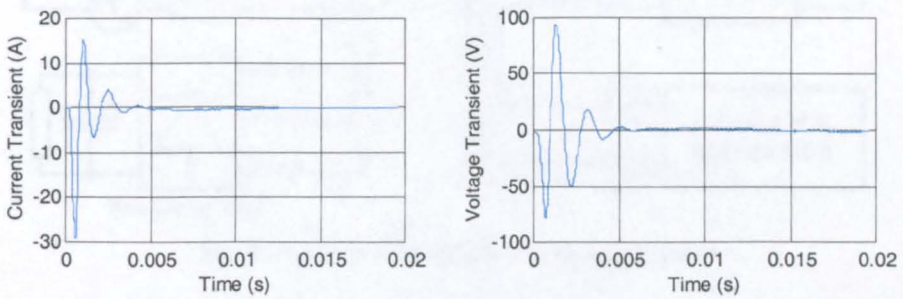

Fig. 6. Transient waveforms for the on-line supply system

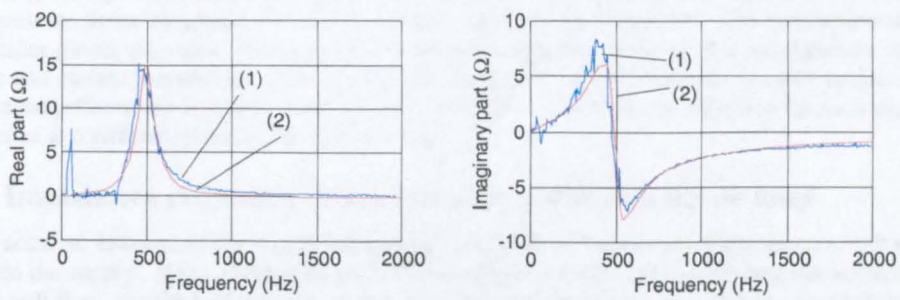

Fig. 7. Impedance estimate for connected supply

(Blue (1) – estimated using new technique, Red (2) – measured using calibrator)

It can clearly be seen from fig. 7 that the technique works very effectively in identifying the impedance of the supply. Indeed, the technique has been tried on several more complex structures with similar accuracy in measurement. Furthermore, if the SNR is decreased due to increased measurement noise or reduced signal injection strength correlation techniques, [4] [5], may be used in order to improve the identification performance. It should be noted that assumption 2 made in section III is not strictly valid. Variations in supply amplitude or frequency mean that the steady state compensation is not exact, leading to a spurious estimate at 50Hz which can be seen in Figure 7.

VI. Non-Linear Impedance Identification

The vast majority of impedance estimation work to date has been concerned with linear systems. Identification problems due to non-linear loads were considered in [10] although no mathematical analysis was used to compensate. In [7] non-linear loads are again considered, in this instance using the concept of running quantities. The effect that non-linear elements have on the impedance estimate obtained by the described technique shall be examined. Furthermore, an additional data processing technique shall also be used to improve estimated results.

Consider the circuit shown in fig. 8. An additional non-linear load – a capacitively smoothed diode bridge rectifier with a resistive load - has been connected to the supply. The experimental supply is rated at 50kVA and the additional non linear component is used to power a 1.6kW load.

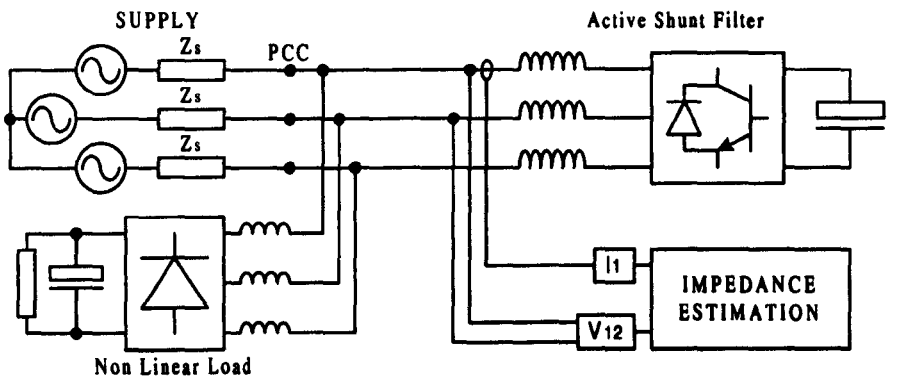

Fig. 8. Non-linear load connected to the supply system

If a measurement is made as before the resulting estimation of the supply impedance may be adversely affected by the presence of the NLL. If any of the diodes in the bridge rectifier are conducting during the transient data capture then they can be considered to be acting as short circuits. As a result the linear components of the additional load must be considered. The conduction state of the rectifier diodes may also change due to the transient injection resulting in discontinuities in the voltage and current waveforms. This will further corrupt the supply estimate. In order to demonstrate the potential effects two injection cases will be considered. The transient injection for each case will commence at a different point in the supply cycle.

VII. Impedance estimates in the presence of the non linear load

For an accurate estimate of the supply impedance ideally all of the measured transient current should flow into the supply. If the diode bridge rectifier interferes with the estimation process, some of the current will flow into the bridge itself. In test 1 the injected transient was timed to occur just before the conduction of the diodes in phases 1 and 3 (approximately 0.02 s in Fig 9). Fig. 9 shows the line current and DC link of the capacitively smoothed diode bridge.

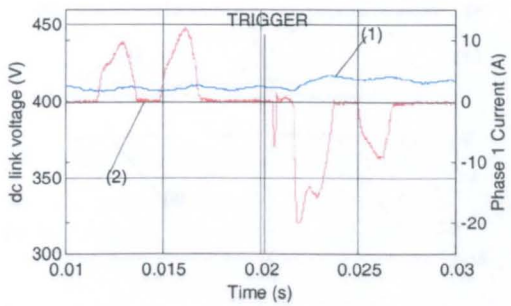

Fig. 9. DC link voltage (blue) (1) and diode bridge current (red) (2) for test 1

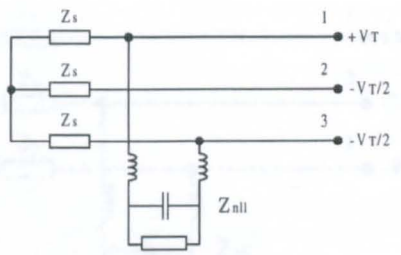

Fig. 10. Equivalent injection circuit for test

A small pulse of current is drawn by the bridge at approximately 0.021 s, i.e. before natural conduction of the diode in this line. Further distortion can be seen at approximately 0.022 s; the current drawn by the conducting diode is quite distorted. In addition the dc link voltage of the diode bridge rectifier increases to a value larger than its pre transient value. These changes to the conduction of the diode and DC link voltage indicate that some of the injected transient current has penetrated the diode bridge and consequently the transient decay and impedance estimate will be distorted. The impedance which is now being estimated is now a combination of the supply impedance and the DC link impedance (as shown in Fig. 10), although the discontinuities in the current measurement will distort the estimate. The impedance estimate from this data is illustrated in Fig. 11.

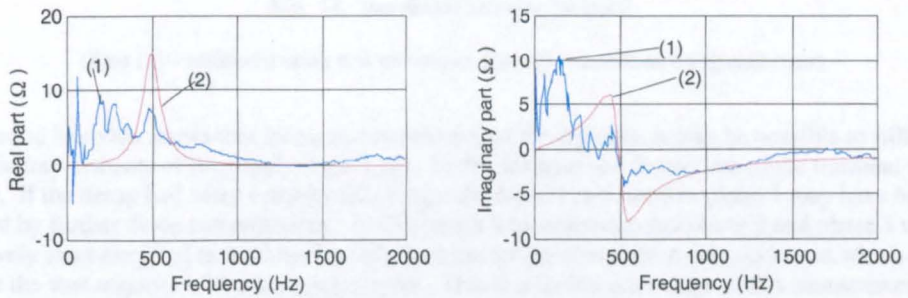

Fig. 11. Impedance estimate test 1

(Blue) (1) – estimated using new technique, Red (2) – measured using calibrator)

A second test (test 2) was performed whereby the transient was injected well away from the conduction points for the diodes in phases 1 and 3. The diode bridge line current and DC link voltage are illustrated in Fig. 12; neither are significantly changed by the transient injection. This shows that the DC link has not been greatly affected by the transient. Fig. 13 shows the equivalent circuit topology for test 2. As the transient voltages for phase 2 and phase 3 are controlled to be the same, no transient current should flow between them. Hence the injection measurements should still estimate solely the supply impedance. The transient has decayed almost completely by the end of this test and further decays during the next time period where no diodes are conducting. The transient data from this injection was used to calculate a supply estimate. This impedance estimation is shown in fig. 14. Fig. 14 verifies that the supply estimation was still fairly good as was expected.

The two different estimates made in the presence of the NLL clearly show how this small additional load can affect the supply estimate. Test 1 illustrates that the time at which the injection is applied is critical. The amplitude of the voltage disturbance is also very important.

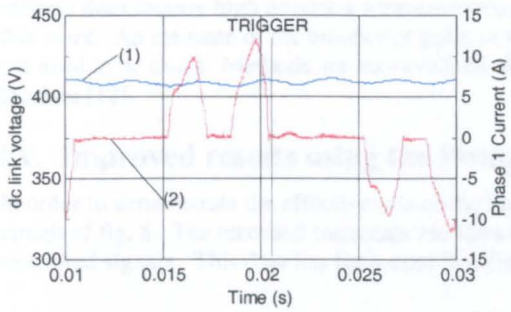

Fig. 12. Second injection line current

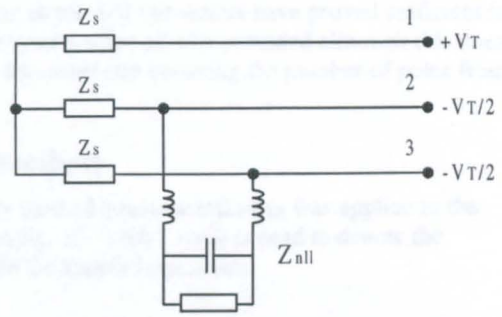

Fig. 13. Equivalent circuit for second injection

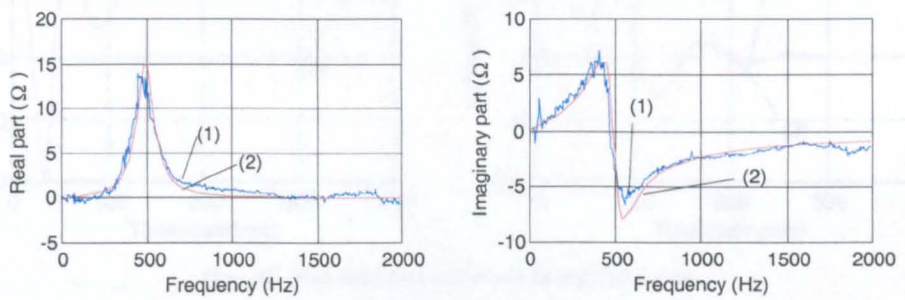

Fig. 14. Impedance estimate for test 2

(Blue (1) – estimated using new technique, Red (2) – measured using calibrator)

The second injection shows that by careful positioning of the injection it may be possible to still gain a satisfactory estimate of the supply impedance. In this instance the decay time of the transient was critical. If the decay had taken considerably longer the current measured in phase 1 may have been affected by further diode commutations. In this case it was important that phase 2 and phase 3 were effectively short circuited as it allowed a sufficient uncorrupted measurement window in which to capture the vast majority of the decaying signals. This is a further advantage of this measurement system although significant alterations would be required for an unbalanced system.

VIII. Extensions to the data processing algorithm

A numerical data processing technique has been used in order to improve the measurement technique and to overcome some of the problems introduced by non linear loads. The time domain extended Prony method [11] can be used to estimate a decaying transient signal from very few sampled data points. This is a parametric method that assumes the decay can be modelled as the solution to a homogenous differential equation. If a continuous section of transient data is recorded in a stage of the injection when transient current is only flowing into the supply a sufficient response may be extrapolated for the existing technique. Hence by recording only a small section of transient data a reasonable estimate of the supply may still be made. Using this method may allow far superior supply impedance estimation in the presence of non linear loads by removing discontinuities in the waveforms and so only estimating the supply impedance. There are further possible advantages to such an approach. The amount of measurement data may be reduced greatly, although this is at the expense of more processing power. Reducing the measurement duration will ensure that the technique is less vulnerable to variations in supply frequency, supply amplitude and changes in supply impedance. As the Prony method calculates the time domain response as a sum of exponential terms it is a simple task to directly calculate equivalent parameters of the supply as in fig. 3. The method involves a least squares approach so that noise rejection will be high. The Prony extrapolation

method does require high accuracy measurements, the 16 bit A/D converters have proved sufficient in this work. An estimate of the number of poles in the system must also be provided although this does not need to be exact. Methods are also available for automatically choosing the number of poles from the data [12].

IX. Improved results using the Prony method

In order to demonstrate the effectiveness of the Prony method a further injection was applied to the circuit of fig. 8. The recorded transients are shown in fig. 15. Line 2 (red) is used to denote the measured signals. This data has been used to estimate the supply impedance.

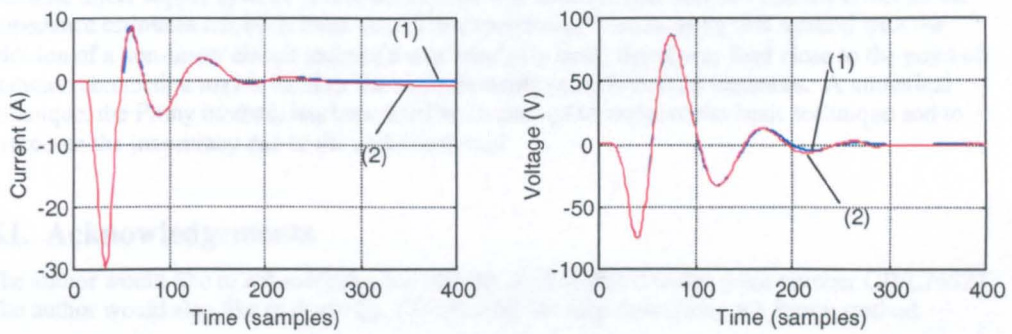

Fig. 15. Measured data and Prony extrapolated data

The Prony method was then applied to both the current and voltage waveforms. 90 samples of the transient were taken starting at time samples 53. These sections of data were extrapolated using the time domain extended Prony method. The number of system poles was automatically chosen by examining the magnitude and frequency of the poles initially generated. The extrapolated signals are recombined with the first measured samples. The reconstructed waveforms are shown in fig. 15. Line 1 (blue) is used to display the predicted waveforms. Fig. 16. Shows a comparison between the impedance estimate made with the unprocessed data and with the estimate made with the extrapolated waveforms. Line 1 (red) shows the result of using the unprocessed data. Line 3 (green) is used for the supply estimate made using the processed data. Line 2 (blue) shows the comparison estimate from earlier figures (measurement using the calibrator)

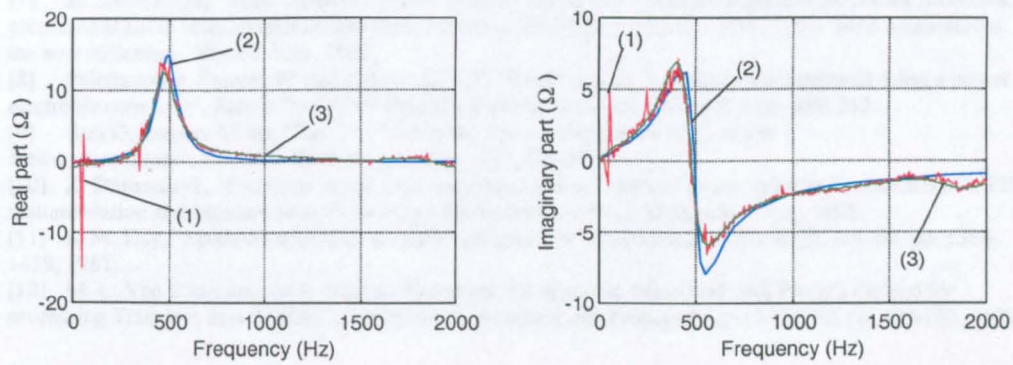

Fig. 16. Impedance estimate using Prony data extrapolation

A clear improvement can be seen when using the extrapolated data set. In this case the a diode commutation occurred towards the end of the transient decay. The Prony method allowed an estimation to be made without using this section of the measured data. As a result a large improvement was possible. The initial stages of the injection must still be made whilst no injection current is flowing through the NLL. A minimum length of continuous data is also required for a reasonable estimate. Work is currently being conducted on these problems with the aim of developing an on-line measurement system as part of the ASF.

X. Conclusion

An impedance measurement technique has been successfully demonstrated experimentally on an example linear supply system. A non-linear load was added to this network and the effect on the impedance estimates has been illustrated. The experimental results using this method with the addition of a non-linear circuit indicate that a relatively small non-linear load close to the point of common connection may invalidate the measurements made in certain instances. A numerical technique, the Prony method, has been used in an attempt to improve the basic technique and to overcome the inaccuracy due to the additional load.

XI. Acknowledgements

The author would like to acknowledge the support of the EPSRC under grant number GR/L76527. The author would also like to thank Dr. J.D. Paul for his help concerning the Prony method.

XII. References

[1] R. C. Dugan, M. F. McGranaghan, and H. W. Beaty, Electrical Power Systems Quality, 1 ed: McGraw Hill, 1996.

[2] A. Oliveira, J. C. Oliveira, J. W. Resende, and M. S. Miskulin, "Practical approaches for ac system harmonic impedance measurements," IEEE Transactions on Power Delivery, vol. 6, pp. 1721-1726, 1991.

[3] J. P. Rhode, A. W. Kelley, and M. E. Baran, "Line impedance measurement: A non disruptive wideband technique," presented at IAS Annual Meeting, Orlando, Florida, USA, 1995.

[4] A. S. Morched and P. Kundur, "Identification and modelling of load characteristics at high frequencies," IEEE Transactions on Power Systems, vol. PWRS-2, pp. 153-160, 1987.

[5] A. A. Girgis and R. B. McManis, "Frequency domain techniques for modelling distribution or transmission networks using capacitor switching induced transients," IEEE Transactions on Power Delivery, vol. 4, pp. 1882-1890, 1989.

[6] M. Nagpal, W. Xu, and J. Sawada, "Harmonic impedance measurement using three phase transients," IEEE Transactions on Power Delivery, vol. 13, pp. 272-277, 1998.

[7] Z. Staroszczyk, "Time dependant power systems impedance - Interpretation and measuring problems," presented at IEEE instrumentation and measurement technology conference (IMTC99): Measurements for the new millenium, Venice, Italy, 1999.

[8] Palethorpe B, Sumner M and Thomas D W P, "Power system impedance measurement using a power electronic converter", Proc ICHPQ2000 Orlando, Florida, USA Oct 2000, vol. 1 pp. 208-213

[9] Butt D, Sumner M and Clare J C, "A novel control technique for high power active shunt filters", Proc PEMC'98 Prague, Sept 1998, CD-ROM

[10] Z. Staroszczyk, "Problems in real time wide band identification of power systems," presented at IEEE Instumentation and Measurement Technology Conference, St. Paul, Minnesota, USA, 1998.

[11] S. M. Kay, "Spectrum analysis - a modern perspective," Proceedings of the IEEE, vol. 69, pp. 1380-1419, 1981.

[12] M. L. Van Blaricum and R. Mittra, "Problems and solutions associated with Prony's method for processing Transient data," IEEE Transactions on Antennas and Propagation, vol. AP-26, pp. 174-182, 1978.

Estimation of Power Supply Harmonic Impedance Using a Controlled Voltage Disturbance

Mark Sumner, Ben Palethorpe, David Thomas
School of Electrical and Electronic Engineering
University of Nottingham, UK

Pericle Zanchetta
Politecnico di Bari, Italy

Maria Carmela Di Piazza
University of Palermo, Italy

Abstract: **A novel method for power system impedance estimation is presented. The method employs a power converter to inject a voltage transient onto the supply system. The impedance is estimated through correlation of the measured voltage and current transients. Simulations and experimental results demonstrate the effectiveness of this measurement technique.**

I. INTRODUCTION

The estimation of the effective source impedance of a power system from a particular point of connection is an important and challenging task. An accurate knowledge of the harmonic impedance allows the identification of potential system harmonics and resonance problems and is useful for passive harmonic filter design [1]. Additionally it can provide significant improvements to the design and operation of active filters, particularly if the impedance can be monitored in real-time [2,3]. The lack of a good knowledge of network structure and parameters usually leads to difficulty in simulation or prediction of harmonic propagation.

Several methods have been proposed in the literature to measure on-line the frequency characteristic of the impedance in a power system and they are usually based on the injection of a current disturbance onto the energised system and on the measurement of the resulting voltage transient [2-9]. This may be through the connection of a transformer (inrush current) [8] or a capacitor bank (normally used for power factor correction) [7]. These measurements are then evaluated using signal-processing techniques to provide an impedance estimation. In both cases there is no true control over the disturbance, and no facility for continual on-line measurement. This paper describes a novel technique for measuring the power system impedance back to source. The technique employs a power electronic converter, which injects a voltage transient onto the network via an inductor. The resulting current is correlated with the disturbance voltage to determine the impedance [3]. As the technique employs controlled power electronic devices it may be used as a stand alone piece of a portable measurement equipment, or it may be embedded into the functions of an Active Shunt Filter for improved harmonic control [2,11].

The algorithms have been evaluated using the MATLAB maths processing package, on data obtained from circuit simulation using the SIMULINK Power Systems Blockset (PSB). A very good impedance estimation is achieved and the simulation results indicate that this technique works effectively for various simple network topologies. Experimental validation is also presented for several test impedance structures.

II. THE IMPEDANCE ESTIMATION METHOD

The basic principle of operation is simple, and is described in more detail in [3]. A voltage transient is injected onto the network via a coupling inductor. The transient current and voltage measured at the point of coupling to the supply are recorded over the transient period – in this case 160 ms. To remove the effects of the source voltage itself from the transient, the current and voltage measured during the 160 ms before the transient are recorded and subtracted from the transient data. The resultant data set is processed using the MATLAB embedded function TFE (Transfer Function Estimation). The TFE function estimates the transfer function of a system with measured input and output quantities using *Welch's averaged periodogram* method [10]. I this case the measured voltage is the input vector and the measured current is the output vector. The voltage magnitudes at each frequency (calculated from a DFT) are squared to form the Power Spectral Density of the input quantity, P_{XX}. The products of the DFTs of the voltage and current sections are averaged to form P_{XY}, i.e. the Cross Spectral Density of input and output quantities. (The data is windowed using a Hanning Window). The system transfer function is then found by dividing P_{XX} by P_{XY}. Finally, the estimated impedance characteristic is compared with the ideal one obtained by means of the Bode diagram of the calculated theoretical impedance of each model, in order to evaluate the accuracy of the estimation.

For the simulation work three system/load models have been adopted, as illustrated in Figs. 1 - 3. (In each figure, the point of coupling of the transient injection circuit is the left-hand side of the model.) The representation of Figure 1 is a very simplified system where only an inductive load is taken into

account [7]. In models 2 and 3 the representation is more detailed to include components such as power transformers, transmission lines, feeder load etc. In particular in load model 2 a 1 MVA power transformer is represented by an R-L series branch, and a 3 km long transmission line is represented by an R-L series branch and a capacitance shunt branch. In this case a shunt R-L branch represents the system load. Model 3 accurately represent a medium scale power system. In particular a 1 MVA transformer is represented by a series inductive branch while an R-L series branch and an R-C shunt branch represent a 3-km long transmission line. In addition, two R-L loads are represented in model 3 as shunt R-L branches: the one placed before the transmission line, in particular, is represented together with its reactive power compensating capacitor.

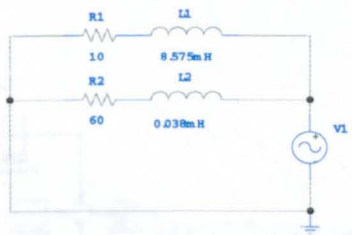

Fig. 1 - Model 1 – a simplified system considering only the transformer inductance

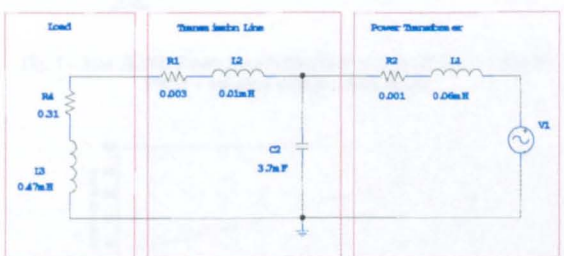

Fig. 2 - Model 2 – including transformer, transmission line and a load.

For the simulations carried out in this work, a PWM voltage source was implemented, as this best represents the controlled voltage source used in the experimental rig. The transient reference is shown in Fig. 4. This waveform injects a signal rich in the harmonics of 50 Hz, and has sufficient resolution (6.25 Hz) to provide a useful impedance map.

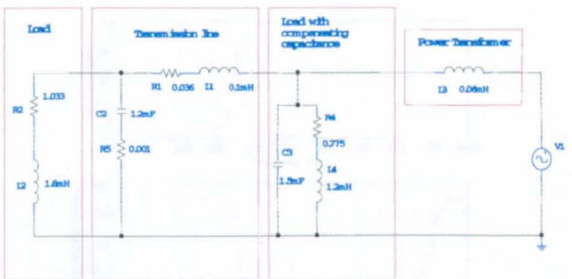

Fig. 3 - Model 3 including transformer, transmission line, load and power factor correction capacitor

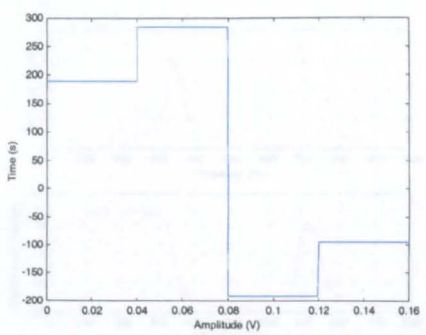

Fig. 4 – Modulating transient voltage (160ms)

It is necessary, to incorporate a current control within the transient injection block to ensure that the injected current has a small magnitude – 10 A – to prevent damage to the power converter or power system components. This control comprises a current feedback control loop through a PID regulator (with a reference of 0 A). Added to the output of this regulator is a replica of the supply, as a feed-forward compensation, and the transient signal itself. The full simulation circuit is shown in Fig. 4, with the transient injection system expanded.

The simulation results presented show the identified amplitude and phase vs frequency of the estimated impedance, as well as the ideal impedance. It can be seen from Figs. 6 to 8 that the estimates are very good for all the models – the two traces are barely distinguishable from each other. Moreover the measured current maintains an average value within 10A – within the currents limits of even small power electronic devices. It should be noted that these results include a white noise signal with amplitude of 1% of the maximum current amplitude. All quantities are sampled using an appropriate anti-aliasing filter.

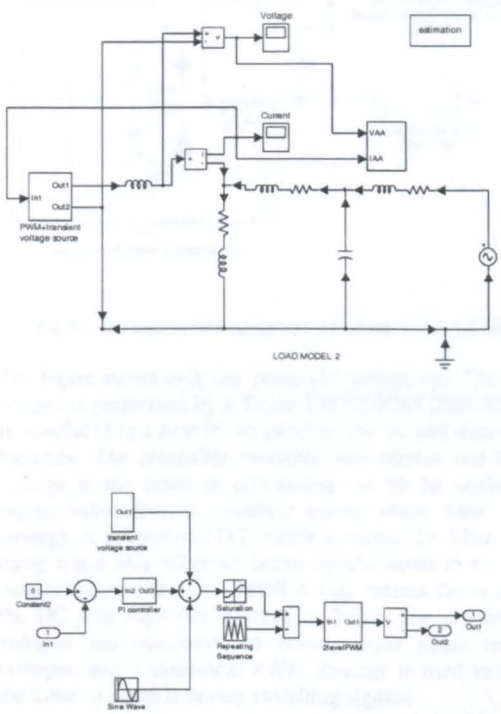

Fig. 5 – SIMULINK Power System Blockset scheme of model 2 and the PWM + transient voltage source block.

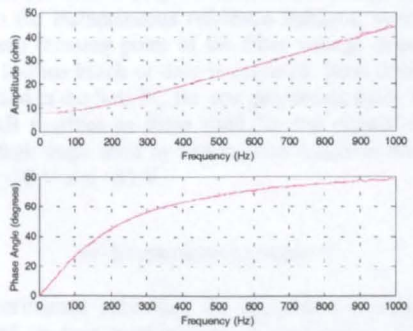

Fig. 6 – Estimate of model 1 impedance (the magenta trace is the ideal impedance, the red trace is the estimated impedance)

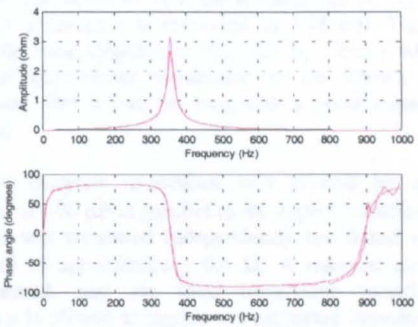

Fig. 7 – Estimate of model 2 impedance (the magenta trace is the ideal impedance, the red trace is the estimated impedance)

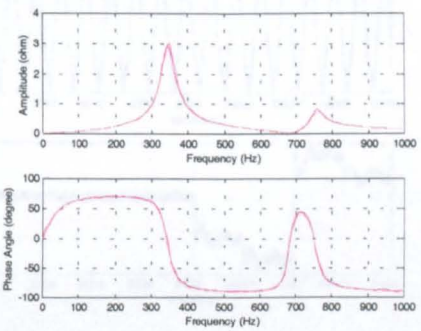

Fig. 8 – Estimate of model 3 impedance superimposed with noise (the magenta trace is the ideal impedance, the red trace is the estimated impedance)

In general, the simulation results show that linear system impedances can be estimated to a good accuracy using this technique. Resonant peaks are correctly identified, and the resolution of 6.25 Hz is entirely adequate for impedance estimation purposes. The duration of the transient and steady state data capture time is therefore 320 ms total. There is obviously a tradeoff between length of transient and data capture time (ie speed of estimate update) vs resolution.

III. EXPERIMENTAL PROCEDURE

The initial simulation work was carried out using a single phase circuit approximation only. The method was developed for three phase power systems and therefore the impedance estimation method was validated using a three phase experimental facility based upon a typical active shunt circuit configuration [11]. The experimental setup is illustrated in Fig 9. The initial work reported here assumes a balanced three phase load.

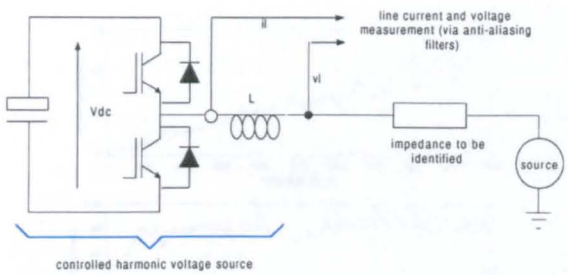

Fig. 9 – The experimental equipment (one phase only is illustrated)

The figure shows only one phase (for simplicity). The overall control is performed by a Texas TMS320C44 DSP. The DSP is interfaced to a host PC to provide user i/o and data capture facilities. The controller measures line current and the line voltage at the point of connection via 16 bit analogue to digital converters; a standard active shunt filter control strategy is employed [11], which controls the filter current using a d-q axis reference frame synchronised to the supply fundamental voltage. (A small d axis current flows to keep the DC link capacitor charged to Vdc). The d-q reference voltages are modulated to instantaneous phase reference voltages, and a sinusoidal PWM strategy is used to convert the these to suitable device switching signals.

The transient injection is stimulated by a user request. Before the transient is injected a 160 ms period of data is captured to assess the 'steady state' harmonics present. The transient waveform (of similar shape to that shown in Fig. 4.) is then added to the instantaneous reference voltages, synchronised to the zero crossing point of the filter voltage demand, and again a 160 ms block of data is captured. Both data sets are then passed to the host PC for post processing using the same MATLAB routines as those used for the simulation work. The voltage steps used by the injected transient are +70 V, +105 V, -70 V and –35 V.

IV. EXPERIMENTAL RESULTS

The experimental procedure for impedance estimation was performed on four combinations of components. Firstly the impedance of the supply transformer alone was estimated. This was assumed to be predominantly inductive. The measured line voltage and current are illustrated in Fig. 10, and the resultant impedance estimate is shown in Fig. 11. Again amplitude and phase versus frequency are plotted for the estimated impedance. It can be seen that supply transformer has a leakage inductance of 1.15 mH.

To verify this a known inductance of 0.6 mH was connected in series with the supply transformer and the experiment repeated. The result of this test is illustrated in Fig 12. The combined inductance is measured as 1.78 mH. Fig 12 also shows the ideal impedance obtained by simply adding the measured transformer impedance to the known inductor impedance, and it can be seen that a good correlation is obtained.

A more complex impedance was created by adding a capacitor of 100 μF in parallel to the supply transformer. The capacitor was measured independently and found to have a resistance of approximately 0.4 Ω. A resonant circuit was now formed, and the ideal impedance variation with frequency is plotted alongside the estimated impedance from voltage injection in Fig 13.

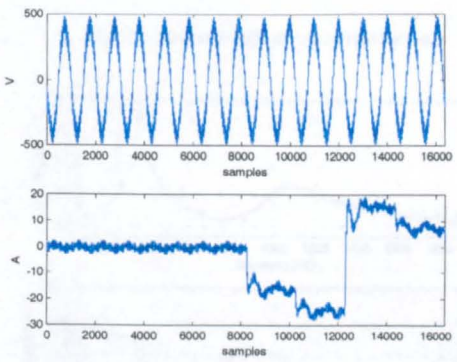

Fig 10 – The transient line voltage and current for the supply transformer only

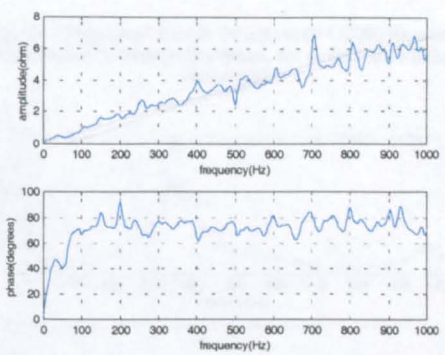

Fig 11 – The supply tranformer impedance estimate

The fourth test was performed on a pi connected circuit as shown in Fig 14. In this case R1 and L1 are the supply transformer, C1 is the 100 μF capacitor, L2 is the 0.6 mH inductor, and C2 is a 50 μF capacitor. The measured voltage and current during the transient are shown in Fig 15, and the ideal and estimated impedances are shown in Figures 16a and 16b, for different frequency scales.

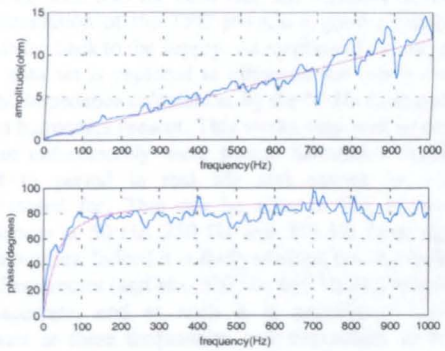

Figure 12 – The supply transformer in series with the 0.65 mH inductor (The blue trace is the impedance estimate, the magenta trace is the ideal impedance)

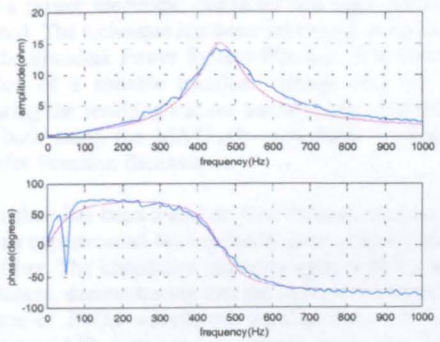

Figure 13 – The supply transformer with a 100 uF capacitor connected in parallel. (The blue trace is the impedance estimate, the magenta trace is the ideal impedance)

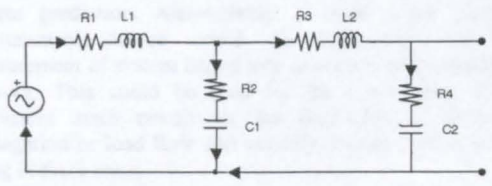

Fig 14 - equivalent single phase circuit for test 4

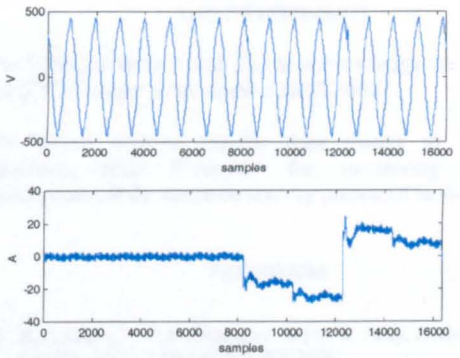

Fig 15 – Measured voltage and current for test 4

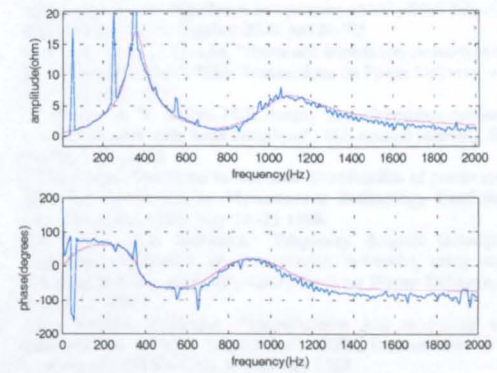

Fig 16a – Impedance estimate for test circuit 4 (2000 Hz scale). (The blue trace is the impedance estimate, the magenta trace is the ideal impedance)

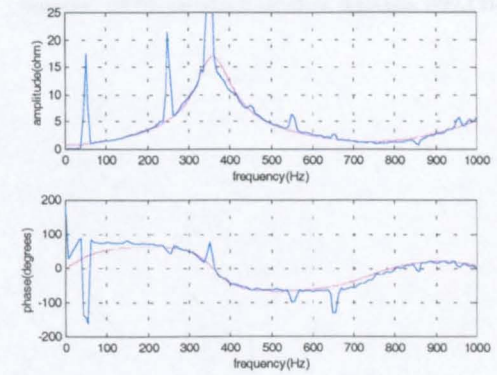

Fig 16b – Impedance estimate for test circuit 4 (1000 Hz scale). (The blue trace is the impedance estimate, the magenta trace is the ideal impedance)

It can be seen that for each test, the transient injection and implementation of the TFE provide a good estimate of the impedance back to the supply. As mentioned earlier, a 'steady state' data set is captured to eliminate the errors introduced into the impedance calculation, by the 50 Hz source and other system harmonics present. This works very well in simulation [3], but unfortunately these source harmonics change from period to period in real life and cannot be accurately compensated for. This can be seen in Fig 16 where the impedances at 50 Hz, 250 Hz and 350 Hz form significant discontinuities. Indeed it is fairly obvious that the estimates at these frequencies (and also 550 Hz, 650 Hz etc) will probably be inaccurate, and as such it is possible to ignore the estimates at these frequencies and interpolate, as has been carried out for Figs 11,12 and 13.

V. CONCLUSIONS

A new method to estimate impedance of a power system using a power electronic converter has been proposed and validated. The technique has been developed using simulation with the Simulink Power System Blockset. It is based on the injection of a suitable transient voltage onto the system, measuring the resulting current transient and then processing them both using the MATLAB embedded function - TFE (Transfer Function Estimation).

The method has been tested on four different passive circuits using an experimental facility based upon a three phase active shunt filter. The impedance estimates agree with the predicted impedances, demonstrating that the method works well in the presence of PWM waveforms, measurement noise, limited resolution (A/D converters), general noise due to power system harmonics and the switching noise present in a large experimental power electronic laboratory.

The estimation method can be embedded into the control algorithm for an active shunt filter to provide on-line impedance estimates for control optimisation and reference current prediction. Alternatively, a stand alone portable measurement device could be constructed for the measurement of system impedance at several points around a network. This could be used for the construction of an equivalent mesh circuit for the prediction of harmonic propagation or load flow and stability studies. Work is on-going in these areas.

ACKNOWLEDGMENTS

The British authors would like to acknowledge the support of the EPSRC under grant number GR/L76527.

The Italian authors express their thanks to "Consiglio Nazionale delle Ricerche" for sponsoring them in development of the research activity presented in this paper.

REFERENCES

[1] R. C. Dugan, M. F. McGranaghan, and H. W. Beaty, *Electrical Power Systems Quality*, 1 ed: McGraw Hill, 1996.

[2] B. Palethorpe, M. Sumner and D.W.P Thomas, "System impedance measurement for use with active filter control", IEE PEVD 2000, London UK, Sept 2000, pp 24-28.

[3] M.C di Piazza, P Zanchetta, M Sumner and D.W.P. Thomas, "Estimation of load impedance in a power system", IEEE PES ICHQP 2000, Orlando USA, October 2000, pp520-525

[4] M.Nagpal, W.Xu, J.Sawada, "Harmonic impedance measurement using three phase transients", IEEE Transactions on Power Delivery, vol. 13, No. 1, January 1998.

[5] J. P. Rhode, A. W. Kelley, M.E. Baran, "Line impedance measurement: a non- disruptive wide band technique", IAS Annual Meeting, Orlando, Florida, USA, 1995

[6] Z. Straszczyk, "Problems in real time identification of power systems", IEEE Instrumentation an Measurement Technology Conference, St Paul, Minnesota, USA, May 18 -21 1998.

[7] A.A Girgis, R.B McManis, "Frequency domain techniques for modelling distribution or transmission networks using capacitor switching induced transient", IEEE Trans on Power Delivery, vol. 4, No.3, July 1989.

[8] A.S. Morched, P.Kundur ,"Identification and modelling of load characteristics at high frequencies", IEEE Transactions on Power Systems, vol. PWRS-2 No. 1, February 1987.

[9] Oliveira, J. C. Oliveira, J. W. Resende, and M. S. Miskulin, "Practical approaches for ac system harmonic impedance measurements," *IEEE Transactions on Power Delivery*, vol. 6, pp. 1721-1726, 1991.

[10] MATLAB Reference Guide, The MathWorks Inc, 1992

[11] D Butt, M Sumner and J.C. Clare, "Harmonic compensation in active shunt filters using controllers employing harmonic rotating frames of reference", EPE99, Lausanne Switzerland, September 1999, CD-ROM.

IEEE TRANSACTIONS ON POWER ELECTRONICS, VOL. 17, NO. 2, MARCH 2002 207

A Technique for Power Supply Harmonic Impedance Estimation Using a Controlled Voltage Disturbance

Mark Sumner, Ben Palethorpe, David W. P. Thomas, Pericle Zanchetta, and Maria Carmela Di Piazza

***Abstract*—A method for power system impedance estimation is presented. The method employs a power converter to inject a voltage transient onto the supply system. As the technique employs controlled power electronic devices it may be used as a stand alone piece of a portable measurement equipment, or it may be embedded into the functions of an active shunt filter for improved harmonic control. The impedance is estimated through correlation of the measured voltage and current transients. Simulations and experimental results demonstrate the measurement technique is highly accurate and effective.**

***Index Terms*—Impedance measurement, industrial power systems, power quality, power system measurements.**

I. INTRODUCTION

THE estimation of the effective source and load harmonic impedance from a particular point of connection is an important and challenging task. Harmonic penetration studies, transient analysis, and passive harmonic filter design [1]–[3] would all benefit from an accurate knowledge of the harmonic impedance of the power system. Additionally, it can provide significant improvements to the design and operation of active filters, particularly if the impedance can be monitored in real time [4], [5], [7], [11]. Usually there is very little data available, but, even with adequate documentation the complexity and dynamic nature of the power system may prohibit reliable estimation of the harmonic impedance. Measurement of the harmonic impedance is also very difficult because the power system is a coupled three phase circuit; the power supply and loads may contain harmonic sources and signals of significant or measurable levels have to be injected across the whole range of frequencies of interest.

Several methods have been proposed to measure the on-line frequency dependent characteristics of the power system impedance. Usually these methods involve the creation of a disturbance on the power system and the measurement of the voltage and current transients from which the harmonic impedance is evaluated using suitable signal processing techniques based on Fourier analysis. In [1], [2], [6] high frequency voltage and current transients are created through capacitor bank switching and then spectral analysis of the transients provides the frequency domain impedance characteristics. Switching of a load to provide a 100–500 μs/10–100 A current pulse has also been suggested in [7] where the harmonic impedance is derived from the analysis of the voltages and currents before and after the disturbance. In all these methods, however, the disturbances are uncontrolled and the presence of power system harmonics are not adequately accounted for [12]. In addition, the accuracy of these methods is not quantified. Rhode *et al.* [10] proposed using a network analyzer to measure the system harmonic line impedance, but this is a relatively expensive solution which is not appropriate for real time monitoring of the three phase power system. The work is further developed in [14], [15] to provide an inexpensive measurement technique using a standard PC with good audio band i/o capabilities. A more advanced technique which uses fully controlled current injection and can distinguish between the load and source characteristics has been proposed by Tsukamoto [8]. In [8] inter-harmonics are injected assuming the source and load only provide voltage and current distortion at the harmonic frequencies. The power system harmonic impedance is then interpolated from the inter-harmonic measurements, with a standard deviation of 10% quoted for experimental measurement of a supply transformer. In [16], Vermeulen employs a MOSFET bridge to inject a pseudo random binary sequence, to identify the impedance of a voltage transformer. However, this work identifies the impedance of pieces of equipment when they are disconnected from the supply utility, as opposed to when they are fully operational.

This paper describes a novel technique for measuring the power system harmonic impedance back to the source. The technique involves a power electronic converter, which injects a voltage transient on to the energized network via an inductor. The injected voltage transient has a frequency resolution of 6.25 Hz which provides inter-harmonic values and thus allows for the interpolation of the system impedance at the harmonic frequencies. The resulting transient current is correlated with the disturbance voltage to determine the frequency dependent impedance [5]. As the technique employs controlled power electronic devices it may be used as a stand alone piece of portable measurement equipment, or alternatively can be embedded into the functions of an active shunt filter for improved harmonic control [4], [5]. The major advantage of this method when compared to those described in [1], [2], [6], [7] is that the injected transient is fully controlled. It can be triggered at any instant (or on a periodic basis), and employs current controllers which can be used to limit the size of the peak of the current disturbance. When compared to the methods described in [8], [10], the work described here uses a much

Manuscript received May 15, 2001; revised September 15, 2001. This work was supported by the EPSRC under Grant GR/L76527 and Consiglio Nazionale delle Ricerche. Recommended by Associate Editor J. H. R. Enslin.

M. Sumner, B. Palethorpe, D. W. P. Thomas, and P. Zanchetta are with the School of Electrical and Electronic Engineering, University of Nottingham, University Park, Nottingham NG7 2RD, U.K.

M. C. Di Piazza is with the Department of Electrical Engineering, University of Palermo, Palermo 90128, Italy.

Publisher Item Identifier S 0885-8993(02)02241-X.

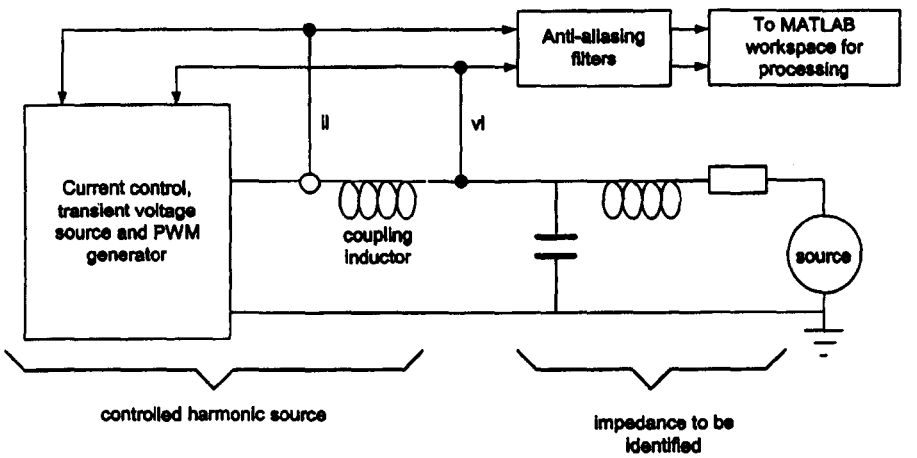

Fig. 1. Simplified scheme of the overall system simulation.

shorter transient duration and provides a faster update of the impedance measurement.

The algorithms have first been evaluated using the MATLAB [9] maths processing package, on data obtained from the circuit simulation using the SIMULINK [9] Power Systems Blockset (PSB). A very good harmonic impedance estimation is achieved with the simulation data and experimental results indicate that this technique works effectively for various simple network topologies.

II. The Impedance Estimation Method

The basic principle of operation is simple. A voltage transient is injected onto the power network via a coupling inductor. The transient current and voltage measured at the point of coupling to the supply are recorded over the transient period—in this case 160 ms. This duration was chosen simply to provide a frequency resolution of 6.25 Hz. This resolution means that a reasonably smooth plot of impedance versus frequency can be obtained, easing the process of deriving a transfer function for the impedance. In addition, the method provides a significant number of points other than the common noninteger harmonics (fifth, seventh, eleventh, and thirteenth). This is advantageous in providing sufficient results to interpolate around these common harmonics, as will be seen in Section IV. The 160 ms duration provides a compromise between frequency resolution and transient duration/update time.

The shape of the voltage transient should excite the harmonic frequencies of interest. The resultant data set, is processed by examining the frequency content of both measurements. The obvious approach is to obtain a discrete fourier transform (DFT) of both of the captured waveforms, and an impedance estimate can be found by dividing the DFT of the voltage measurement by the DFT of the current measurement. A better approach is to use the MATLAB embedded function transfer function estimation (TFE). The TFE function estimates the transfer function of a system with measured input and output quantities using *Welch's averaged periodogram* method [9]. In essence, the voltage data

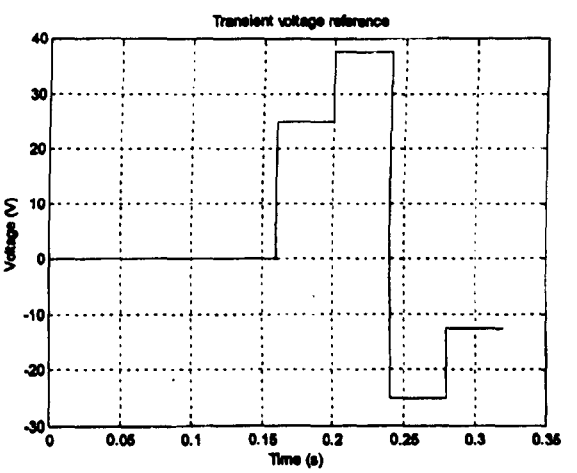

Fig. 2. Modulating transient voltage (160 ms).

set is auto correlated, and a cross correlation is obtained of the voltage and current data sets, before the DFT is employed. This approach improves the signal to noise ratio by filtering out the uncorrelated noise. In particular this reduces the large absolute errors in the impedance estimate at the frequencies where the voltage and current signal strengths are low. The correlated noise is either at much higher frequencies (converter switching frequency) or can be corrected for directly (such as by subtracting 160 ms of the pre-transient data from the transient data).

The system simulated is illustrated in Fig. 1. A controlled voltage source is connected to the supply network via a coupling inductor. In this case, the network comprises a 50 Hz source with predominantly inductive impedance and with a capacitor connected in parallel. At the fundamental frequency (50 Hz) there are thus two sources; the supply and the 50 Hz component of the injected transient. By the superposition theorem the total fundamental currents and voltages must be the superposition of the contribution from the two sources. The contribution from the

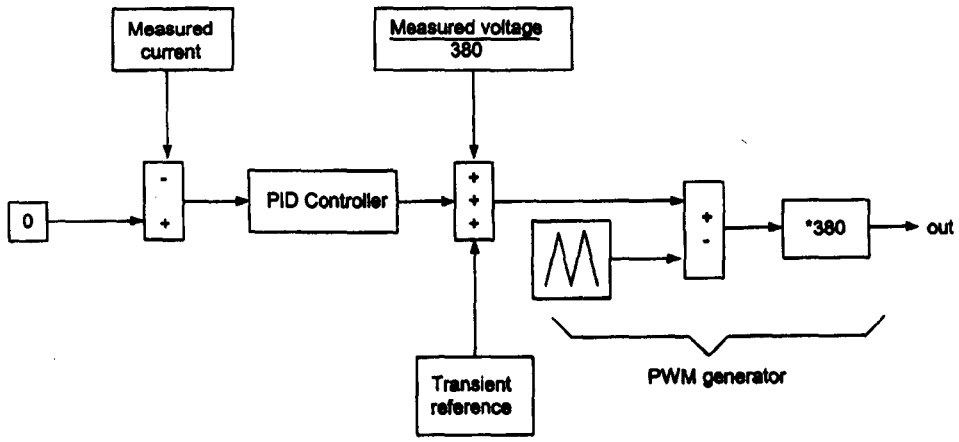

Fig. 3. Simplified scheme of the current control and transient source block.

supply can be compensated for by assuming that it is static over the measurement period. The voltages and currents are recorded for eight cycles just before the injection of the transients (T = 160 ms) and then subtracting this from the subsequent transient voltage and current. If the sample period is Δt, then the superimposed transient data samples $D_S(k\Delta t)$ are given in terms of the sampled pre-injection samples $D_P(k\Delta t - T)$ and the sampled post-injection transients $D_T(k\Delta t)$ by

$$D_S(k\Delta t) = D_T(k\Delta t) - D_P(k\Delta t - T) \qquad (1)$$

where $k = 1$ to $(T/\Delta t)$ and is an integer number.

The supply will also be a source of harmonics on a practical system, but it can be shown that (1) will also compensate for the supply harmonics.

The transient voltage signal must excite the frequency range of interest. For this project, the frequency range was limited to 1 kHz, as this contained the predominant low order harmonics associated with large nonlinear loads such as power electronic converters. The waveform shown in Fig. 2 was found to contain sufficient spectral excitation over this frequency range, and provided a frequency resolution of 6.25 Hz. The magnitude has been chosen experimentally to prevent an excessive injection current. Initial research assumed an ideal source [5]. In the simulations presented here, a more realistic source was chosen—a pulse width modulated (PWM) inverter. As this is no longer an ideal source, the supply fundamental and harmonics would cause a large circulating current through the transient source. Therefore, a current controller must be employed to reduce this current to zero; a PID controller is used, with additional feedforward control obtained using the voltage measurement at the point of coupling. The final control for the transient voltage source is shown in Fig. 3.

Three system/load models have been adopted, as illustrated in Figs. 4–6. These loads correspond to the experimental loads used. The representation of Fig. 4 is a simplified system where only the supply inductance is estimated. In models 2 and 3 the representation is more detailed to include resonances caused by

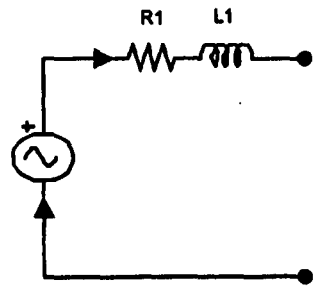

Fig. 4. Model 1—a simplified system considering only the transformer inductance ($R1$ = 0.4 Ω, $L1$ = 1.15 mH).

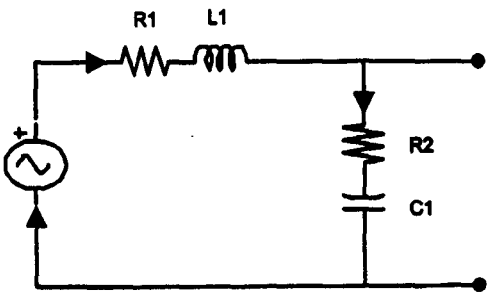

Fig. 5. Model 2—including transformer, and a parallel capacitance ($C1$ = 100 μF, $R1$ = 0.4 Ω).

added parallel capacitance. It should be noted that the work reported in [5] considers distribution level components such as power transformers, transmission lines, feeder load etc. To complete the simulated system, random noise and truncation have been incorporated onto the measurements to simulate the effects of a real digital data acquisition system. The noise has an amplitude of 0.1 A, and the truncation is chosen such that a 16 bit analogue to digital converter is simulated.

The simulation results presented show the identified amplitude and phase versus frequency of the estimated impedance.

210 IEEE TRANSACTIONS ON POWER ELECTRONICS, VOL. 17, NO. 2, MARCH 2002

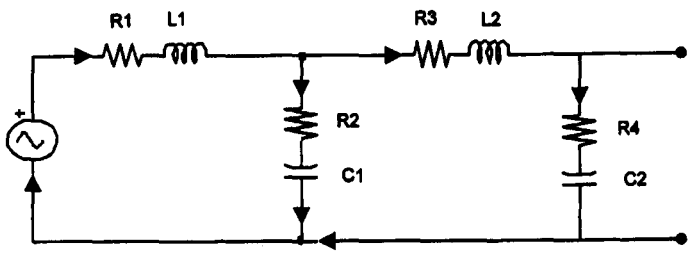

Fig. 6. Model 3 including transformer, parallel capacitor, line inductor and further parallel capacitor ($R3 = 0.04\,\Omega$, $R4 = 0.4\,\Omega$, $L2 = 0.6$ mH, $C2 = 50$ mF).

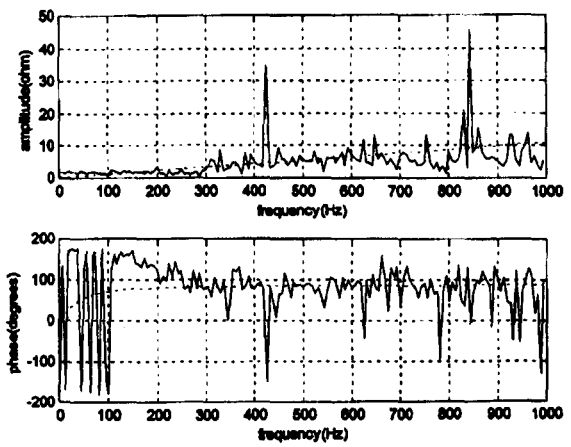

(a)

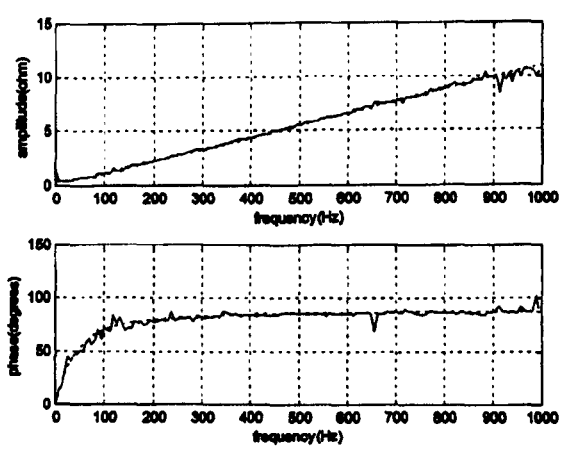

(b)

Fig. 7. (a) Estimate of model 1 impedance (dotted trace is the ideal impedance, solid trace is the estimated impedance), using straightforward DFT. (b) Estimate of model 1 impedance (dotted trace is the ideal impedance, solid trace is the estimated impedance), using TFE function.

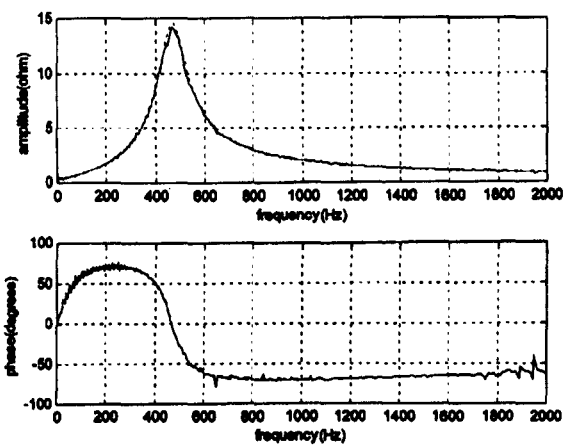

Fig. 8. Estimate of model 2 impedance (dotted trace is the ideal impedance, solid trace is the estimated impedance).

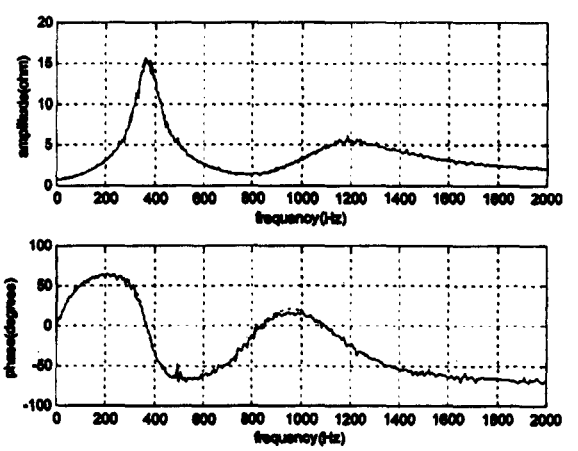

Fig. 9. Estimate of model 3 impedance (dotted trace is the ideal impedance, solid trace is the estimated impedance).

as well as the ideal impedance. Fig. 7(a) shows an estimate of the impedance of circuit 1 when the impedance is calculated directly from a DFT of the voltage measurement divided by a DFT of the current measurement. This estimate is extremely inaccurate. At the frequencies where there is low excitation and low current strength, the uncorrelated noise dominates, and this can be particularly seen in the phase estimate. By contrast, Fig. 7(b) illustrates the impedance estimate when the TFE function is employed. It can be seen from Figs. 7(b), 8 and 9 that the estimates are very good for all the models—the estimated and ideal

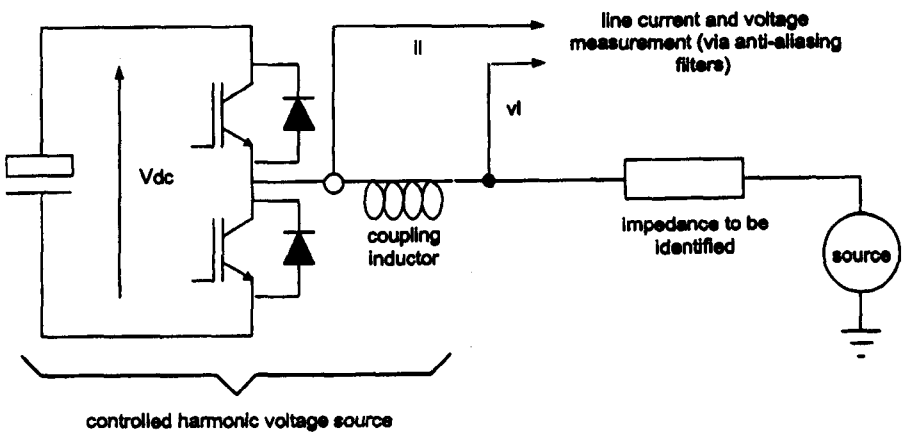

Fig. 10. Experimental facility (one phase only is illustrated).

impedances are barely distinguishable from each other. Moreover the measured current maintains an average value within 20 A—within the currents limits of even small power electronic equipment. In general, the simulation results show that linear system impedances can be estimated to a good accuracy using this technique. Resonant peaks are correctly identified, and the resolution of 6.25 Hz is entirely adequate for impedance estimation purposes. The duration of the transient and steady state data capture time is therefore 320 ms total. There is obviously a trade-off between length of transient and data capture time (i.e., speed of estimate update) versus resolution.

III. Experimental Procedure

Although the initial simulation work was carried out using a single phase circuit approximation only (for simplicity and to improve processing speed), the method was intended for three phase power systems and therefore the impedance estimation method was validated using a three phase experimental facility. The controlled source required for the voltage injection was simply a voltage source inverter employed in a standard, active shunt filter configuration [13]. The experimental facility is illustrated in Fig. 10.

Fig. 10 shows only one phase for clarity. The power electronic converter is an FKI Industrial Drives 45 kW IGBT inverter, coupled to the point of injection via a 1.2 mH "filter" inductor. The source voltage for these tests is supplied from a transformer to provide a 240 V, 50 Hz supply. The dc link capacitance is 1.2 mF, and the dc link voltage is maintained constant at 720 V using a control loop. The reduction in supply voltage is due to the overall nature of this particular experimental facility. It is also used for research into advanced active filter control strategies [13], and the larger ratio of dc link voltage to supply peak voltage allows for greater flexibility in the control laws. Several combinations of line inductor and ac capacitors were available to create networks for the "impedance to be identified" as shown in Fig. 9.

A Texas TMS320C44 digital signal processor (DSP) performs the overall control functions. The DSP is interfaced to a host PC to provide user input/output and data capture facilities. The controller measures the line current and the line voltage at the point of injection using 16 bit analogue to digital converters, to provide a good signal to noise ratio (SNR). A standard active shunt filter control strategy is employed [13], which controls the filter current using a d–q axis reference frame synchronized to the supply fundamental voltage. A small d axis current flows to keep the dc link capacitor charged to V_{dc} (720 V). The d–q reference voltages are modulated to instantaneous phase reference voltages, and a sinusoidal PWM strategy is used to convert these to suitable device switching signals. The switching frequency used was 4 kHz, and therefore the control sample period was 125 μs.

The impedance identification is obtained through a small modification to this current control strategy. The transient injection is stimulated by a user request. Before the transient is injected a 160 ms period of data (measured line voltage and current) is captured to allow compensation of the "steady state" harmonics present as described in Section II. The transient is then added to the instantaneous reference voltages. A transient waveform which has the same shape to that shown in Fig. 2 is added to the phase A reference voltage. The voltage steps used are +70 V, +105 V, −70 V and −35 V. Transient waveforms of opposite polarity and half the magnitude are added to the remaining two phase reference voltages to maintain a balanced three phase set. The controller synchronises this transient to the zero crossing point of the filter voltage demand. Again a 160 ms block of data is captured.

The data used for impedance estimation is captured using a second processor system—in this case a Siemens SAB167 microcontroller. The data capture is triggered by the C44 processor to coordinate it with the transient injection. It does not interfere with the operation of the power electronic circuit. Again, in this circuit 16 bit AD converters are used to provide a good SNR, and particular attention has been made to matching the frequency characteristics of the voltage and current transducer and filter circuits. A sampling frequency of 51.2 kHz has been used although it is not strictly necessary as the frequency range of interest is below 2 kHz. The anti-aliasing

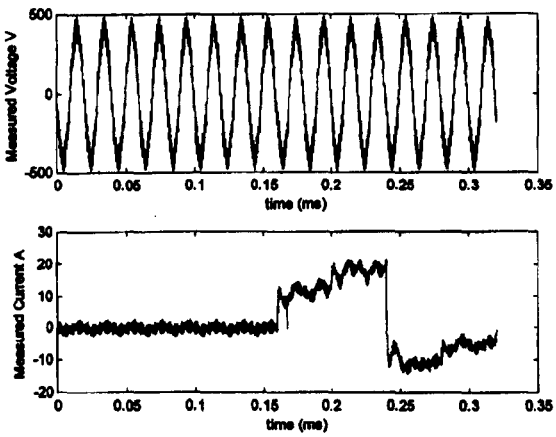

Fig. 11. Transient line voltage and current for the supply transformer only.

filters have been designed with a cut-off frequency of 10 kHz. Note that the switching frequency components contained in the measurements will be processed, but are outside the range of interest for this project. The captured data sets are then passed to the host PC for post processing using the same MATLAB routines as those used for the simulation work.

IV. Experimental Results

The experimental procedure for impedance estimation was performed on four combinations of components. Firstly the impedance of the supply alone was estimated. The measured line voltage and current are illustrated in Fig. 11, and the resultant impedance estimate is shown in Fig. 12(a)–(c). Amplitude and phase versus frequency are plotted for the estimated impedance. It can be seen that supply transformer was predominantly inductive, suggesting that the transformer has a leakage inductance of 1.15 mH. This was confirmed from the nameplate data.

For the test of Fig. 12(a), no steady state compensation has been included. Therefore the measured voltage waveform contains significant fundamental, fifth, seventh, eleventh, and thirteenth harmonics although very little current flows at these frequencies (the current control minimizes currents flowing from the injection source at these frequencies). The identified impedance is therefore much too high at these frequencies. In Fig. 12(b), steady state compensation has been implemented, as described by (1). Although the nature of the impedance illustrated in Fig. 12(b) now appears inductive, two problems are apparent. Firstly, significant discontinuities still appear at 50 Hz, 250 Hz etc. This problem arises due to the time varying nature of the magnitude and phase of the source harmonic voltages (i.e., varying from cycle to cycle). This means that exact cancellation will not occur, and therefore the impedance estimates at these specific frequencies will be in error. As the frequencies at which these discontinuities occur can be easily predicted, it is possible to ignore these inaccurate measurements and interpolate between the points. A revised impedance plot using interpolation at 50, 250, 550, and 650 Hz is shown in Fig. 12(c). Most of the subsequent impedance plots will include this interpolation. Finally, Fig. 12(d) shows the impedance estimated from the same data, but using the DFT directly, rather than the TFE function. Steady state compensation, and main harmonic interpolation have been included. The TFE method clearly provides the superior estimate.

The second problem arises from the fact that the magnitude of the voltage injected at higher frequencies will be small. Therefore, with predominantly inductive loads, the resultant injection current at higher frequencies will be small. The impedance estimate will be swamped in measurement and resolution noise. This is clearly seen at frequencies above 700 Hz, where there is more "deviation" from the lines provided for an ideal inductance. The impedance measurement technique has been developed specifically for a frequency range up to the 13th harmonic (650 Hz) as these are the most significant harmonics when considering power electronic equipment. Therefore the results for the inductive impedance are entirely adequate.

The measured supply impedance can be verified by connecting a known inductance (in this case 0.6 mH) in series with the supply transformer. The result of this test is illustrated in Fig. 13. The combined inductance is measured as 1.78 mH. Fig. 13 also shows the ideal impedance obtained by simply adding the measured transformer impedance to the known inductor impedance, and it can be seen that a good correlation is obtained.

A more complicated network was created by adding a capacitor of 100 μF in parallel to the supply transformer. The capacitor was measured independently and found to have a resistance of approximately 0.4 Ω. A resonant circuit was now formed, with a predicted resonant peak at 469 Hz. The ideal impedance variation with frequency (estimated from nameplate data) is plotted alongside the estimated impedance from voltage injection in Fig. 14. It can be seen that this peak is clearly identified.

The fourth test was performed on a Π connected circuit as shown in Fig. 6. In this case $R1$ and $L1$ are the supply transformer, $C1$ is the 100 μF capacitor, $L2$ is the 0.6 mH inductor, and $C2$ is a 50 μF capacitor. The resultant network creates resonant peaks at 374 and 1130 Hz. The ideal and estimated impedances are shown in Fig. 15(a) and (b), for different frequency scales. Again the resonant peaks are accurately identified.

A noticeable feature of the results from Figs. 14 and 15 is that the high frequency impedance is estimated correctly. This results from the fact that with a capacitor connected in the circuit, the high frequency impedance is now small compared to the purely inductive case. Therefore, the magnitude of the higher frequency injection currents are large, and no longer swamped by measurement or resolution noise.

One point to note from the experimental results is that although the general waveshape of the impedance estimates is correct, some discontinuities occasionally appear at the main harmonic frequencies. The work was carried out in a power electronics experimental laboratory when there is considerable supply noise due to local power electronic equipment. The

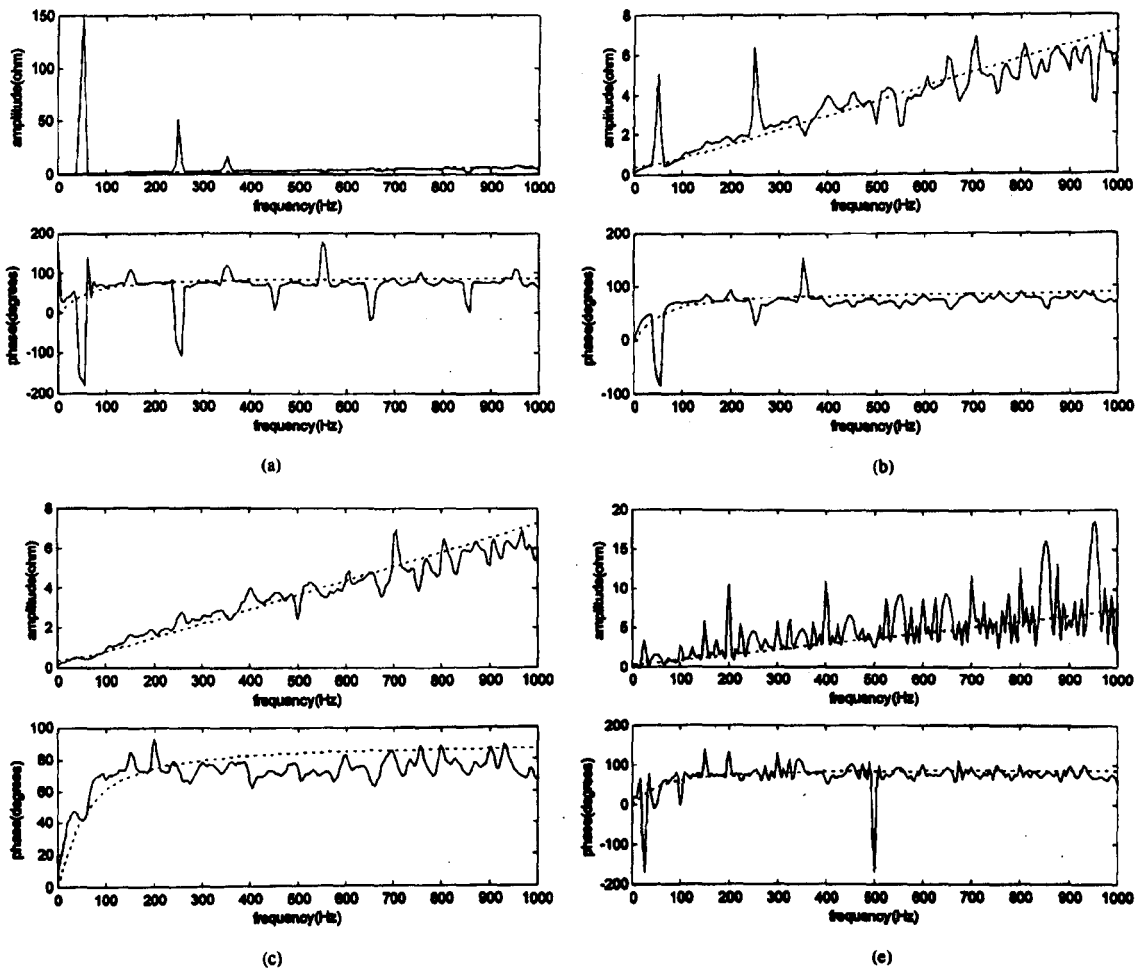

Fig. 12. Impedance estimate for the supply transformer (a) without steady state compensation, or main harmonic interpolation, (b) without main harmonic interpolation, (c) with main harmonic interpolation, and (d) with main harmonic interpolation using the DFT (solid trace is the impedance estimate and dotted trace is the ideal impedance).

method works well in the presence of moderate power electronic loads. However, when severe discontinuities appear on the supply voltage due to switching of high currents in other equipment, this estimation technique can be disrupted. The authors are therefore developing an alternative injection strategy [17], which can be used in the presence of significant power electronic loads. This method employs a current injection of only 500 μs duration, but requires significant signal processing to extrapolate the transient and obtain a less accurate impedance estimation.

V. Conclusion

A new method to estimate impedance of a power system using a power electronic converter has been proposed and validated. The technique has been developed using simulation with the Simulink Power System Blockset. It is based on the injection of a suitable transient voltage onto the system, measuring the resulting current transient and then processing them both using the MATLAB embedded function—transfer function estimation (*TFE*).

The method has been tested on four different passive circuits using an experimental facility based upon a three phase active shunt filter. The impedance estimates agree with the predicted impedances, demonstrating that the method works well in the presence of PWM waveforms, measurement noise, limited resolution (A/D converters), general noise due to power system harmonics and the switching noise present in a large experimental power electronic laboratory. It can be seen that for each test, the transient injection and implementation of the TFE provide a good estimate of the impedance back to the supply. A "steady state" data set can be used to reduce the errors introduced into the impedance calculation, by the 50 Hz source and other system harmonics present. This works very well in simulation [3], but unfortunately, in real life, these source harmonics can change from period to period and cannot be accurately compensated

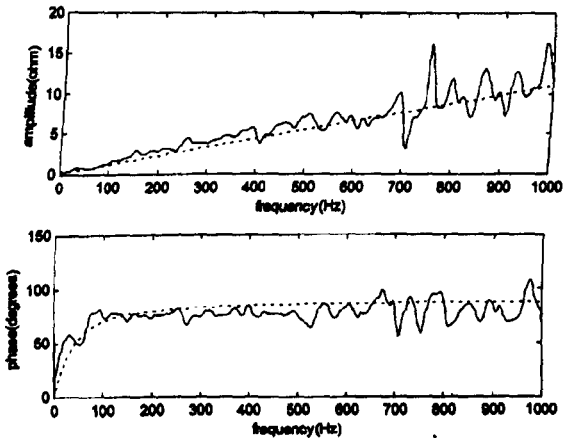

Fig. 13. Impedance estimate for the supply transformer in series with the 0.65 mH inductor—with interpolation. (The solid trace is the impedance estimate, the dotted trace is the ideal impedance.)

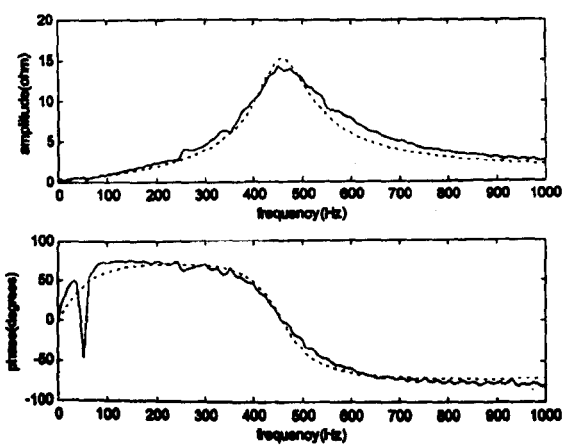

Fig. 14. Supply transformer with a 100 uF capacitor connected in parallel (no interpolation). (The solid trace is the impedance estimate, the dotted trace is the ideal impedance.)

for. Interpolation has been shown to effectively remove the discontinuities.

The estimation method may provide improvements to several areas of Power Quality control. Firstly, used within a stand alone piece of instrumentation it will be possible to build up mesh equivalent networks of unknown power and distribution systems, which can then be used for load flow studies, protection or harmonic penetration prediction (and stable passive filter design). Secondly, the method can be embedded into the control algorithm for an active shunt filter to provide on-line impedance estimates for control optimization, and also a mechanism for reference current calculation which does not require instrumentation outside of the active shunt filter. The method will also find application within embedded generation systems, where on-line impedance estimation can be used for load flow control and also the detection of islanding. Work is on-going in these areas.

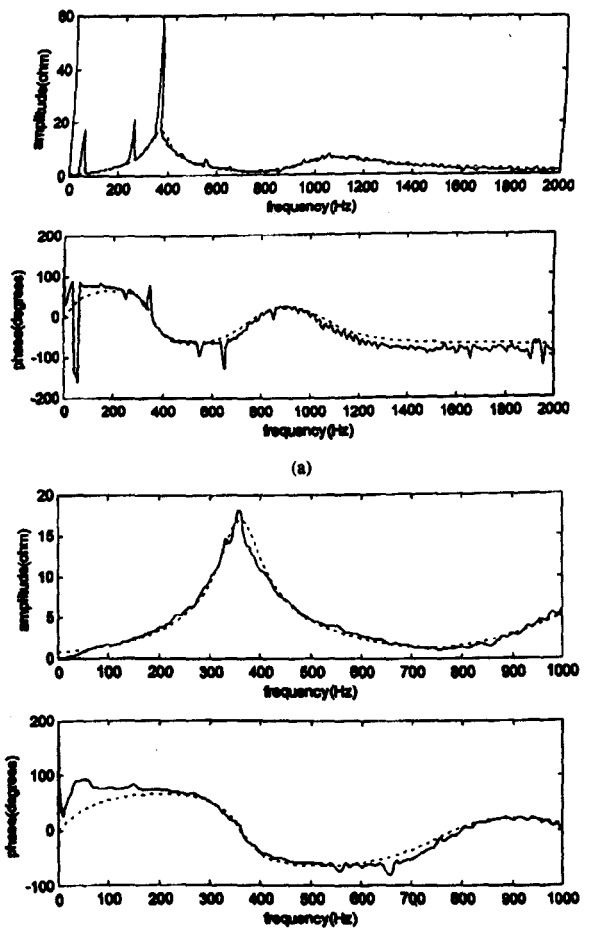

Fig. 15. (a) Impedance estimate for test circuit 4 (2000 Hz scale, no interpolation). (The solid trace is the impedance estimate, the dotted trace is the ideal impedance). (b) Impedance estimate for test circuit 4 (1000 Hz scale, with interpolation). (The solid trace is the impedance estimate, the dotted trace is the ideal impedance.)

REFERENCES

[1] A. A. Girgis and R. B. McMania, "Frequency domain techniques for modeling distribution or tranamission networks using capacitor switching induced transient," *IEEE Trans. Power Del.*, vol. 4, pp. 1882–1890, July 1989.

[2] A. S. Morched and P. Kundur, "Identification and modeling of load characteristics at high frequencies," *IEEE Trans. Power Syst.*, vol. PWRS-2, Feb. 1987.

[3] R. C. Dugan, M. F. McGranaghan, and H. W. Beaty, *Electrical Power Systems Quality*, 1st ed: McGraw Hill, 1996.

[4] B. Palethorpe, M. Sumner, and D. W. P. Thomas, "System impedance measurement for use with active filter control," in *Proc. IEE PEVD'00 Conf.*, London, U.K., Sept. 2000, pp. 24–28.

[5] M. C. di Piazza, P. Zanchetta, M. Sumner, and D. W. P. Thomas, "Estimation of load impedance in a power system," in *Proc. IEEE PES ICHQP'00*, Orlando, FL, Oct. 2000, pp. 520–525.

[6] M. Nagpal, W. Xu, and J. Sawada, "Harmonic impedance measurement using three phase transients," *IEEE Trans. Power Del.*, vol. 13, pp. 272–277, Jan. 1998.

[7] Z. Staroszczyk and K. Mikolajuk, "Time-dependent power systems impedance—Interpretation and measuring problems," in *Proc. IEEE Instrum. Meas. Technol. Conf. (IMTC99): Meas. New Millenium*, Venice, Italy, 1999.

[8] M. Tsukamoto, S. Ogawa, Y. Natsuda, Y. Minowa, and S. Nishimura, "Advanced technology to identify harmonics characteristics and results of measuring," in *Proc. 9th Int. Conf. Harmonics Qual. Power*, Orlando, FL, Oct. 1–4, 2000, pp. 341–346.

[9] *MATLAB Reference Guide*, 1992.

[10] J. P. Rhode, A. W. Kelley, and M. E. Baran, "Line impedance measurement: A nondisruptive wide band technique," in *Proc. IAS Annu. Meeting*, Orlando, FL, 1995.

[11] Z. Straszczyk, "Problems in real time identification of power systems," in *IEEE Instrum. Meas. Technol. Conf.*, St. Paul, MN, May 18–21, 1998.

[12] A. de Oliveira, J. C. de Oliveira, J. W. Resende, and M. S. Miskulin, "Practical approaches for ac system harmonic impedance measurements," *IEEE Trans. Power Del.*, vol. 6, pp. 1721–1726, Oct. 1991.

[13] D. Butt, M. Sumner, and J. C. Clare, "Harmonic compensation in active shunt filters using controllers employing harmonic rotating frames of reference," in *Proc. EPE'99 Conf.*, Lausanne, Switzerland, Sept. 1999.

[14] J. P. Rhode, A. W. Kelley, and M. E. Baran, "Complete characterization of utilization-voltage power system impedance using wideband measurement," in *Proc. Ind. Comm. Power Syst. Tech. Conf.*, 1996, pp. 123–130.

[15] ——, "Complete characterization of utilization-voltage power system impedance using wideband measurement," *IEEE Trans. Ind. Applicat.*, vol. 33, pp. 1472–1479, Nov.–Dec. 1997.

[16] J. Van Rooijen and H. J. Vermeulen, "A perturbation source for in-situ parameter estimation applications," in *Proc. IECON'94 Conf.*, 1994, pp. 1819–1823.

[17] B. Palethorpe, M. Sumner, and D. W. P. Thomas, "Power system impedance measurement in the presence of nonlinear loads," in *Proc. EPE'01 Conf.*, Graz, Austria, Aug. 2001.

Mark Sumner received the B.Eng. degree in electrical and electronic engineering from Leeds University, U.K., in 1986 and the Ph.D. degree from Nottingham University, U.K., in 1990.

He worked for Rolls Royce, Ltd., Ansty, U.K., for a short time before embarking on research work in vector controlled induction motor drives at Nottingham University, where he was a Research Assistant, and later appointed Lecturer in October 1992. His research interests cover microprocessor control of power electronic systems including advanced sensored and sensorless induction motor drives research, active shunt filters, system identification, and the development of new converter topologies.

Ben Palethorpe was born in Farnham, U.K., in 1974. He received the M.Eng. degree in engineering science from the University of Oxford, U.K., in 1996 and is currently pursuing the Ph.D. degree at the University of Nottingham, U.K.

He is currently a Research Assistant within the Power Electronics and Machine Control Group, University of Nottingham. His research interests include active filter control, system impedance identification, and power quality.

David W. P. Thomas received the B.Sc. degree in physics from the Imperial College of Science and Technology, London, U.K., in 1981, the M.Phil. degree in space physics from Sheffield University, U.K., in 1987, and the Ph.D. degree in electrical engineering from Nottingham University, U.K., in 1990.

After working as a Research Assistant he was appointed as a Lecturer in 1990. His research interests are in electromagnetic compatibility, protection and simulation of power networks, electrostatic precipitation, and high voltage insulation testing.

Pericle Zanchetta received the Laurea degree in electronic engineering and the Ph.D. degree in electrical engineering from the Politecnico di Bari, Italy, in 1994 and 1997, respectively.

Since then he's been working with the Converters, Electrical Machines, and Drives Research Team, Politecnico di Bari. After working in Bari as a Research Assistant, in November 1998 he became Assistant Professor of power electronics at the Department of Electrical and Electronic Engineering, Politecnico di Bari. He is also a Visiting Lecturer at the University of Nottingham, U.K. His main research interests are in the field of modeling and measurement of low frequency conducted EMI, virtual instrumentation, modeling and simulation of power converters, active power filters, multilevel inverters, and fuzzy logic controllers.

Maria Carmela Di Piazza received the M.S. and Ph.D. degrees from the University of Palermo, Italy, in 1997 and 2001, respectively, both in electrical engineering.

She then joined the Converters, Electrical Machines, and Drives Research Group, Department of Electrical Engineering, University of Palermo. Since November 2000, she has been with the Research Centre on Electrical Power Systems (CERISEP) [part of the National Council of the Research (CNR)], Palermo. Her main research interests are electrical drive systems, electromagnetic compatibility, and power quality.